UNIVERSITA' DEGLI STUDI DI FIRENZE
&
CRANFIELD UNIVERSITY

ADOLFO CARLONI

A NOVEL OPTICAL CHIP FOR AFFINITY BIOSENSORS BASED ON FLUORESCENCE ANISOTROPY

PhD THESIS

UNIVERSITA' DEGLI STUDI DI FIRENZE
&
CRANFIELD UNIVERSITY

DOTTORATO IN SCIENZE CHIMICHE
XX CYCLE

CRANFIELD HEALTH

PhD THESIS

Academic years 2005-2007

ADOLFO CARLONI

A NOVEL OPTICAL CHIP FOR AFFINITY BIOSENSORS BASED ON FLUORESCENCE ANISOTROPY

Supervisors:
Professor Marco Mascini
Professor Anthony P.F. Turner

July 2008

This thesis is submitted in partial fulfilment of the requirements for the degree of Doctor of Philosophy in co-tutela between University of Firenze and Cranfield University.

ABSTRACT

The subject of this thesis relates to the realisation of a novel biochip for sensors based on optical principles. In particular, affinity biosensors for antigens (IgG/anti-IgG), for a transcription factor, and for mRNA were studied and developed. The interrogation of the biosensors implied the development of a novel and innovative optical platform based on fluorescence which was designed, implemented and thoroughly characterised. The biosensors developed were integrated within an optical biochip connected to an innovative platform. The optical biochip was fabricated from polymethylmethacrylate (PMMA) formed by two pieces of PMMA complementary shaped in order to obtain four micro-channels. The lower part included the micro-channels and the inlet and outlet for the fluidic, while the sensing biolayer was immobilised on the upper part. The optical signal comprised the fluorescence emitted by the layer, which was anisotropically coupled to the cover and suitably guided by the chip. Several chemical treatments of the surface were investigated to obtain the most effective distribution of carboxylic groups for the covalent immobilisation of antibodies. Deposition of the polymers, in particular by Langmuir-Blodgett method, can enhance the performances of the chip going through lower detection limits. The potential of the optical chip as a biosensor was investigated in depth by means of a direct IgG/anti-IgG interaction carried out inside the flow channels. Following this, bioassays for the determination of the NF-kB transcription factor and for the mRNA that codifies for MGMT protein were implemented on the optical platform. The development and characterisation of the biosensors, the identification of the protocol for the bioassays and the design and characterisation of the optical platform were performed at the Institute of Physics Applied Carrara of National Research Council (IFAC-CNR), Firenze, Italy. The research devoted to the development of biosensing surfaces for the realisation of affinity biosensors able to detect and quantify antigens, transcription factors and RNA sequences were carried out at the laboratories of the Institute of Clinical Physiology of National Research Council (IFC-CNR), in Pisa, Italy. Langmuir-Blodgett deposition of polymers, Atomic Force Microscopy imaging and further fluorescence measurements of proteins covalently bound on the surfaces were performed at Cranfield University in Silsoe, England. The overall project starts from a first characterisation of the optical system, and comprehend the enhanced optimisation of the biochip performances until the realisation of the biosensors previously mentioned.

ACKNOWLEDGEMENTS

This research study was supported by the European Community within the Framework 6 Programme (FP6) of the five-year EU funded project under IST priority, CAREMAN (HealthCARE by Biosensor Measurements and Networking).

I would like to thank all my colleagues for the exchange of scientific knowledge inside the Institute of Applied Physics *"Nello Carrara"* (IFAC-CNR).
The strategic role of CNR, in collaboration with Datamed S.r.l., was determinant for the development of the chip and for the measurements performed.

In particular, I would like to thank Dr. Francesco Baldini, Dr. Andrea Mencaglia from IFAC-CNR, Dr. Ph.D. Cosimo Trono, Dr. Ph.D. Ambra Giannetti, for the support in the implementation of the opto-chemical instruments.

I would like to thank also Prof. Lorenzo Citti and Dr. PhD. Lorena Tedeschi from IFC-CNR for their help in the laboratories of Pisa.

Thanks finally to Prof. Marco Mascini and to Prof. Anthony Turner for the trust that they placed in me for this highly multidisciplinary project enriched by nice periods spent in Firenze and Pisa in Italy and in Silsoe in the UK.

The most important thanks go to my girlfriend, "the doctor" Linda, and to my family, especially to my parents which supported me for the entire period of my Ph.D.

LIST OF CONTENTS

LIST OF FIGURES

LIST OF TABLES

NOTATION

AFM	Atomic force microscopy
Anti-IgG_Cy5	Goat-antimouse immunoglobulin antibody labelled Cy5
APTES	Aminopropyltriethoxysilane
APTMS	Aminopropyltrimethoxysilane
BP	Band pass filter
CCD	Charge-coupled device
$CHCl_3$	Chloroform
Cy5 (NHS)	Cyanine 5-N-pentil-succinimidyl ester
$C_6H_8O_7$	Citric acid
DMF	Dimethylformamide
DMSO	Dimethylsulfoxide
DNA	Deoxyribonucleic Acid
DTT	Dithiothreitol
EDC	1-Ethyl-3-[3-dimethylaminopropyl] carbodiimide hydrochloride
EDTA	ethylenediaminetetraacetic acid
EtOH	Ethanol
Eudragit L100	Copolymer 1:1 of PMMA and carboxylic acid
Eudragit RL100	Copolymer 1:1 of PMMA and propyltrimethylammonium chloride
FITC	Fluorescein isothiocyanate
5-FAM-X, SE	6-(Fluorescein-5-carboxamido)hexanoic acid, succinimidyl ester
GRIN	Graded index lens
HCl	Chloridric acid
HEPES	N-2-Hydroxyethylpiperazine-N'-2-Ethanesulfonic Acid
HMDA	Hexamethylendiammina
HP	High pass filter
H_2O_2	Hydrogen peroxide
H_2SO_4	Sulphuric acid
IgG	Mouse immunoglobulin antibody
IKK	Inhibitor kinase complex
ITC	Input Trigger Connector
KCl	Potassium chloride
LASER	Light Amplification by Stimulated Emission Radiation
LB	Langmuir-Blodgett trough
LC	Liquid condensed phase
LD	laser diode
LE	Liquid expanded phase
LED	Light emitting diode
LP	Low pass filter
LWF	Long wavelength fluorophore
MeOH	Methanol
MES	2-morpholinoethanesulfonic acid
NHS	N-hydroxy-succynimide
NaOH	Sodium Hydroxide
Na_2HPO_4	Disodium hydrogen phosphate
NF-kB	Nuclear Factor kappa B
NP-40	nonyl phenoxylpolyethoxylethanol
PBS	Phosphate buffer solution
PLLA	Poly L-lactic acid

PMMA	Polymethylmethacrylate
PMT	Photo multiplier tube
PTFE	Polytetrafluoroethylene (Teflon)
PVC	Polyvinylchloride
p50	protein 50 kDa
p65	protein 65 kDa
p50/p50	homodimer protein
p50/p65	heterodimer protein
Π	Surface Pressure
RNA	Ribonucleic Acid
2'OMe-RNA	2'-O-methyl ribonucleic acid
S	Solid state
SiO_2	Silica glass
s-NHS	Sulfo-N-hydroxysuccinimide
s-SDTB	Sulfo-succinimidyl-4-O-(4,4-dimethoxytrityl) butyrate
SMA	Subminiature version A connector for optical fibre
SMCC	sulfo-succinimidyl 4-(N-maleimidomethyl) cicloesan-1-carboxylate
SNR	Signal to noise ratio

1. PREFACE

Affinity biosensors allow the detection of affinity based interactions between bio-molecules and their corresponding components (e.g., avidin/biotin, antigen/antibody, complementary single-stranded DNA sequences). A suitable design of the biosensor ensures that binding of target molecules and their corresponding components takes place on the transducer surface. The sensors are thus implicitly heterogeneous. A key aspect in the development of biosensors concerns the interaction between inorganic (i.e., the transducer) and organic material (i.e., the biological receptors). The increasing miniaturisation of biosensor transducers (and thus of their active areas) and the demand for high sensitivity, require a covalent and tailored coupling of bio-molecules to the transducer surface. In order to meet the requirements of miniaturised affinity based biosensors regarding sensitivity, selectivity, stability and reproducibility, tailored bio-interfaces have to be developed and evaluated. Affinity biosensors have generally proved more amenable to optical detection methods [1]. As for the optical approach, a major distinction can be made between label-free sensors [2-4], in which the interaction analyte/sensitive layer gives rise to a modification of the optical signal due to a change in the refractive index of the layer deposited on the substrate, and label-based sensors [5-8], in which fluorescent labelling is used to obtain an optical signal that depends on the analyte investigated. There are both advantages and disadvantages with these two methods. The main advantage of a direct detection method is its capability to make analyses without the application of labels [9]. In fact, fluorescence-based biosensors require either multi-step detection protocols or delicately-balanced affinities of interacting biomolecules for displacement assays, which can cause sensor cross-sensitivity to non-target analytes. However, for complex sample monitoring, the label-free methods continue to be susceptible to problems such as low sensitivity and increased backgrounds due to non-specific binding. Therefore, in clinical applications in which the sample matrix can be very complex (as in the case of whole blood and even serum) the use of a label-based system may be preferable [10].

In particular, affinity biosensors for the IgG/anti-IgG, for the NF-kB transcription factor/DNA consensus sequence and for complementary RNA/RNA sequences, one of which is the mRNA codifying for MGMT protein, were studied and developed.

The interrogation of the biosensors implied the development of a novel and innovative optical platform based on fluorescence which was designed, implemented and thoroughly characterised.

The biosensors developed were integrated within an optical biochip connected to the optical platform.

The optical signal comprised the fluorescence emitted by the layer, which was anisotropically coupled to the PMMA cover and suitably guided by the PMMA chip.

Several chemical treatments of the PMMA surface were investigated. In particular the deposition of one copolymer of PMMA by Langmuir-Blodgett method, offers an impressive enhancement of the performances of the biochip.

The potential of the optical chip as a biosensor was investigated in depth by means of a direct IgG/anti-IgG interaction carried out inside the flow channels. The mouse-IgG was covalently immobilised on the internal wall of the PMMA cover and the Cy5-labeled anti-mouse IgG was used for the specific interaction.

Bioassays for the determination of the NF-kB transcription factor and for the mRNA that codifies for MGMT protein were implemented on the optical platform.

An improvement in the sensitivity of the system and a lower limit of detection (linear range 1 ng/ml- 1mg/ml) for the IgG/anti-IgG assay was revealed with the PMMA chip.

2. INTRODUCTION

2.1 General features of biosensors

According to the modern definition [11-12], a biosensor is an analytical device comprising a biological or biologically derived sensing element either integrated within or intimately associated with a physicochemical transducer which generates selective and reversible signals reflecting the concentration of analytes present in the sample.
The general principles of operation of an affinity biosensor are shown in Fig. 2.1 and it is conceptually easy to understand: the bioreceptor immobilised on a surface of a solid support takes part in one or more processes that determine the variation of a chemical, physical or physical-chemical parameter, which are then converted by the transducer into an electrical signal that can be amplified, elaborated and visualised.

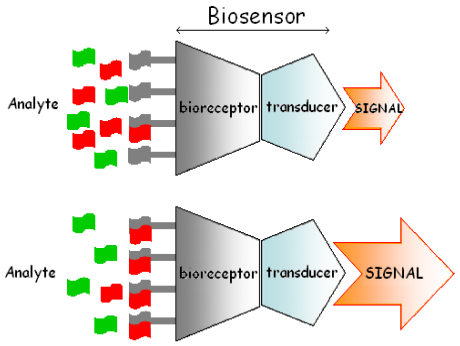

BIORECEPTOR	TRANSDUCTION	SIGNAL
Proteins Antibodies Oligonucleotides DNA,RNA	Electrochemical Optical Calorimetric Acoustic or micromechanical Magnetic	Current Potential Conductibility Absorption Fluorescence Refraction Temperature Frequency piezoelectric Magnetic field

Figure 2.1 General constituents of a biosensor (left) and list of possible types of bioreceptor, transduction systems and signal (right).

For most modern industrial production methods, process monitoring plays a key role; bioprocess systems are no exception to this rule. Effective methods of control are required so that the development and optimisation of efficient biosensors is a key component for biological process monitoring. An optimised biosensor should lead to a streamlined procedure, reducing material costs and improving performance in the control of several parameters. A number of bioprocess monitoring instruments and kits have been developed for industry quality control over many years, in particular biosensors capable of measuring physical or chemical parameters. The challenge in this branch of research is

to develop cost-effective and robust devices capable of measuring a much wider range of parameters, providing process operators with a deeper insight into their processes.

In addition to the variety of monitoring devices available, a number of methods for carrying out the measurement exist. Sampling and sample handling is a vital issue, affecting both the accuracy and frequency of measurement [13]. Broadly, the main approaches to sampling can be described in one of several ways:

1) "Off-line monitoring" involves taking a sample from the measuring site and carrying out the measurement at a different location, usually under laboratory conditions. Off-line sampling suffers from the disadvantages of high cost and low efficiency. Manually removing and measuring a sample requires technical labour, involves the introduction of possible errors during the sample transportation and implies a delay between sampling and the measurement.

2) "At-line monitoring" involves decentralised equipment and allows measurements to be made simply close to the production process reducing lot of delays associated with the sample transportation and laboratory analysis.

3) "On-line monitoring" involves automatic sampling facilitated by the proximity of the analytical instrumentation.

4) "In-line monitoring" involves the use of sensors placed directly *in situ* inside the bioprocess vessel.

The use of *in situ* sensors has long been established in the bioprocess industry [14] where immersed devices are used to monitor a number of parameters such as pH and dissolved gas concentrations. A number of advantages are gained by operating sensors in this fashion, including "real-time monitoring" (delays due to sampling are eliminated) with the sensors operating continuously (any change in the analyte concentration can be readily observed), and problems of contamination being significantly reduced. However, *in situ* sensors can have a number of drawbacks, for example, if the sensor lifetime is short and the sensing element looses its recognition properties, it has to be easily renewed or replaced, which may be difficult during a process run. Methods of "on-line monitoring" involve the automatic removal and measurement of sample or sample stream from the bioreactor. One example of this has been the development (since the early 1980s) of flow injection analysis. This is a liquid handling technique that has proved flexible in adapting to most chemical and biochemical reaction procedures [13], representing an effective compromise between the desirability of *in-situ* monitoring and off-line measurements. The main advantages of on-line methods include the following:

sensor sterilisation can be readily accomplished, sample pre-treatment (e.g. dilution, removal of interferents) and sensor calibration can be performed on the system.
The main disadvantage is represented by a need for an effective and reliable sampling system; the frequency of measurements is limited by the overall flow-injection analysis arrangement.
Further developments came from wireless technologies that now allow sensors to be controlled directly from a portable device at an affordable price using appropriate software. The improvement of this technology allows a much more constant frequency rate and can avoid certain discontinuities of the signal due to previously used slower telecommunications. In summary, all of these methods have their advantages and disadvantages. The choice of an appropriate approach depends on a number of factors, not least of which will be the availability of both sensor and system. Eventually effective monitoring will lead to better control systems, providing costs and quality benefits. For any measurement technique, there are a number of criteria that the device must satisfy if it is to be accepted by commercial bioprocess operators. The following subset covers the main characteristics of a monitoring process [15]:

Reliability

Reliability is a key issue for bioprocess monitoring equipment. Confidence in the ability of an instrument to maintain its credibility in terms of performance is a fundamental parameter. This encompasses a number of features relating to the operation of the instrument, for example, ease of use, maintenance, repair and replacement. A successful monitoring instrument will have a low failure rate.

Accuracy

Accuracy can be described as the relationship between the measured value (by the instrument) and the actual value of a bioprocess variable.
An accurate instrument will achieve a low percentage error between these two values. Generally this can be stated as:

% error = (measured value - true value) / true value

Precision

Precision is a measure of instrument reproducibility, that is, the ability to obtain the same value with repeated measurements of a process variable (at constant level, such as in the same buffer solution). A precise instrument may not be accurate. Therefore it is important to distinguish between these two parameters.

Response time

The measurement of any process variable will entail a time delay between change in the parameter and display of the measured value. This response time should be appropriate for the progress of the bioprocess, particularly if the measurements are linked to a control action. Response times will be affected not only by the type of instrument but also by the method of measurements. Off-line sampling and measuring can involve a number of time consuming steps. In contrast, an *in situ* device can provide a real-time measurement.
According to IUPAC (International Union of Pure and Applied Chemistry) the response time is based on the differential quotient Δsignal / Δtime (where signal is normally expressed in volts).
The IUPAC recommendations outline two experimental procedures for measuring the response time. In the "dipping method", the sensor is instantaneously immersed into a solution of known activity of the test analyte. With the "injection method", the sensor is kept immersed in a solution and after beginning to record the response, a measured aliquot of a concentrated solution of the analyte is added.
The response time determined by the first procedure has been termed "the static response time", whereas, the approach delivers the "dynamic response time".
The response time is not a univocal parameter and it depends on the particular working conditions [16].

Calibration

In order to maintain the accuracy of a sensor it is desirable to carry out a calibration step. The effects of calibration can damage the process, or, in other words, it may be difficult to carry out calibration of an *in situ* sensor, whereas an online device could easily incorporate calibration steps during routine running.

Linearity

Under ideal condition the output signal from a sensor would be directly proportional to the analyte concentration. However, this is not always the case and other models have to be used to reach a true value. Despite this drawback, linearity is not an overriding prerequisite for a successful monitoring instrument. In fact, developments in modern software can be adapted to compensate for non-linearity.

Sensitivity

Sensitivity is the magnitude of the output signal per unit change in the target analyte concentration. The lowest level of detection is related to the sensitivity and the signal-to-noise ratio. A number of factors influence the sensitivity of a monitoring device, including sensor design, the operating environment, periods of maintenance, and interfering noise levels. The sensitivity will influence the dynamic range above which the device becomes saturated; the highest level of detection will be the threshold limit for the device. The limit of detection (LOD) and limit of quantification (LOQ) are defined by IUPAC as three times and ten times respectively the average of the single noise value signal (standard deviation).

Selectivity

Selectivity indicates how free from interferences the method of measurement is. In practice, all analytical methods can be perturbed by interfering species and this effect has to be minimised in order to obtain higher accuracy of the measurement.

Specificity

It is a statistical measure of how well a binary classification test correctly identifies the negative cases, or those cases that do not meet the condition under study. Specificity is defined as the number of true negatives divided the total sum of true negatives and false positives.

2.2 General features of optical biosensors

The argument of this thesis will refer to the use of different types of bioreceptors to characterise the potentiality of a novel optical biochip, measuring the signals in absorption and mainly focusing on fluorescence (Fig. 2.1).

In literature are plenty described various systems obtained following precise conditions dictated by opto-chemical rules involved in the engineering of an instrumental device.

In this chapter several optical principles and literature references are reported and illustrate an overall idea of the recent thirty years development in the field of optical biosensors.

In literature various optical technique for detecting and monitoring antibody-antigen reactions at a solid-liquid interface are reported.

Extremely important are the theoretical studies and the applications developed determined by the study of the optical coupling of the laser light with a surface chemically modified.

This part will start from formulations on the general principles of internal reflection spectroscopy, models for refractive index, evanescent wave and fluorescence theory in immunoassays, going towards modern optical systems such as fluorescence capillary fill device.

Satisfactory results were also obtained based on surface plasmon resonance sensors, optical biosensors, resonant mirror, array biosensor, flow injection analysis, fiber optic sensor, near infrared sensor, fluorescence sensor and dipstick sensor.

Recently a comparison between two modern techniques (optical biosensors and ELISA) to measure a protein assay was also considered and discussed.

Lateral flow biosensors, fluorescence enhancement due to metal nanoparticles, and the presentation of a multi-analyte array biosensor product in the market were the last articles reported.

2.2.1 Internal Reflection Spectroscopy (IRS)

Between two transparent media when a light beam strikes the interface from the medium with a higher refractive index ($n_1 > n_2$), total internal reflection occurs [17] (Fig. 2.2A) if the angle of reflection θ is larger than the critical angle θ_C, defined as:

$$\theta_C = \arcsin (n_2 / n_1)$$

In this case the evanescent wave penetrates a distance (d_P), on the order of a fraction of a wavelength, beyond the reflecting surface into the rarer medium with the lower refractive index n_2. According [17] to Maxwell's equations, a standing sinusoidal wave, perpendicular to the reflecting surface, is established in the denser medium (Fig. 2.2B).

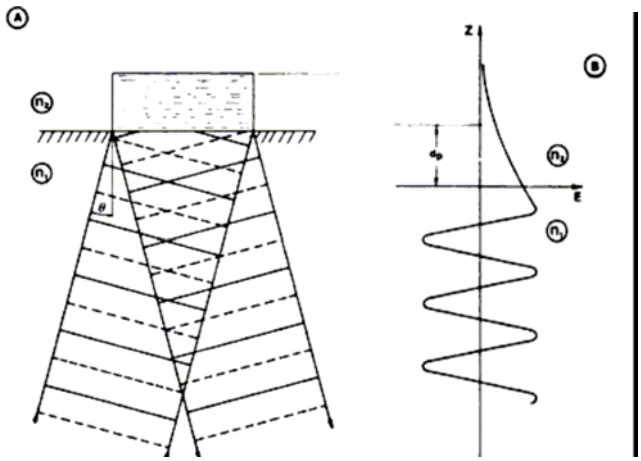

Figure 2.2 Generation of the evanescent wave at an interface between two optical media: (A) Where $n_1 > n_2$ and $\theta > \theta_c$ the critical angle at which refraction occurs, the evanescent wave is generated at the point of reflection. (B) Plotted on a different axis (where E = field strength, Z = distance into the rarer medium), the evanescent wave is represented as a standing sinusoidal wave perpendicular to the reflecting surface with a characteristic generation depth (d_P). [17]

Although [17] there is no net flow of energy into the non absorbing, rarer medium, there is an evanescent, non propagating field in that medium, the electric field amplitude (E) of which is largest at the surface interface (E_0) and decays exponentially with distance (Z) from the surface:

$$E = E_o \cdot \exp(-Z/d_P)$$

The depth of penetration (d_P), defined as the distance required for the electric field amplitude to fall to exp (-1) of its value at the surface, is given by:

$$d_P = \frac{\lambda / n_1}{2\pi[\sin^2\theta - (n_2/n_1)^2]^{1/2}}$$

Starting from 90°, as θ approaches θ_C, d_P becomes infinitely large and, at a fixed angle, increases with closer index matching (i.e., as $n_2/n_1 \rightarrow 1$).

Also, because d_P is proportional to wavelength, it is greater at longer wavelengths.

Thus, by an appropriate choice of the refractive index n_1 of the transparent support material, the incident angle, and the wavelength, one can select a d_P to promote optical interaction mainly with compounds close to or affixed at the interface, and minimally with the bulk solution.

For example, if the denser medium is a quartz microscope slide ($n_1 = 1.54$) and the rarer medium is aqueous sample solution ($n_2 = 1.34$), θ is 70°, and if λ is either 495 nm or 310 nm, thus the d_P is approximately 145 nm or 90 nm, respectively.

One [17] can enhance assay sensitivity by combining the evanescent-wave principle with multiple internal reflections. The number of reflections (N) for both sides of the slide is a function of the length (L) and thickness (T) of the waveguide and of the angle of incidence (θ):

$$N = L/T \cdot \cot\theta$$

In 1985, optical techniques for monitoring immunological reactions on continuous surfaces were investigated and reviewed [18]. Techniques such ellipsometry, light scattering, surface plasmon resonance and more general internal reflection spectroscopy (IRS) systems were discussed.

The latter includes attenuated total reflection (ATR) and total internal reflection fluorescence (TIRF). Overall, it was considered that the IRS systems and ellipsometric approaches offered the most promise for the design of a specific immunosensor device.

In particular. the ellipsometric methods are the most sensitive but also the most vulnerable to non-specific signal interference. Although lacking in extreme sensitivity, the IRS approaches reviewed were more robust in signal transduction. [18]

2.2.2 Models for refractive index

A recent well appreciated formulation [19] in a an asymmetric slab (planar) waveguide setup (Fig. 2.3) was plenty explained on a clear class with the equations shown on the:

1) Determination of the core thin film refractive index, n_{core} .

2) Calculation of the superstrate refractive index, $n_{superstrate}$, if n_{core} is known.

3) Calculation of the effective refractive index, $(n_{eff})_p$, if n_{core} is known.

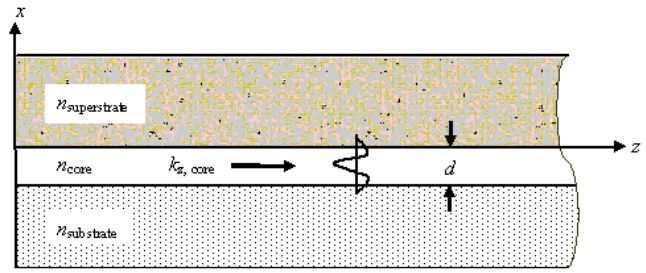

Figure 2.3 A typical coupling arrangement in a an asymmetric slab (planar) waveguide. [19]

Derivation of these equations were referred previously [20], and applications of these procedures are well reported elsewhere [21-23].

Again another exhaustive formulation in the excitation of a planar waveguide using a grating coupler (Fig. 2.4) was discussed [24] on the:

1) Determination of the core thin film refractive index, n_{core};

2) Determination of an analyte solution, i.e. the superstrate, refractive index, $n_{superstrate}$;

3) Calculation of the effective refractive index, $(n_{eff})_p$, if n_{core} is known;

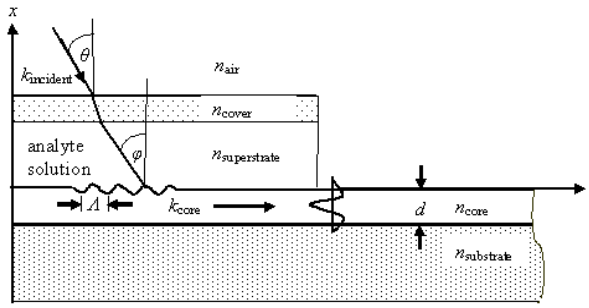

Figure 2.4 A typical coupling arrangement in a grating coupling sensor is shown. [24]

2.2.3 The evanescent wave

Fluorescence emission generated at a waveguide-liquid interface can be monitored at the waveguide output.

Fluorescence emission in a waveguide/liquid interface must be considered as an evanescent wave as depicted by the theory of reciprocity, and demonstrated with dye molecules in both monomolecular layers [25] and in monodispersed spheres [26].

In effect, excitation of fluorescence by an evanescent wave produces fluorescence emission generating an internally reflected beam of fluorescent light.

The direction of fluorescence emission is mainly a function of the respective refractive index ratio and has the major feature [25] that photon emission has a distribution of "preferred" angular probability close to the critical angle (θ_C).

Practically the fluorescence can be monitored at the output of the waveguide in the same optical plane as the excitation light. Theoretically, this has the advantage to concentrate the fluorescent emission intensity within a small angle, called anisotropic angle; also, these fluorescent photons do not pass through the bulk of the solution and thus are not subject to major optical interference (e.g., absorption, scattering).[27]

Antibodies covalently immobilized onto the surface of either a planar (microscope slide) or cylindrical (fibre optic) waveguide made of quartz were described in literature.[27]

The reaction of immobilized antibody with antigen in solution was detected through use of the evanescent wave, which has a characteristic depth of penetration of a fraction of a wavelength into the aqueous phase, thus optically interacting, as previously mentioned, with substances bound or located very close to the interface and only minimally with the bulk solution.

An immunoassay for methotrexate (MTX) was monitored by the decrease in transmittance at 310 nm and achieved a detection limit of about 270 nmol/l; a two-site immunofluorometric assay for human IgG was able to detect until 30 nmol/l; binding of fluorescein-labeled antibody was monitored by the increase in signal at > 520 nm (λ exc. = 495 nm).

With both immunoassays the signal-generating phase was monitored kinetically and was completed within 15 min. The completion time in a procedure for an immunoassay (commonly due to the biological response of the bioreceptor to the analyte) represents one of the most important parameters in a point-of-care unit device.

Following the pioneering work of Berson and Yalow in 1959 [28], immunoassay procedures have rapidly assumed a major role in the clinical investigation of disease and monitoring of therapy [29, 30]. Extremely important is the optimization of the chemical protocol which can ensure robust performances of detection in a short period of time.

The evanescent field technique was used to monitor the deposition of inorganic compounds at various solid-liquid interfaces [31, 32].
Similarly, the generation of thin protein films at solid liquid interfaces has been investigated by infrared spectroscopy techniques [33, 34] and fluorescence [35].

In particular fluorescent detection in antibody-antigen reactions has been demonstrated in 1975 when the monitoring of fluorescein-labeled antibody bound to antigen (phenyl arsonic acid) immobilized on a quartz waveguide has been reported [36].
In 1983 an examination of the binding kinetics of rhodamine-labeled antibodies to dinitrophenol, immobilized to a quartz waveguide, was also presented [37].

Elsewhere [38] were presented data using the evanescent wave to measure human IgG, captured by an immobilized antigen, by the increase in light scattered perpendicular to the optical axis.
Moreover, in 1984, another application [39] based upon theoretical principles, described an optical detection technique for monitoring antibody-antigen reactions at a quartz-liquid interface.

A two-site immunofluorescent assay for human IgG is described using fluorescein.
The assay detection limit is approximately 0.8 μg/ml and individual fluorescence measurements were completed in this case within 10 min [39].

Going towards the development of commercial biomedical devices, a U.S. Patent, in 1987 was registered describing a waveguide placed in contact with an illuminated sample; fluorescence from bound material produces an evanescent wave above the critical angle. Fluorescence from unbound material is refracted at the interface, and can therefore only exit the waveguide at an angle below the critical angle [40].

2.2.4 Fluorescence Capillary Fill Device

In 1987, detail of a novel type of optical biosensor for immunoassays, the fluorescence capillary-fill device (FCFD), was reported [41]. This is based on a straightforward adaptation of the technology used to mass manufacture liquid-crystal display (LCD) cells to give cheap disposable immunosensors. The optical characteristics of the FCFD were described on a competitive immunoassay for human immunoglobulin G (hIgG).

The demonstration of this assay resulted in a significant achievement, because the format of the FCFD, its manufacturing process and its instrumentation were modern and deeply studied [41].

In addition, sensors that exploit the evanescent field associated with the reflection of light at dielectric/ dielectric interface or at dielectric/metal interface enhanced optical biosensing [42].

The development [43] of FCFD, in which the additional reagent was temporarily immobilized has removed several shortcoming and the use of a metal/dielectric interface at which a surface plasma wave was generated has provided a robust idea in the biosensor construction.

Immunosensors make use of antibodies and can be extremely specific if appropriate monoclonal antibodies are used. The development [44] of an optical immunosensor based on the detection of rubella antibody in serum, plasma and whole blood was reported in an assay time of less than 10 min.

Optical technologies currently proved very attractive ideas for the construction of reliable biosensors in a fast response time.

Using FCFD, in 1991 was developed [45] an assay for human chorionic gonadotrophin (hCG) for a variety of body fluids (whole blood, serum, urine and saliva) demonstrating the enhanced versatility for the assay performances of this method.

Maximum analytical performance from an optical immunosensor which uses whole blood as the sample matrix, needs a rigorous selection of the fluorophore and this was studied in 1995 [46].

Three fluorophores, allophycocyanin (APC), carboxymethylindocyanine succinimidyl ester (CY5) and fluorescein isothiocyanate (FITC), were evaluated in whole blood and serum assays using the FCFD immunosensor. FITC is a well known and readily available fluorophore; however, the wavelengths of its fuorescent spectrum coincide with the intrinsic fluorescence of human serum and it was suspected that the performance of

assays using FITC would suffer accordingly. APC and CY5 were evaluated as alternative fluorophores because of their longer excitation and emission wavelengths. APC is a phycobiliprotein extracted from algae whilst CY5 is a synthetic dye whose properties are similar to those of APC. APC and CY5 gave the best result in terms of analytical performance using FCFD setup [46]. Whole-blood patient samples were assayed using APC as label and an excellent correlation was obtained with a commercially available immunoassay.

A most desirable feature of such sensors would be the ability to use untreated whole blood samples thus removing the need, with associated time, cost and safety implications, for the preparation of serum and/or plasma samples prior to analysis.

The use of whole blood is also advantageous from an optical point of view because the self-fluorescence of the sample was much reduced.

The samples were examined again by FCFD, discriminating between fluorophores bound to the surface and free in solution without the need for a wash and/or separation step.

The model analyte chosen [46] for this study was prostate-specific antigen (PSA). PSA is a glycoprotein of approximately 30 000 molecular weight which is secreted exclusively by the prostate gland in the male and finds an important role in the diagnosis of prostate disease [47].

The FCFD is currently undergoing rigorous product developments targeting the point-of-care market of biomedical instruments.

2.2.5 Surface plasmon resonance

Surface plasmons are electromagnetic waves that propagate parallel along a metal/dielectric interface [48]. The antibody was immobilised on a metal surface on which the surface wave was generated. On binding a large analyte the refractive index within the region of the surface plasmon evanescent field changes, and the matching requirements for surface plasmon generation are correspondingly alterations which may be observed, e.g. as a change in the angle of the incident light required to achieve resonance.

Immunosensors have dominated those biosensors that exploit an evanescent field. Most workers see decentralized testing as the natural market niche for evanescent field biosensors, e.g. testing within the doctor's office, rapid screening within blood collection

centres and, possibly, home monitoring. Anyway, such applications are less demanding than in vivo monitoring.

Nonetheless, there are still many problems to solve in this area. Non-specific binding is one of the major troubles in surface plasmon resonance (SPR) biosensing because any large molecule that diffuses into the evanescent field will cause a change in the resonance shift. [48]

An attractive approach, that embodies the philosophy to join plasmon effects and fluorescence technique, was to combine them to give an SPR enhanced fluoroimmunoassay [49].

"Indirect" sensors (for example, those employing a fluorescently labelled reagent) overcome many problems of non-specific binding and poor sensitivity to small molecules, but they require more sophisticated and expensive instrumentation because of the low power of the light detected.

In an attempt to combine the best features of these two techniques, an indirect SPR fluoroimmunoassay (SPRF) technique was investigated in 1991. The surface field intensity enhancement produced by SPR was used to boost the emission from a fluorescently labelled immunoassay complex on a metal surface.

The potential of the method was demonstrated by assaying for human chorionic Gonadotrophin (hCG) in serum. Enhanced sensitivity over conventional using total internal reflection fluorescence (TIRF) and SPR techniques was achieved. [50]

2.2.6 Optical biosensors

Biosensors are increasingly becoming practical and useful, if not essential, tools in medicine, food quality control, environmental monitoring and research. In principle, they can be tailored to match individual analytical demands for almost any target molecule or compound that interacts specifically with a biological system.

A biosensor makes use of a biological molecule that is immobilized in proximity to a transducer to detect an analyte, and ultimately transduces the chemical signal produced by the interaction into a measurable response, most often an electronic signal. The immobilization of robust biomolecules permits the regeneration of a biosensor, and allows a simplification of the analytical apparatus. [51]

It has long been known that spontaneously formed structures such as bilayer lipid membranes can be used as models of biological membrane. This has led to the

development of biosensors based on structures similar to bilayer lipid membranes, which are films composed of multiple layers of organized lipid-like molecules. Insoluble, amphiphilic molecules (i.e. those having a hydrophilic end and a hydrophobic end), including phospholipids and fatty acids, will spontaneously form a monolayer film if deposited at an air-water interface. Bilayer lipid membrane structures may be immobilized on surfaces by transferring the amphiphilic monolayers from an air-water interface using the Langmuir-Blodgett (LB) method [52].

This transfer is usually accomplished by slow insertion, or withdrawal, of the support through the air-water interface. Repeated insertion/withdrawal cycles can be used to obtain bilayers and multilayers. An important characteristic of immobilized films is that, while they are stabilized on the surface, there is still a high degree of lateral mobility of membrane molecules which simulates the behaviour in natural membranes. Films prepared by the LB method have been deposited on both electrochemical [53] and optical [54] supports, and used for the detection of analytes in solution.

However, further investigations were required before practical biosensors using LB membranes became available. [55]

Optical systems depend more on traditional immobilization methods that were developed some time ago, when immobilized enzymes on substrates such as porous glass were thought to be the next generation of industrial catalysts. Research has demonstrated the possibility in the past that functioning biological molecules could be encapsulated in silicate glasses using the sol-gel method. The sol-gel entrapment process is a relatively gentle chemical procedure that is carried out at room temperature so that many of the molecules can survive entrapment.

In the sol-gel procedure, the silicate matrix is formed by hydrolyzing an alkoxide precursor, such as tetramethyl orthosilicate (TMOS), followed by condensation, to yield a polymeric oxobridged SiO_2 network. Therefore, if a protein is added after the partial hydrolysis of the TMOS precursor, a porous matrix is formed around the protein molecule, entrapping it in an aqueous microenvironment.

It should be noted that the structure and properties of the gel continue to change as long as solvent remains in the pores, since cross-linking is still taking place in the solid amorphous phase.

The control of cross-linking to produce a sol-gel with reproducible and controllable pore sizes must be achieved before the procedure can be considered for practical applications in biosensor construction [55]. In many sensor applications the sol-gel film is used to

provide a microporous support matrix in which analyte-sensitive fluorophores are entrapped and into which smaller analyte species may diffuse and interact [56, 57].
Sol-gel films have many advantages as support matrices over polymer supports, including for example, strong adhesion, good mechanical strength, and excellent optical transparency.
The versatility of the process facilitates tailoring of the physicochemical film properties to optimize sensor performance. For example films can be designed to have optimum porosity while minimizing leaching of the fluorophore.

2.2.7 Resonant mirror

The potential of a new compact optical biosensor, the so called resonant mirror (RM), for detecting whole cells was demonstrated in 1994 [58]. The RM is a biosensor based on frustrated total internal reflection which combines the enhanced sensitivity of waveguide devices [59] with the facile construction of surface plasmon resonance sensor for the study of biomolecular interactions at interfaces. A thin (circa 100 nm) layer of a high refractive index dielectric material, such as titania or hafnia, and a thicker layer (circa 1 μm) of a low refractive index material, such as silica, were deposited on a prism of high refractive index glass.
At certain angles of incidence, light is coupled into the high refractive index dielectric layer where it undergoes multiple total internal reflections at the top interface, allowing the evanescent wave, to penetrate into the sample overlayer.
The angle at which this resonance occurs is sensitive to changes in refractive index and thickness in the biological overlayer within a few hundred nanometers of the interface. On reflection, the light undergoes a 2π phase change, and by monitoring the angle at which this occurs, it is possible to detect changes within the evanescent field.
As the two components of the light, the transverse magnetic (TM) and the transverse electric (TE), undergo this phase change at different angles, one mode can be utilized as the reference for the other. By interference of the two components, a bright resonant peak can be generated, the position of which can be monitored to detect changes in the biological overlayer [58].
The biosensor surface was functionalized with an aminosilane and IgG immobilized via a glutaraldehyde linker. Subsequent addition of S. aureus (Cowan-1) cells produced a shift

in resonance position proportional to the cell concentration applied from $8 \cdot 10^6$ to $8 \cdot 10^7$ cells / ml . Sensitivity was increased to $8 \cdot 10^3$ cells / ml by using colloidal gold-IgG conjugates in a sandwich assay format. The specificity of the method was also demonstrated by measuring S. aureus in milk by the colloidal gold-IgG conjugate sandwich assay. The Staphylococcus aureus strain Cowan-1, which expresses protein-A at its surface, can be detected by binding to immobilized human immunoglobulin G (IgG), whereas the non-protein-A expressing S. aureus strain Wood-46 produced no significant resonance shift. [58]

2.2.8 Anisotropic emission

A novel model configuration for fluorescence-based optical sensors was presented in 1998 [60]. The fluorescence emitted from a dye-doped sol-gel film was captured efficiently and guided along a planar waveguide. The study on anisotropy of the fluorescence emission brought to the best angular separation between the excitation light and the fluorescence emission.

In the spectroscopic mechanisms which may be employed in biosensors construction, fluorescence is the still probably the most attractive because of its simplicity and inherently low detection limits. So, with the increasing trend towards miniaturised, low cost and disposable devices, there is a great interest in optical configurations which are compatible with mass production and inexpensive components [60].

The general principle is the efficient capture of fluorescence emitted from a coating on a planar waveguide. This allows the realisation of compact and low cost devices where the discrimination of excitation and emission light is performed without the use of expensive optical filters.

A schematic drawing of an extremely interesting and simple optical setup is shown in Fig.2.5.

The sensing element was a multimode waveguiding substrate (for example, a simple microscope slide) coated with a sol-gel film made of a fluorescent reagent entrapped in a polymer matrix.

The fluorescent reagent used in this work was ruthenium II-tris (4,7-diphenyl-1l-o-phenantroline) which has been widely used in optical oxygen sensors based on fluorescence quenching. The dye was excited in the blue region of the spectrum (λ_{exc} =

450nm) and emitted in the orange (λ_{em} = 600nm). The sol-gel process [61, 62] was used to produce glass-like coatings from the hydrolysis and condensation polymerisation of a silicon alkoxide precursor. This precursor solution was doped with the fluorescent dye. The microscope slide was then dip-coated by withdrawal from the doped sol, and after thermal treatment a thin layer of fluorescent porous glass was obtained on the surface of the slide [60]. A substantial fraction of the fluorescence emitted in the thin film was captured by the microscope slide, which acts as a waveguide. The guided fluorescence was detected at the end-face of the slide by a photodiode which was placed at an angle θ to the plane of the slide (Fig. 2.5).

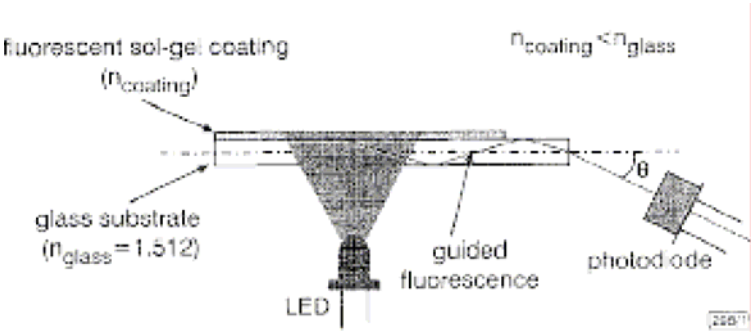

Figure 2.5 Schematic drawing of experimental setup. Fluorescence emitted in the thin film was captured by the microscope slide, which acts as a waveguide [60]

The detection angle θ was a very important parameter in this optical setup. Plots of the fluorescence intensity collected by the photodiode against the angle θ, for various coating refractive indices, were also investigated (Fig. 2.6) in this experiment.

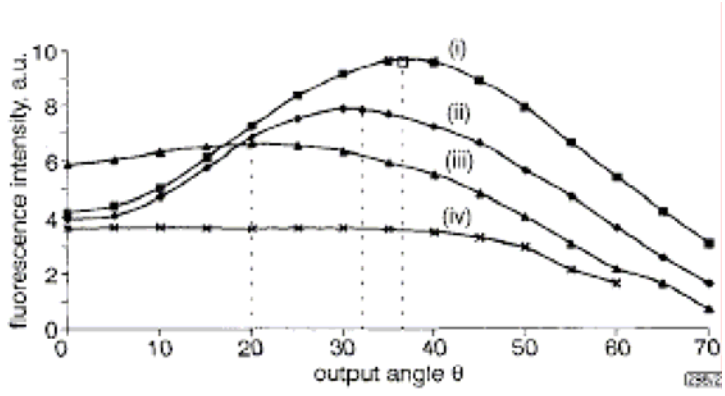

Figure 2.6 Angular dependence of light detected at end-face for range of coating refractive index values: $n_{coating}$ = (i) 1.44, (ii) 1.47, (iii) 1.50, (iv) 1.51. Dotted lines indicate the maximum. [60]

A device where fluorescence was captured and detected at the end face of a waveguide has been also reported elsewhere [63].

However, no mention was made before this article on the refractive index optimisations or on the angular distribution of the detected fluorescence. The performance of a fluorescence-based sensor can be significantly improved by exploiting the optimum angular dependence. The fluorescence was captured preferentially by the high order modes of the waveguide, thereby indicating that it was based on the evanescent wave mode coupling.

Contrary to the fluorescence, only a very small amount of the excitation light from the LED was coupled into the slide, mainly by scattering. Thus, by selecting an optimum angle for detection, a spatial separation of fluorescence and excitation light, thereby eliminating the need for optical filters was accomplished [60].

As a proof of principle, this concept was applied to the sensing of oxygen. The sensitivity of this economic device, particularly at low oxygen concentration, was evidenced [60].

This technique was able to achieve a good separation of fluorescence and emission light without the use of optical filters. The device obtained was simple and compact and was successfully applied to the sensing of oxygen in the market of biosensors [60].

2.2.9 Array biosensor

Array biosensors are small, portable instruments for analysis of immunofluids and are designed for ease of use by untrained personnel, for rapid assay times, and for sensitivity comparable to ELISA methods. In recent years, the fabrication of biosensors able to distinguish multiple analytes in a single sample has become an increasingly well recognized research goal [64].

There are several recent reports describing multianalyte immunosensors. Many describe a method for multianalyte sensing but demonstrate the detection of only a single analyte [65-69].

Others combine discrete sensing substrates, such as optical fibers [70], capillaries [71], microtiter wells [72], or dipsticks [73], to detect multiple analytes simultaneously.

Another general approach employs different capture molecules in different regions of a sensing substrate and detects binding using a label-free approach [74, 75].

These label-free methods were initially susceptible to low sensitivity and increased backgrounds due to non-specific binding.

Such problems were avoided by using fluorescent tracer antibodies and performing a measurement insensitive to non-specifically bound proteins (other than the tracer antibody).

However, while this example used a single substrate with multiple capture spots, the individual tracer antibodies were added in sequential steps [76, 77].

The array biosensor [78] utilised a standard sandwich immunoassay format: antigen-specific capture antibodies were immobilized in a patterned array on the surface of a planar waveguide and bound analyte was subsequently detected using fluorescent tracer antibodies. Mixtures of analytes were also assayed to demonstrate the sensor's ability to detect more than a single specie at the same time.

The biosensor array developed was employed also in other studies [79] and it was relatively simple in its configuration.

It was consisted of a thermoelectrically cooled CCD camera, a microscope slide (waveguide) coated with vertical columns of capture antibody, a diode laser with a line generator to launch light into the end of the waveguide, and a removable poly-dimethylsiloxane (PDMS) flow cell for introduction of samples and fluorescent tracer antibody.

Also in this case the array biosensor utilised evanescent wave excitation to interrogate patterns of fluorescent compounds immobilized on a planar waveguide.

The array biosensor analyzed multiple samples simultaneously and detected mixtures of different types of analytes in buffer in the multianalyte format and in a number of physiological fluids [79] and was relatively unaffected by non-specifically bound components from complex samples.

The array biosensor was able to identify samples containing bacterial spores, virus particles, or protein antigens in a statistically significant number of blind samples [78].

Moreover the biosensor performed the assays quickly and in a format that is amenable to automation and portability.

Simultaneous immunoassays performed on the array biosensor correctly detected and identified bacterial, viral, and protein analytes in 126 blind samples, each containing a single analyte.

Limits of detection and sensitivities were similar to those obtained with confirmatory ELISA but with significantly shorter assay times (14 min versus several hours) [78].

These experiments exemplified a significant reduction in the complexity of performing multianalyte assays.

The planar waveguide provided a vehicle not only for simultaneously assaying a sample for multiple analytes but also for assaying multiple samples in parallel.

Combining several analyte-specific reagents into a single solution reduces both the assay time and complexity of the fluidics (compared to sequential addition of the reagents).

This approach may be scaled up to accommodate a potentially unlimited number of analytes for which antibodies can be generated.

The image analysis has been successfully automated and will be followed by the automation of the fluidics for increased ease of use and reproducibility of quantitative determinations [78].

Effective process control and modelling is a basic requirement for the optimal utilization of biological material. Automated systems can provide a continuous stream of information instead of repeated sampling and off-line analyses.

Optical systems do not interfere with the metabolism of the cells, permitting non invasive *in vivo* monitoring and offering intracellular information that is nearly impossible to obtain with other methods [80].

Measurements of both intracellular and extracellular analytes can be performed, to provide both qualitative and quantitative data.

For measuring cell growth and biomass concentration, the on-line and off-line optical density were often used as reference method.

Commercially available in situ optical sensors for the on-line determination of microbial growth measure light absorption (turbidity) or scattering (nephelometry) continuously in the visible and near-infrared (NIR) ranges [80].

These devices can allow accurate on-line determination of cell density with no need for intermittent calibration procedures.

Commercially available on-line and in situ probes for monitoring cell density, including experimental observations, are reported. [81–84].

This optimization procedure seems to be a very promising development for optical sensor systems in general [85-87].

On-line characterization of cell populations in bioreactors can also be performed by in situ microscopy and, is important to remember that cell-concentration measurements are already performed in this way.

A microscope can be mounted directly in a port of a bioreactor to generate in situ images from the agitated broth using pulsed illumination.

This technique was successfully tested during yeast fermentations and gave optimal results that correlated well with those obtained from a hemocytometer.
This technique also allows morphological parameters of cells to be determined on line [80, 88].

2.2.10 Fiber-optic sensors

Improving the reliability of *in situ* biosensors for industrial applications and the integration of biosensors into flow-injection analysis (FIA) brought towards the developments directed to overcome some of the common disadvantages of biosensors [89].
Evanescent-wave sensor integrated with a flow injection system was used to detect DNA–DNA hybridization in real time.
Biotinylated oligonucleotide probes were immobilized on the sensor surface and hybridization of a complementary target oligonucleotide was monitored.
The limit of detection was lower than other optical biosensors using surface-plasmon resonance, fiber-optic fluorescence or light-activated potentiometric devices [89].
Fiber optic sensors (known as optodes) are based on a change in the optical properties (such as absorption, fluorescence or luminescence) of a particular indicator molecule.
For example fiber optic oxygen sensors are produced by the immobilization of suitable oxygen-sensitive dyes at the tip of an optical fiber.
The principle of these measurements is the decrease in fluorescence intensity of an organometallic dye, caused by the interactions with oxygen.
A blue LED is guided through an optical fiber, on the tip in which the dye is immobilized; the fluorescence of this dye is back scattered from the tip and offers information about the oxygen concentration [89].
Sensors of this type have their highest sensitivity at lower oxygen concentrations (<20%).
In contrast to conventional amperometric sensors (Clark type), no oxygen was consumed and the signal was not dependent on the stirring rate or velocity of the media.
Biosensors for glucose or H_2O_2 can be manufactured by adding biological compounds such as oxidases to the optode [80, 89].

2.2.11 Near-infrared biosensors

NIR spectroscopy are used to measure the concentration of certain organic species, even in complex media. Biologically important bonds (aliphatic C–H, aromatic or alkene C=C, amine N–H and O–H) absorb in the NIR range, at 2.0 to 2.5 μm. Each chemical structure is related to a specific position, shape and size of the analyte's absorption bands.

Because the absorption bands are very similar, advanced data-analysis algorithms are required to extract the analytical information in a reliable manner. Multivariate calibration models generated by using partial-least-squares (PLS) analysis provide analytical information from NIR measurements. A pre-processing digital-Fourier-filtering step improves the results and, with this technique, glucose, glutamine, ammonia, lactate and glutamate were measured simultaneously in aqueous solution [90].

By NIR methods were measured glucose, glutamine and lactate concentrations also during the cultivation of human prostate-cancer cells [91].

NIR spectroscopy was used for glycerol, ammonium and acetate monitoring for control and fault analysis of an industrial high-cell-density *E. coli* cultivation [92].

During lactic acid production in batch, fed-batch and continuous fermentation processes, this technique was used on line to measure the lactic acid, glucose and biomass concentrations, and the results agreed well with those obtained by conventional methods [93].

Moreover, a fiber refractometer was used as a sensing element for NIR spectrometry applied to the in-line determination of fermentable sugars during the mashing process in breweries [80, 94].

2.2.12 Fluorescence biosensors

Fluorescence sensors based on the measurement of the reduced form of nicotinamide adenine dinucleotide phosphate (NADPH), were studied for in vivo measurements [80].

The use of these sensors is thus limited to cultivation processes with a well-defined medium and so, generally, restricted to special applications [80].

More information can be obtained by *in situ* scanning fluorimetry [95]. A number of different fluorophores (e.g. aminoacids, vitamins) can be detected simultaneously. A fluorescence spectrometer has been developed for the on-line monitoring of different

cultivation of *Cyathus striatus*, *Eurotium cristatum* and *Crinipellis stipitaria*. The excitation and emission wavelengths were set independently, using a diode array to detect the fluorescence. The spectrometer was connected by a quartz light guide to the reactor, and it was possible to detect several fluorophores simultaneously, including aromatic amino acids, NADPH and polycyclic aromatic hydrocarbons (PAHs), *in situ* and on line [95].

A fluorescence spectrometer has been used to measure the total culture fluorescence.

The spectrometer was connected to the bioreactor by a bifurcated liquid light guide, one end of which was placed inside the cuvette in the spectrometer and the other end in a standard port of the reactor with quartz window. A sensor for 2D-fluorescence measurements with multiple excitation and emission wavelengths was developed. [96]

This is the so called BioView™ sensor which demonstrated to be highly robust and well suited to use in a process environment. It was optimized for fully automatic fluorescence measurements under industrial applications. A liquid light guide is used to link the spectrometer with the bioreactor. Contamination and sterilization problems are avoided by mounting the light guide into a standard port in the reactor, sealed with a quartz window. Interference filters are used to select the different excitation and emission wavelengths. Although several factors may interfere with measurements in complex or poorly defined culture media, this technique, in combination with modern chemometric methods, offers a number of interesting features for non-invasive process monitoring. Special filter combinations allow both fluorescence measurements and the turbidity measurements. The optical density and the biomass concentration can thus be estimated, rather than needing to use specialized turbidity sensors and it has been tested on different cultivation processes at laboratory and pilot-plant-scale conditions, and it was found that this sensor showed a high level of signal reproducibility during cultivations with *S. cerevisiae, Claviceps purpurea, Acremonium crysogenum, Schizosaccharomyces pombe, Tetrahymena thermophila, Bacillus licheniformis, Enterobacter aerogenes, Sphingomonas yanoikuyae* and *E. coli*. [96].

Other process parameters such as enzyme activity, product formation and consumption of substrates could be observed by their fluorescence intensity.

In combination with scanning fluorimetry, time resolved fluorimetry has a high potential for resolving individual components of complex mixtures [97].

Oxygen, pH, CO_2 and glucose modern sensors were compared with their phase-fluorimetric alternatives. Oxygen levels in spinner flasks used for hybridoma growth

were monitored in situ by fluorescence-lifetime measurements. The change in lifetime of a donor fluorophore induced by fluorescence resonance energy transfer (FRET) to a pH-sensitive non fluorescent acceptor, was used [98] to measure carbon dioxide in the exhaust gas of a bioreactor.

The fluorescence decay times of polycyclic aromatic hydrocarbons in sea water was examinated [99], and Szemacinski and Lakowicz [100], have described two simple methods for fluorescence lifetime measurements in highly scattering media.

These measurements can be performed in correlation to a reference fluorophore with a known lifetime. Alternatively, an intensity-decay law can be used that take in account the time delays and pulse-broadening effects of multiple light-scattering events. [80]

Another nice configuration after the results obtained in the 1998 [60], was accomplished in 2000 by the group directed by McCraith [101].

A dual-analyte optical chemical sensor platform based on the surface patterning of fluorescent dyes immobilized in sol–gel thin films was demonstrated as a proof of principle for a potential multi-analyte detection system with implications for lab-on-a-chip technology. A combination of hot embossing and an eccentric spin-coating technique was used to achieve discrete deposition of oxygen and carbon dioxide sensitive zones on a single wave guiding platform (Fig. 2.7A). Imaging of fluorescence from the oxygen and carbon dioxide sensing areas were performed using a low-cost CCD camera (Fig. 2.7B) and fluorescence quenching on analyte exposure was characterized [101].

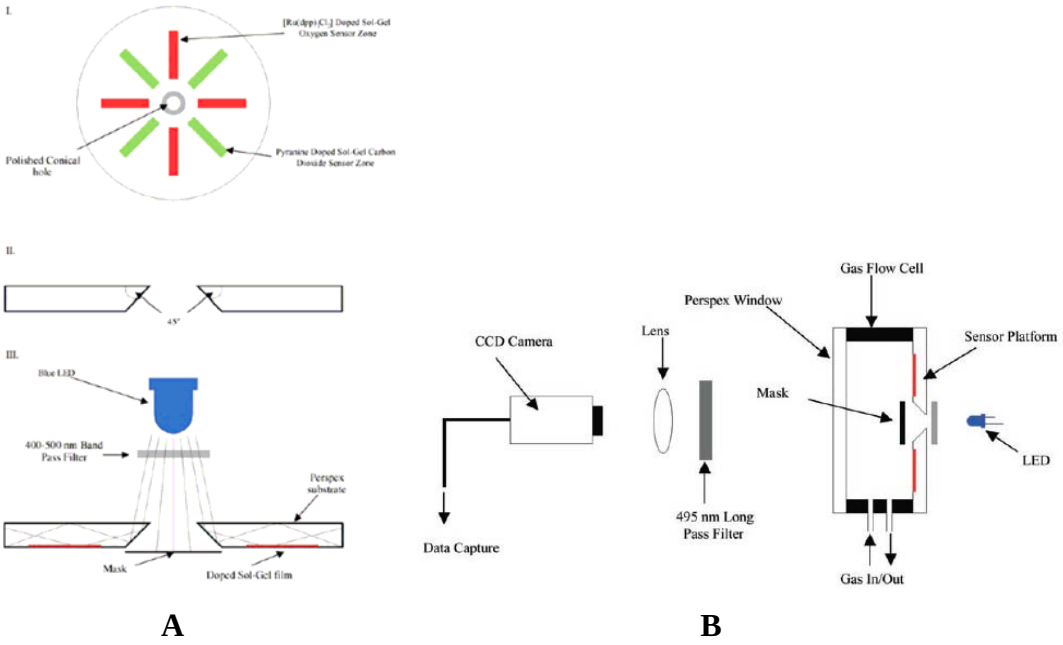

Figure 2.7. A) I) Frontal view of the sensor. II) Central cut view. III) LED optical coupling to the sensor. B) Section view of the oxygen and carbon dioxide chamber with a CCD camera faced on a window [101].

Many chemical sensors and biosensors are based on the fluorescence emitted from thin layers or patterned arrays of fluorophores deposited on a dielectric interface, such as a waveguide surface or a transparent substrate [102]. For example, a wide range of fluoroimmunosensors that are based on the evanescent wave excitation of fluorescently labeled antibodies immobilized on the surface of decladded optical fibers has been reported [103].

It was found that the interface enhances the energy transfer of the radiating dipole, which results in a shortening of the fluorescence lifetime. Another important effect of the interface that is more relevant to optical sensor applications is the significant alteration in the angular distribution of the radiated intensity when the distance of the radiating dipoles is small or comparable with the wavelength of radiation of the dipole. It was shown experimentally that the angular distribution of the radiated intensity exhibits considerable anisotropy [104].

2.2.13 Anisotropic emission theoretical approach

A qualitative explanations of this phenomenon has been proposed but there are quite limiting theories due to the consideration of single dipole behaviour near a dielectric interface [105] or a metal layer [104].

However, many optical sensor configurations employ a layer of dipoles in which the layer thickness is comparable with or greater than the wavelength of the radiation of the dipole. Moreover, the optical properties of the media adjacent to the dipole layer may be of greater complexity, such as in a multilayer system.

Therefore a rigorous electromagnetic theory that can predict the direction of the radiation produced by dipoles embedded inside an arbitrary multilayer system was necessary. First, a single dipole (or a very thin layer of the dipoles) of the order of 0.01 λ was considered, such in the articles mentioned above, and the expressions for the radiated electromagnetic field and intensity were derived. Then, under the assumption of mutual incoherence of the dipole radiation, the calculations were extended to a layer of radiating dipoles.

Expressions for the angular distribution of the intensity that is radiated by a single dipole as well as by a layer of dipoles into the surrounding media are quite complex and rich in parameters and are discussed elsewhere. In particular, this study seeks to establish expressions for the functions $I_0(\theta, \phi)$ and $I_{N+1}(\theta, \phi)$ that represent, respectively, the

angular distributions of the signal in the media with refractive-index values n_0 and n_{N+1} (Fig. 2.8).

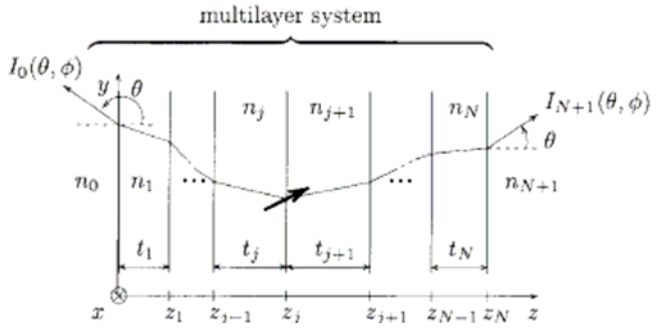

Figure 2.8 Schematic drawing of the radiating dipole placed within a multilayer system. The dipole, depicted by the bold arrow, is placed at the interface of the j_0 and the (j+1) layer. Media with refractive indices n_0 and n_{N+1} are semi-infinite toward -∞ and +∞, respectively. The interface between the medium n_0 and the first layer is at z = 0. [102]

In sensor applications involving luminescent coatings, one typically has a thin dielectric layer doped with radiating dipoles. Therefore it is useful to find expressions for the radiated intensity produced by an ensemble of dipoles that are distributed across a layer that is embedded inside a multilayer system. Expressions that represent the distributions of the intensity radiated by a single dipole and by a layer of dipoles embedded inside a multilayer system were depicted and a rigorous theory of the radiation of a dipole placed inside a multilayer system consisting of layers of arbitrary optical properties separated by plane interfaces was proposed. [102]

Assuming that an arbitrarily oriented dipole is the only source of the electromagnetic field across a multilayer system and that the generated field does not influence the dipole radiation, an explicit formula for the electromagnetic field radiated outside the multilayer system was derived. Because of its form, the expression for the radiated field of an oscillating dipole inside a multilayer system can be used for derivation of the electromagnetic field produced by any set of radiating dipoles embedded inside a multilayer system of arbitrary complexity. [102]

Assuming that the radiated dipoles are evenly distributed across a layer inside the multilayer system and that any of two dipoles radiate mutually incoherently, an expression that describes the angular distribution of the intensity radiated by an ensemble of dipoles embedded inside the layer was derived. [102]

This theoretical formula can be used to calculate the distribution of the intensity produced by dipoles with an arbitrary distribution of orientations. In addition to the general theory,

a number of specific system configurations and found implications that could be important for the design of opto-chemical sensors and biosensors that use luminescent coatings was considered. [102]

In the case of configurations that use a thin dielectric layer doped with fluorescent dipoles coated on top of a bulk substrate, a relatively large amount of energy radiated by means of the so-called [$e_0\, p_1\, p_2$] modes propagating in the higher-refractive-index medium and it is shown in Fig. 2.9.

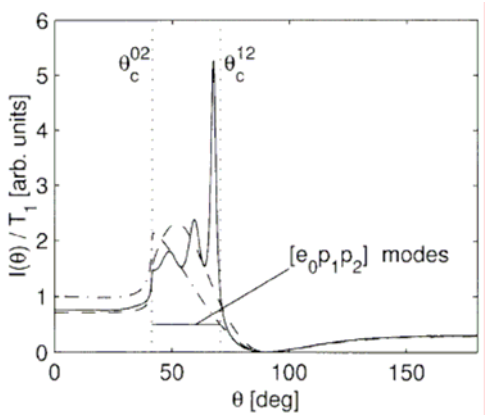

Figure 2.9 Distributions of normalized intensity $I(\theta)/T_1$ radiated by a layer of randomly oriented dipoles that are evenly distributed across a layer with a refractive index of n_1= 1.43 and a thickness T_1. This layer is surrounded by media with refractive indices of n_0=1.0 and n_2 = 1.515. The solid, dashed and dashed dotted curves correspond to thicknesses = 1.5 λ, 0.3 λ, 0.01 λ, respectively. Angles θ_c^{02} = 41.3° and θ_c^{12} = 70.7° represent the critical angles of the n_0-n_2 and n_1-n_2 interfaces, respectively. The values of $I(\theta)/T_1$ for the angle ranges between 0 and 180° correspond to the radiation into the media with refractive indices n_2 and n_0 respectively. [102]

This result suggested that one should detect the fluorescence at angles of $\theta_c^{02} > \theta > \theta_c^{12}$ rather than at angles outside this interval to optimize the optical efficiency.

In particular, the critical angles depend on the refractive indexes of the surrounding media;

$\theta_c^{02} = \arcsin(n_0/n_2)$

$\theta_c^{12} = \arcsin(n_1/n_2)$.

A particularly important example concerns the case of a layer of fluorescent dipoles deposited on the top of a dielectric substrate, e.g., a glass slide, in which the whole system is surrounded by air (or some other material, the refractive index of which is lower than that of the glass slide).

The fact that a relatively large amount of radiated energy is coupled into the [e_0 p_1 p_2] modes suggests that it is not very efficient to detect the fluorescence emitted into the air above the dipole layer or below the substrate.

Instead, because the electromagnetic field of the [e_0 p_1 p_2] modes is totally reflected by the glass–air interface and thus guided along the glass slide, better results should be provided by the detection of the fluorescence at the edge of the glass-slide (Fig. 2.10). This particular configuration and its efficiency were also reported previously [60].

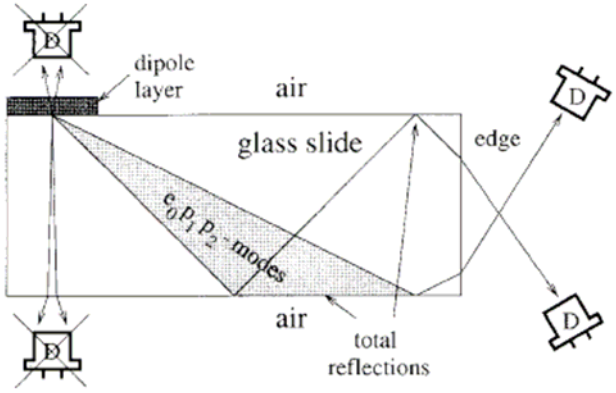

Figure 2.10 Configuration of an optical sensor with a dipole layer that is coated on top of a glass slide. The fluorescence should be (preferably) detected at the edge of the glass slide rather than at its sides. D= detector. [102]

Although only the modes propagating in the higher-refractive-index medium at angles $\theta_c^{02} > \theta > \theta_c^{12}$ are considered, the statement is valid for modes propagating in the entire range of angles $90° > \theta > -90°$.

In general terms this study establishes a theoretical framework for optimizing the design of optical chemical sensors and biosensors that are based on luminescent coatings offering a clear and detailed explanation of radiation of dipoles within a multilayer system. [102]

2.2.14 Dipstick sensor

The design and performance of a rugged dissolved oxygen (DO) probe, which is based on phase fluorometric detection of the quenched fluorescence of an oxygen-sensitive ruthenium complex, was fabricated [106].

The complex was entrapped in a porous hydrophobic sol-gel matrix that has been optimised for this application (Fig. 2.11). The LED excitation and photodiode detection were employed in a dipstick probe configuration, with the oxygen-sensitive film coated on a disposable PMMA disc, which in turn is designed to guide light into the film by total internal reflection.

A key element of the design is the common mode rejection of phase between the signal and reference channels, requiring careful selection of the relevant optoelectronic components.

The advantages of the phase fluorimetric approach over intensity measurement are highlighted. [106]

The determination of oxygen concentration is important in many areas of industry, medicine and the environment.

The amount of oxygen dissolved in water is an indication of the quality of the water and careful control of oxygen levels is important in waste-water management and in fermentation processes. Sensor operation is usually based on the quenching of fluorescence in the presence of oxygen.

The fluorescent ruthenium complex, [Ru^{II}-Tris(4,7-diphenyl-1,10-phenanthroline)]2., (Ru-(Ph2phen)3^{2+}) was chosen as dye and entrapped in a porous sol-gel film.

The oxygen quenching process is described by the following Stern-Volmer equations:

$$\frac{\tau}{\tau_0} = 1 + K_{SV} \cdot pO2$$

where τ is the excited state lifetime of the fluorophore, τ_0 denotes the absence of oxygen, K_{SV} the Stern-Volmer constant and pO_2 the oxygen partial pressure.

The measured lifetime is an intrinsic property of the fluorophore which, unlike intensity, is virtually independent of external perturbations. [106]

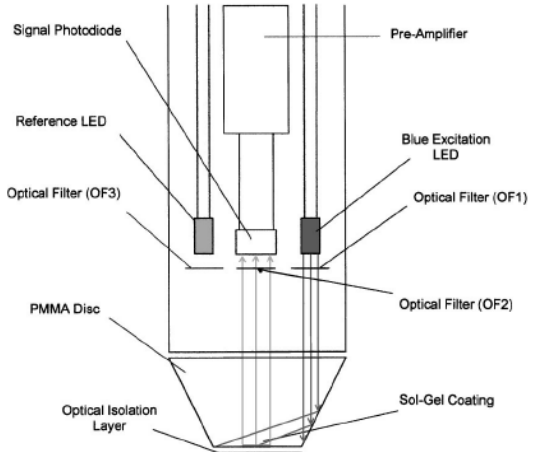

Figure 2.11 Schematic view of dipstick sensor. A compact probe configuration was used to be compatible with the requirements of the particular application (waste-water monitoring). The probe measures approximately 15 cm in length with a diameter of 4 cm. Apart from the optoelectronics and sensor film, a compact preamplifier is also housed in the probe. The excitation source is a blue LED filtered using a blue glass BP filter. The second LED is part of an internal dual referencing scheme and is also filtered by a bandpass (BP) filter. The detector is a silicon photodiode. The PMMA was chosen as a substrate for the sensor film because of the ease of machining and with a view to ultimately designing an injection moulded sensor cap to facilitate mass production. [106]

2.2.15 optical biosensor and ELISA comparison for a recombinant protein assay

The development of label-free optical biosensor technologies, based on either surface plasmon resonance technology (SPR) [107] such as BIAcore AB (Sweden) or resonant mirror technology [108] IAsys, Affinity Biosensors, (UK) dominate the market and so were compared to ELISA ones [112]. The BIAcore biosensors, which is capable of rapid monitoring of recombinant product concentration in crude fermentation broth was used [109], although IAsys sensors have been used for a similar purpose [110].
The principle of the assay is described in Figure 2.12.

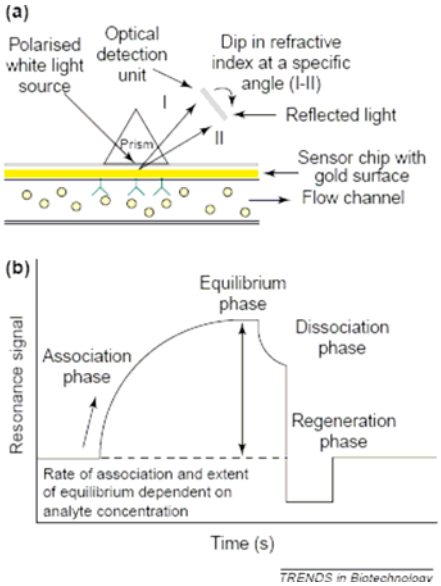

Figure 2.12 Principle of the optical biosensor assay using surface plasmon resonance technology. (a) A schematic representation of the technology. Capture ligand is covalently linked to the surface of the sensor chip. Analyte solution is passed over the bound ligand in a continuous flow. As binding occurs, polarized white light is totally internally reflected, leading to the formation of an evanescent wave. This results in a change in refractive index (a sharp dip in the intensity of reflected light at a specific resonance angle) detected at an optical interface [111]. (b) A typical realtime optical biosensor response. As biosensor output (measured as resonance units) is directly related to the amount of analyte bound to sensor surface, automated data analysis facilitates easy calculation of analyte concentration in solution based on either the initial rate of analyte binding (by monitoring the first dew seconds of binding data) or the total change in resonance units at equilibrium (requiring minutes of binding data) [112].
See also: http://www.biacore.com and http://www.affinity-sensors.com.

Advantages of the BIAcore optical biosensor assay include the abolition of ligand or analyte labeling and multiple flow cells for rapid (<10 minutes) quantification of undiluted proteins and key contaminants. Both manual and fully automated systems are available in the market.

A variety of sensor chip chemistries are available: carboxymethyl-dextran, amino, hydrophilic and hydrophobic surfaces, biotin (IAsys) and streptavidin, lipophilic and metal chelated surfaces (BIAcore). Consumables such as the sensor chips themselves are moderately expensive but are reusable and can remain viable for several months.

A disadvantage of the BIAcore systems is the requirement for specific training before the full benefit of its state-of-the-art software can be appreciated. [112]

Specific measurement of recombinant protein titer in a complex environment during industrial bioprocessing has traditionally relied on labour-intensive and time-consuming immunoassays.

In recent years, however, developments in analytical technology have resulted in improved methods for protein product monitoring during bioprocessing.

The advantages of optical biosensors for measuring both small and large recombinant therapeutic proteins were compared with a conventional enzyme-linked immunosorbent assay (ELISA) technique. [112] Given that conventional ELISA-based immunoassays are labour intensive and typically take 3–5 hours to complete, alternative means of monitoring recombinant protein products have been developed.

Ultimately, robust and rapid monitoring techniques are needed that are as effective and easy to use as a modern home pregnancy test, which measures the concentration of the pregnancy hormone human chorionic gonadotrophin (hCG) in urine, for example [1]. The home pregnancy test is specific, rapid and provides the required data (albeit a semi-quantitative 'yes/no' answer) in <5 min. The technology uses sterilized freeze-dried anti-hCG antibodies encased in a specific polymer coating that maintains sterility *in situ* until it is dissolved on contact with urine[112]. Following the development of monoclonal antibody production, which led to the creation of antibody clones specific for a single target antigen, ELISA became increasingly popular in the 1980s and 1990s.

This assay provided sensitivity and specificity without the requirement for radioactive labeling of ligands. ELISA is still widely used for many industrial and non-industrial applications to provide an accurate and sensitive test for a particular antigen of interest (Fig. 2.13). ELISA was performed in the protein range 0–200 ng/ml. [112]

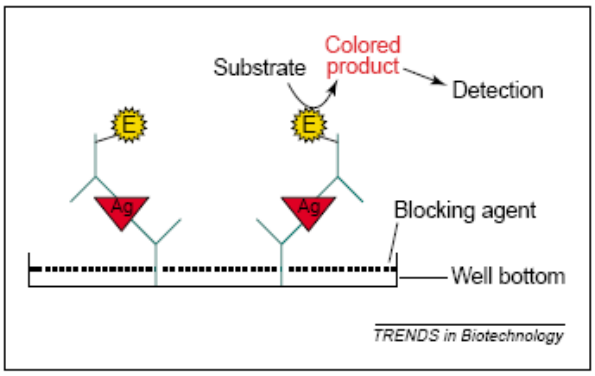

Figure 2.13. Principle of a simple sandwich ELISA. Following non-covalent binding of a purified primary ligand (green) to a solid phase, a blocking reagent is added to prevent any non-specific binding. The test solution containing antigen (Ag) is then allowed to bind specifically to the primary ligand. Unbound proteins are then removed by washing and a secondary antibody (black) conjugated with a reactive enzyme (e.g. horseradish peroxidase) is added. Following a wash step to remove unbound secondary ligand, the extent to which a chromogenic substrate is converted to a soluble colored product by the conjugated enzyme in a given time is determined by spectrophotometry using a standard microplate absorbance reader. [112]

New developments in ELISA include the numerous companies providing off-the-shelf ELISA formats that require very little optimization for a given recombinant or natural protein product.

Fast semi-automated plate-washing and reader systems are available, which reduce handling-associated errors. In addition, 96 samples per plate can be assayed simultaneously, thus assay time per sample is very economical. [112]

As previously described, potential problems associated with ELISA can include long assay development times and, particularly for smaller molecules, low dynamic linear ranges.

In addition, the requirement for extensive sample dilution (and the associated risk of fluid-handling-derived errors) is an undesirable feature of most ELISA-based assays. ELISA can also require large amounts of substrate and other non-recoverable consumables.

Availability of assays targeting recombinant products in development or production in the current pharmaceutical market is limited and can only be purchased in many cases at considerable cost. [112]

2.2.16 Optical biosensor vs ELISA assay performance summary

Except at very low concentrations (below 1 μg/ml), the instrument provided reproducible wide dynamic linear ranges concomitant with very low within- and between assay variation. The automated assay, once set up, was easy to use but data analysis took many hours and required a moderate amount of training before use. The assay required few consumables other than the BIAcore sensor chip, which is stable for 3–6 months.

In this comparison, it was provided an overview of the current major technologies for rapid monitoring of recombinant protein production. Each has advantages and disadvantages that are particular to the assay design and instrumentation. With respect to assay format, it is important to note that both ELISA and microplate electrochemiluminescence permitted assay of up to 24 samples in triplicate (including internal standards) per microwell plate. This is not possible using the optical biosensor. For example, if you want to monitor a bioprocess in real-time, then single quick assays taking <15 mins might be preferable (optical biosensor). However, to monitor multiple

samples retrospectively, or for another purpose, then ELISA or chemiluminescence can be better choices. ELISA assays generally gave higher coefficients of variation than the optical biosensor assay format [112].

Assay method	ELISA	Optical biosensor
Ease of assay optimization	Long rhIgG$_1$ Long TIMP1	Short rhIgG1 Medium TIMP1
Total assay time	3–5 hours	5–15 min
Samples per assay	96	1
Linear dynamic range	10–220 ng ml^{-1} TIMP 10.2–25 ng ml^{-1} rhIgG1	1–200 µg ml^{-1} rhIgG1 1–200 µg ml^{-1} TIMP1
Sensitivity of detection	High <1 ng ml^{-1}	Medium <1 µg ml^{-1}
Within assay variation (CV%) n = 6	<10% rhIgG1 < 5% TIMP1	<5% rhIgG1 <5% TIMP1
Relative variability (%) between assays n = 3	>10% rhIgG1 >10% TIMP1	<5% rhIgG1 <5% TIMP1
Recovery of free sample	No	Yes
Number of ligands	2	1

Assay method	ELISA	Optical biosensor
Instrument standardization	N/A	Good
Automation	Part	Part or full
Maintenance	None required	Simple to moderate
Calibration and validation	Simple to moderate	Simple
Technical expertise required	Little	Moderate
Ease of data manipulation and analysis	Simple	Moderate
Approximate capital costs (×1000)	Plate reader from US$ 3	BIAcore™ US$ 110–US$ 275 IAsys™ US$ 45–165
Running costs	Moderate	Moderate–high
Expensive reagents	Two antibodies (non re-usable)	Sensor chips (re-usable)

Table 2.1 Comparison between performances of ELISA and optical biosensor [112]

2.2.17 Lateral flow biosensors

Lateral flow (LF) biodetectors facilitate low-cost, rapid identification of various analytes at the point of care. The LF cell consists of a porous membrane containing immobilized ligands at various locations. There are many examples of the application of LF reactors in the health care industry [114].

It was listed just a few examples such as home pregnancy tests, human fecal occult blood detection, HIV-1 diagnostics, mycobacterium tuberculosis diagnostics, and detection of drugs of abuse. Although LF immunoassay technology is widely used in the health care industry, in home care, and in the monitoring of the quality of the water and food supply, the format suffers from certain shortcomings such as signal saturation and eventual decline when the target analyte concentration increases. [113]

The lateral flow (LF) immunoassay was invented as a popular diagnostic tool because it eliminates the need for trained personnel and expensive equipment. [114]

Various antibodies and/or oligonucleotides, to which we refer collectively as ligands, are immobilized at predetermined locations (capture zones) along the porous membrane.

A sample containing target analytes is mixed with a buffer solution and preengineered reporters such as colloidal gold, carbon black, dyed polystyrene, phosphor, and dye-

encapsulating liposomes. The mixture then is introduced into the membrane by capillary forces (Fig. 2.14).

As the mixture flows along the capture zones, the analytes and/or the reporters bind to the immobilized ligands. Two common formats are the sandwich and the competitive assays. When the sandwich assay is used, some of the target analytes bind to the reporters and some remain free in the solution. When the mixture passes through the capture zone, both unbound analytes and bound analytes bind to the ligands.

After some time, the LF strip is scanned and the concentration of the reporters is measured as a function of location. An elevated concentration in the capture zone indicates the presence of the target analytes.

The sandwich assay has the advantage that the presence of a signal indicates the presence of target analytes. Unfortunately, this is not true at high target analyte concentrations. Once the target analyte concentration exceeds a certain critical value, further increases in the target analyte concentration lead to a reduction in the signal.

LF immunoassay technology is widely used in hospitals, laboratory medicine, life science research, and the monitoring of water and food quality. [114]

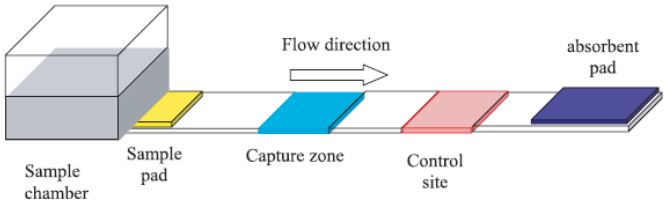

Figure 2.14 In the first format of competitive assay, the target analytes bind to the ligands in the capture zone and block the ligands from binding to the reporters. The control site consists of an immobilized ligand that can bind to the reporter but not to the target analytes. [114]

Confirmatory detection of diseases, such as HIV and HIV-associated pathogens in a rapid point-of-care (POC) diagnostic remains a goal for disease control, prevention, and therapy.

If a sample could be analyzed on-site with a verified result, the individual could be counseled immediately and appropriate therapy initiated. In this article [115] is described the development of a microfluidic "lab-on-a-chip" that simultaneously identify antigens, antibodies, RNA, and DNA using a single oral sample.

Lateral flow (LF) strips were developed for the detection of human antibodies against human immunodeficiency virus type-1 and -2 (HIV-1 and -2) with additional capture zones to detect antibodies against Myobacterium tuberculosis (TB) and hepatitis C Virus (HCV).

The bench-top CF format was converted to a microfluidic platform and a first prototype semi-automated chip capable of performing CF was presented [116].

A similar lab-on-a-chip system for detecting bacterial pathogens in oral fluid samples was again considered. The microfluidic chip hosts a fluidic network for cell lysis, nucleic acid extraction and isolation, PCR, and labeling of the PCR product with bioconjugated, upconverting phosphor particles for detection on the lateral flow strip [117].

2.2.18 Fluorescence enhancement due to metal nanoparticles

In 2005, was reported [118], on the so-called plasmonic enhancement effect, that the presence of metallic surfaces or particles in the vicinity of a fluorophore can dramatically alter the fluorescence emission and absorption properties of a fluorophore. The effect, which was associated with the surface plasmon resonance of the metallic surface, depends on parameters such as metal type, particle size, fluorophore type, and fluorophore-particle separation.

Ordered arrays of metallic nano-islands were fabricated on glass substrates by a process of natural lithography using monodisperse polystyrene nanospheres. The metal particle dimensions were tailored in order to tune the plasmon resonance wavelength to match the spectral absorption of the fluorophore. The fluorophore, Cy5 dye, which was widely used in optical immunoassays and had a medium quantum efficiency, was used in preliminary studies on the plasmonic enhancement effect. [118]

A fluorescent dye (FD) in the proximity of the NP senses the altered electromagnetic field and its fluorescence properties are changed. There are two enhancement effects: an increase in the excitation of the FD and an increase in the quantum efficiency **(**QE**)** of the FD. The biggest technical challenge in achieving plasmonic enhancement is in the preparation of the metallic nanoparticles (NPs). Several methods exist and are quoted in the literature, such as electron beam lithography [119], atom-light interaction lithography [120], chemical production of nanoparticles [121,122], electro-deposition of metal nanoparticles [123], and electrochemical template synthesis of metal nanoparticles [124].

2.2.19 Enhanced detection efficiency in luminescence-based sensors

Fluorescent labels (such as cyanine dyes and quantum dots) are employed routinely in bio-assays to transduce the biomolecular binding event. Such sensors, often referred to as microarray biochips, are of significant interest, especially in applications such as point-of-care testing, water quality monitoring and biowarfare detection [125].

The biochips are typically fabricated from glass or polymer, often incorporate microfluidic functionality, and are treated as single-use disposable components. This platform is generic in nature and is compatible with microfabricated, mass produced biochips, especially in the case of polymer materials. The enhancement strategy that was presented in this article [126] had major significance for the future design and fabrication of low-cost, high sensitivity platforms.

For example, the particular case where the thin luminescent layer is sol-gel-derived silica doped with a luminescent indicator and deposited on a glass substrate is shown in Fig. 2.15. This Figure illustrates the spatial emission pattern as a 2-D cross-section. A comparison of Fig. 2.15a and b indicates the sensitivity of the mission pattern to the superstrate, air or water respectively, refractive index.

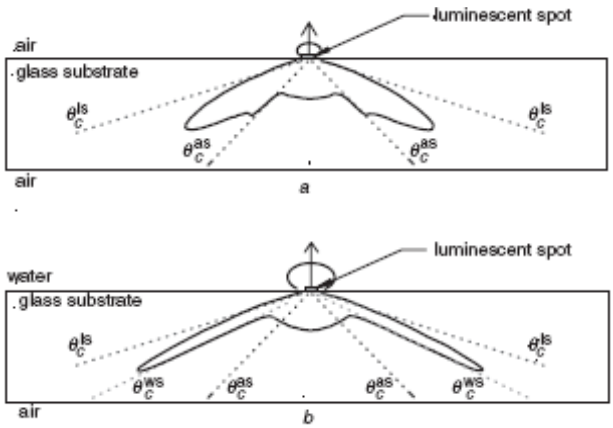

Figure 2.15 Angular properties of luminescence radiated from a thin luminescent spot deposited on a glass membrane over air (a) or over water (b).[126]

Consequently, in the case of planar substrates with parallel sides as shown, this light will undergo total internal reflection at the bottom interface and become substrate-confined (SC) or trapped in a 'conventional' detection technique, where a detector is placed above

or below the substrate in the vicinity of the luminescent layer, it is clear that a significant amount (the majority) of the generated luminescent signal will be waveguided away as SC modes and will go undetected.

The modes radiated from the luminescent spot are redirected towards the detector (Fig. 2.16) placed below the substrate. [127]

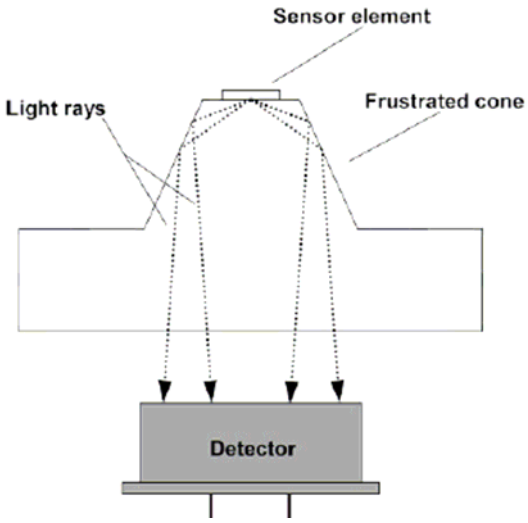

Figure 2.16 Cross section of the configuration facilitating improved efficiency of luminescence capture. The configuration exploits a frustrated cone located at the top side of the substrate.

2.2.20 A multi-analyte array biosensor product

With recent advances in surface chemistry, microfluidics, and data analysis, there are ever increasing reports of array based methods for detecting and quantifying multiple targets.

However, only a few systems have been described that require minimal preparation of complex samples and possess a means of quantitatively assessing matrix effects.

The first one is the NRL Array Biosensor, [128] which was developed with the goal of rapid and sensitive detection of multiple targets from multiple samples analyzed simultaneously.

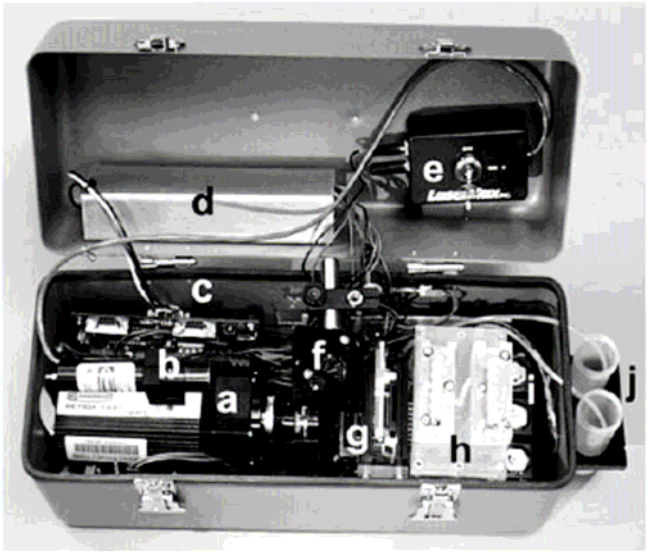

Figure 2.17 Portable array biosensor components: (a) CCD camera, (b) diode laser, (c) RS32 interface board, (d) power supply, (e) laser power switch, (f) mirror, (g) slide mount, (h) removable reservoir modules, (i) peristaltic pumps, (j) waste and buffer reservoirs. Electronic control boards for pumps and valves are not visible. The valves are underneath the reservoir modules [129].

The NRL Array Biosensor was developed [128] to analyze multiple samples for multiple analytes and was designed to be portable and easy to use for untrained personnel (Fig. 2.17). The sensor system consists of a 50 W power supply, a cooled CCD camera, peristaltic pumps and valves, and machined fluidics chambers.

Also contained within the carrying case is a 635 nm diode laser equipped with a line generator to spread the laser beam into a fan pattern. The expanded laser beam is launched into the edge of the microscope slide waveguide, thus providing even fluorescence excitation.

The CCD images the fluorescent array on the microscope slide through a 700 ± 35 nm BP filter and a 665 nm longpass filter. The image was acquired through a Firewire (IEEE 1394) connection, eliminating the need for a bulky frame grabber board and allows all aspects of sensor function to be controlled by a laptop. [128]

The NRL Array Biosensor has recently been used in the development of multiplexed assays for screening of human sera for antibodies directed against bacterial and viral antigens, including SEB, tetanus toxin, diphtheria toxin and hepatitis B. Such a biosensor could potentially be used in a clinical setting to monitor individuals for exposure to various pathogens or to study the efficacy of vaccination. [128]

Three companies, Hanson Technologies, Constellation Technology Corp. and Precision Photonics Corp., have licensed the technology relevant for operating the NRL Array Biosensor and are producing the biosensor to sell for a host of different applications. [128]

Hanson Technologies (www.hansontechnologies.com) has modified the NRL Array Biosensor laboratory prototype into an instrument ready for commercial production (Fig. 2.18a).

A proprietary software control interface is now provided for ease of operation and test result interpretation. The software is combined with a much improved series of fluidic sections for

consistent and repeated operation of the instrument. The result is a rugged, easy to use, and reliable biosensor. It can be used both by skilled and highly educated laboratory staff, and by less skilled technicians in a commercial environment. [128]

Constellation Technologies (www.contech.com) has developed a completely automated and self-contained (no external computer) instrument, called the CT-ABS (Fig. 2.18b), which allows a user in the field to manually execute the immunoassay process or to integrate the CT-ABS unit into an automated biodetection system.

The CT-ABS consumables are contained in mass producible cartridges. One cartridge contains the waveguide patterned with capture antibody and the flow chamber. A separated cartridge contains detection antibody reservoirs. These cartridges allow a user in the field to easily replace consumables. After sample introduction, the unit automatically executes all the CT-ABS immunoassay steps, as well as analyzes the resulting image and provides the user with a positive or negative evaluation. Constellation has demonstrated the CT-ABS integrated with a number of sample collection devices including an aerosol-to-hydrosol air collector and a filter/concentrator for biological agent detection in water systems. Over a dozen assays, which provide results in 10 – 15 minutes, have been developed for the CT-ABS unit.

Manufacturing of the CT-ABS and cartridges has progressed significantly. Constellation now uses an automated non-contact dispensing machine to mass produce patterned waveguides. The design of the CT-ABS unit has been optimized for cost, reliability, and manufacturability. [128]

Precision Photonics (www.precisionphotonics.com) is adapting the NRL Array Biosensor for clinical detection of disease markers, with an emphasis on point-of-care diagnostics in resource limited settings, ranging from clinics in developing countries to the frontlines of

a bioterrorist attack. To date the technology has been used for detection of both proteins and antibodies. When adapted for detection of antibodies, the platform provides a useful test for HIV and its common coinfections, a key set of tests to manage clinical treatment (Fig.2.18c). [128]

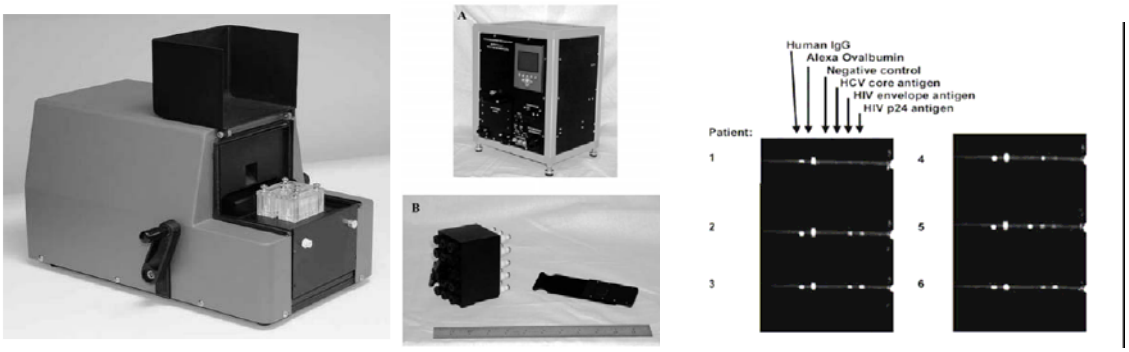

a) **b)** **c)**

Figure 2.18 a) The Hanson Technologies Leopard array biosensor. b) The Constellation Technologies corp. A) the ABS unit, B) Consumable reagent kit and waveguide. c) Results from a set of six tests from 6 patient sera using Precision Photonics instrument. The first patient has negative serology, while patients 2 - 6 are positive for HIV and patient 5 is positive for HCV. Each test strip shows six potential spots with reactivity. As labelled, the first two are positive controls, the third is a negative control, and the last three test for reactivity to the viral antigens.

The design of a microfluidic lab-on-a-chip system for point-of-care cancer screening and diagnosis of oral squamous cell carcinoma (OSCC) was also described in literature [130]. The chip was based on determining a approximately 30-gene transcription profile in cancer cells isolated from oral fluid samples. Microfluidic cell sorting using magnetic beads functionalized with an antibody against cancer-specific cell-surface antigens was described. A comprehensive cancer diagnostics chip will integrate microfluidic components for cell lysis, nucleic acid extraction, and amplification and detection of a panel of mRNA isolated from a subpopulation of cancer cells contained in a clinical specimen. [130]

2.3 General immunology:

2.3.1 Lymphocytes

The immunologic response towards an antigen depends on the interaction between an antigen and two classes of lymphoid cells, named B lymphocytes and T lymphocytes; both originate from primitive stem cell in the bone marrow [131, 132]. B Lymphocytes are derived from lymphoblast of the lymphoid tissue in the bone marrow and here they differentiate into mature B cells. In contrast, T lymphocytes are derived from lymphoblast previously differentiated in the thymus gland. Lymphocytes are present at various levels in organs, lymphatic tissues and blood. They act against infections through two different mechanisms. Firstly, they work against external antigens (i.e. toxic products, viruses etc); in the extra cellular environment, the immunological response is mainly represented by a humoral immunoresponse governed by B lymphocytes (although activated by a specific population of T lymphocytes) that are able to interact with the antigen through a mediation with antibodies. Secondly, lymphocytes work against internal antigens (i.e. viral proteins); in the intracellular environment of an infected cell, where antibodies cannot penetrate, a cell-mediated immunoresponse by a particular population of T lymphocytes act directly to destroy the infected cell. B lymphocyte receptors are molecules (approximately 10^5 per cell) identical to the antibody that the cell is programmed to produce, and that differ only in a specific configuration of the variable region. Humoral immunoresponse occurs when an external antigen interacts, on one side, with the specific receptor of B lymphocytes, and, on the other side, with other cells (macrophagocytes) that are able to phagocytes the antigen and to present it to the T lymphocytes in a contest called “antigen presenting cell” (APC) [132].

Hence, T helper lymphocytes, using their specific receptors, recognize the antigen presented by APC, and cause the conversion of lymphocytes B into plasma cells able to produce antibodies specific for the antigen of interest, and further “memory” B lymphocytes, are able to enter into the interaction to generate an eventual recall response. Plasma cells possess a relatively short lifetime (one week) and during this period they produce a great quantity of antibodies with a lifetime of six months in biological fluids (blood and lymph). Memory B lymphocytes, in contrast, have a lifetime of several years, and dispose themselves to be transformed rapidly into plasma cells (producing antibodies) in the presence of antigens.

2.3.2 Immunoglobulins

Antibodies are serum molecules produced by B lymphocytes; they represent the soluble form of specific receptors for the antigen expressed by B lymphocytes [131, 132].

In cooperation with the complement system (a complex cascade reaction that activates identification of bacteria, so that phagocytes can recognise and eliminate them), antibodies are the mediators of the humoral immunity [133] and their presence on the surface of mucous membranes provides resistance and prevents multiple infections.

In plasma subjected to electrophoresis, antibodies are found as proteins related to the gamma fraction, the highest in molecular weight (globulins) portion. Hence, the protein fraction that contains antibodies is usually called immunoglobulin or Ig.

Different types (fig. 2.19) of Ig exist: IgG, IgA, IgM, IgD, IgE. All the antibodies have the same base structure, but they differ in the region that binds the antigen i.e. the Fab region. Another region of the antibody binds to phagocytes or other proteins of the complement system and is called the Fc region. Hence, an antibody can be phagocyted using Fc segments, if it binds to an antigen.

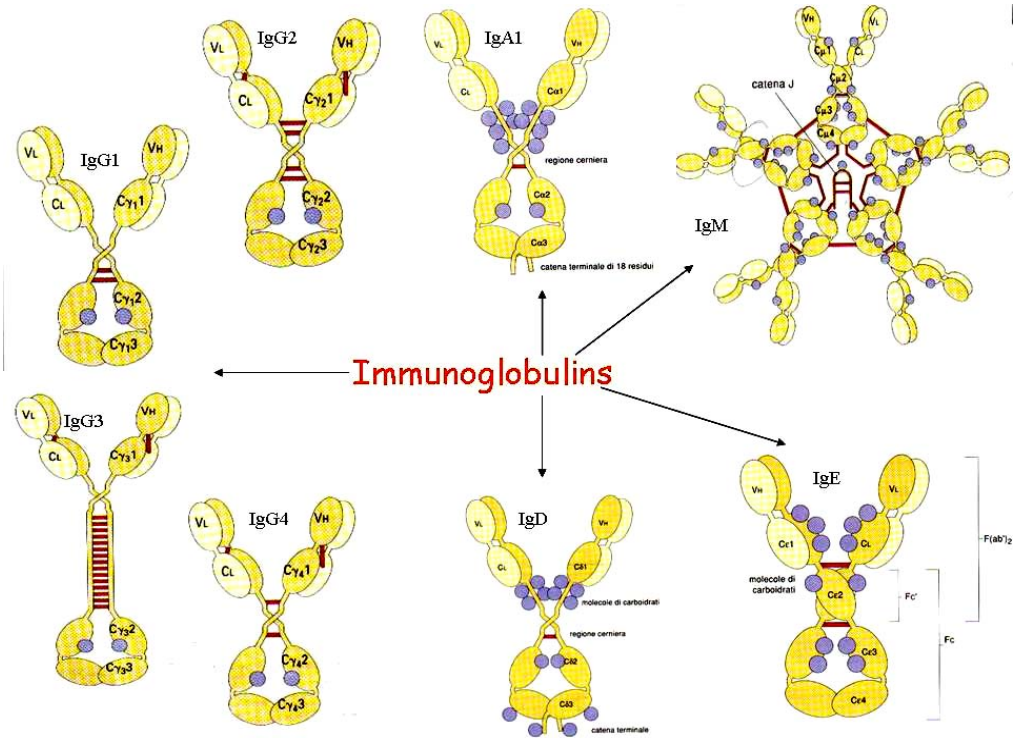

Figure 2.19 Structure of immunoglobulin classes. V = variable domain; C = constant domain; L = light chain; H = heavy chain; Fab = Fragment antigen binding; Fc= fragment crystallisable. Source of diagram is [133].

The IgG molecule is a typical example of the structure of every immunoglobulin.

In 1962, Rodney Porter proposed [132] a structural model of immunoglobulins: four chains, constituted by two light chains and two heavy chains (Fig. 2.20).

Every light chain (L) has a molecular weight of 25 kDa and both chains are the same for all immunoglobulins. In 1965, Hilschmann and Craig found that the light chain has two regions: the COOH terminal region constant (called region C_L), of 107 amino acids and the N-terminal region variable (called region V_L) of 105 amino acids. Heavy chains present four internal disulphuric bridges, whereas light chains have two. The N terminal region of an IgG is characterised by variability for the heavy chain as well as for the light chain (V_H and V_L). The other part of the macromolecule has constant sequences such as C_H1, C_H2, C_H3, called domains. Antibodies bind to the antigens in the variable region. The flexibility of the clasp region permits the two sites to act separately, where antigens can bind. Carbohydrates bind to the C_H2 domain.

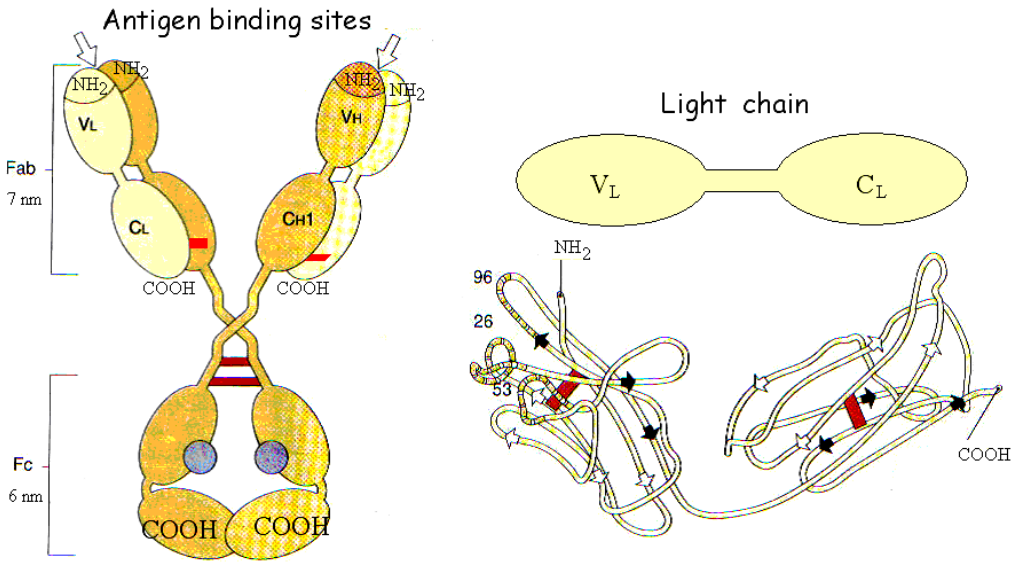

Figure 2.20 On the left part is shown a common immunoglobulin IgG. In red are shown the disulphuric bridges. On the right part is shown the light chain. Source of figure is [133].

IgG are the most prevalent immunoglobulins in human serum (75 % of total Ig in serum); IgG present in all biological fluids are the most important class of antibodies in response to bacterial toxins and extracellular viruses. IgG's comprise four distinct subclasses:

IgG1, IgG2, IgG3, IgG4 [131-133]. These subclasses are distinguished by the number of disulphuric bridges that bind together the heavy chains (HC). These subclasses of IgG differ also in some biological features. IgG1 and IgG3 possess better efficiency in the recognition of the antigen ("opsonisation") and in the complement activation. IgG2 are produced against polysaccharide antigens present on the surface of various bacteria such as S*treptococcus pneumonia*.

IgA represent 15-20% of the immunoglobulins present in human serum [133]. In human beings IgA are 80% monomer proteins, whereas in other mammals IgA prevail in the dimeric form; Ig in dimeric form is prevalent in man as antibodies in the intestinal mucous membrane. The IgA of secretions (sIgA) is in the dimeric form and is associated with a short polypeptide chain called secretor component. The concentration of sIgA in serum is really low, whereas in the secretions of intestine, it is really high. The IgA's consist of two different subclasses of molecules which possess different heavy chains: IgA1, IgA2 [131].

IgM represents 10% of total immunoglobulins in serum; the molecule is a pentamer of five immunoglobulins linked together by Fc segment. IgM's are present in the serum and represent an antibody class prevalent in the primary response towards microorganisms complexed by antigens. IgD's represent 1% of all immunoglobulins in serum and they are present in huge quantities on the surface of lymphocytes B; these immunoglobulins are involved in the process of differentiation of lymphocytes. IgE's represent 0.002 % of the total immunoglobulins in serum; they are located on the surface of mastocytes and basophiles cells of mucous membranes and bronchial tubes. They are really important in the defence against parasites and in relation with bronchial asthma and allergic rhinitis.

General properties that concern the variability of the heavy chain, the concentration of immunoglobulin in serum, the sedimentation constant, and other parameters of interest are shown in the Table 2.2.

PROPERTIES	IgG1	IgG2	IgG3	IgG4	IgM	IgA1	IgA2	sIgA	IgD	IgE
concentration in serum (mg/ml)	9	3	1	0.5	1.5	3.0	0.5	0.05	0.03	0.00005
sedimentation constant	7s	7s	7s	7s	19s	7s	7s	11s	7s	8s
Molecular weight (kDa)	146	146	170	146	970	160	160	385	184	188
half-life (days)	21	20	7	21	10	6	6	?	3	2
Intravascular distribution (%)	45	45	45	45	80	42	42	tracce	75	50
Carbohydrates (%)	2-3	2-3	2-3	2-3	12	7-11	7-11	7-11	9-14	12

Table 2.2 Properties of general immunoglobulins. Source of table is [133].

2.3.3 Antigen/Antibody interactions

Antigenic molecules are surrounded and trapped inside a pocket formed by the light and heavy chains of an antibody. This is called the *combinatory site* and is where a protein can be captured (i.e. Fig. 2.21).

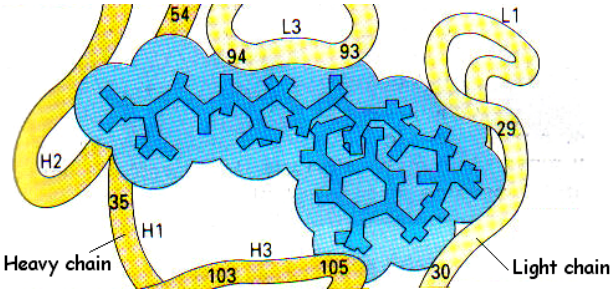

Figure 2.21 A human IgG can trap a protein of myeloma called g-hydroxyl vitamin K in 12 different aminoacidic points. The instrument used to detect this type of 3-D interactions is the X-ray crystallography. Source of the image (132).

The union between an antigen and an antibody is the result of non-covalent interactions between the amino acidic residuals of the antigens and of the combinatory site of the antibody. These bonds are weak interactions (Figure 2.22) of different types such as hydrogen bonds, electrostatic forces, Van der Waals forces and hydrophobic interactions [133], but they contribute all together to a binding of relevant energy. The strength of these bonds depends critically on the distance d between reagent groups. This strength is

proportional to $1/d^2$ in the case of electrostatic forces and $1/d^7$ in the case of Van der Waals forces.

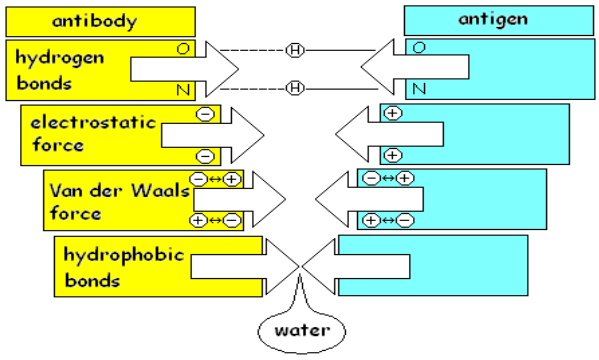

Figure 2.22 Overview of the forces that take place in antigen-antibody interactions. Image adapted by [133]

2.3.4 Specificity, affinity, avidity

If the electronic clouds of the antigen-antibody residuals overlap but do not fit exactly, repulsive forces, which are proportional to $1/d^{12}$, prevail on the attractive weak forces [133]. These forces play an important role in the determination of the specificity of an antibody to a particular antigen and the strength of the bond decreases suddenly if something changes in the complementary ideal fit form (Fig.2.23).

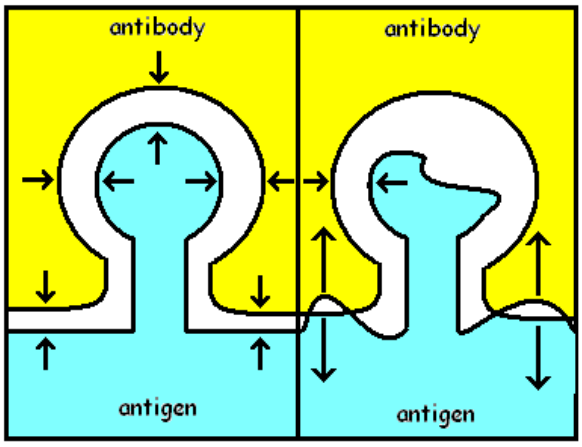

Figure 2.23 The ideal fitting of an antigen in the antibody is shown on the left image. Specificity of an antibody to its antigen is ensured by the fact that a non ideal overlapping causes greater repulsive forces compared to smaller internal forces. Image adapted by [133].

The affinity of an antibody towards an antigen can be expressed by the strength of repulsive and attractive forces (Fig.2.24). An antibody with high affinity for an antigen fits perfectly to its specific antigen. The law of mass action can be used to calculate the affinity which is given by the equilibrium constant K_A.

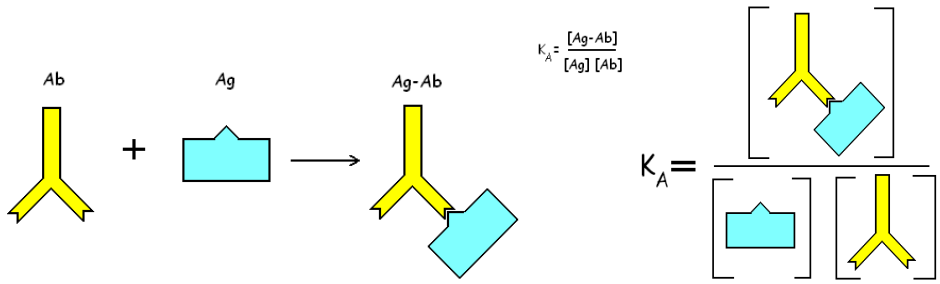

Figure 2.24 Affinity depends on the affinity constant value. Equilibrium constant K_A is defined as the affinity constant. Image adapted by [133].

An antibody has two combinatorial sites for an antigen; this means that antibodies are potentially polyvalent to form bonds with an antigen. Antigens can be monovalent (such as haptens) or polyvalent (such as microorganisms). When a polyvalent antigen binds to an antibody, the total energy of the bond is higher than the normal strength of a single bond. This total force is called the avidity of the antibody and differs from affinity which is related to a single combinatory site for a single antigenic determinant (see table 2.3). In physiological conditions avidity is fundamental because almost all the antigens are polyvalent.

affinity and avidity Biosensors

antibody	Fab	IgG	IgG	IgM
valence Ab	1	1	2	up to 10
valence Ag	1	1	n	n
equilibrium konstant	10^4	10^4	10^7	10^{11}
polyvalence gain	-	-	$+10^3$	$+10^7$
definition	affinity	affinity	avidity	avidity

Table 2.3 Multi-valence bonds between antigen and antibody (avidity) increase stability in comparison to mono-valence bonds. This effect is defined as positive effect of multivalence. The gain in polyvalence corresponds to 10^3 if both binding sites of IgG are occupied and 10^7 if the sites of IgM are occupied simultaneously. Table source is adapted by [133].

2.4 Transcription factors

A transcription factor is a protein that has the capability to enter inside the nucleus and binds to specific parts of DNA using DNA binding domains and is part of the system that controls the transcription of genetic information from DNA to RNA [134-135].
Transcription factors perform this function alone or by using other proteins in a complex, by increasing (as an activator), or preventing (as a repressor) the presence of RNA polymerase, the protein is responsible for genetic transcription [136, 137].
The genome contains thousands of genes and an enormously diverse regulatory system is necessary to obtain induction or repression of the expression of the right gene at the right time. The expression of a gene can be regulated at many different levels, e.g. initiation and elongation of transcription, RNA processing, RNA transport, RNA stability, initiation and elongation of translation, post-translational modification, protein transport and protein activity. The first step, initiation of transcription, represents a major control point for the regulation of gene expression.
The transcription of a gene X depends on which transcription factor binding sites are present in the control regions of gene X, and on whether an appropriate set of transcription factors which is capable of binding those DNA sequences is expressed and active in the cell type in question. Thus, the control of the activity of transcription factors plays an important role in transcriptional regulation and is achieved at distinct levels in response to signals. For example, the nuclear factor-kappa B (NF-kB), a transcription factor involved as important regulator of the host immune and inflammatory response and also in protecting cells from apoptosis, is regulated at the level of sub-cellular localisation. Phosphorylation has been shown to affect transcription factors at many levels, such as nuclear transport, DNA binding activity and transactivating function [138, 139]. A transcription factor is a protein that binds DNA at a specific promoter (that is a DNA sequence that enables a gene to be transcribed) or at an enhancer region (a short region of DNA which can be bound with proteins to enhance transcription) or at a site, where it regulates transcription. Transcription factors can be selectively activated or deactivated by other proteins.

Transcription factors are classified in three main groups: basal, upstream and inducible transcription factors [140]. The first class is comprised of the group of proteins that

directly interact with RNA Polymerase. This mechanism is directly responsible for transcription. The upstream factors are unregulated proteins that bind somewhere upstream of the initiation site to stimulate or repress transcription. These are ubiquitous factors that increase the efficiency of transcription initiation. Finally, some factors are turned in a temporal or spatial manner, or directly in response to the environment. These factors provide the final link in controlling gene expression. The inducible factors act in the same manner as an upstream factor but their synthesis is regulated in a temporal or spatial manner. In particular, NF-kB, the transcription factor which is studied in this thesis, is part of this category. A more general and complete list of transcription factors is reported on the web-site: http://www.gene-regulation.com/pub/databases/transfac/cl.html

2.4.1 The transcription factor NF-kB

The Transcription Factor NF-kB represent a signalling system evolutionarily conserved.
Crystallographic-structure studies of NF-kB binding DNA have shown that each subunit consists of two immunoglobulin-like domains connected by a 10 aminoacid flexible linker. Dimers are formed through a β-sheet sandwich of the carboxy-terminal domains. Unlike most DNA-binding proteins, which use α-helices for base-pare recognition, NF-kB dimers use loops from the edges of the N- and C-terminal domains to mediate DNA contacts.
Secondary structures of the subunits are equivalent, apart from 32-aminoacid insert in the N-terminal part of p50 that adds a second α-helix. Dimerisation in the heterodimer is localized to the C-terminal domains and consists of a hydrophobic core stapled by various polar interactions.
NF-kB was first described in 1986 as a nuclear factor necessary for immunoglobulin kappa light chain transcription in B cells (hence the name, nuclear factor-kB) [141].
In mature B cells and plasma cells, NF-kB is localized to the nucleus where it binds a 10 base-pair region of the kappa intronic enhancer and activates transcription.
It was originally thought that NF-kB was not produced in other cells, including pre-B cells, because it could not be detected in these cell types by a sensitive gel-shift assay using the Igκ DNA-binding site. Subsequently however, it was found that the DNA-binding ability of NF-kB in these cells was masked by the presence of an inhibitor [142].
It is now known that NF-kB pre-exists in the cytoplasm of most cells in an inactive form

bound to the inhibitor, IkB. Since the discovery of NF-kB, its responsive sites (kB sites) have been characterised in the promoters and enhancers of numerous genes, making NF-kB an important component in the inducible expression of many proteins, including cytokines, acute phase response proteins, and cell adhesion molecules [143, 144].

Nature has not overlooked the elegance of the NF-kB signalling system. Indeed, this system has been conserved to operate on divergent genes in many different species [145]. In Drosophila three NF-kB molecules have been described: Dorsal, Dif, and relish [146-148]. The first Drosophila rel protein described was the Dorsal/ventral morphogen, Dorsal, which delineates polarity by specifically activating genes on one side of the Drosophila embryo and repressing genes on the other [149]. The signal activating Dorsal passes through a transmembrane protein called Toll, which bears a remarkable likeness to the cytoplasmic domain of the type I IL-1 receptor [150] and passes through a serine/threonine protein kinase, pelle, which is also homologous to IRAK (IL-1 receptor-associated kinase) from mammalian cells [151, 152]. Dorsal, like NF-kB, is retained in the cytoplasm by an inhibitory protein called cactus [153, 154]. The release of Dorsal from cactus [155] requires the kinase pelle and, although the exact sequence of events has not been determined, Dorsal itself is also phosphorylated (151, 156, 157). A more striking similarity in function is observed in the case of the second Rel protein described in Drosophila, known as Dif [147]. Dif appears to be the fly equivalent of the inducible form of NF-kB because it is active only under certain circumstances and upregulates transcription of insect immunity genes. Dif pre-exists in the fat body of insects, an organ that is thought to be the ancestral equivalent of the liver in vertebrates [158]. Interestingly, the liver is the centre for production of the acute phase proteins in the acute phase response to inflammation, a condition partly regulated by NF-kB [159]. Dif becomes activated as a result of infection; the Dif-activated response is therefore part of a primitive innate immune system controlled by rel proteins [158].

Although NF-kB sites have been found in the promoters of many of the insect antibacterial and antifungal genes, including cecropin, attacin, defensin, diptericin, drosocin, and drosomycin, a recent report suggests that not all the genes are regulated by Dorsal or Dif [160]. The gene most dependent on Dorsal and Dif was that encoding the antifungal protein drosomycin, while the genes encoding the antibacterial proteins cecropin, attacin, and defensin were only partly dependent. These results suggested an additional signalling pathway in insects that is involved in responses to microbial infection [161]. The third known member of the Rel-family in Drosophila is Relish,

which appears to be the homolog of the mammalian p105 and p100 proteins, with the exception that it has a serine-rich region in the place of the glycine-rich region. This protein was reported recently, and as yet very little is known about its regulation except that it is highly upregulated upon bacterial infection. Nevertheless, its similarity to p105 and p100 once again reinforces the striking evolutionary conservation of the Rel/NF-kB family.

An intriguing parallel to the Toll/Dorsal/Dif system exists in plants. The product of the plant N gene is homologous to Toll and the IL-1R [162]. This gene encodes a transmembrane receptor that confers resistance to tobacco mosaic virus infection probably by signalling the upregulation of the pathogenesis resistance proteins. Although an NF-kB-like protein has not been described in plants, the N protein may ultimately communicate with a similar transcription factor enabling the plant to activate an innate type of immune system. Recently, however, the gene encoding the NIM1 (noninducible immunity) gene in Arabidopsis, which plays a critical role in systemic acquired resistance and disease resistance in plants, has been cloned and found to be homologous to IkB [163]. The signalling system of Toll and Dorsal/Dif also led to the search for an equivalent system in mammals. It is gratifying that a mammalian Toll homolog has now been identified, that appears to be able to induce the expression of cytokines and genes known to play an important role in innate and adaptive immunity [164]. Therefore, Toll appears to function in vertebrates as a nonclonal receptor that modulates the immune response by activating NF-kB. These findings also further strengthen the notion that signalling in disease resistance responses from flies to mammals utilises an ancient, evolutionarily conserved, and ubiquitous pathway that involves the Toll/NF-kB/IkB family of proteins.

Recent years have witnessed remarkable interest in the study of the cellular pathway of transcription factors, due to their abnormal production in the presence of several diseases [165, 166]. Therefore, an in depth knowledge of their cellular mechanisms is of great importance both at the medical diagnostic and pharmacological level. In particular, the transcription factor NF-kB is involved in a wide variety of human diseases including inflammation, asthma, atherosclerosis, AIDS, septic shock, arthritis and cancer. NF-kB is a protein complex found in all types of cells and is involved in cellular responses to stimuli such as stress, cytokines, free radicals, ultraviolet radiation and bacterial or viral antigens. This protein is ubiquitously expressed in an inactive form and, after these external stimuli, it becomes active and capable to regulate a large number of genes [167].

Thereafter, when a therapy is applied to the above diseases, for which the detection of the efficacy of the therapeutic agent is particularly important, the monitoring of NF-kB concentration, in cellular extracts, is an important target, especially in pharmacological studies where a direct verification of the effectiveness of therapeutic agents is necessary [168]. In general, the dramatic difference between a healthy tissue and a chronically inflamed one is due to the excessive protein expression that is normally present in the organism, but in a limited or controlled amount [169]. The gene expression for the synthesis of some of these proteins is activated from the NF-kB, present in the cytoplasm in an inactive form and activated by a great variety of inflammatory and injurious stimuli. In mammalians five members of the Rel family are known: Rel A (also known as p65), Rel B, c-Rel, NF-kB1 (p50 and its precursor p105) and NF-kB2 (p52 and its precursor p100) [169]. Hence, various shapes of NF-kB proteins are present in nature in the cytoplasm: the p50 and p52 NF-kB members play critical roles in modulating the specificity of kB site transcription. Homodimers of p50 and p52 (such as p50/p50, p52/p52) are generally repressors of kB site transcription. Instead, if p50 or p52 form heterodimers with Rel A, Rel B, or c-Rel (such as p50/p65), these protein complexes participate in target gene activation. NF-kB indicates, in general, each homodimer or heterodimer of this family, even if the heterodimer p50/p65 is the most represented and the most diffuse in mammals [143, 144, 170].

As previously mentioned, NF-kB was discovered in the nucleus of mature B cells as an active protein bound to a 10 base-pair DNA [141]. Briefly, what ensures that NF-kB is not active in healthy tissues is its tight association with a specific inhibitory class of proteins, called IkB [171], which prevent the crossover in the nuclear membrane and the consequent binding of the transcription factor NF to the kB site of DNA. In answer to inflammatory stimulations, IkB is detached and the released NF-kB is transported into the nucleus, where it begin the gene transcription on the specific sites of DNA (Fig.2.25).

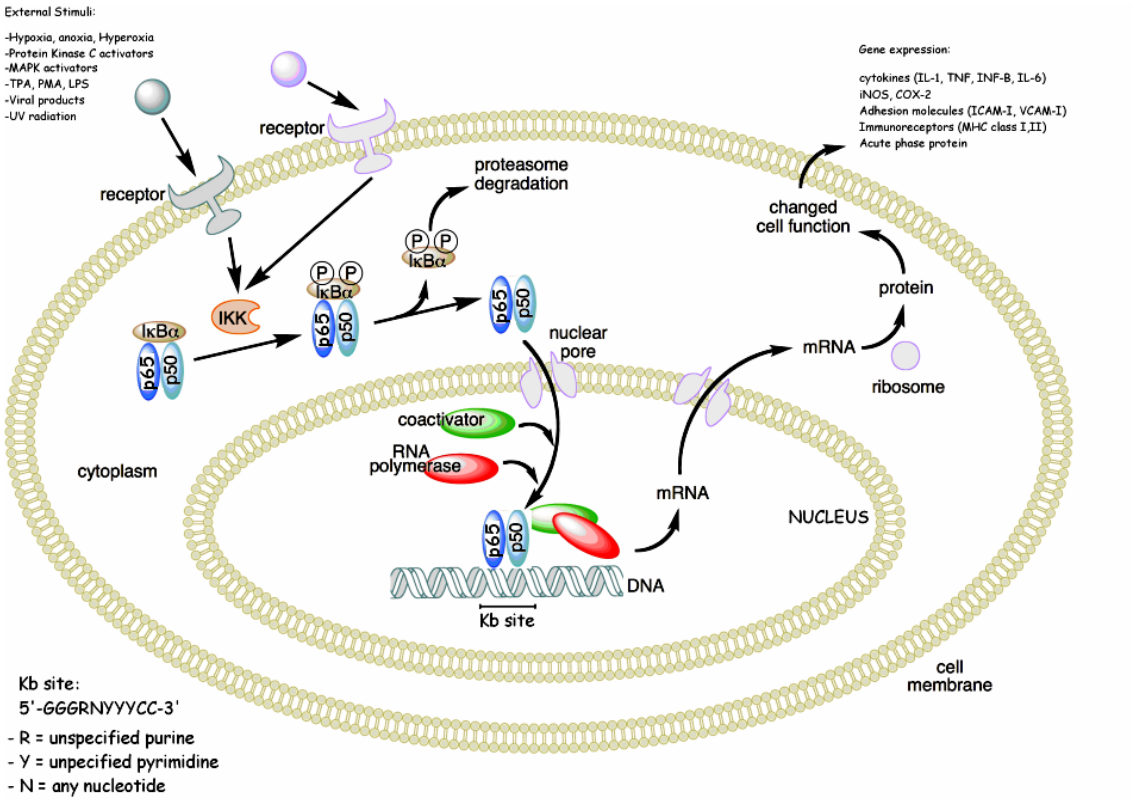

Figure 2.25 NF-kB pathway is well known; IkB inhibitor bonded to the heterodimer protein p50/p65, in answer to extra cellular inflammatory stimuli, separates from the dimer protein and is degraded from the protease. Therefore, the heterodimer p50/p65 is activated and can enter the nucleus of a cell where it causes the activation of transcription on the specific Kb site of DNA. The image is available online at http://it.wikipedia.org/wiki/NF-kB and was adapted to show external stimuli, Kb site and gene espression.

It was demonstrated that more than 60 pro-inflammatory genes are involved in the control provided by NF-kB protein. Among the genes activated by this transcription factor, there is also one related to the formation of the IkB inhibitor protein, that it is quickly synthesised after its degradation [171]. The inactive complex NF-kB/IkB is transported back in the cytoplasm, completing therefore an entire cycle of activation and deactivation of NF-kB.

2.4.2 Characteristics of NF-kB in the active and inactive form

The first NF-kB molecule described was a heterodimer of p50 (50 kDa) and p65 (65 kDa) subunits (Fig. 2.26). This protein is still what is commonly referred to as NF-kB despite the diversity of other members now known. Because the two Rel proteins making up the complex each contact one half of the DNA binding site, the slight variations possible in the 10 base pair consensus sequence, 5'-GGGRNYYYCC-3' (R is an unspecified purine,

Y is an unspecified pyrimidine, and N is any nucleotide), confer a preference for selected Rel combinations [172].

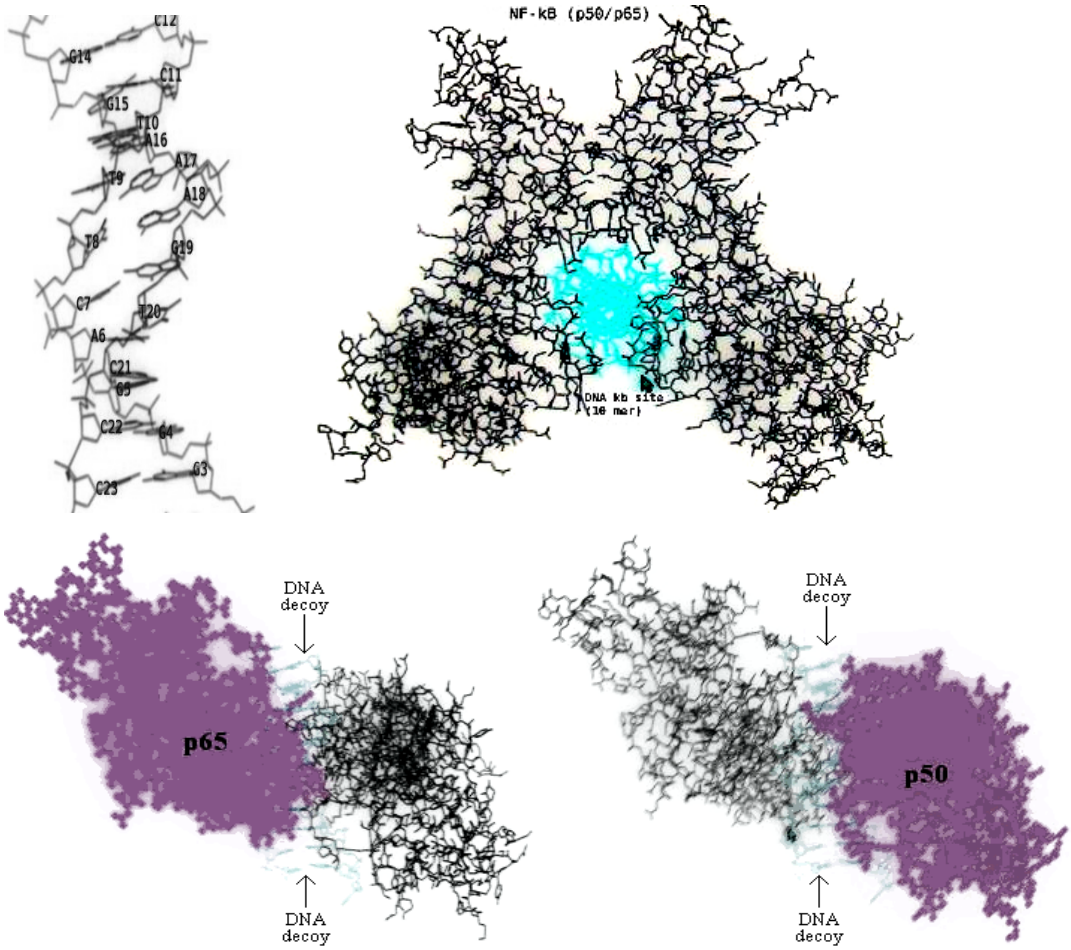

Figure 2.26 The DNA kb binding site is shown on the top left. The protein p50/p65 bound to DNA kb binding site is shown on the top right. At the bottom (left and right) is shown a frontal view where proteins bound to DNA are highlighted. The image rendering was executed using Lycos Tripod ™ software at Cranfield University, UK. These 3D images were captured by Protein Data Bank and refer to the work of Ghosh, Chen and Huang published on Nature in 1998 [173].

Although most of the NF-kB proteins are transcriptionally active, some combinations are thought to act as inactive or repressive complexes. Thus, p50/p65, p50/c-Rel, p65/p65, and p65/c-Rel are all transcriptionally active, whereas p50 homodimer and p52 homodimer repress transcription [174]. Because p50 and p52 lack a variable C-terminal domain found in the activating Rel proteins, this domain is most likely responsible for transactivation of NF-kB responsive genes.

The first glimpse of how proteins of the Rel-family bind to DNA came from the crystal structure of p50 homodimers bound to a kB site [175, 176]. Each p50 molecule is comprised of two domains joined by a flexible link. Dimerisation occurs exclusively via

the C-terminal domains where a set of hydrophobic side chains interdigitate, clamping these regions together.

In both immunoglobulin-like domains, β-strands are connected by loops that are responsible for an unusual DNA-contact interface. Both N- and C- terminal regions are involved in DNA binding, and the dimerisation and DNA-binding contacts of the C-terminal domain form a novel continuous interface that essentially "locks" NF-kB to the major groove. This DNA-binding method is also noteworthy in the extensive number of contacts made by the loops to both the sugar-phosphate backbone and the bases (Fig. 2.27).

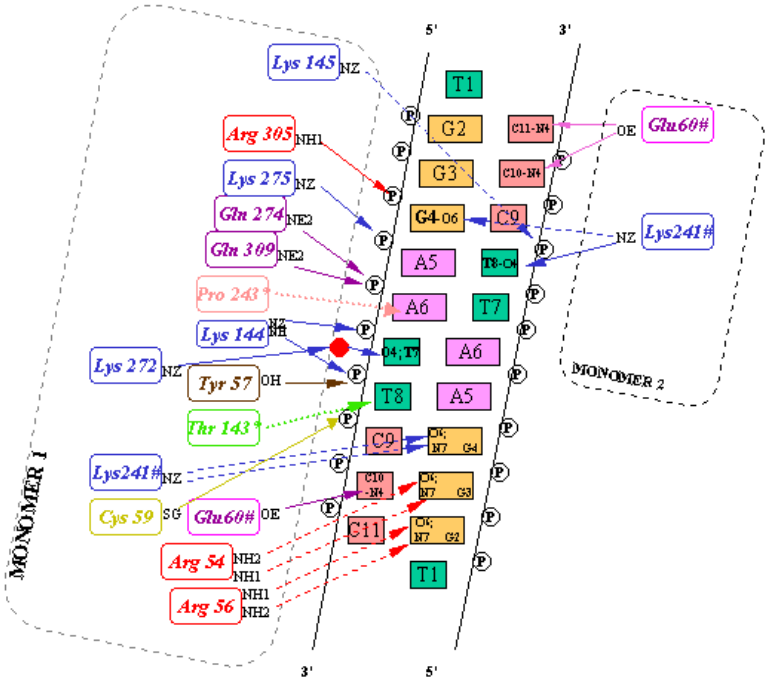

Figure 2.27. Schematic model of specific interface between NF-kB p50/p50 homodimer and central 11 base pairs of DNA [176]. The arrows represent the interaction between p50 and DNA, the red-dot represents a water mediated hydrogen bond, # represents asymmetry of residue bonding compared between DNA chains and p50 units.

The crystal structure of human NF-kB p52 in its specific complex with the natural kB DNA binding site MHC H-2 (major histocompatibility complex proteins) has been solved [177]. Compared with NF-kB p50, the compact α-helical insert region element is rotated away from the core of the N-terminal domain, opening up a mainly polar cleft. The insert region presents potential interaction surfaces to other proteins. The high resolution of the structure reveals many water molecules which mediate interactions in the protein–DNA interface. Additional complexity in Rel protein–DNA interaction comes from an

extended interfacial water cavity that connects residues at the edge of the dimer interface to the central DNA bases. The observed water network might account for differences in binding specificity between NF-kB p52 and NF-kB p50 homodimers (Fig. 2.28).

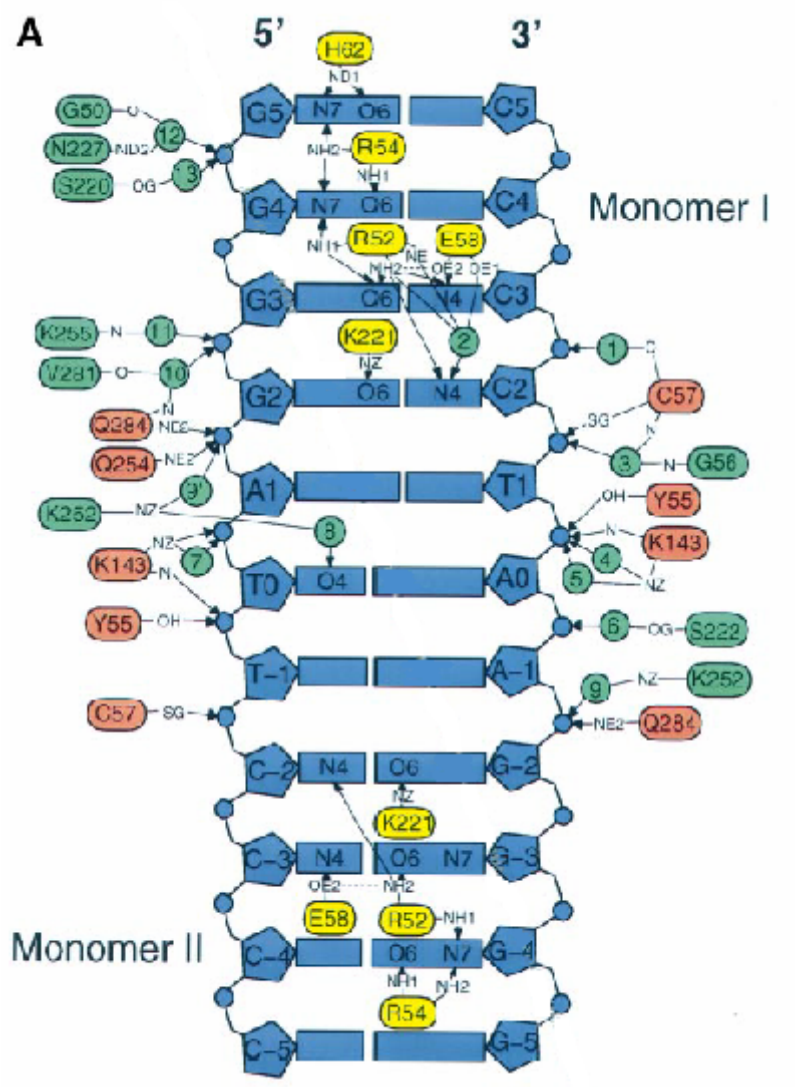

Figure 2.28. Schematic diagram of polar interactions between the homodimer p52/p52 and DNA. Contacts to DNA bases (yellow boxes), to the DNA backbone (red boxes) and water-mediated contacts (green boxes) in both half sites are shown. Water molecules are depicted as green spheres. [177]

The structure of the p65 RHD bound to DNA has also been solved [178]. Although the overall architecture of the complex is quite similar to that of p50, the p65-DNA complex reveals a few novel features. Unlike the p50 homodimer, p65 subunits are not symmetrically arranged on the DNA target. While one of the subunits binds a four base-pair DNA half site with sequence specificity, the other subunit displays a remarkably different mode of DNA recognition, retaining only partial specificity for the other half

site (Fig. 2.29). This novel model of DNA recognition exhibited by p65 probably helps to explain the wide range of DNA sequences recognised by NF-kB.

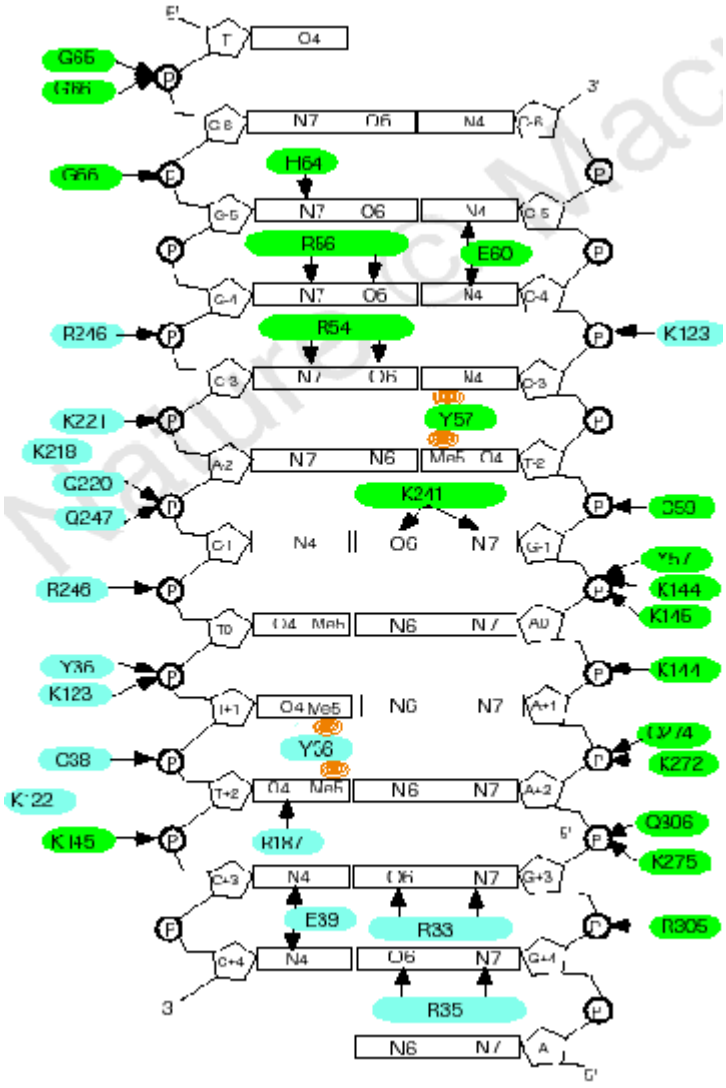

Figure 2.29. The DNA contacts the p50/p65 NF-kB heterodimer. Blue and green distinguish the p65 and the p50 subunits, respectively. Arrows denote hydrogen bonds; brown ovals indicate van der Waals contacts. The p50 subunit binds to the 5' five-base-pair subsite; the p65 subunit binds to the 3' four-base-pair sub site [178].

The mRNA retrieved from the cloning of p50, surprisingly, was found to encode for a much larger protein of approximately 105 kDa. Likewise, the mRNA for p52 also encodes a protein of 100 kDa. The N-terminal regions of p105 and p100 are identical to the p50 and p52 proteins, respectively. Inspection of the C-terminal portion of these molecules revealed several ankyrin repeats (tandemly repeated molecules of about 33 amino acids, it is one of the most common protein-protein interaction motifs in nature), reminiscent of the ankyrin repeats found in the NF-kB inhibitor molecule, IkB.

Later it was demonstrated that p100 and p105 are post-translationally cleaved to produce the smaller p50 and p52 products [179].

This processing is ATP-dependent and requires phosphorylation, polyubiquitination and proteasomic degradation. Probably it represents a further level of control of the activation of NF-kB, in fact the longer p105 and p100 proteins are exclusively cytosolic because of the masking of the nuclear localisation signals on p50 and p52 by the C-terminal ankyrin repeat region. Stimulation of cells with agents that activate NF-kB causes an increase in the rate of degradation of the C-terminal region of these proteins, and consequently increased amounts of p50 and p52, complexed with p65, are produced [181, 182].

In Figure 2.30 members of the NF-kB/rel and IkB families of proteins are shown.

The activation of NF-kB is also regulated by its cytoplasmic inhibitor, IkB. It binds NF-kB and masks its nuclear localisation signal, thus retaining it in the cytoplasm [169].

Like NF-kB, IkB is a member of a larger family of inhibitory molecules that includes IkBα, IkBβ, IkBε, IkBγ, and Bcl-3 (Fig. 2.30).

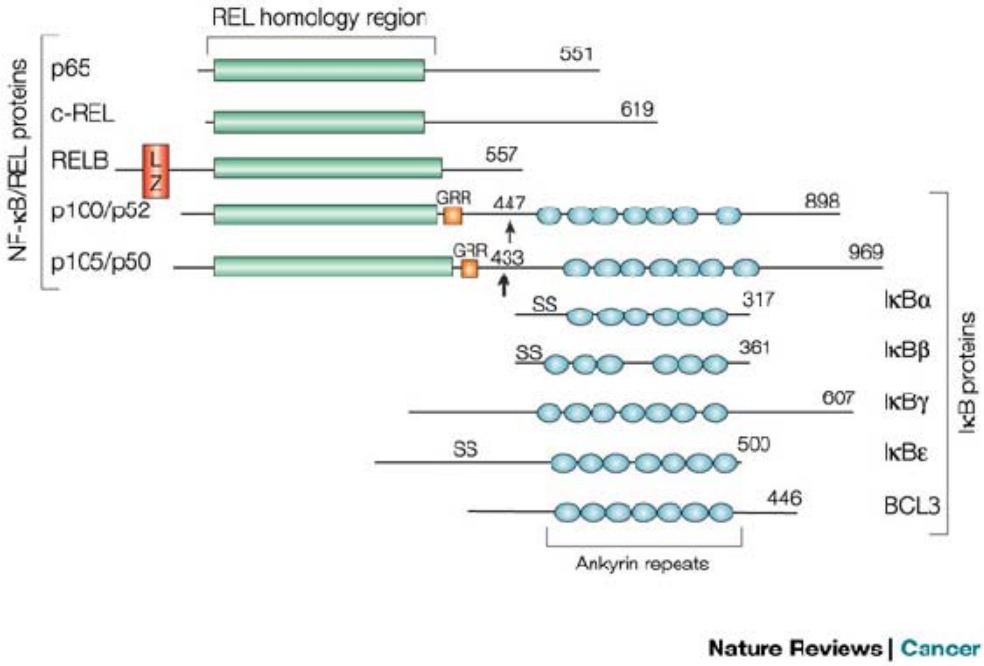

Figure 2.30. The Rel/NF-kB/IkB family of protein [180]. The number of amino acids in each protein is shown on the right. The arrows point to the endoproteolytic cleavage sites of p100/p52 and p105/p50, LZ is the leucine zipper domain of rel-B; GRR is the glycine-rich region, IκBα, IkBβ and IkBε contain an amino-terminal regulatory domain, within which there are two conserved serines (SS).

All of these inhibitors contain multiple regions of homology known as the ankyrin-repeat motifs. The ankyrin repeats are regions of protein/protein interaction, and the specific interaction between ankyrin repeats and rel-homology domains appears to be a crucial, evolutionarily conserved feature of the regulation of NF-kB proteins. Each IkB differs in the number of ankyrin repeats, and this number appears to influence the specificity with which IkB pairs with a rel dimer. As mentioned above, p100 and p105 also contain ankyrin repeats and are sometimes included in the IkB family.

The best characterised IkB protein is IkBα, a 37 kDa unit that has a tripartite organisation also seen in IkBβ: 1) an N-terminal domain that is phosphorylated in response to signals, 2) a central ankyrin repeat domain, and 3) a C-terminal domain that is involved in the basal turnover of the protein [170].

In order to clarify the structural basis for inhibition of both nuclear entry and DNA binding of NF-kB by IkBα, some authors [183, 171] have determined the crystal structure of the NF-kB p50/p65 heterodimer in complex with IkBα.

The crystal structure demonstrates how IkBα/NF-kB interactions promote cytoplasmic retention and transcriptional inactivation of NF-kB. Amino acid residues vicinal to both the p50 and p65 NLSs are tethered to the first two ankyrin repeats of IkBα, suggesting a mechanism for cytoplasmic retention of NF-kB. In the presence of IkBα, the p65 subunit of NF-kB undergoes a profound conformation change. Adoption of this closed conformation by NF-kB impedes DNA binding through the occlusion of basic DNA-contacting surfaces.

Physiologically the defining characteristic of IkBα is its ability to regulate rapid but transient induction of NF-kB activity, owing to the participation of IkBα in an autoregulatory feedback loop; that is, the activation of NF-kB causes the upregulation of transcription of IkBα, which serves to shut off the signal. There is some evidence that IkBα, which is very rapidly resynthesized after degradation, can enter the nucleus and remove NF-kB from DNA. The inactive NF-kB/IkB complex is then transported back into the cytoplasm thereby completing a cycle of activation and inactivation of NF-kB [184]. The continuing presence of certain inducing agents, for example Lypopolysaccharide (LPS), however causes NF-kB to be maintained in the nucleus despite the upregulation of IkBα mRNA synthesis, and this persistent activation of NF-kB is regulated by IkBβ [185].

IkBβ is a 45 kDa molecule that was cloned later and hence is less well characterised than IkBα [71]. Surprisingly, IkBβ binds the same rel subunits as IkBα, the divergence appears to be at the level of the incoming signal and at the timing of the onset and duration of the response. Both IkBα and IkBβ are rapidly degraded after cells are treated with the inducing agents Interleukin-1 (IL-1) and LPS; however, IkBα is re-transcribed as a result of NF-kB activation, whereas IkBβ is not. Thus, IkBβ levels remain low until the NF-kB activating signal is attenuated.

The most recent member of the IkB family to be described is IkBε. The characterisation of the protein revealed that it was unable to interact with either p50 or p52; instead it appeared to be a specific inhibitor of p65 and c-Rel complexes. IkBε can be degraded with slow kinetics upon stimulation of cells with the majority of inducers of NF-kB, and as with the other IkBs, this degradation requires two N-terminal serine residues (see NF-kB pathway). At present it seems that IkBε acts as a specific inhibitor of a subset of Rel complexes, and it therefore probably regulates the expression of specific genes, e.g. IL-8, whose promoters bind preferentially to p65 and c-Rel complexes.

Bcl-3 is the most unusual member of the IkB family. Structurally, Bcl-3 is very much like the other IkB family members in that its predicted protein structure contains 7 ankyrin repeats. However, unlike IkBα and IkBβ which are located in the cytoplasm, Bcl-3 appears to be located in the nucleus and has a binding specificity for p50 and p52 homodimers [186, 187]. Bcl-3 acts like other IkB proteins forming an inactive complex with NF-kB, unable to bind the double stranded DNA. Since the p50/p50 and p52/p52 homodimers are transcriptionally repressive, Bcl-3 may function as a transactivator by removing these inhibitory NF-kB complexes from kB sites. The complex p52/Bcl-3 can also directly bind to kB sites and activate the transcription [188]. Thus, Bcl-3 is apparently unique among the IkB proteins in that its binding to rel proteins leads to transcriptional activation rather than repression.

Finally, very little is known about the IkB family member IkBγ, which is a 70-kDa molecule detected only in lymphoid cells. Its sequence is identical to the IkB-like C-terminal region of p105, and indeed IkB is the product of an alternate promoter usage that produces an mRNA encoding the C-terminal portion of p105. Although the initial report of IkB suggested that it functioned as a *trans*-inhibitor of Rel-proteins, similar to the other IkB proteins, subsequent studies have suggested that IkB probably plays a more limited role, probably inhibiting only p50 or p52 homodimers [189].

2.4.3 Signalling pathway of the Nuclear Factor kB

As mentioned above, the activation of NF-kB is achieved primarily through the degradation of IkB proteins.

This process, which is mediated by the 26S proteasome [190], depends on the phosphorylation of two conserved serines (ser-32 and ser-36 in human IkBα) in the N-terminal regulatory domain of IkBs. Once phosphorylated, the IkBs, still bound to NF-kB, almost immediately undergo a second post-translational modification, a polyubiquitination. The major ubiquitin acceptor sites in human IkBα are lysines 21 and 22.

The enzymes that catalyze the ubiquitination of phospho-IkB are constitutively active. Hence, the only regulated step that dictates the fate of IkB and NF-kB is in most cases the phosphorylation of the two N-terminal serines in the IkB molecule. There are only two exceptions to this universal pathway for NF-kB activation. The first is the activation of NF-kB in response to UV radiation, which although dependent on IkB degradation does not involve N-terminal IkB phosphorylation. The second exception is anoxia, which stimulate phosphorylation of IkBα at tyrosine 42.

The control of IkB phosphorylation in response to all other NF-kB activating stimuli is dependent on the IkB kinase (IKK) complex, a large (700 to 900 kDa) multisubunit cytoplasmic complex [191].

By means of protein purification, microsequencing, and molecular cloning, three components of IKK were unambiguously identified. IKKα and IKKβ (also referred to as IKK1 and IKK2) are 85- and 87- kDa proteins, respectively. IKKα and IKKβ are highly homologous proteins and contain N-terminal protein kinase domains as well as leucine zipper (LZ) and helix-loop-helix (HLH) motifs. IKKα and IKKβ serve as the catalytic subunits of the IKK complex.

The third component of IKK is a 48-kDa regulatory subunit named IKKγ, or NF-kB essential modulator (NEMO), or IKK-associated protein 1 (IKKAP1), or 14.7 interacting protein (FIP-3) [192].

Secondary-structure prediction algorithms indicate that IKKγ is predominantly helical with large stretches of coiled-coil structure, including an LZ motif near the C terminal.

Extensive research over the last few years indicates that NF-kB activation is highly complex and may involve as many as 20 different protein kinases. These kinases may form a cascade, and different cascades may be formed depending on the NF-kB activator.

For instance, IKK can undergo phosphorylation by NIK (NF-kB inducing kinase), MEKK (mitogen activated protein kinase kinase) or AKT (protein kinase Bα). Although several signalling proteins and protein kinases have been recently identified that mediate IKK activation, the exact role of these kinases and their placement within the activation cascade is controversial. The activation of some of these kinases may be specific for cell type and to the stimulus employed to activate NF-kB. For instance, NIK, while found to be critical for NF-kB activation by LT and CD40L (receptor ligands), was found to have no role in TNF-induced NF-kB activation [193].

In the IKK complex the kinase activity of IKKα and IKKβ and their abilities to be activated depend on their LZ-mediated dimerisation, and LZ mutations, that interfere with this process, abolish IkB kinase activity. IKKα and IKKβ activity is also abolished by mutations within the HLH motif. The HLH mutations, however, do not interfere with dimerisation or binding to IKKγ. IKK activation is also dependent on the presence of an intact IKKγ subunit. Several authors [194, 195] provide proof for the importance of IKK in the NF-kB activation and suggest that the C-terminal region of the IKKγ is necessary for recruitment for upstream activators. In addition, overexpression of IKKγ can inhibit IKK activation due to titration of limiting IKK activators.

Activation of IKK depends on phosphorylation of its IKKβ subunit. Although IKKα phosphorylation is concurrent with that of IKKβ, it is not essential for stimulation of IkB kinase activity. These activators are recruited to the complex via the IKKγ subunit, most likely through interaction with its C-terminal domain. Phosphorylation can also result in negative regulation of IKK activity. In addition to its activation loop, IKKβ is extensively phosphorylated within a region located between its HLH motif and the C-terminus, which contains multiple serines. Phosphorylation of these serines depends on autokinase activity and presumably occurs subsequent to phosphorylation of the activation loop. Mutagenesis experiments indicate that the C-terminal autophosphorylation sites are involved in downregulation of kinase activity [196]. Initially, the inactive IKK complex is not phosphorylated. In response to upstream stimuli IKK kinases are activated and recruited to the IKK complex via the IKKγ subunit. It results in phosphorylation of the IKKβ activation loop and consequently in activation of IKK. Through trans-autophosphorylation the activated IKKβ subunit can phosphorylate an adjacent subunit, which can be either IKKα or IKKβ as well as other inactive IKK complexes through an intermolecular reaction. The activated IKK complexes then phosphorylate IkB subunits

in NF-kB/IkB complexes, triggering their ubiquitin-dependent degradation, and the activation of NF-kB. Concurrently and maybe due to the decrease of IkB abundance, the activated IKKβ subunits (and presumably the IKKα subunit as well) undergo C-terminal autophosphorylation. This reaction, which could be regulated by the level of IkB, operates as a timing device so that when at least 9 of the C-terminal serines are phosphorylated, the enzyme reaches a low activity state. Once in this state, IKK become sensitive to inactivation by phosphatases. As the C-terminal autophosphorylation sites are adjacent to the HLH motif they may exert their negative effect on kinase activity by changing the conformation of this intrinsic kinase activator domain and affecting its interaction with the catalytic domain.

A model representing the regulation of IKK is shown in figure 2.31.

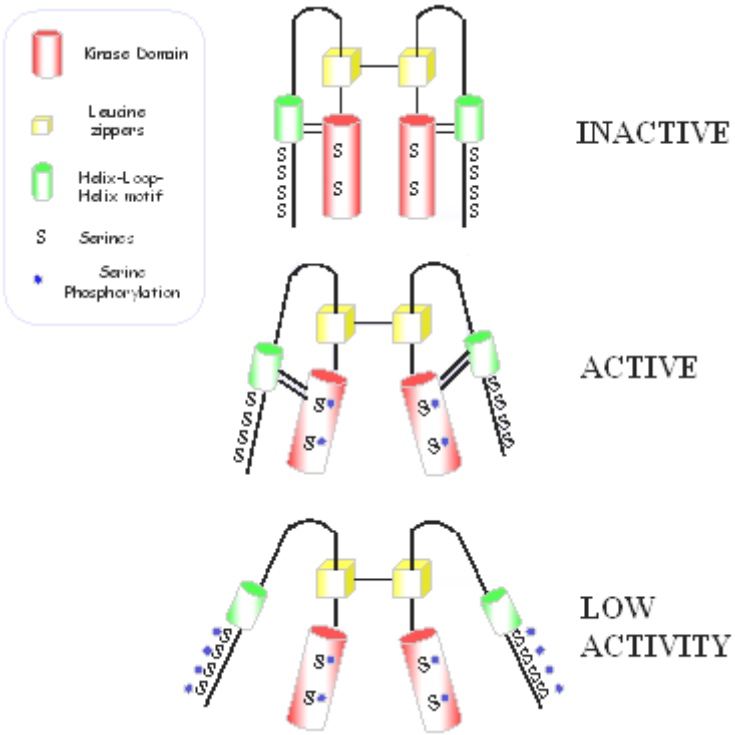

Figure 2.31 A model for IKK activity regulation by phosphorylation. The two catalytic subunit of IKK are associated in a heterodimer via their leucine zippers. In non-stimulated cells, the activation loop within the kinase domain is not phosphorylated and the helix-loop-helix (HLH) motif contacts the kinase domain. Upon cell stimulation the activation loop of IKKβ is phosphorylated and through trans-autophosphorylation of the second subunit IKK is activated. Once activated, in addition to phosphorylation of IkBs, IKK undergoes progressive autophosphorylation at its C-terminal serine cluster. When at least nine of the C-terminal serines are phosphorylated, electrostatic repulsion alters the interaction between the activating HLH motif and the kinase domain such that the kinase reaches a low activity state. In this situation the IKK activity decreases [196].

Due to the ability of IKKβ to propagate its active state via autophosphorylation it is important to have a mechanism for decreasing its kinase activity thus rendering it sensitive to inactivation by phosphatase. Without negative autoregulation, a single bolus of a proinflammatory cytokine could result in prolonged IKK activation leading to prolonged NF-kB activation followed by increased production of both primary and secondary inflammatory mediators. As these mediators can cause further NF-kB activation, there is a risk that in the absence of efficient negative feedback mechanisms even a minor proinflammatory insult would result in a major catastrophe, such as septic shock [197].

One of the most interesting aspects of NF-kB is the variety and the nature of the inducers that lead to its activation. A summary of all stimuli that are known to activate NF-kB are shown online (http://www.nf-kb.org).

Many different inducers initiate their pathways through distinct receptors and all of these different responses result in the activation of NF-kB. Depending on the stimulus, the mechanism of activation involves overlapping and non-overlapping steps.

Though a wide variety of stimuli can activate NF-kB, among the most potent inducers are gram-negative endotoxin or lipopolysaccharide (LPS), TNF-α, and IL-1β which activate NF-kB via receptor-dependent signal transduction that involves specific intracellular protein-protein interaction. A wide array of receptor-independent stimuli, including UV radiation, physical stress or deformation, ischemia-reperfusion, and exposure to H_2O_2, are capable of activating NF-kB but the mechanism is unknown [198].

A simplified version of the key events that link these kinds of stimuli to NF-kB activation is shown in figure 2.32.

TNF-α binds to the type 1 TNF receptor (TNFR1), which results in an association with TNFR1 associated death domain protein (TRADD), the receptor-interacting protein (RIP), and the TNF receptor-associated factor-2 (TRAF-2). These cytoplasmic proteins form an active signaling complex that interacts with NF-kB-inducing kinase (NIK). Activation of NIK results in phosphorylation of IKK, which cause phosphorylation IkB. Phosphorylated IkB is targeted for destruction by the ubiquination/proteosome degradation pathway, allowing the translocation of NF-kB to the nucleus [199].

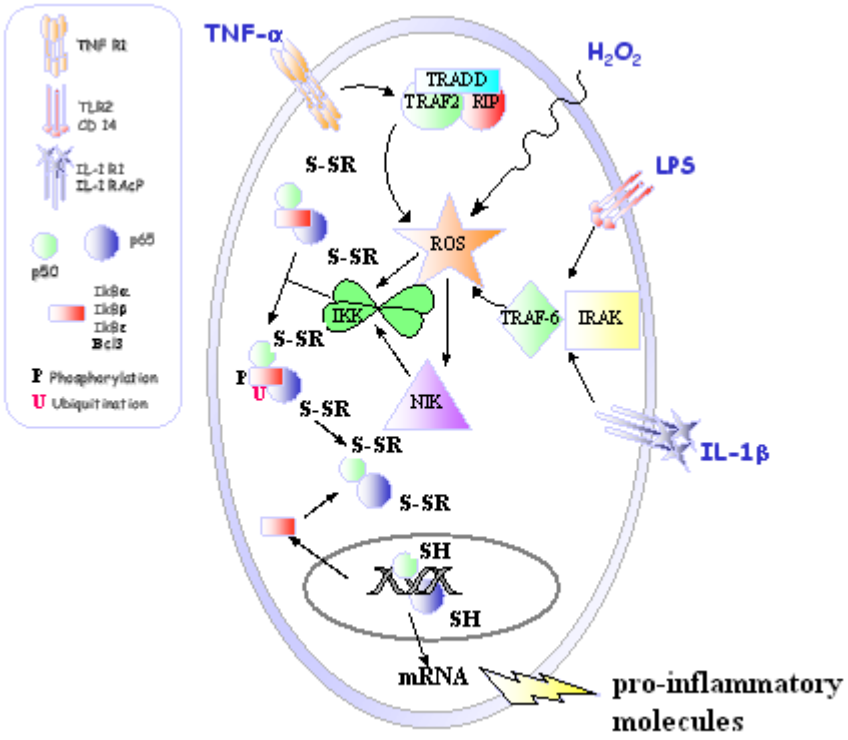

Figure 2.32. A schematic view of different stimuli that activate NF-kB towards the production of inflammatory proteins [199].

IL-1 binds to the type 1 IL-1 receptor (IL-1R1) and the IL-1 receptor accessory protein (IL-1RAcP) which facilitates an interaction between IL-1 receptor-associated kinase (IRAK) and TNR receptor-associated factor-6 (TRAF-6). The interaction between IRAK and TRAF-6 can also be triggered by endotoxin, as LPS (Lipopolysaccharide).

LPS binds with high affinity to CD-14 (the LPS receptor), and to Toll-like Receptor 2 (TLR2). These proteins form an active signally complex that also result in activation of NIK and IKK leading to the sequence of events that results in activation of NF-kB. Activation of NF-kB results in expression of mRNA of a variety of pro-inflammatory mediators which are involved in the inflammatory process. IkB is also induced by NF-kB activation and contributes to the down-regulation of this intracellular signaling cascade [85]. Also depicted are the potential points in this intracellular cascade where reactive oxygen species (ROS) modulate the activation process. Any process that increases intracellular ROS, like TNF, IL-1 or H_2O_2, might influence the activity of NIK or the IKK signalsome. An interrupted line links ROS, NIK, and IKK because this point of interaction has not been proven. Modulation of the sulfhydryl (SH) group in the conserved Cys62 in RelA and p50 by cellular redox can dramatically alter DNA binding, oxidation (-S-SR) decreases binding affinity while a reductive process (-SH) is critical for

strong NF-kB binding to DNA. This sulfhydryl group is shown in the cytoplasm in the oxidised state (-S-SR) and in the nucleus in the reduced state (SH) to correspond with effects on binding activity [198].

Reactive oxygen species (ROS), including hydrogen peroxide, superoxide anion and the hydroxyl radical have been implicated in the pathogenesis of most inflammatory diseases including cerebral vascular disease. Since pro-inflammatory molecules are involved in the pathogenesis of these inflammatory diseases, interactions between ROS and NF-kB might be a component of the intracellular signalling process that leads to activation. Four areas of evidence indicate that NF-kB activation is linked to the generation of ROS. First, treatment with hydrogen peroxide directly activates NF-kB in some cells [200].

In addition, overexpression of superoxide dismutase (SOD), the enzyme that converts superoxide anion to hydrogen peroxide, enhances the TNFα-induced activation of NF-kB. Second, most of the known stimuli for NF-kB activation, including LPS, TNFα, and IL-1β, produce oxidative stress in cells [201].

Third, treatment with N-acetylcysteine (NAC), α-lipoic acid, membrane permeable hydroxyl scavengers, metallothionein and the iron chelator, PDTC, blocks NF-kB activation that is induced by a wide variety of stimuli. These antioxidants are also effective in attenuating inflammation in rodent models of neutrophilic lung and cerebral inflammation. Fourth, overexpression of catalase, an enzyme that scavenges hydrogen peroxide, as well as overexpression of glutathione (GSH) peroxidase, an enzyme that scavenges hydrogen peroxide as well as organic peroxides using GSH as the electron donor, inhibits the cytokine-induced activation of NF-kB. Moreover, over-expression of γ-glutamylcysteine synthetase, the rate-limiting enzyme for GSH synthesis attenuates TNFα-induced NF-kB activation [202].

These observations suggest that ROS act as a common second messenger following cellular exposure to agents that induce NF-kB activation [203]. However, the main site of the interaction between ROS on the NF-kB activation pathway has not been completely defined. The most likely scenario is that ROS promote the activation pathway by activating a critical redox-sensitive kinase, probably NIK or the IKK signalsome since these molecules lead to phosphorylation of critical serine residues in IkB, resulting in liberation of cytoplasmic RelA/p50 heterodimers. However, the exact biochemical nature of the interaction between ROS and kinase activity of IKKα, IKKβ, or NIK has not yet been delineated. A recent study demonstrates that the IKK activity is blocked by apocynin (400 μM), a specific NADPH oxidase inhibitor, and diphenyleneiodonium

chloride (DPI; 10 μM), an inhibitor of flavin-containing oxidases like NADPH oxidases. Determination of ROS also demonstrated an increased generation in low shear stress that could be blocked by DPI. These results suggest that the source of ROS generation in endothelial cells in response to low shear stress is NADPH oxidase. The DPI-inhibitable component of ROS is the primary regulator of specific upstream kinases that determine the persistent NF-κB activation selectively in low shear-induced endothelial cells [204].

It is also possible, though not proven, that the redox state of critical cysteine residues could reversibly modulate kinase activity and regulates NF-kB activation [198].

Besides NIK and IKK signalsome, a second potential point of interaction of ROS on the NF-kB activation pathway has been suggested using cell-free *in vitro* systems. These studies have shown that redox changes can have a direct effect on DNA binding activity. The N-terminal region of NF-kB/Rel proteins, including p50 and RelA, contain a cysteine residue at position 62 (Cys62) which is critical for DNA binding activity but is not essential for dimerisation or interaction with IkB family members. While mutation of Cys62 to Serine does not affect DNA-binding activity, mutation to Asparagine markedly impairs DNA binding activity in response to redox changes. This implies that the conserved Cys62 in the N-terminal region of the Rel homology domain is susceptible to redox changes that govern binding activity to DNA. Modulation of the sulfhydryl (SH) group in Cys62 by cellular redox can dramatically alter DNA binding.

Oxidation (-S-SR) decreases binding affinity while a reductive process (-SH) is critical for strong NF-kB binding to its cognate DNA sequence.

These observations suggest that cellular oxidative stress has a paradoxical action on NF-kB by facilitating activation yet inhibiting DNA binding activity. Under conditions of oxidative stress, the sulfhydryl group of Cys62 should be in the oxidised state in the cytoplasm, but conversion to the reduced state must occur in the nucleus in order for strong DNA binding to occur.

As mentioned above, once activated, in the nucleus, NF-kB dimers bind to target DNA elements and activate transcription of genes which encode for proteins involved with immune or inflammation responses and with cell growth control.

A complete list of the target genes, inducers and inhibitors of NF-kB is available online at: http://people.bu.edu/gilmore/nf-kb/

Because of its direct role in regulating responses to inflammatory cytokines and endotoxin, the activation of NF-kB may play a role in the development of chronic diseases such as rheumatoid arthritis or in acute situations such as septic shock.

Support for a critical role for NF-kB activation in arthritis comes from two observations: NF-kB is activated in the arthritic synovium and therapies that are used for treatment, such as prednisone and gold compounds [205], are now known to block NF-kB.

Septic shock is a systemic inflammatory response that develops when LPS or other microbial products stimulate expression of various inflammatory cytokines. The massive production of these proteins ultimately leads to reduction in blood pressure and to general organ failure. It has recently been proposed that the production of nitric oxide in response to LPS regulates important aspects of septic shock [206]. These experiments showed that iNOS-deficient mice were protected from septic shock. Since NF-kB activates transcription of the iNOS gene, activation of NF-kB by LPS may play a role in the development of septic shock. Other activators of NF-kB, such as TNFα, may also mediate septic shock [207]. Autoimmune diseases such as systemic lupus erythromatus (SLE) may involve activation of NF-kB as well. Additionally, Alzheimer's disease may also involve activation of NF-kB in a chronic setting, since the amyloid β peptide causes production of ROS and activates gene expression through kB sites [208].

Moreover, NF-kB plays an important role in the activation of HIV gene expression. The influenza virus protein hemagglutinin activates NF-kB, and this activation may contribute to viral induction of cytokines and to some of the symptoms associated with flu [209].

Products of the genes that are regulated by NF-kB also cause the activation of NF-kB. The proinflammatory cytokines IL-1β and TNF-α both activate and are activated by NF-kB. This type of positive regulatory loop may amplify and perpetuate local inflammatory response [210].

NF-kB may also play a role in the development of atherosclerosis by transducing pathogenic stimulation to expression of genes that promote recruitment and activation of inflammatory cells in the plaque.

The NF-kB-regulated inflammatory mediators such as cytokines, inducible NO synthase and leukocyte adhesion molecules have been detected in atherosclerosis lesions. Activated NF-kB has been identified in macrophages, smooth muscle cells and endothelial cells in human atherosclerotic plaques but not in healthy vessels [211, 212].

As mentioned above, NF-kB has a fundamental role also in the regulation of cellular growth and it might have both pro-apoptotic and anti-apoptotic effects. TNFα, for example, is a proinflammatory cytokine that is produced by cytokine and other activators, such as LPS and viruses. It has several functions, including roles in inflammation, immunoregulation, proliferation, and anti-viral response [213].

The diverse actions of TNFα are mediated by two receptors, TNF-R1 (p60) and TNF-R2 (p80). TNFα binding to TNF-R1 leads to activation of NF-kB and AP-1, which culminates in a proinflammatory and immunomodulatory response [214]. However, in certain cell types and under certain conditions, TNFα can induce apoptosis [215]. The duality of TNF-R1 signalling became clear through the identification of two distinct TNF-R1 intracellular pathways: a pro-apoptotic pathway, which is mediated by FADD, and an anti-apoptotic pathway, which is mediated by TRAF2 [216] and, in some cell types, by the Akt kinase [217], that leads to activation of NF-kB.

Several studies have also shown that NF-kB has a pro-apoptotic and an anti-apoptotic role on nervous system. For example, treatment of rat primary neuronal cultures and hippocampal slices with the neurotoxin glutamate induces NF-kB activity and apoptosis, and activation of NF-kB in these cells can be inhibited by some common anti-inflammatory drugs, as aspirin and salicylates [218]. On the other side, the β-amyloid peptide associated with Alzheimer's disease my cause its neurodegenerative effects by down regulating NF-kB activity [219].

The protective role of NF-kB in Alzheimer's disease was also reported [220], demonstrating that the neuroprotective form of soluble β-amyloid peptide precursor protein can activate NF-kB and prevent apoptosis induced by the β-amyloid peptide.

Moreover, NF-kB may have a pro-apoptotic or an anti-apoptotic role in response to a viral infection. For example, NF-kB can protect HIV-1-infected myeloid cells from apoptosis [221]; however, HIV-1 may also induce apoptosis through NF-kB in some situations: the HIV-1 encoded transcriptional transactivator TAT has been shown to render cells sensitive to apoptosis by inducing NF-kB [222].

An emerging picture is that, depending on a variety of circumstances, including the cell type and the inducing agent, NF-kB can have pro- or anti-apoptotic effects. These effects are likely carried out by the activation of target genes that lead to different outcomes.

As a consequence of which types of genes are expressed after NF-kB activation, it seems that the pro- or anti-apoptotic effects of NF-kB may be part of a more complex process, namely the development of cancer. Cancer is a hyperproliferative disorder that involves transformation, initiation, promotion, angiogenesis, invasion, and metastasis. NF-kB activation participates at multiple steps in this pathway not only because it blocks apoptosis and promotes cell proliferation [223-225] but also because:

1) NF-kB mediates the expression of genes that are involved in tumour promotion, angiogenesis, and metastasis [226]. For example, NF-kB may regulate the production of

prostaglandins via the proinflammatory gene cyclooxygenase-2 (COX2), which has been shown to be overexpressed in a variety of cancers including colorectal cancer and mesothelioma [227]. Moreover, Tumour cells, just like normal cells, need oxygen to survive and this can be a limiting factor to progression of tumours. Vascularisation of tumours requires the release of angiogenic growth factors (e.g. VEGF, MCP-1) from tumour cells and/or inflammatory cells such as macrophages and neutrophils or in response to pro-inflammatory cytokines (e.g. TNF). NF-kB regulates the expression of such growth factors and cytokines (VEGF, TNF, MCP-1) necessary for angiogenesis [228, 229, 230]. And also, the metastasis of cancer requires the migration of cancerous cells both into and out of the vessel walls that transport them to other parts of the body. The ability to cross vessel walls is mediated by specific molecules that are expressed in response to a number of signals from inflammatory cells, tumour cells, etc. Among those special molecules are ICAM-1, ELAM-1, and VCAM-1, all of which have been shown to be expressed in response to NF-kB activation [231, 232].

2) It has been shown that NF-kB is activated by hypoxia and acidic pH, both indigenous to the tumour microenvironment [233]. The stress of fluctuation in blood flow in the microenvironment of solid tumours and the resultant intermittent hypoxia has been shown to activate NF-kB [234, 235]. Since oxygen is needed for a tumour to grow, the tumour must secrete chemotactic signals such as growth factors and cytokines in order to induce neovascularisation. Many of these growth factors and necessary signals for tumour progression are target genes of NF-kB and utilize its activation for their transcription.

3) Several tumour types show a persistent constitutive nuclear activation of NF-kB [236-241].

4) NF-kB activation has been shown to induce resistance to various chemotherapeutic agents [242]. Likewise, the precise mechanism for NF-kB's involvement in chemotherapeutic efficacy is not clear, but its enhanced activity has been shown to be linked to decreased apoptosis via expression of the anti-apoptotic gene A1/Bfl-1 and enhanced expression of the multiple-drug resistance gene product or MDR gene (prevents the intracellular accumulation of toxic drugs such as those used in chemotherapy), both likely factors in the progression of tumours [243, 244].

5) NF-kB gene products can be oncogenic when aberrantly expressed and are implicated in a number of tumour types. While the expression of a large number of genes involved in the development of cancer are regulated by NF-kB, the genes that code for individual

NF-kB proteins themselves have also been implicated in the development of several types of cancers, both hematopoietic and solid tumours. These genes are expressed aberrantly, i.e. amplification of gene on chromosome, rearrangement, overexpression, substitution, mutation, truncation, etc. [245, 246].

Because of the multitude of cellular and organism processes affected by NF-kB signaling, there has been great interest in modulators of this pathway and, for this reason, specific and efficient inhibitors of NF-kB have been sought. Due to the large number of inducers of NF-kB and the various levels of the regulation of this pathway, inhibitors also include a large variety of molecules that act at multiple levels.

2.4.4 NF-kB: a target for therapeutic agents

As mentioned above, NF-kB regulates the transcription of an exceptionally large number of genes [247], particularly those involved in immune and inflammatory responses (248, 249, 210]. NF-kB activation also plays an important role in the antiviral response through interferon gene induction [250, 251]. Yet, through adaptation, many viruses, including human immunodeficiency virus type 1 (HIV-1) [252] and human T-lymphotrophic virus type 1 (HTLV-1) [253], which do not cause interferon induction, exploit NF-kB to activate their own genes and to stimulate the survival and proliferation of lymphoid cells in which they replicate. In most cells, NF-kB activation protects from apoptosis, through induction of survival genes, although under certain conditions and in certain cell types it may also induce apoptosis [254, 255]. Inappropriate regulation of NF-kB is directly involved in a wide range of human disorders, including a variety of cancers [256], neurodegenerative diseases [257], arthritis [258], asthma [259], inflammatory bowel disease [260], and numerous other inflammatory conditions.

Because of the multitude of cellular and organism processes affected by NF-kB signalling, there has been great interest in modulators of this pathway.

Intense efforts are currently made to develop novel drugs that specifically block NF-kB activating pathways. Due to the large number of inducers of NF-kB and the various levels of regulation of this pathway, inhibitors also include a large variety of molecules that act at multiple levels.

The cascade of NF-kB signalling events provide several key steps for specific inhibition of NF-kB activity that could be classified as follow:

1) blocking the incoming stimulating signal at an early stage and thus blocking its general effect; 2) interfering with any step in the NF-kB activation pathway by blocking a specific member of the cascade; 3) blocking NF-kB nuclear activity, that is, inhibiting its translocation to the nucleus, its binding to DNA or its interactions with the basal transcription machinery. Each of these three major steps would not be susceptible to the same types of inhibitors. The following Tables give examples of a NF-kB-inhibitors classification. In a great number of cell types, NF-kB can be activated by oxidants and its induced activity can be inhibited by anti-oxidants.

A list of anti-oxidants that have been shown to inhibit activation of NF-kB is available online on the website: http://people.bu.edu/gilmore/nf-kb/inhibitors/index.html

The last common step before NF-kB is freed from the cytoplasm is the degradation of ubiquitinated IkB by the 26S proteasome [190, 261].

Thus, inhibitors of the ubiquitin-proteasome pathway suppress activation of NF-kB by stabilizing IkB. The inhibitors described below can all penetrate cells and inhibit NF-kB activation in a dose-dependent manner by blocking proteasome-mediated degradation of IkB (but not its phosphorylation).

A list of proteasome and proteases inhibitors that inhibit NF-kB is available online on the website: http://people.bu.edu/gilmore/nf-kb/inhibitors/index.html

In addition to the proteasome inhibitors, several other molecules inhibit NF-kB by maintaining a high level of IkB proteins in the cytoplasm and thereby preventing NF-kB nuclear translocation. Among these molecules, some inhibit IkBα phosphorylation and its subsequent ubiquitination, while others block IkBα degradation. Those molecules can be grouped into two classes: (1) natural molecules, that is, molecules produced by cells under specific condition or synthesized by diverse organisms (plants or micro-organisms), and (2) artificial compounds, designed and produced by chemical, pharmacological or molecular biological processes.

A list of IkBα phosphorylation and/or degradation inhibitors is available online on the website: http://people.bu.edu/gilmore/nf-kb/inhibitors/index.html

Direct inhibition of NF-kB-specific trans-activation could involve several other molecules with different mechanisms of action blocking either nuclear translocation, DNA binding, or transactivation by NF-kB dimers.

Because many of NF-kB target genes are involved in the acute phase or inflammatory response, inhibition of NF-kB has been used to minimise the pathologic effects induced by the immune system misregulation. As such, several of the most commonly used drugs

can inhibit NF-kB activity. An example of that are the anti-inflammatory drugs (aspirin, sodium salycilate, glucocorticoids, etc.) and the immunosuppressive agents (Cyclosporin A, FK506, PG490, etc.).

Another general strategy for inhibiting NF-kB activity is to develop genetically-engineered proteins that block specific steps in the activation process.

It has been possible to block the activation of NF-kB by manipulating the genes that encode proteins (eg TRAF2, TRAF6, I-TRAF, NIK, MEKK1, and IKK) found directly in the known activation pathways [262].

TRAF2 (TNF receptor-associated factor) and TRAF6 interact with TNF receptors and serve as adapters for the activation of NF-kB.

Dominant negative mutants of TRAF2 and TRAF6 have been shown to repress NF-kB activity in response to TNFα and IL-1, respectively [216].

I-TRAF interacts with TRAF2, and its overexpression inhibits TRAF2 activation of NF-kB [263]. NIK (NF-kB-inducing kinase) is induced by several proteins in the activation pathway, including TRAF-2 and TRAF-6, and activates IKK (as does MEKK1).

Therefore it has been shown that a dominant-negative mutant of NIK (and MEKK1) represses NF-kB activation [264-266].

The IKKs (IkB kinases, alpha and beta) phosphorylate IkBα to subsequently cause its ubiquitination and ultimate degradation.

Thus, alterations in the ATP-binding site of the IKK complex (IKKβ more so than IKKα) or its activation loop have been shown to block the activation of NF-kB as well (267-272].

From the commonly-used aspirin to the IkBα super repressor, numerous inhibitors of the NF-kB activity have been described. Their mode of action is sometimes known, other times it has simply been noticed that such molecules inhibit NF-kB-induced DNA binding. Some NF-kB inhibitors are “broad-range” inhibitors, such as the many anti-oxidants and proteasome inhibitors, which can block most NF-kB activating signals. Other inhibitors of NF-kB block activation when induced by only certain stimuli, for example by acting on a particular protein in the signalling cascade or by blocking specific NF-kB complexes. From the pharmacological point of view, it is moreover important, not only the transcription factor inhibition, but also its control, useful to evaluate the efficacy of the drug-therapy applied. This could be obtained quantifying the concentration decrease of the active factor, related to the dispensed drug. In order to have the possibility to detect the active NF-kB, several methods have been developed.

A list of miscellanous inhibitors of NF-kB is available online on the website: http://people.bu.edu/gilmore/nf-kb/inhibitors/index.html

2.4.5 Different methods for NF-kB detection

NF-kB is involved in so many human diseases, including inflammation, asthma, atherosclerosis, AIDS, septic shock, arthritis, cancer.
Several efforts for the development of a successful method, capable to detect the active form of the protein, have been done.
Different methods have been proposed and successively used for the determination of the transcription factor, even if many of these are unable to discriminate the active form from the inactive one.
Basic classical assays currently used for NF-kB detection include: Southwestern blotting [273, 274] enzyme-linked immunosorbent assay (ELISA) [275], electrophoresis mobility-shift assay (EMSA) on gel [276], free solution capillary electrophoresis (FSCE) [277]. Moreover some modern techniques, often combining two different classical approaches in order to take advantage of the value of both, have been proposed and commercial kits have been developed.

2.4.6 Detection kits commercially available

The common aspect of simple and fast assay-kits for NF-kB detection commercially available is the research of a non-radioactive labelling method, in order to avoid the tedious and time consuming aspect of these assays. Furthermore, all of them are based on the antigen-antibody interaction.

Different assay kits for detection of NF-kB, p50 are available on the market:
ASSAY DESIGNS/STRESSGEN BIOREAGENTS Company produce an assay which uses streptavidin-coated plates with bound NFkappaB biotinylated-consensus sequence to capture only the active form of NFkappaB. The captured active NFkappaB is incubated with a specific NFkappaB p50 antibody which is subsequently detected using an HRP conjugated secondary antibody. The assay is developed with a chemiluminescent substrate and the signal is detected using a luminometer.

The CAYMAN CHEMICAL® Company provide a NF-kB (human p50) Transcription Factor Assay non-radioactive method for detecting specific transcription factor DNA binding activity in nuclear extracts and whole cell lysates. A 96 well enzyme-linked immunosorbent assay (ELISA) replaces the cumbersome radioactive electrophoretic mobility shift assay (EMSA). A specific double stranded DNA (dsDNA) sequence containing the NF-kB response element is immobilised onto the bottom of wells of a 96 well plate. NF-kB contained in a nuclear extract, binds specifically to the NF-kB response element. NF-kB (p50) is detected by addition of specific primary antibody directed against NF-kB (p50). A secondary antibody conjugated to HRP is added to provide a sensitive colorimetric readout at 450 nm. The Cayman Chemical NF-kB (human p50) Transcription Factor Assay detects human NF-kB (p50) is specific and does not cross-react with NF-kB (p65).

The CHEMICON® (Millipore™ Corporation Company) sells non-radioactive NF-kB p50/p65 Transcription Factor Assay which provides a method to detect specific DNA binding activity for transcription factor in nuclear extracts. This assay combines the principle of the EMSA with the 96-well based ELISA, enabling manual or high-throughput sample analysis with significantly greater sensitivity than conventional EMSA assays. The entire assay takes less than 4 hours to complete with minimal hands-on time. The versatile set up allows a flexible assay design and because the binding reaction occurs in solution, various parameters can be optimised such as probe titration, competitive oligonucleotide concentration, or treatment conditions. The system is similar to the one described before, actually the non-radioactive NF-kB p50/p65 Transcription Factor Assay kit is provided in a 96-well format. During the assay, the Capture Probe, a double stranded biotinylated oligonucleotide containing the consensus sequence for NF-kB binding (5'-GGGACTTTCC-3'), is mixed with cellular (nuclear) extract in the Transcription Factor Assay Buffer provided. When incubated together, the active form of NF-kB contained in the nuclear extract binds to its consensus sequence. After incubation, the extract/probe/buffer mixture is then directly transferred to the streptavidin coated plate. The biotinylated double stranded oligonucleotide bound by active NF-kB protein is immobilised and any inactive, unbound material is washed away. The bound NF-kB transcription factor subunits, p50 and p65, are detected with specific primary antibodies, a Rabbit anti-NF-kB p50 (active form) and a Rabbit anti-NF-kB p65. An HRP-

conjugated secondary antibody is then used for detection and provides sensitive colorimetric detection that can be read in a spectrophotometric plate reader.

NOVAGEN® Company proposes an identification of DNA binding protein using the NoShift™ Transcription Factor Assay Kit. The NoShift™ assay is a microassay plate–based test to identify proteins that bind to a specific DNA sequence. One advantage of this plate-based assay over traditional gel shift assays is the remarkable specificity of the test. The shift in mobility of a DNA probe in an EMSA indicates that some protein in a crude extract binds, but the identity of the protein is unknown unless a supershift is performed with a protein-specific antibody. The NoShift assay has dual specificity: that of the protein for the DNA probe and of the antibody for the interacting protein. The convenient 96-well format of the NoShift assay permits screening for multiple DNA binding proteins in the same plate. The basic NoShift kit consists of a streptavidin-coated microassay plate. A NF-kB reagent kit contains biotinylated oligonucleotides that include a consensus recognition sequence, specific and non-specific competitors, a transcription factor–specific antibody, secondary antibody conjugated to HRP, and positive control nuclear extract. The NoShift assay kits, as the others described before, offers a fast, sensitive, non-radioactive alternative to gel shift assays.

These interesting kits solved the problem of an unspecific active-inactive NF-kB bound by means of a DNA consensus sequence in the ELISA assay. In spite of that, it seems a laborious approach that takes several hours before the sandwich antigen-antibody was ready to be measured.

2.4.7 In vivo imaging of NF-kB activity

An original contribution for the control of NF-kB activity has been recently given [278]. As NF-kB is involved in a number of diseases, their model offers a tool for studying NF-kB regulation in condition were NF-kB is a key player. Their goal is to define mechanisms through which NF-kB leads to the development of disease, for that they have developed transgenic mice that express a luciferase reporter whose transcription is dependent upon NF-kB. The relative amount of luminescence can be assayed uninvasively by real-time imaging.

Reporter gene expression in vivo has previously been assessed using optical techniques such as microscopy of green fluorescent protein [279] or near-infrared fluorescence [280], both of which have limited depth penetration. Nuclear imaging techniques using gamma cameras [281], positron emission tomography [282], or single-photon emission computed tomography [283] have satisfactory depth penetration, but they have a lower spatial resolution. Magnetic resonance imaging techniques [284] provide excellent spatial resolutions, but the temporal resolution is limited, and the technique is several orders of magnitude less sensitive than optical and nuclear techniques. Their detection system was adapted from one described by Contag and colleagues [285]. In their study of mice infected with recombinant bacteria containing the luciferase gene, the displayed luminescence was sufficiently intense to be detected externally. The transgenic mice expressing luciferase prepared by Carlsen and co-workers gives the possibility to monitor changes in NF-kB activity in living animals as a function of cytokines, endotoxin, physical agent, and state of disease. In other words, it is an interesting model to observe exogenous factors, such as nutrients, pharmaceuticals, and pollutants, for modulation of gene expression related to NF-kB, but it is not able to quantify the active protein that is increased after an external stimulus and decreased after the appropriate drug therapy.

2.4.8 dsDNA microarrays for DNA/protein interactions studying

An array of dsDNA specific for transcription factor was recently realized by Wang and co-workers [286]. They proposed as an alternative to the classical techniques, the immobilization on a glass surface of dsDNA interacting specifically with a fluorescent labelled protein. The oligonucleotide chain was covalently immobilised on a glass slide, consequently the p50 subunit of NF-kB was labelled with the fluorescent dye Cy3 and the interaction with the DNA fragment was performed. The construction of an array carrying different DNA sequences could be potentially used to study: screening sequence-specific DNA-binding proteins; predicting new DNA-binding sites of transcription factors in genome; assessing importance of nucleotides in DNA-binding sites for DNA/protein interactions; monitoring the expression of drug-induced DNA-binding proteins; and screening sequence-specific DNA-binding drugs.Taking advantage of this biosensing method described for the NF-kB detection, during this work an optical sensor-model for active NF-kB quantification was proposed. The reliability of a reusable biosensor, important for the construction of a cheap device, was also demonstrated.

2.4.9 Idea of biosensor for NF-kB

Standard techniques to quantify the protein NF-kB (e.g. ELISA) are not able to discriminate the active structure from the inactive one, and other methods (such as electrophoresis mobility shift assay, EMSA) are laborious and time consuming. The critical need for a simple and direct method to evaluate the quantity of a transcription factor in a biological sample can be addressed using a suitable, renewable biosensor, consisting of two basic elements: the biological recognition system which interacts selectively with the analyte of interest, and the transduction process, able to convert the molecular recognition into a detectable optical signal.

In particular, an optical detection method based on fluorescence has been considered, in which the active form of NF-kB is detected by its binding to a specific DNA sequence. An optical biosensor for the NF-kB based on fluorescence resonance energy transfer (FRET) is reported in literature [168]. The principle of operation of the biosensor is based on the DNA *binding activity* of NF-kB, which relies on its ability to bind to one particular sequence of DNA.

The device described in this thesis was constructed using a bioreceptor made of a synthetic double filament (dsDNA) that represents the site of binding (kB site) of the transcription activator NF-kB1 (p50/p50).

The biosensor, therefore, is required to transduce the binding event with an unknown quantity of the factor to a measurable and quantifiable physical phenomenon (a variation in fluorescence) induced from the formation of the complex DNA/protein [175, 176].

The achievement of direct and quantitative detection of activated NF-kB would be far preferable to the traditional assay methods (EMSA, western blot, immunoprecipitation) that are extremely laborious, have insufficient reproducibility and are only capable of providing semi-quantitative results.

The optical biosensor developed here and suitable for the specific measurements of the levels of factor NF-kB in biological samples is based on a sandwich assay.

The first step was the immobilisation of an oligonucleotidic probe (which mimics the DNA sequence kB) on the internal wall of a flow channel. Then, in a second step, a protein (p50) was inserted in the channel interacting with the DNA probe. Cy5-labeled antibodies specific for the interaction with p50 were then inserted, as a third step, and the intensity of fluorescence, which was proportional to the concentration of p50, was measured (Fig. 2.33).

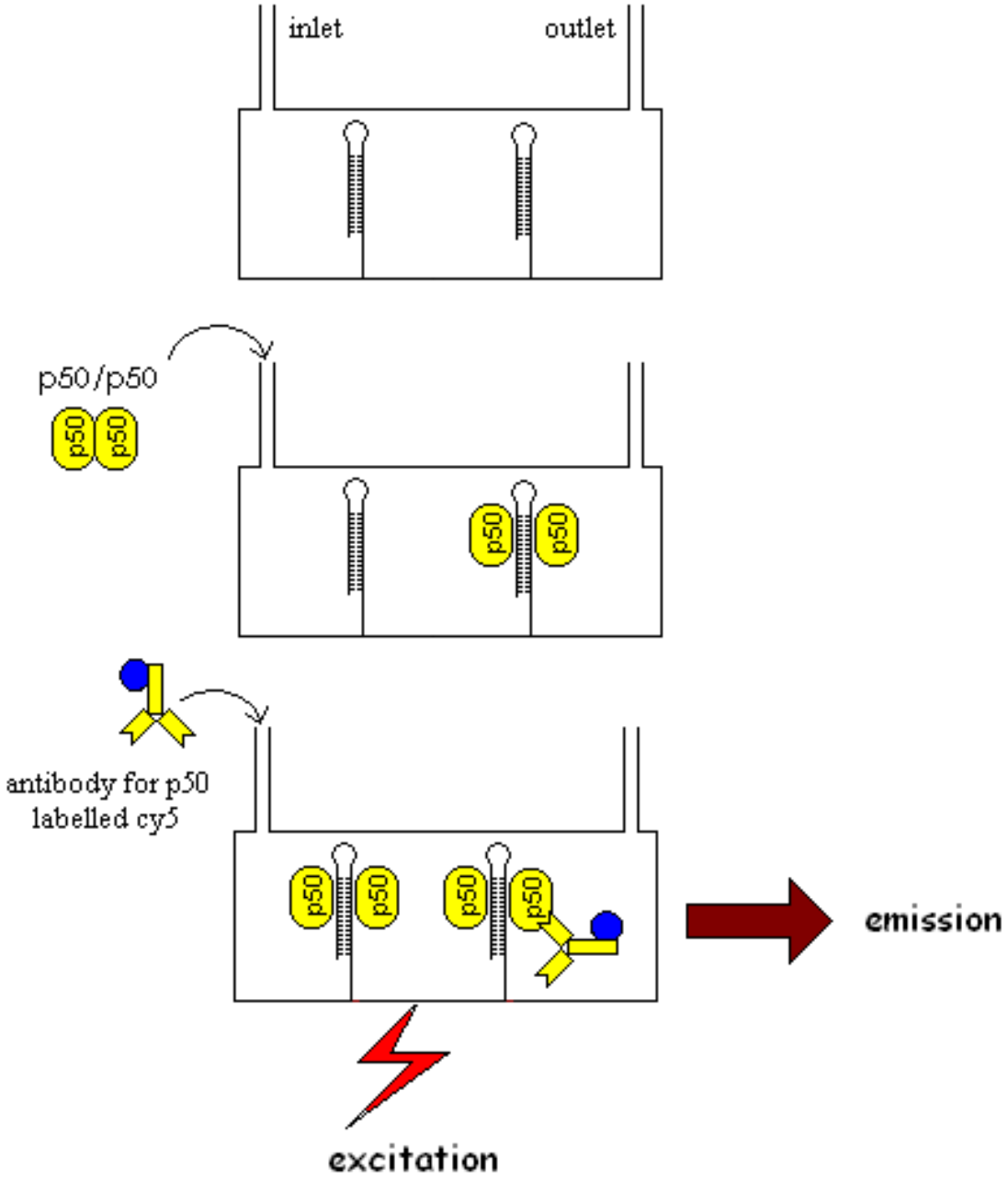

Figure 2.33 A diagrammatic representation of the two step operation idea for the optical biosensor for NF-kB. Top: dsDNA is immobilised on the wall of the flow channel; binding between protein p50/p50 and DNA takes place. Bottom: the protein p50/p50, bound to dsDNA, is measured by means of a labelled (Cy5) antibody specific for p50, causing a variation in the fluorescence signal.

2.5 MGMT

MGMT (O^6-Methylguanine-DNA methyltransferase) is a ubiquitous DNA repair protein that removes O^6-alkyl-guanine lesions, primarily O^6-methyl-guanine from damaged DNA. It is a major contributor to cellular protection from the mutagenic, carcinogenic, and cytotoxic effects of DNA alkylation [287]. Recent studies define the role of MGMT in protecting from alkylating agent-induced toxicity and mutations in mammals [288]. The alkylation of DNA occurs in the O6 position of the guanine and the MGMT protein is able to remove these residual agents that constitute a condition of mutagenic lesion of the DNA. In fact the presence of O6-methylguanine during the replication of the DNA can cause a mutation from cytosine into thymine; in O6-Metilguanina, thymine is the favoured complementary partner rather than cytosine, the correct complementary base of guanine. [289]. A brief representation of the chemical reactions in play is shown in fig. 2.34. DNA mutation caused by a methyl group in position O6 can be favoured considering the rearrangement of electrons if a methyl group reacts in the oxygen position number 6. This fact can cause a modification of guanine into O6-methylguanine [290]. The part highlighted in red in O6-methylguanine (Fig. 2.34) looks chemically similar to the same part of adenine molecule. Consequently during the transcription from DNA into RNA, RNA recognises the O6-methylguanine as if it is an adenine base, with the consequent conversion of O6-methylguanine into a thymine instead of cytosine.

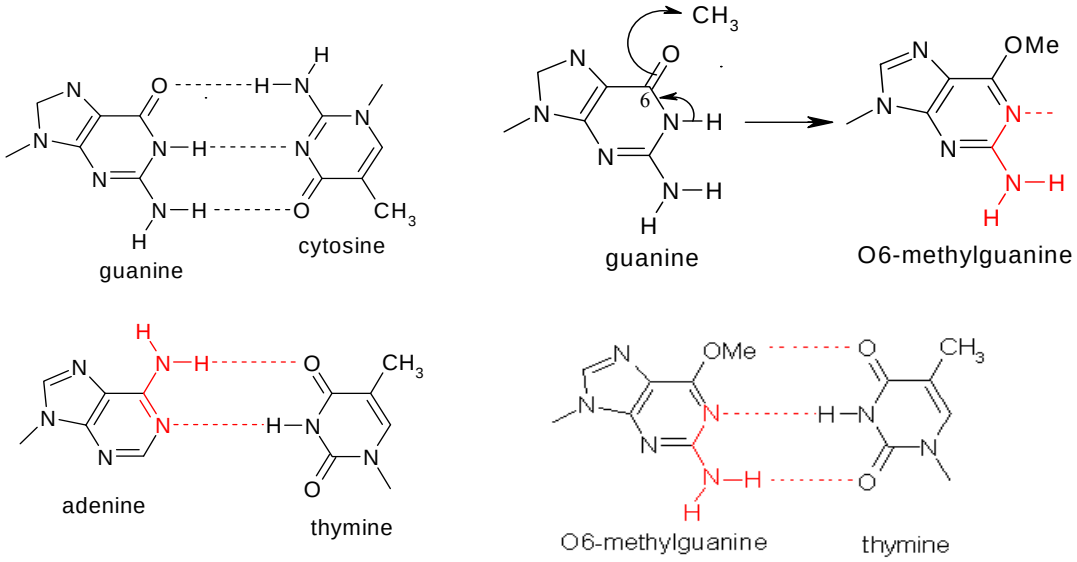

Figure 2.34 The normal complementary pairs of DNA bases are shown on the left. On the right (top) the modification due to alkylating agents (in this case a methyl group) is shown. On the right (bottom) the DNA wrong transcription due to O6-methylguanine is represented. I personally depicted this image.

In recent years, it was plenty demonstrated that MGMT protein is able to play a fundamental role in the cellular defence against the alkylating agents, especially in the case of undesirable methylation of guanine base [291-309].

All these works about MGMT protein reveal the potentiality that SH group, belonging to cysteine, possess in prevention of mutagenicity. In fact, the evolution of mutagenic nucleotides can cause an unnatural cellular revolution caused by low levels of MGMT. On the contrary, high level of this parameter tends to preserve the DNA replication process [291, 293].

In particular, Glioblastoma multiform (GBM) is the most common and aggressive type of primary brain tumour. Treatment can involve chemotherapy, radiotherapy and surgery. The use of temolozide (Temodar ©) alongside radiotherapy has shown survival benefit and is currently considered the standard of care by the National Cancer Institute [294-298]. In particular, the gene silencing of MGMT can help temolozide drug activation in radiotherapy in glioblastomas brain tumour. mRNA silencing is usually performed using a promoter of methylation (methylation-specific polymerase-chain-reaction) preventing its DNA repair function when temolozide is involved as specific drug in brain cellular processes [299-301].

In low-grade diffuse astrocytomas, promoter hypermethylation of MGMT has been shown to predict an increased sensitivity to alkylating chemotherapeutic agents; earlier chemotherapy could serve to improve an unfavorable natural history in tumors with MGMT methylation [291].

The DNA-repair enzyme MGMT inhibits the killing of tumor cells by alkylating agents. MGMT activity is controlled by a promoter; methylation of the promoter silences the gene in cancer, and the cells no longer produce MGMT. Methylation of the MGMT promoter is related to the responsiveness of the gliomas (primary central nervous system tumour) to alkylating agents; research studies were conducted on clinical patients with gliomas treated with carmustine (1,3-bis(2-chloroethyl)-1-nitrosourea, or BCNU).

The MGMT promoter was methylated in gliomas from 19 of 47 patients (40 percent). This finding was associated with regression of the tumor and prolonged overall and disease-free survival. It was an independent and stronger prognostic factor than age, stage, tumor grade, or performance status. Hence, methylation of the MGMT promoter in gliomas is a useful predictor of the responsiveness of the tumors to alkylating agents [292].

Methylation of the promoter region of the O(6)-methylguanine-DNA methyltransferase (MGMT) gene is known to be predictive of response to temozolomide treatment in patients with glioblastoma [294]. Little is known about variations in the methylation status of the MGMT promoter after temozolomide treatment or across different regions of the same tumor. A study about the variation in the methylation status of the MGMT promoter after this treatment or across different regions of the same tumor suggests that variation in MGMT promoter methylation can occur within the same tumor, necessitating caution in clinical decision-making based on this analysis [294].

A study conducted in these days relates on MGMT activity in primary and recurrent glioblastomas of patients who received radiation therapy (RT) or RT plus chemotherapy with alkylating agents (temozolomide, chloroethylnitrosoureas). The data revealed a threshold of MGMT expression below which patients respond better to alkylating agents. Therefore, determination of MGMT activity in the primary tumor appears to be useful in predicting the outcome of glioblastoma therapy [295]. Other investigations revealed that MGMT immunoexpression predicts responsiveness of pituitary tumors to temozolomide therapy [296].

In general, the use of triazene compounds for clinical approaches (i.e. dacarbazine and temozolomide) and their mechanism of action related to DNA repair systems were recently well described in literature [298]. Triazene compounds have excellent pharmacokinetic properties and limited toxicity. Dacarbazine requires hepatic activation whereas temozolomide is spontaneously converted into active metabolite in aqueous solution at physiological pH. Moreover, temozolomide is fully active when administrated orally (100% bioavailability) [298].

Recent published articles conclude that MGMT is widely expressed in primary neuroblastoma tumors, and is a relevant therapeutic target in neuroblastoma. Both in vitro and in vivo studies suggest inactivation of MGMT with O(6)-benzylguanine may increase the activity of temozolomide against neuroblastoma [299].

Epigenetic silencing of the MGMT by promoter methylation compromises DNA repair and has been associated with longer survival in patients with glioblastoma who receive alkylating agents. Patients (206 cases) with glioblastoma containing a methylated MGMT promoter benefited from temozolomide, whereas those who did not have a methylated MGMT promoter did not have such a benefit [300-301].

The above citations reveal the potentiality which could possess a biosensor able to measure variations of MGMT in glioblastoma samples, representing a key factor in temozolomide treatment.

MGMT activity is also involved in positive studies on the treatment of lung cancer as a DNA repair gene [302], and in vitro studies on promoted methylation during Human Papilloma Virus (HPV-16, HPV-18) induced by cervical carcinogenesis [303, 304]. MGMT activity is also frequent in human oral cancer cells [305].
A recent clinical study, reported among Singapore Chinese, investigated the role in colorectal cancer, due to mutations in the colorectal lumen caused by smoking and alcohol drinking, of single-nucleotide polymorphisms in MGMT (Leu (84) Phe). This research conducted on 310 cases (180 colon, 130 rectum cancer) revealed, in the case of colon cancer a positive association of PARP (codon 940 Lys/Arg and Arg/Arg genotypes and colorectal cancer risk, and an inverse association between the MGMT codon 84 Leu/Phe or Phe/Phe genotypes and colon cancer risk, but not rectal cancer [293].
On the other side, on a population based San Francisco Adult Glioma study, associations between XRCC1 Arg399Gln, MGMT Leu(84)Phe, and MGMT Ile(143)Val polymorphisms with glioma risk was evaluated. No evidence of an association between XRCC1 genotypes and glioma was found. Instead, a weak positive association for the MGMT Leu(84)Phe polymorphism (Leu or Phe/Phe versus Leu/Leu) and the MGMT Ile143Val polymorphism (Ile or Val/Val versus Ile/Ile) was found [297].
In general MGMT expression has been found to be drastically inferior in carcinogenic tissue compared to normal values measured on healthy tissue on pateints [310, 311].
It is now evident that the realisation of a device able to estimate in cellular extracts the concentration of mRNA sequence that codifies for MGMT is of a primary importance.

2.5.1 Three dimensional structure of MGMT protein

Human O(6)-alkylguanine-DNA alkyltransferase (AGT), which directly reverses endogenous alkylation at the O(6)-position of guanine, confers resistance to alkylation chemotherapies and is therefore an active anticancer drug target [312].
Crystal structures of active human AGT and its biologically and therapeutically relevant methylated and benzylated product complexes reveal an unexpected zinc-stabilised helical bridge joining a two-domain alpha/beta structure. An asparagine hinge couples the

active site motif to a helix-turn-helix (HTH) motif implicated in DNA binding. The reactive cysteine environment, its position within a groove adjacent to the alkyl-binding cavity and mutational analyses characterize DNA-damage recognition and inhibitor specificity, support a structure-based dealkylation mechanism and suggest a molecular basis for destabilization of the alkylated protein. These results support damaged nucleotide flipping facilitated by an arginine finger within the HTH motif to stabilize the extrahelical O(6)-alkylguanine without the protein conformational change originally proposed from the empty Ada structure. Cysteine alkylation sterically shifts the HTH recognition helix to evidently mechanistically couple release of repaired DNA to an opening of the protein fold to promote the biological turnover of the alkylated protein (Fig. 2.35).

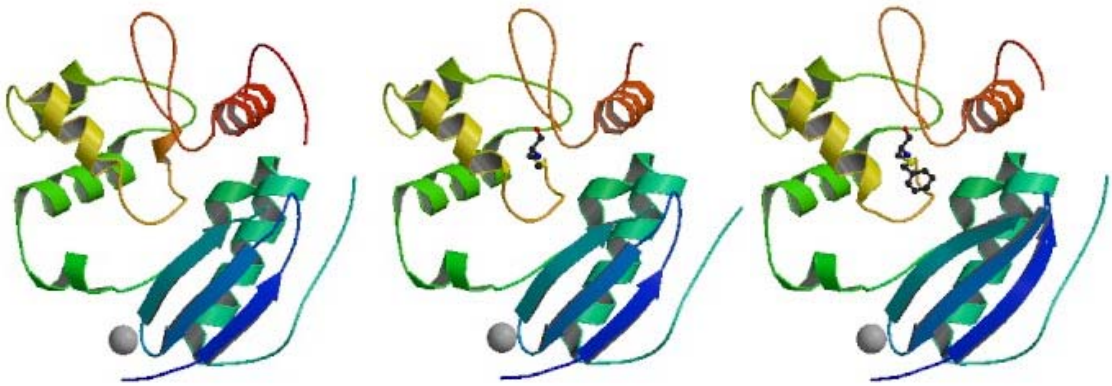

Figure 2.35 Human O6-alkylguanine methyltransferase (left), methylated human O6-alkylguanine-DNA alkyltransferase (middle) and benzylated human O6-alkylguanine-DNA alkyltransferase structures determined by X-ray diffraction (Daniels, Tainer et al.). Image source is Protein Data Bank.

In 2004, a study evidence of DNA binding and nucleotide flipping by the human repair protein MGMT was determined by X-ray diffraction (Fig. 2.36, left).

As mentioned above, O(6)-alkylguanine-DNA alkyltransferase (AGT), or O(6)-methylguanine-DNA methyltransferase (MGMT), prevents mutations and apoptosis resulting from alkylation damage to guanines. AGT irreversibly transfers the alkyl lesion to an active site cysteine in a stoichiometric, direct damage reversal pathway. AGT expression therefore elicits tumour resistance to alkylating chemotherapies, and AGT inhibitors are in clinical trials. The structures of human AGT in complex with double-stranded DNA containing the biological substrate O(6)-methylguanine or crosslinked to the mechanistic inhibitor N(1),O(6)-ethanoxanthosine is reported in literature.

The prototypical DNA major groove-binding helix-turn-helix (HTH) motif mediates unprecedented minor groove DNA binding. This binding architecture has advantages for

DNA repair and nucleotide flipping, and provides a paradigm for HTH interactions in sequence-independent DNA-binding proteins like RecQ and BRCA2. Structural and biochemical results further support an unpredicted role for Tyr114 in nucleotide flipping through phosphate rotation and an efficient kinetic mechanism for locating alkylated bases [200].

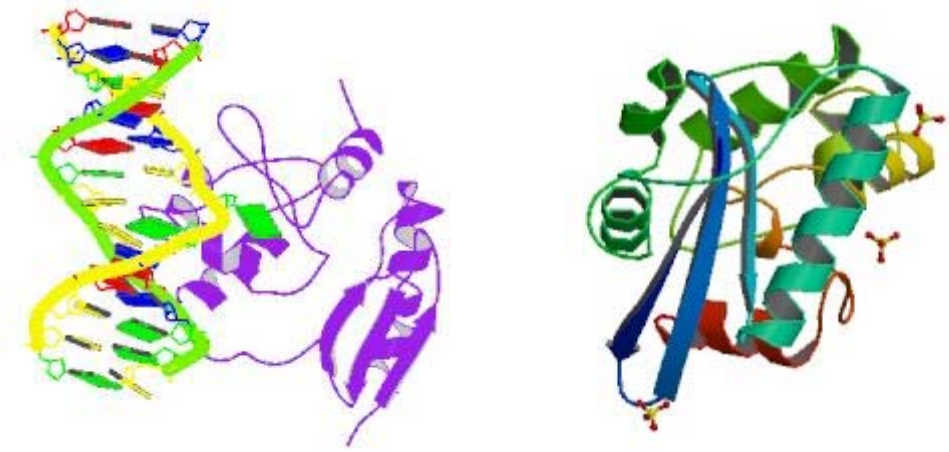

Figure 2.36 Left: Human O6-alkylguanine-DNA alkyltransferase bound to DNA containing O6-methylguanine. Right: Crystal structure of O6-methylguanine-DNA methyltransferase from hyperthermophilic archaeon Pyrococcus Kodakaraensis strains KOD1 (Pk -MGMT).

Another published work is in literature about crystal structure of MGMT and it was accomplished on Archaea, a group of prokaryotic and single celled microorganisms. Archaea are similar to bacteria but these two groups evolved differently, and are classified as different domains in the three-domain system. A single individual or species from this domain is called archaeon, while the adjective is archaeal or archaean. The etymology is greek meaning “ancient things”.

In particular, the crystal structure (Fig. 2.36, right) of O6-methylguanine-DNA methyltransferase of hyperthermophilic archaeon Pyrococcus Kodakaraensis strain KOD1 (Pk -MGMT) was determined by single isomorphous replacement method with anomalous scattering (SIRAS) [201].

The archaeal protein is extremely thermostable and repairs alkylated DNA by suicidal alkyl transfer from guanine O6 to its own cysteine residue. Archaea constitute the third primary kingdom of living organisms, sharing characteristics with procaryotic and eucaryotic cells. They live in various extreme environments and are thought, as previously mentioned, to include the most ancient organisms on the earth. Structural studies on hyperthermophilic archaeal proteins reveal the structural features essential for

stability under the extreme environments in which these organisms live, and will provide the structural basis required for stabilizing various mesophilic proteins for industrial applications. The crystal structure of Pk-MGMT and structural comparison of Pk-MGMT and methyltransferase homologue from Escherichia coli (AdaC, C-terminal fragment of Ada protein) was reported. Analyses of solvent-accessible surface area (SASA) reveals a large discrepancy between Pk-MGMT and AdaC with respect to the property of the ASA. In the Pk-MGMT structure, the intra-helix ion-pairs contribute to reinforce stability of alpha-helices. The inter-helix ion-pairs exist in the interior of Pk-MGMT and stabilize internal packing of tertiary structure. Furthermore, structural features of helix cappings, intra and inter-helix ion-pairs are found around the active-site structure in Pk-MGMT [201]. Therefore, archaeal protein is a suicidal enzyme able to remove O6-guanine repairing DNA and transferring the alkyl group from DNA to its cysteine.

2.5.2 Idea of a device able to quantify mRNA for MGMT

Research to obtain an optical biosensor for MGMT derives from this overall idea.
RNA interference (RNAi) by double strand formation (RNA/RNA) of molecules of approximately 25-30 nucleotides, represent a modern solution to regulate the expression of a protein. This mechanism is called the short interfering method (siRNAs) and is a powerful way of preventing the expression of a particular gene [306]. This means that the specific base-pairing of ribonucleic acids can be usefully adopted for RNA biosensing. Hence, the idea of the synthesis of RNA probes by virtue of their more stable pairing to target (RNA/RNA duplexes) rather than DNA probes (DNA/RNA duplexes) was planned. In particular, for the design of oligonucleotidic bioreceptor probes, the stability of the duplex, the conformational accessibility (favourable for probe binding), and the absence of any recurrence in other known transcribed sequences (uniqueness) must be considered. As previously mentioned, sequences of mRNA encoding for human MGMT were chosen.
With the aim to assemble a RNA biosensor for MGMT, particular attention was focused on the bioreceptor and on its integration with the surface of the transducer. Starting from a computational selection of targets, complementary probe sequences were derived and synthesised. During the automated synthesis, some chemical modifications were introduced in order to confer resistance against RNA-ase to probes, increased binding

strength and anchoring ability, useful for conjugation to the sensing surface for the realisation of the optical mRNA biosensor. In addition, to overcome the extreme sensitivity of native RNA oligonucleotides to chemical and enzymatic hydrolyses, 2'-O-methyl modified RNA monomers were used. In fact, they had been previously recognised to produce 2'-O-methyl RNA able to survive ribonucleases and alkali attack [307, 308]. Syntheses were performed on a DNA synthesiser and in order to evaluate the resistance of the probes to nucleases, different tests were conducted in serum, and then compared with experiments using unmodified RNA oligonucleotide. They were finally analysed for integrity by acrylamide gel electrophoresis (SDS-PAGE) as reported in literature [309]. The results of these experiments demonstrated good stability of the modified RNA compared with the unmodified one.
The modified RNA was suitable and stable and could be immobilised and used as bioreceptor.

2.5.3 The selection of RNA probes and targets

The priorities in probe preparation were high selectivity and good affinity for the desired target, in order to make a stable duplex without interference and spurious hybridisation with non-target nucleic acid sequences. In order to prepare such probes, a study of folding of the target mRNA molecule was necessary. More generally, the folding of RNA is an unimolecular process occurring spontaneously in the cell and depends on the thermodynamics of pairing between complementary stretches of different regions of the RNA sequence and produces a number of secondary structures [315, 316].
There are computer algorithms, based on energy minimisation, able to predict secondary structures of RNA sequences and their sources of thermodynamic parameters are continuously improving [317]. A recent study [318] describes an "in silico" strategy to detect suitable targets within a given mRNA sequence to be used for hammerhead ribozyme design [319]. Such a computational method was exploited for selecting accessible regions in the human MGMT transcript and planning our probes. The program analyses the score of pairing events among the different structures nucleotide by nucleotide (the freedom of each nucleotide), considering the probability of existence of each structure. On these bases, for each sequence of desired length, an algorithm gives the accessibility score (AS) which was a basic parameter for selecting our target strings

[318]. All sequences of the MGMT transcript were classified [320] in four accessibility classes according to their accessibility score (see Table 2.4).

Probe	Length (nucleotides)	Position	Access. (%)	Self-struct. ΔG (kcal/mol)	T_m (°C)	ΔT_m (°C)
7	**25**	**101–125**	**63.6**	**−0.4**	**73.57**	**29.39**
27	25	141–165	64	−2.1	84.77	6.33
36	25	285–309	60	−4.5	82.26	13.03
42	25	291–315	64	−4.6	83.53	19.17
43	25	292–316	68	−4.2	82.53	18.17
44	25	293–317	68	−4.2	82.38	16.72
45	25	294–318	68	−4.2	82.62	16.96
46	**25**	**295–319**	**68**	**−4.8**	**84.05**	**18.39**
47	25	296–320	64	−4.8	86.53	15.66
48	25	297–321	60	−5.0	87.35	16.48
49	25	298–322	60	−4.4	86.59	15.72
50	25	299–323	60	−4.7	84.31	13.44
51	25	300–324	60	−4.7	82.86	11.99
52	25	301–325	60	−5.1	83.35	12.48
53	25	302–326	60	−5.6	84.23	13.36
54	25	303–327	60	−7.2	84.03	13.16
64	**25**	**420–444**	**60**	**−1.7**	**75.84**	**28.92**
38	30	293–322	60	−5.0	88.6	17.73
39	30	294–323	63.3	−5.0	88.16	17.29
40	30	295–324	66.7	−5.5	88.16	17.29
41	**30**	**294–325**	**66.7**	**−5.1**	**89.46**	**18.59**
42	30	297–326	66.7	−5.6	89.88	19.01
43	30	298–327	66.7	−6.9	89.28	18.41
44	30	299–328	63.3	−7.0	88.14	17.27
45	30	300–329	60	−7.0	86.89	16.02

Table 2.4 Main features of a set of potential probes for MGMT mRNA. All these putative probes are complementary to accessible regions of target mRNA (accessibility > 60%). For each probe six characteristics are shown: length, position of the complementary sequence in the mRNA sequence, accessibility, Gibbs energy of the self-structuring of probe, melting temperature (T_m) of the target-probe duplex and difference between the T_m of the correct duplex and the T_m of the most stable incorrect one. The most favourable ones are highlighted in bold. [320]

The sequences were then evaluated for their pairing energy ΔG° using the Nearest Neighbour Nucleotide algorithm at standard conditions (25°C, 1 atm). Once the most accessible target sequences and their pairing energy suitable for probe binding were evaluated, the uniqueness of each target among the entire human known trascriptome was checked. Partial homologies between the target sequence and other unwanted mRNA sequences were searched. A homology threshold value of 70% was imposed and the partially homologous sequences which passed the limit were evaluated for their affinity towards the selected probes. The melting temperature (T_m) of these mismatched duplexes was then calculated and compared with the T_m of the correct duplex. The resulting ΔT_m expresses the difference in melting temperature between the correct duplex and the most stable of the incorrect ones. The higher ΔT_m corresponds to the most selective binding between the probe and its target. Probe sequences displaying a ΔT_m for mismatched duplexes under a threshold of 10°C were discarded. This gap in temperature can be exploited to reach stringent conditions. Increasing the temperature above the T_m of the

incorrect duplex but below the denaturing temperature of the right hybrid causes a selective detachment of unwanted sequences [320].

Finally the evaluation of the thermodynamic properties of each selected probe was also performed in order to evaluate the tendency of the probes to intra-molecular pairing.

For each potential probe the $\Delta G°$ of *self-structuring* was calculated and probes with high negative values were discarded. In Table 2.3 a set of potentially active probes (accessibility of the target sequence $\geq 60\%$) is reported and each probe is described by an identification number, by the position of its complementary sequence in the MGMT transcript and by a set of values corresponding to different criteria of the selection method. The probes selected according to this computing method, synthesised and employed in these experiments [320].

The final choice of these probes was done by in collaboration with the group Pisa based on a compromise between different criteria. For probes 7 and 64 uniqueness and absence of self-structuring were preferred, while in choosing probe 46 and 41, accessibility was the leading criterion and $\Delta G°$, T_m and ΔTm the auxiliary ones.

In particular, in this thesis an experimental study on a new optical platform of hybridisation interactions between probe 7 and probe 46 (bioreceptor) with their respective complementary RNA sequences was investigated.

2.5.4 Biosensor for mRNA

The plan was to realise an assay for the development of a RNA biosensor able to detect hybridisation between RNA probes (25 nucleotides) and RNA complementary targets. For this purpose, a sequence of oligonucleotide that mimics the complementary sequence of mRNA for the protein MGMT was selected to be used. Hence, the bioreceptor will be a probe for RNA, complementary to the mRNA sequence, which was opportunely realised by means of DNA synthesiser and chromatography purification.

For the measurements, a flow channel was designed and prepared containing the chain of synthetic RNA complementary to the target RNA by which measurements could be carried out to establish the RNA/RNA interactions.

When hybridisation occurs and an opportune detection of the target is realised, a further step based on RNA/RNA duplex interaction can be performed. In the first step the

bioreceptor (probe) is covalently attached to the internal wall of a transparent flow channel (Fig 2.37, top).

In the second step the RNA target is inserted in the flow channel and the RNA/RNA hybridisation takes place (Fig. 2.37, middle).

In the third step (Fig. 2.37, bottom) an oligo probe opportunely planned and synthesised flows into the channel to obtain a second hybridisation with the accessible free parts of the mRNA previously linked to the bioreceptor. The second oligo probe, labelled with a fluorophore, is then introduced at known concentration, so that a fluorescence signal is observed which is dependent on the mRNA present.

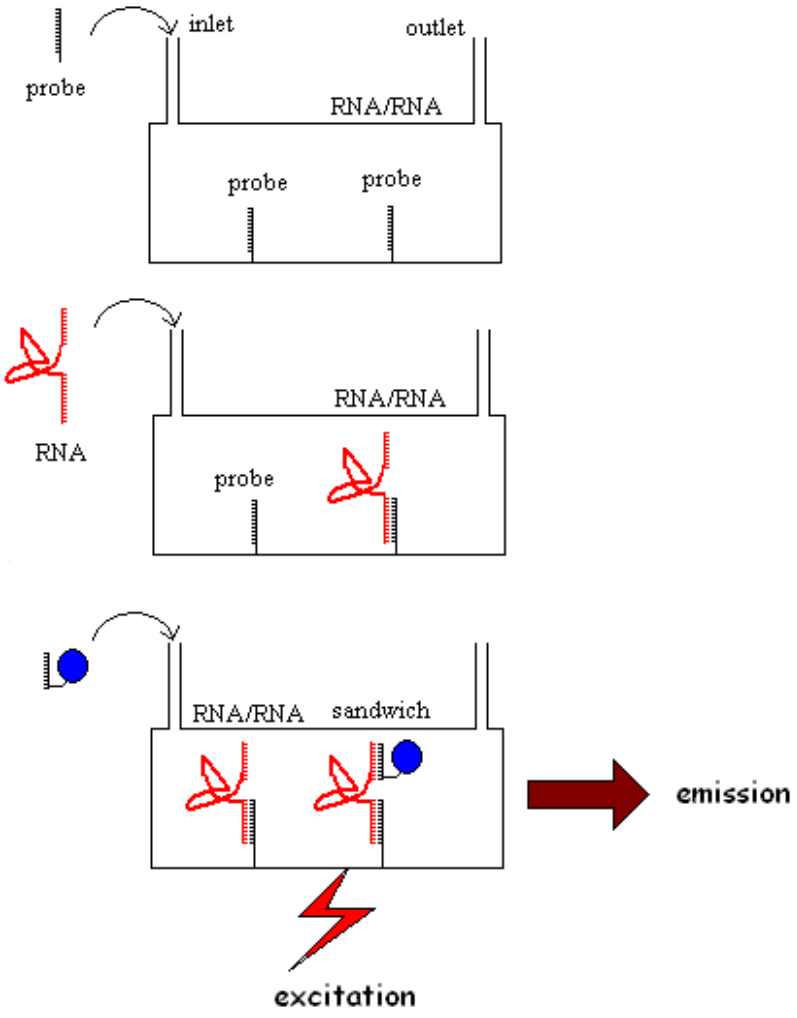

Figure 2.20 Three-step operation for the optical biosensor for mRNA. Top: RNA is immobilised on the wall of the flow channel; middle: RNA/RNA duplex hybridization takes place. Bottom: a second probe of Cy5-labeled RNA, complementary to a second target of mRNA, hybridizes the free part of mRNA enhancing the fluorescence signal.

2.5.5 Commercial kits available for MGMT

Only one type of detection kits able to determine MGMT protein is available on the market and is sold by Sigma-Aldrich ^{TM}. Sigma's MGMT assay kit is based on the formation of a new restriction site in a 23-mer ^{32}P labeled ds-oligonucleotide after removal of the O6-methyl-guanine lesion. Cleavage of the new restriction site results in two smaller oligonucleotides that can be resolved on a denaturing SDS-PAGE gel.

This assay is based on a radioactivity method that utilizes ^{32}P, an isotope of phosphorus, beta-emitter, primarily used to produce radiolabeled DNA or RNA probes for use in Northern or Southern Blot. Because the high energy beta particles produced by penetrate skin and corneas, and because any ^{32}P ingested, inhaled, or absorbed is readily incorporated into bone and nucleic acids, Occupational Safety and Health Administration requires that a lab coat, disposable gloves, and safety glasses or goggles be worn when working with ^{32}P, and that working directly over an open container be avoided in order to protect the eyes. Monitoring personal, clothing, and surface contamination is also required. In addition, due to the high energy of the beta particles, shielding this radiation with the normally used dense materials (e.g. lead), gives rise to secondary emission of X-rays via a process known as Bremsstrahlung, meaning braking radiation. Therefore shielding must be accomplished with low density materials, *e.g.* Plexiglas, Lucite, plastic, wood, or water (http://www.oseh.umich.edu/TrainP32.pdf).

All these precautions represent an awful, tedious limit for MGMT detection; moreover this dangerous labour requires specialised human handling.

The research to obtain a novel clean and economic method based on fluorescence for sensing mRNA codifying in MGMT protein represents a challenge for the actual standard of measurements.

3. AIMS & OBJECTIVES

This thesis consists in the realisation of optical affinity biosensors based considering all the scientific aspects mentioned in the Introduction-part of this thesis.
The aim is the obtainment of an optical biochip able to detect several biological parameters in a multianalyte optical setup.
In the multidisciplinary path of this work the aim is the design, hence the realization of a modern device, the fluorescence enhanced optimization of its performances and the miniaturised setup which will combines optics and microfluidics based on it.
Optical sensors able to detect pH and antigen-antibody affinities have to be obtained in order to investigate the better performances gathered from the results changing chemical reactants and optical properties.
This experimental knowledge will be directly applied into the biochip system.
After that, it will be possible to start investigations on the immobilization of short sequences of DNA and RNA to the substrate.
When those will be properly reached the DNA and RNA bioreceptors will be able to detect rispectively:

- The transcription factor (NF-kB) by DNA/NF-kB binding.
- The mRNA sequence that codify in MGMT protein by RNA/mRNA binding.

Several chemical treatments of the surfaces have to be properly investigated in order to obtain the most effective chemical deposition of an hydrophilic substrate which will represent the “floor” for the attachement of proteins, DNA and RNA.
A key objective is to find the appropriate polymer to obtain a reproducible surface enhanced for the fluorescence measurements.
Several steps are considered in the obtainment of the biochip;
as first, a sensor for pH made by immobilizing pH fluorescent dyes on a receptor channel will be considered and an optimisation of the maximum fluorescence intensity will be set up.
Secondarily, an immunoassay for immunoglobulins Ig will be investigated contributing useful informations on the best chemical-physical conditions which will determine a proper coverage of bioreceptors on the transduction surface area.

This represents in fact a critical issue. An objective is the improvement in the sensitivity of the system until a linear range from 1 ng/ml to 1mg/ml covering with IgG the bioreceptor channel and measuring the anti-IgG diluted in buffered solutions.
Further chemical treatments must be considered and the deposition of the polymers selected has to be compared to detect the most effective one.
The deposition method of the polymer should be well considered because is crucial for reproducible sensing. The concentration of the chosen polymer in its solvent must keep integral the optical transparency. The polymer must possess chemical ON/OFF properties in the sense that activation of chemical groups on the surface (ON) and inactivation of these groups on the surface (OFF) can be selected.
Finally, the chemical nature of the polymer have to combine transparency, dissolution in a low temperature solvent, low cost, reproducibility, reliability.
Reuse of the biosensor or reuse of the substrate will depend on the configuration adopted and will be extremely useful to provide an easy-handling solution for the user.
The reuse of the biosensor will imply that the substrate has to be sterilised properly without the need of a heating procedure. This, in fact, could be detrimental for the biosensing activity and for the optical transparency.
On the other side, the reuse of the substrate will depend on the total remove of the bioreceptors immobilised and consequently on its sterilisation. If the substrate is not more usable because, for example, it lost its optical properties, it becomes waste material. Fortunately, transparent substrates are made of recyclable materials such as plastic or glass.
The measurement of the affinity biosensors, the identification of the protocol bioassays and the design and characterisation of the optical platform was mainly held in the Institute of Applied Physics at National Research Council (IFAC-CNR), Firenze, Italy.
The biochemical aspects devoted to the design and synthesis of the chemical components for the realisation of affinity biosensors able to detect and quantify antigens, transcription factors and RNA sequences is carried out in collaboration with the Institute of Clinical Physiology at the National Research Council (IFC-CNR), in Pisa, Italy.
AFM Imaging and deposition studies of the surfaces were experimentally carried out in the Biomedical Department in Cranfield Health, Cranfield University, Silsoe, UK.

4. MATERIALS AND METHODS

4.1 pH sensing of fluorescein solutions in glass capillary

Optical setup:

A silica glass capillary was firstly used as flow chamber to detect a fluorescence signal of dyes dissolved in buffer pH solutions. Dimensions of the capillary are: 127 mm in length, 1 mm in external diameter and 500 μm in internal diameter. Inner volume is 10 μl. Bare capillaries were purchased from Drummond Scientific Company, Broomall, PA, U.S.A. Multimode optical fibres (200 μm glass core diameter) were purchased from Polymicro Technologies, Phoenix, Arizona, United States. These fibres were used to transport the optical signal from the excitation source to the biosensing layer and the fluorescent signal from the biosensing layer to a detector. SMA connectors were used for the optical coupling. The method consisted in to couple the capillary with a system of optical fibres able to interrogate the sensing layer in absorbance and fluorescence modes (Figure 4.1).

A tungsten white lamp was used as source in the absorbance mode to detect absorption of immobilised dyes. A blue LED with a 490 nm peak was employed as a source in the fluorescence mode, and was firstly coupled at the input with low pass (LP) filters 480 nm or with one band-pass (BP) filter at 488 nm, set between the source and the sensing layer. Output filter BP at 525 nm and a high-pass HP filter at 546 nm were considered too.

A led source was preferred to an Argon laser because it provided a miniaturized and cheap solution for prototype engineering. A fibre optic spectrometer (S2000) with a wavelength range of 300-900 nm was used as detector and it was purchased from Ocean Optics Inc., Dunedin, FL, United States.

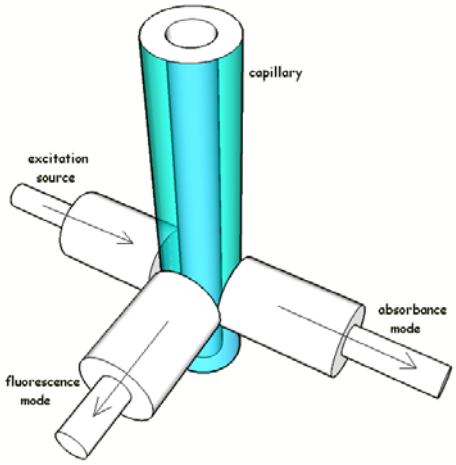

Figure 4.1 Detail of the interface between the capillary and the optical fibres.

Chemical protocols:

Six buffers at different pH were prepared mixing, pure water, citric acid ($C_6H_8O_7$), disodium hydrogen phosphate (Na_2HPO_4), and potassium chloride (KCl) following McIlvaine protocol. Solvents and salts were purchased by Sigma, St. Louis, MO, U.S.

McIlvaine pH buffers were prepared at 1 M of ionic strength in accord with Table 4.1.

pH	g / liter	g / liter	Buffer system Ionic	KCl added g / liter of solution to produce IS of:	
T= 25°C	Na_2HPO_4-12$H_2$0	$H_3C_6H_5O_7$-$H_2$0	strength(IS)	1 M	0.5 M
4.6	33.4	11.2	0.2100	58.9	21.6
5.4	40	9.29	0.3020	52.1	14.8
6.0	45.2	7.74	0.3440	48.9	11.6
6.6	52.1	5.72	0.3850	45.8	8.5
7.2	62.3	2.74	0.4570	40.4	3.1
8.0	69.6	0.59	0.5590	32.9	0.0

Table 4.1. McIlvaine protocol for buffers at different pH.

Fluorescein sodium salt was dissolved in the buffers in a range between 10^{-4}-10^{-9} M to set a preliminary session of pH measurements.

Fluorescein sodium salt was dissolved in a buffer pH 8 to set the measurement for calibration curves.

Fluorescein sodium salt was purchased from Sigma-Aldrich, Riedel de Haen.

For all the experiments a peristaltic pump model Minipuls 3, with a four channel pump head, was used and purchased from Gilson, Middletown, WI, United States.

Tygon tubes, with an internal diameter of 1.02 mm, were purchased from Saint Gobain. Flow speed used in these experiments was 10 μl/min.

4.2 pH sensor in glass capillary

First optical setup:

Silica glass capillary was used as substrate for the immobilisation of fluorescent dyes and as flow chamber to detect a fluorescence signal of dyes dissolved in buffer pH solutions. A tungsten white lamp, coupled via SMA connector with an optical fibre multimode, was used as source in the absorbance mode to detect absorption of immobilised dyes. For fluorescein derivatives a blue LED at 490 nm was employed as a source in the

fluorescence mode. This light source was coupled to a band-pass (BP) filter at 488 nm, set in entrance (source-sensing layer), and a BP filter at 525 nm, set in output (sensing layer-detector). These filters were purchased from Andover Corporation, Salem, NH, U.S. For cyanine derivatives a red LD at 635 nm, 3 mW output power (Hitachi-HL6314MG) was the main source employed in IgG/anti-IgG biosensing.

BP filter, at 635 nm was set in entrance (source-sensing layer) and a high-pass (HP) filter, cut-on at 650 nm was set in output (sensing layer-detector).

These filters were purchased from Thorlabs, Munich, Germany.

Second optical setup:

A second optical system configuration was studied to improve signal to noise ratio.

This was based on a glass capillary coupled with a second fused silica capillary 450 μm fixed using epoxy glue. A PVC sleeve allowed two optical fibres, 200 μm in core diameter, to be located facing the capillary section. The two fibres were interfaced to a double detector system. (Figure 4.2)

As detectors, a fibre optic spectrometer (S2000) with a wavelength range of 300-900 nm (Ocean Optics) and a photomultiplier tube (PMT) connected to a frequency photon counter (PicoQuant 2006) were used.

Transversal excitation with a blue light emitting diode (490 nm) and a filter BP-488 was employed for fluorescein derivatives, whereas a red diode laser source (635 nm) was used for cyanine derivatives.

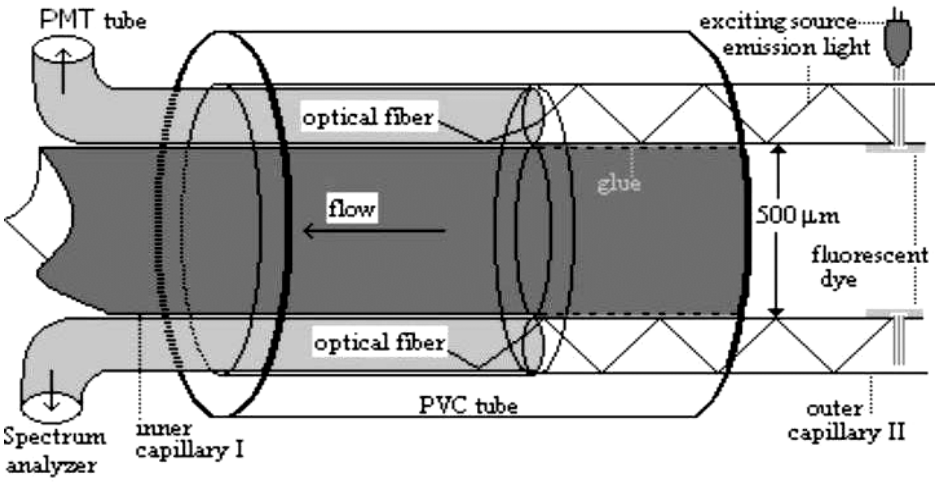

Figure 4.2. Second configuration used to improve the optical efficiency of the system. The dye was immobilised inside a capillary which was used as waveguide to capture the fluorescence signal by coupling with two optical fibres on a photomultiplier tube and on a spectrophotometer.

Chemical protocol:

Activation of the glass surface of capillaries was obtained with sulphuric acid (H_2SO_4), and hydrogen peroxide (H_2O_2, 3:1 v/v). After 1 hour the capillary was rinsed with water.

Modification of the internal wall of the capillary was achieved by filling the capillary with APTES in EtOH (30:70 v/v).

The capillary was kept overnight in the oven at 80°C.

Basilar chemical protocols were considered changing the concentrations of silanes in EtOH (pure, 10%, 20%, 30%), the types of silanes (APTMS, APTES), the solvents (ethanol or methanol) and the temperature environment (25-100°C) for silanisation.

Silanes were purchased from ABCR GmbH, Karlsruhe, Germany; the solvents were purchased from Sigma, St. Louis, MO, U.S.

On exposed amino pendants, fluorescent dyes with reactive functional groups were attached by covalent bonding on the glass (Figure 4.3): fluorescein isothiocyanate (FITC), was dissolved in EtOH in a concentration of 1 mM and succinimidyl derivatives (FAM-X-SE and Cy5) were dissolved in dimethylformamide (DMF) in a concentration of 1 mM and then were inserted filling the entire capillary.

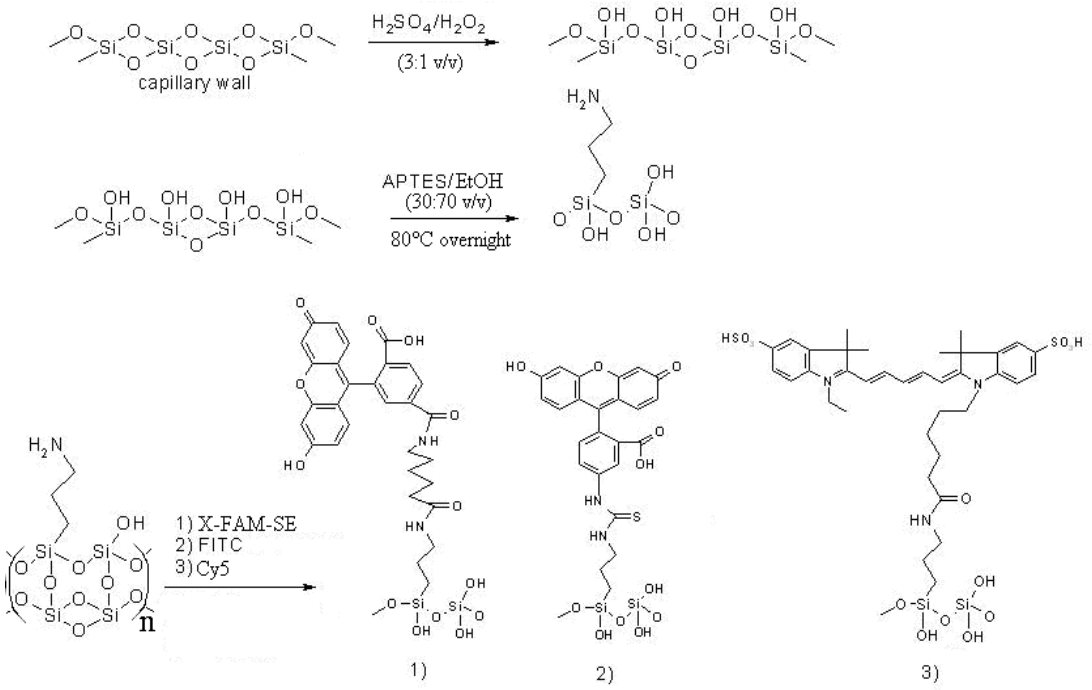

Figure 4.3 Three step reaction for the covalent binding of fluorescent dyes to the glass surface inside a capillary. In the first step the oxidation was performed using the so-called Piranha solution. In the second step silanisation of the substrate was done to obtain exposed amino groups. In the third step the fluorophores were covalently bound to the surface by condensation and peptide bond formation.

Dyes:

- Fluorescein isothiocyanate (FITC) was purchased from Sigma-Aldrich.
- 6-(Fluorescein-5-carboxamido) hexanoic acid, succinimidyl ester (5-FAM-X, SE) was purchased from Fluka.
- N-hydroxysuccinimidyl cyanine or Cy5 was purchased from Amersham Bioscience, GE Healthcare, England, UK.

These type of dye molecules possess functional groups reactive to attach primary amino groups (Figure 4.4). In the case of 5-FAM-X, SE the spacer of six atoms of carbons helps the succinimidyl group to be sterically more reactive to primary amino groups.

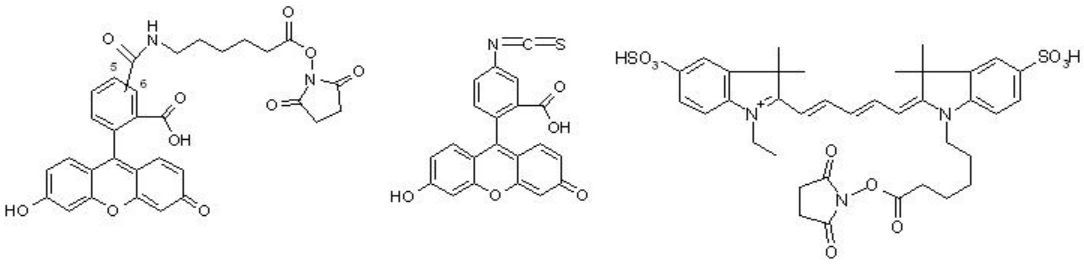

Figure 4.4 From left to right: organic structures of Fluorescein-5-(and-6)-carboxamido) hexanoic acid, succinimidyl ester 5-FAM-X, SE; Fluorescein isothiocyanate (FITC); Cyanine 5-N-pentil-succinimidyl ester (Cy5).

Optical spectra of fluorescein and cyanine derivatives were obtained from literature [332]. Optical behaviour of the fluorophores involved in the experiments are summarized in Figure 4.5 where normalized absorption and fluorescence are reported.

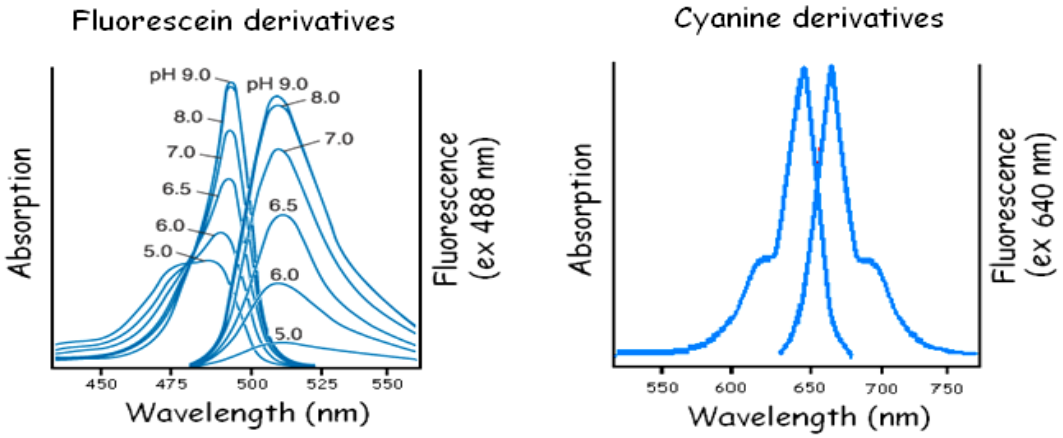

Figure 4.5 Absorbance and emission spectra of fluorescein and cyanine derivatives from literature [332]. In the case of fluorescein it is possible to note a fluorescent pH dependence.

4.3 pH sensor in PMMA chip

Optical setup:

A second transparent substrate, the PMMA biochip, was obtained from a 3 mm-thick planar slide by mechanical processing. The chip consisted of four channels, obtained by combining two pieces: the lower part, which included the four micro-channels and the inlet and outlet for the fluidics (Figure 4.6a), and the upper part, on which the sensing layer was immobilised (Figure 4.6b). The dimensions of a single flow-channel were: 0.5 mm wide, 0.4 mm high and 18 mm long. The model engineering of this innovative prototype for an optical multichannel chip made in PMMA was carried out at IFAC-CNR, Firenze, Italy, and realised in collaboration with DATAMED S.r.l., Milan, Italy.

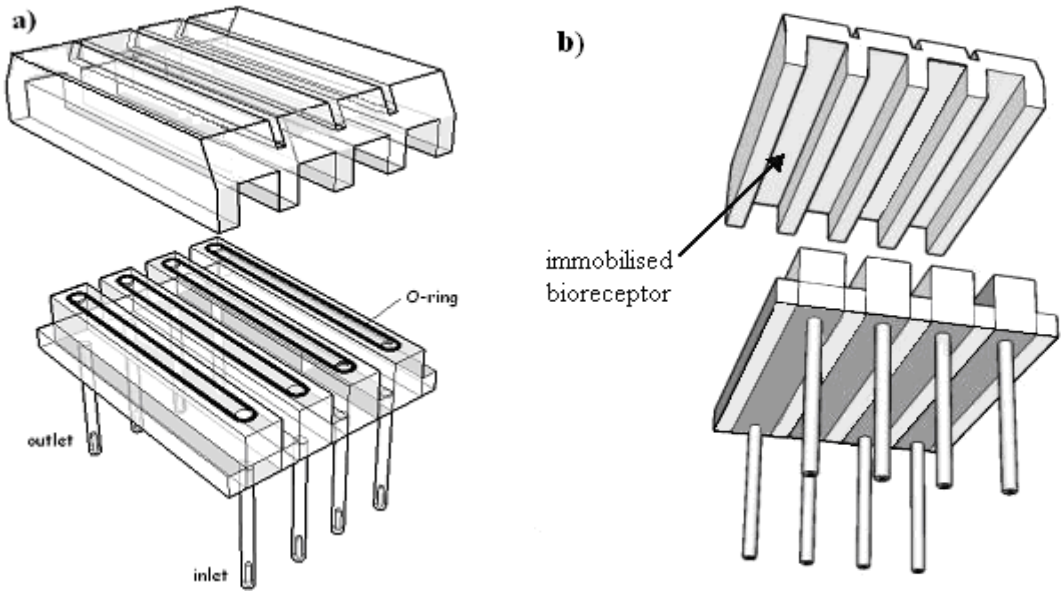

Figure 4.6 a) Top view of PMMA multi-channel chip. b) Bottom view where is shown a single channel surface in which a bioreceptor is immobilised.

The dimensions of a single flow channel were: 0.5 mm wide, 0.4 mm high and 18 mm long. The longitudinal cross section of the flow cell is clearly illustrated in Figure 4.7.

A fraction of the fluorescence emitted by the layer is guided at the end of the cover where it is collected by means of a 200 μm optical fibre. The signal was analysed using an Ocean Optics S2000 spectrometer.

The particular profile of the cover with the air gaps allowed a physical separation of the fluorescence signal coming from the different channels and each channel was optically

separated from the others. The presence of the inlet and outlet for the fluidics on the bottom of the structure facilitated the monitoring of the fluorescence which travelled inside the plastic cap along the same direction as the flow.

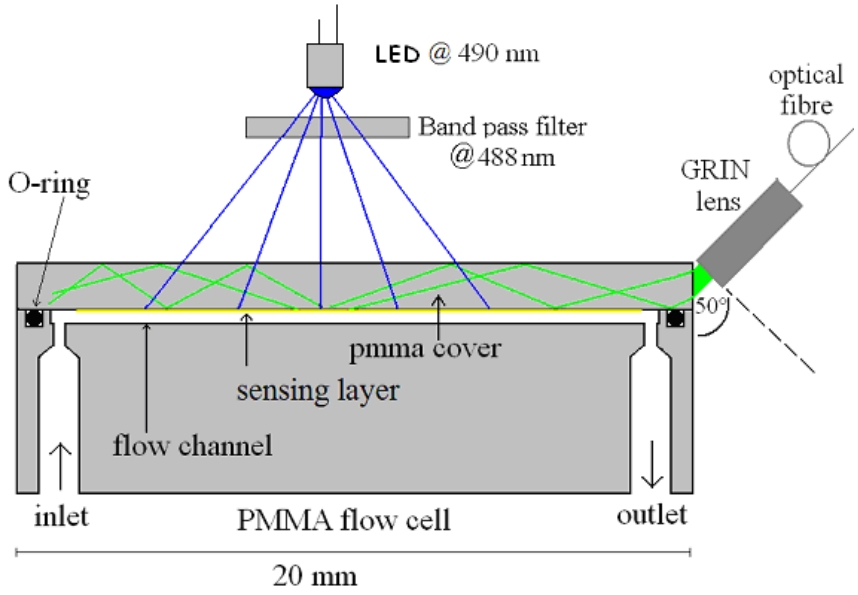

Figure 4.7 Lateral section of the PMMA chip. The cover and the flow cell, both made with PMMA, are complementary shaped. The fluorescence is guided along the PMMA cover and is collected by an optical fibre.

The realisation of the first prototype is shown in Figure 4.8a. Another image of the prototype under working conditions is shown in Figure 4.8b.

a) **b)**

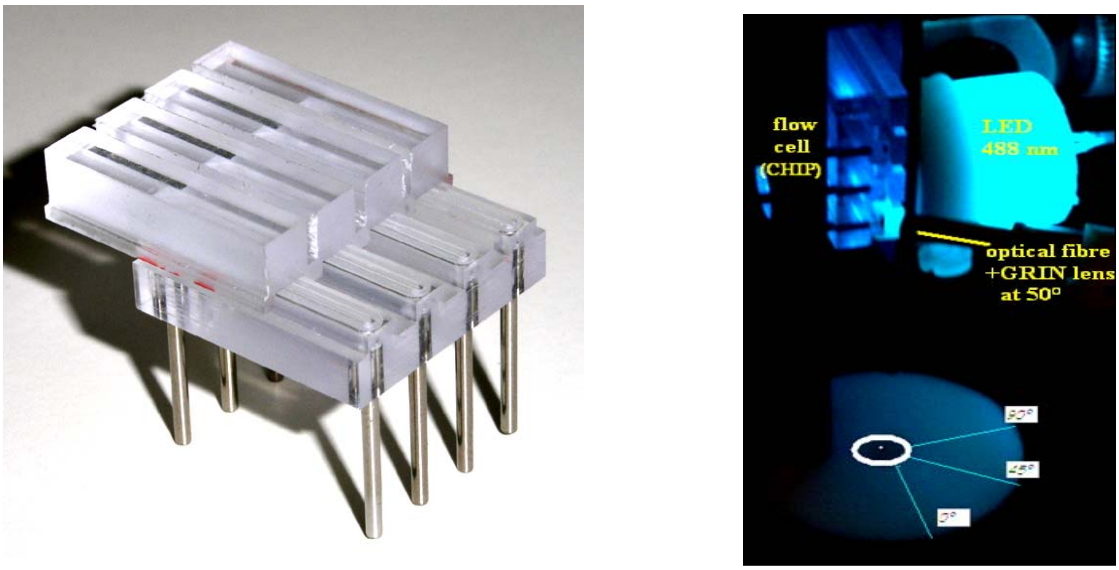

Figure 4.8 a) Image of the initial prototype biochip. b) Optical angular coupling of the LED 490 nm on a channel with a filter BP-488 with the optical fibre and GRIN lens coupled with a side face of the channel cover at an angular position of 50°.

Chemical protocol:

A copolymer of PMMA (Eudragit RL100, MW= 150000) was dissolved in EtOH at 0.1 mM concentration. Eudragit RL100 was purchased from Degussa Röhm Pharma Polymers, Essen, Germany.

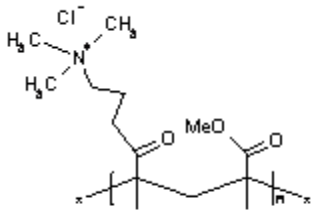

Eudragit RL100

This solution was mixed 1:1 with a solution of FITC in EtOH (1 mM). Few drops of the cocktail were dropped on the PMMA channel of the biochip.

Total evaporation of the solvent occurred at room temperature after few minutes.

The sensing surface was then rinsed abundantly with pure water.

The fluorescent layer, containing fluorescein and Eudragit RL100 was excited by led at 490 nm, with a BP filter at 488 nm.

Buffers at different pH were prepared mixing, pure water, citric acid ($C_6H_8O_7$), disodium hydrogen phosphate (Na_2HPO_4), and potassium chloride (KCl) following McIlvaine protocol. Solvents and salts were purchased by Sigma, St. Louis, MO, U.S.

McIlvaine pH buffers were prepared at 1 M of ionic strength in accord with Table 4.1.

The pH value was increased starting from pH 4.6 to pH 8.0 in six different intermediary steps and the maximum peak of fluorescence was recorded at 539 nm for more than 3 hours and changing pH concentrations every 12 minutes. Flow speed was set at 10 µl/min.

4.4 Antigen sensor in PMMA planar squares

Optical setup:

The potentiality of the PMMA chip, its ease of use and its convenient geometrical configuration for a simple replacement encouraged in-depth examination.

For this reason, a cheaper and easier preliminary substrate was thought and realised and inexpensive proteins such as IgG and anti-IgG-Cy5 were purchased and investigated.

Small squares of PMMA were used as substrates in order to identify a proper immobilisation procedure of the bioreceptor.

The research implied to find the best arrangement for an immunosensor based on interactions between IgG immobilised on the substrate and anti-IgG-Cy5 flowing in solution.

The optical setup shown in figure 4.9 was used because the results in the anisotropic angle for Cy5 were in agreement with the ones for fluorescein.

As source it was used a red DL at 635 nm, 3 mW output power (Hitachi-HL6314MG). Filters were not added for these preliminary experiments (Fig. 4.9).

Fibre optic spectrometer (S2000) with a wavelength range of 300-900 nm was used and purchased from Ocean Optics Inc., Dunedin, FL, United States.

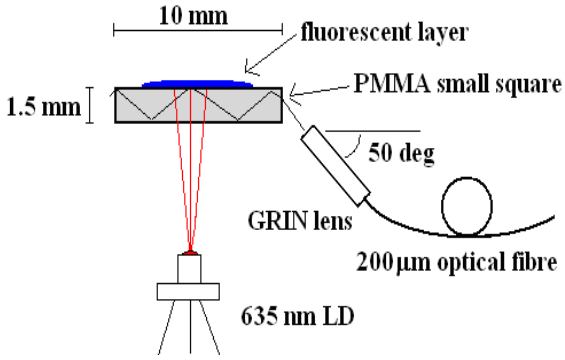

Figure 4.9 The source, a diode laser He/Ne at 635 nm, is perpendicularly directed on a PMMA square surface on which a mixture of Eudragit RL100 and cy5 was deposited. The fluorescence is guided through the channel and collected using an optical fibre.

Chemical protocol:

Large transparent plates of PMMA were cut using a CO_2 laser (2 kW) for industrial applications.

Thousands of single planar squares of size 10 mm x 10 mm x 1.5 mm were thus obtained. These squares where used as a planar configuration of the PMMA chip in order to determine the best operating conditions in the chemical treatments and to improve the optical properties.

Polymethylmetacrylate (PMMA) was purchased from RS Components, Milan, Italy.

Two different polymers were deposited on the surface:

- poly L-lactic acid (PLLA) is currently used in a number of biomedical applications, such as sutures, stents, dialysis media and drug delivery devices, but it has also been evaluated as a material for tissue engineering [336]. PLLA was

dissolved in $CHCl_3$ and then activated into a carboxyl surface by strong basic solutions (e.g. NaOH 2M). Figure 4.10 shows that PLLA is the product resulting from polymerisation of L,L-lactide (also known as L-lactide). The polymer blend

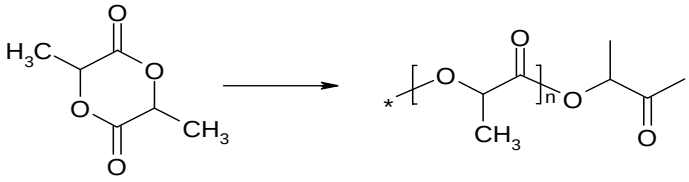

dissolved in $CHCl_3$ is perfectly transparent. PLLA was purchased from DURECT Corporation, Cupertino, CA, U.S.

Figure 4.10 Ring opening polymerisation of lactide into polylactide.

- Copolymer of PMMA (Eudragit L100) deriving from polymethylmethacrylate, possess methacrylic acid groups in their chemical structure (Figure 4.11). Eudragit L100 was dissolved in EtOH. EudragitL100 was purchased from Degussa Röhm Pharma Polymers, Essen, Germany.

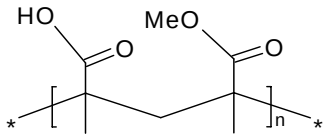

Figure 4.11 Chemical structure of Eudragit L100.

The deposition of these two polymers was compared to two direct chemical modifications of PMMA substrate, considering the idea to convert methyl esters groups of PMMA into carboxylic groups using a strong basic solution or mixtures of pyridine and water.

In summary, the PMMA surface was treated by following several protocols in order to covalently immobilise mouse-IgG through the interaction of their amino groups with carboxylic groups present on the solid support.

The carboxylic groups were obtained (Figure 4.12) by several treatments listed below:

1) Direct surface treatment with NaOH 2M in pure H_2O and in a mixture of H_2O/DMSO (1:1) for 1 hour, and then washing with deionised H_2O;

2) Direct surface treatment with pyridin/water (95:5 and 50:50 v/v) dropping the solutions on the surface for 10, 20 and 30 minutes and then rinsing with deionised water;

3) Deposition of Eudragit L100 in EtOH at different concentrations (0.001-100 mM) until the solvent had evaporated and then washing with deionised water;

4) Deposition of PLLA in $CHCl_3$ at different concentrations (0.01-10 mM) until the solvent had evaporated; then after washing with deionised water, treatment with 2 M NaOH and then further washing with deionised water.

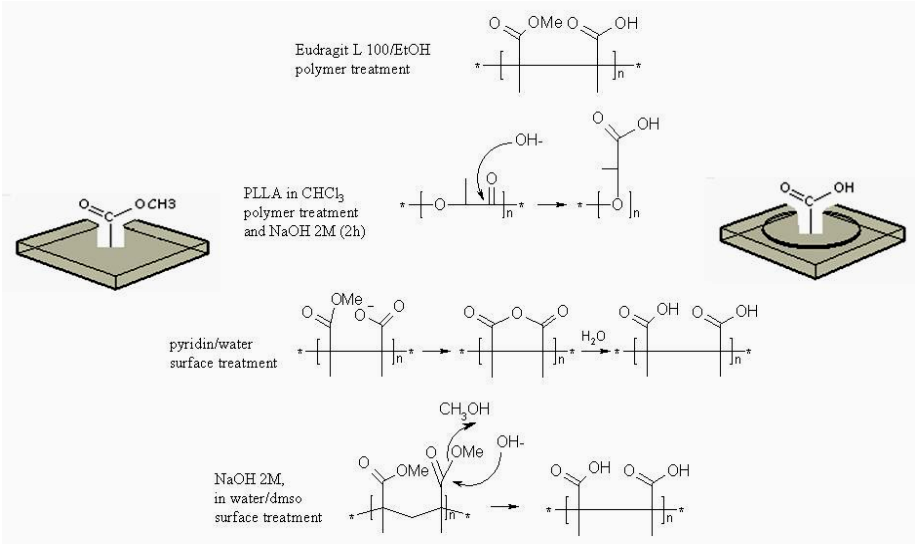

Figure 4.12 Chemical modifications of PMMA to obtain carboxylic groups. Two polymer depositions were compared to two direct surface treatments.

EDC and s-NHS were used to convert surface carboxylic groups into amino reactive NHS esters. This was accomplished by mixing s-NHS with a dehydrating agent such as the carbodiimmide EDC (Figure 4.13). EDC and NHS were dissolved in 2-morpholinoethanesulfonic acid (MES) buffer 0.1 M at pH 6.2 and dropped for 30 minutes on the carboxylic surface following protocols from Pierce. After EDC/NHS procedure, unreacted semi-stable succinimydil esters were inactivated by tris-(hydroxymethyl)-aminomethane (TRIS) buffer pH 7.4, and then washed with a phosphate buffer solution PBS (NaCl 137 mM, $Na_2HPO_4$10 mM, KCl 2.7 mM, pH 7.4). A solution of mouse IgG in PBS (50µl, 1.25 mg/ml) was then dropped on the small squares for 1 hour and the squares were washed with PBS.

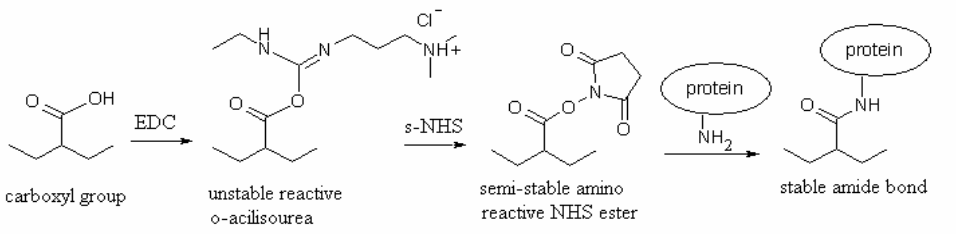

Figure 4.13 Mechanism of catalysis of EDC /s-NHS for amino covalent bonding of a protein on a carboxylic surface.

The immobilisation was then followed by incubation with antiIgG-Cy5 (1 mg/ml) for 1 hour and finally rinsing with PBS buffer to remove unreacted anti-IgG.
Mouse-IgG and goat-antimouse-IgG labeled Cy5 were purchased from Zymed Laboratories, Invitrogen Corporation, Carlsbad, CA, U.S.
The results obtained from these preliminary experiments on planar PMMA squares were applied on the four micro-channel PMMA chip.

4.5 Antigen sensor in PMMA chip

Optical setup:
The PMMA chip was modified cutting the PMMA cover channel with an angle of 30° in order to obtain a perpendicular output area of the guided fluorescence (Figure 4.14a).
Hemi cylindrical lenses made of PMMA were developed in the laboratory and positioned on the top of every single channel to improve the excitation focus in the channel thus increasing the signal (Figure 4.14b).
Graded index (GRIN) lenses, ¼ pitch, 1.8 mm diameter, were used to increase the collection area of the emitted signal and were purchased from SELFOC MicroLens, NSG Europe, Temse, Belgium.
A red DL at 635 nm, 3 mW output power (Hitachi-HL6314MG), was used as source.
The laser diode combo controller ITC 510 was purchased from THORLABS.
This instrument provides a current controller and a temperature controller in one unit. The source requires an external cooling system which was built in our labs around the diode laser and included a Peltier cell coupled with a heat sink.
A filter BP at 635 nm was set between the diode laser and the flow channel.
A second high-pass filter (> 650 nm) was set on the top of the optical fibre at the output.
A more sensitive fibre optic spectrometer (SWNIR CCD, purchased from Hamamatsu Photonics) with a wavelength range of 500-1100 nm was employed for these measurements.

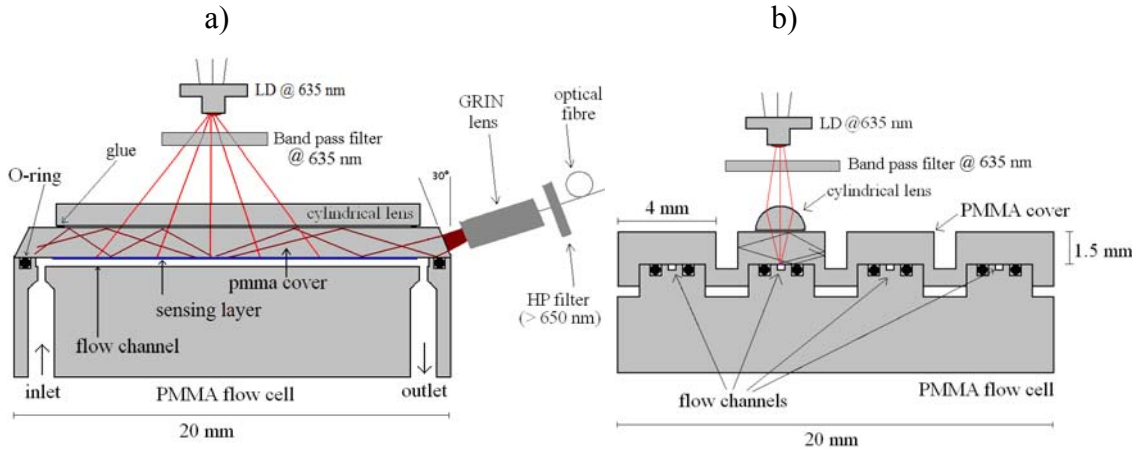

Figure 4.14 Lateral section (a) and cross section (b) of the optical chip for the interrogation in flow of antigen labelled Cy5. On the left is shown the lateral section of the PMMA chip. The fluorescence is guided along the PMMA cover, filtered with a HP > 650 nm, and collected by an optical fibre coupled with a GRIN lens. An hemicylindrical lens was added on the top of the channel in order to increase the focus of the source thus emproving the sensitivity.

Chemical protocol:

After deposition of Eudragit L100 in EtOH and EDC/NHS activation, as described above, the pmma cover part was ready to be inserted on its complementary flow cell part.

In the case of PMMA chip, the IgG immobilisation and the assay were carried out in flow conditions. The PMMA chip was connected to a peristaltic pump by means of the PVC tubing. The flow rate used for IgG immobilisation was 1 µl/min, whereas the speed for assay experiments was 10 µl/min.

Different concentrations of mouse IgG (0.5, 0.05, 0.005 mg/ml) were inserted in the channels for 30 minutes, and sensing efficiency was compared to understand the more convenient concentration of IgG to be deposited for one single channel.

Three different treatments of the surface to obtain carboxylic groups were executed with Eudragit L100/EtOH (0.01 mM); PLLA/$CHCl_3$ (0.01 mM) + NaOH 2M; NaOH/dmso (1:1). These treatments were compared in biosensing efficiency and a final microfluidic assay protocol for antiIgG detection was implemented as follow:

1) A mouse IgG solution in PBS (0.05 mg/ml was chosen) in flow for 30 minutes was inserted on a single channel at speed of 1 µl/ml to obtain a reproducible coverage of the substrate previously modified with Eudragit L100 (0.01 mM) and EDC/NHS method.

2) TRIS buffer pH 7,4 in flow for 5 minutes with a speed of 1 µl/min was used to deactivate the surface.

3) PBS in flow for 5 minutes with a speed of 10 µl/min was used to wash unbound IgG.

4) AntiIgG-Cy5 was diluted in PBS in a range between 1 ng/ml - 1 mg/ml.

5) AntiIgG-Cy5 in flow for 15 minutes spaced out by washing steps of PBS for 5 minutes for every concentration measured.

6) Measurements were performed starting from the more diluted (1 ng/ml) to the more concentrated (1 mg/ml) solutions of antiIgG-Cy5 after PBS wash.

7) The DL (635 nm, 3 mW) was switched on and 10 measurements of the optical spectra were captured with an integration time of 10 sec for a total time of 100 sec.

8) The DL was switched off and an average spectrum of the measurements was collected by the Hamamatsu spectrophotometer.

4.6 mRNA (MGMT) biosensor in PMMA planar squares:

Optical setup:

A led at 490 nm coupled with an optical filter BP at 488 nm was used as excitation source (Figure 4.15). The collection of fluorescence signal was carried out using an optical fibre at 50° angle. Graded index (GRIN) lenses, ¼ pitch, 1.8 mm diameter, were used to increase the collection area of the emitted signal. GRIN lenses were purchased from SELFOC MicroLens, NSG Europe, Temse, Belgium.

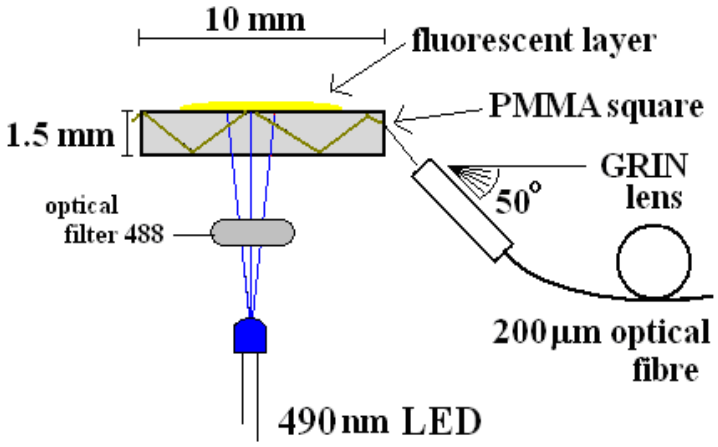

Figure 4.15. A blue led source filtered at 488 nm is perpendicular to the transparent pmma square where the fluorescent layer is deposited. The guided fluorescent signal is captured with a graded index lens coupled with an optical fibre.

Chemical protocols:

A solution of Eudragit L100/EtOH (0.01mM) was prepared and dropped on a small planar square to obtain a surface covered with carboxyl groups.

To obtain a surface with exposed amino groups, hexamethylendiammina (HMDA) was then dropped.

HMDA amino groups react covalently with the carboxyl groups forming peptidic bond and water.

Hexamethylendiammina (HMDA) was diluted in 100 mM borate buffer at pH 9, as reported in literature [5], and dropped on the surface to obtain primary amino groups exposed on the surface (Figure 4.16).

Hexamethylendiammina (HMDA) was purchased from Fluka, Riedel de Haen, Germany.

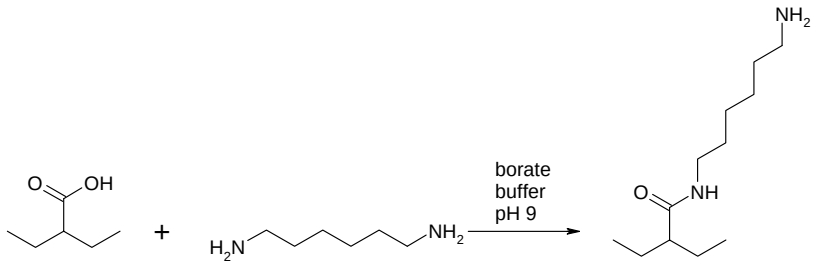

Figure 4.16 HMDA binding to a carboxylate surface.

Surface treatments to activate the PMMA with amino groups were considered and several experiments were conducted to find the better solution in terms of quantity of amino groups present on the surface.

Planar square of PMMA were used as substrate for preliminary studies of the surface chemistry. Amino groups were obtained by means of pre-treatment of the surface with Eudragit L100 and consequently EDC/NHS treatment followed by HMDA treatment. The same reaction was also carried out directly with pure HMDA.

In particular, the following pre-treatments before HMDA treatment were compared:

a) surface deposition of Eudragit L100;

b,c,d) acid hydrolysis of ester groups on PMMA (H_2SO_4 3M; H_2SO_4 1M; HCl 1M)

e,f) alkaline hydrolysis of ester groups (NaOH 4M; NaOH 1M) with PMMA planar square immersed in the solution for 3 h.

g) PMMA chip immersed in HMDA 1M in DMSO;

h) Drop deposition of HMDA 1M in DMSO.

A quantitative measurement of amino groups generated on the surface was achieved with sulfosuccinimidyl-4-O-(4,4-dimethoxytrityl) butyrate (s-SDTB), a molecule that reacts with an amino group releasing a dye (λ_{max} Abs = 498 nm) as by-product of reaction (Figure 4.17) [352].

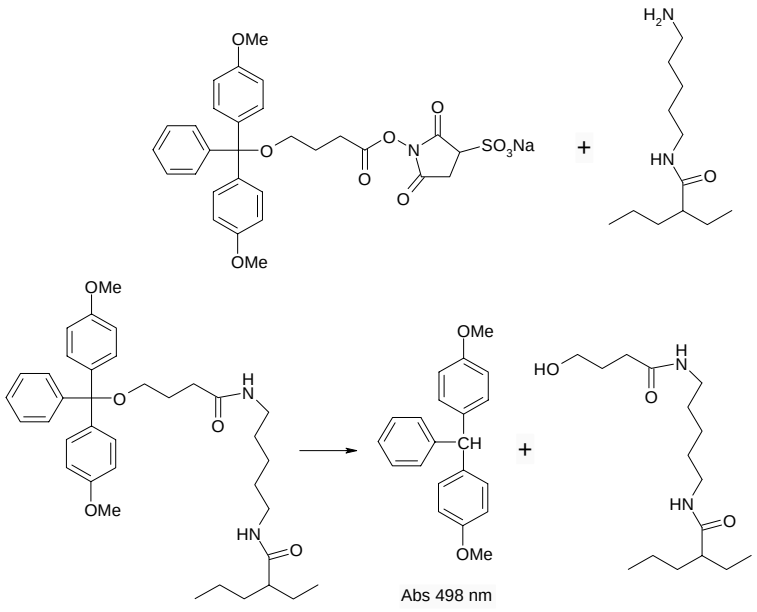

Figure 4.17 Quantification of amino groups with s-SDTB. The quantity of amino groups present on a surface is proportional to the quantity of dye released in solution.

A 0.1 mM solution of sulfosuccinimidyl s-SDTB was prepared by first dissolving it in acetonitrile: sodium bicarbonate (1:50) buffer at pH 8.5.

The s-SDTB solution was dropped for 30 minutes on the planar squares of PMMA pretreated with HMDA.

The samples were then washed abundantly with pure water and placed in vials with perchloric acid (30%).

The absorbance signal was recorded at 498 nm by spectrophotometer and amino groups were quantified.

The reaction between pmma planar square amino modified and thiolated RNA was obtained using an etero-bifunctional cross-linker: sulfo-succinimidyl 4-(N-maleimidomethyl) cicloesan-1-carboxylate (SMCC) was purchased from Pierce, Rockford, IL, United States (Figure 4.18).

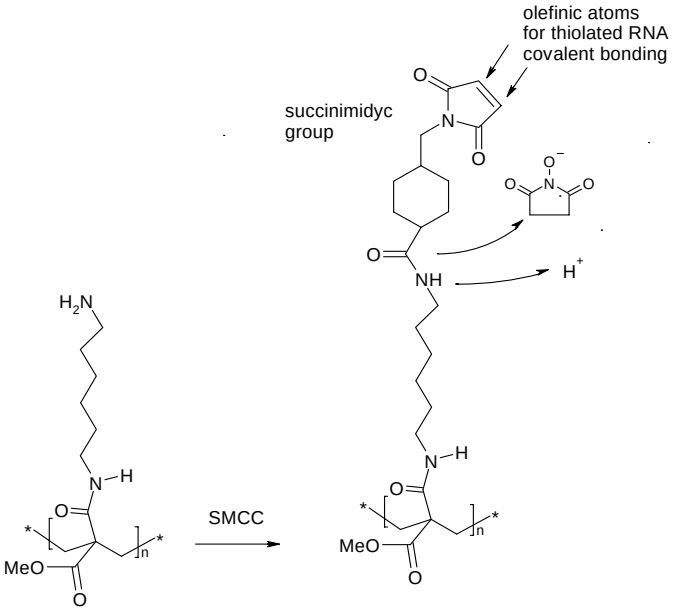

Figure 4.18 Reaction of peptidic bond formation between amino groups and SMCC.

The protocol of SMCC, able to react in an etero-bifunctional manner [337-340] with amine groups and with thiol-modified 2'OMe-RNA (Figure 4.19), was performed following the protocol from Pierce.

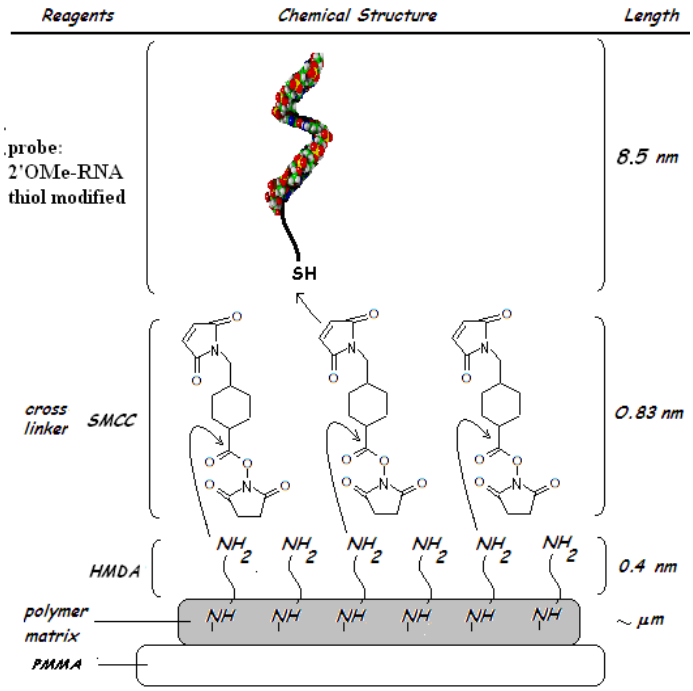

Figure 4.19 Left: Cross-linking reaction of SMCC between an amino carrier and a thiol carrier. Right: 2'OMe-RNA sequence thiol-modified is covalently bound to the PMMA surface The overall structure is about 10 nm in length.

The sequences of RNA synthesised in Dept. of Clinical Physiology, at IFC-CNR, in Pisa, Italy, were chosen in accord with previous experiments carried out and reported in literature [318]. The sequences of RNA were modified with methoxyl group at 2' carbon atom (2'OMe-RNA) to protect RNA from RNAses enzymes.
RNA sequences and concentrations were:

Probe 7: 5'-GUGCGUUUCAUUUCACAAUCCUUGU-3'
Characteristics: 2'-OMe, SH or NH_2 at 3', conc. 234.4 mM.
Probe 46: 5'-CCUCGGGCUGGUGGAAAUAGGCAUU- 3'
Characteristics: 2'-OMe, NH_2 at 3', conc. 246.9 mM.
Probe 7 mism.: 5'-GUGCGU**A**UCAUU**G**CACAA**G**CCUUGU-3'
Characteristics: 2'-OMe, SH at 3', conc. 234.4 mM.
Target 7*: 3'-CACGCAAAGUAAAGUGUUAGGAACA-5'
Characteristics: 2'-OMe, FITC or Cy5 labelled, conc. 100.0 mM.

The RNA probes were dissolved in pure water whereas, the RNA targets were dissolved in an hybridisation buffer (2X) made of 5 ml of formamide (50%), 5 ml of SSC (10X), 0.2 ml of SDS (10%). SSC (20X) buffer was prepared adding NaCl 3 M, sodium citrate 0.3 M, EDTA 1 mM.

4.7 mRNA (MGMT) biosensor in PMMA chip:

Calibration curve regarding the sensitivity for RNA/RNA hybridisation between probe 7 and target 7* was recorded using the PMMA multi-channel chip.
In this case the RNA probe was modified with an amino group instead of a thiol group, in order to simplify the chemical protocol for the self-assembling of the bioreceptor.
The target 7* was labelled with Cy5 instead of FITC to match the source characteristics.
A solution of Eudragit L100/EtOH (0.01 mM) was prepared and 50 µl were dropped on a bare single channel of a PMMA chip.
After solvent evaporation, a solution of EDC/NHS in MES buffer 0.1 M, pH 6.2 was dropped on the surface for 30 minutes.
The PMMA cover part was then ready to be inserted on its complementary flow cell part.
Bioreceptor immobilisation (probe 7) was executed in flow for 30 minutes at 1 µl/min.

TRIS buffer in flow for 5 minutes at 1 µl/min was used to deactivate the surface.
After a washing step of 5 minutes with buffer, the RNA target 7* solution, dissolved in hybridisation buffer at different concentrations was inserted at 10 µl/min speed for 15 minutes.
After a washing step for 5 minutes with pure buffer, the red diode laser was turned on and ten measurements were captured with an integration time of 10 seconds.
After 100 seconds the diode laser was turned off and an average spectrum was saved.
The integral fluorescence area in a range between 650-750 nm was calculated and a calibration curve was plotted for different concentrations of the target 7*.

4.8 NF-kB sensor in PMMA chip:

The DNA sequence for the capture of NF-kB was invented and realised in the laboratory of the institute of Clinical Physiology (IFC-CNR) in Pisa by means of DNA synthesizer.
The specific sequence for NF-kB protein detection was a single chain of 30 nucleotides opportunely synthesised to auto-hybridize folding on itself and leaving a closed loop of four bases.
This specific sequence of DNA binds to NF-kB protein and is known as a NF-kB decoy [168].
The synthesis of the bioreceptor should include primary amino groups (Figure 4.20) on the loop side for further attachment onto an activated surface.
The DNA was dissolved in pure deionised water in a concentration of 0.1 µM and inserted inside a PMMA channel previously treated with Eudragit L100/EtOH (0.01mM) and activated by EDC/NHS method. The PMMA cover part was then ready to be inserted on its complementary flow cell part.

Figure 4.20 The DNA decoy for NF-kB is constituted by the 20 bases surrounded by the dotted line and functional amino groups on the loop side.

The immobilisation of NF-kB decoy was carried out for 30 minutes at a flow speed of 10 μl/min.
Ethanolamine, TRIS or bovine serum albumin (BSA) deactivation treatments were compared and the last one was the most effective one.
After a washing step of 5 minutes with buffer solution, the p50 solution was dissolved in binding buffer (10mM HEPES pH=7.9, 50 mM KCl, 0.1M EDTA, 2.5 mM DTT, 10% glycerol and 0.05% NP-40) in a concentration of 0.1 μM and inserted in flow for 30 minutes at speed of 10 μl/min.
The protein p50/p50 was purchased from Promega, Madison, WI, United States.
After a washing step for 5 minutes with pure buffer, the red diode laser was turned on and ten measurements were captured with an integration time of 10 seconds.
After 100 seconds the diode laser was turned off and an average spectrum was saved.
The integral fluorescence area in a range between 650-750 nm was calculated and this value represents the background signal due to PMMA autofluorescence.
Then, an antibody (clone 19) able to bind to p50, was firstly labelled with Cy5, and then was inserted at different concentrations in the channel at 10 μl/min for 15 minutes plus 5 minutes of washing steps with pure buffer.
After every washing step the measurement was caught integrating the fluorescence area between 650-750 nm.

To detect how many sites are available to interact with the heterodimer protein p50/p65 it was necessary to quantify the quantity of p50 bound to the DNA decoy.
Unfortunately the heterodimer protein p50/p65 (our target) is not actually present on the biotechnology market so the experiment was performed using the most similar dimer protein (p50/p50).

The antibody able to interact with p50 is the clone 19 (C-19), an affinity purified polyclonal antibody raised against a peptide mapping at the C-terminus of NF-kB p50 of human origin, and was purchased from Santa Cruz Biotechnology, CA, U.S.
Clone 19 was previously labelled with Cy5 fluorophore in order to match the characteristics of the optical system.

4.9 Atomic Force Microscope

The AFM is an extremely accurate technique for measuring and analysing films.
It uses a very sharp tip attached to a triangle cantilever of 0.2 mm with a laser beam positioned on it, so the cantilever reflects the light of the laser which is detected by a photo-detector. The tip scans the surface of the sample to be analysed. The interaction forces occurring between the tip and the atoms of the scanned sample surface, of the order of nano-newtons (nN), promote a deflection of the cantilever where the tip is mounted. When there is a change in the surface topography, a change in the cantilever deflection is detected by the position of a laser beam. From a scan over the sample surface, a bi-dimensional and tri-dimensional image can be obtained (see Figure 4.21).

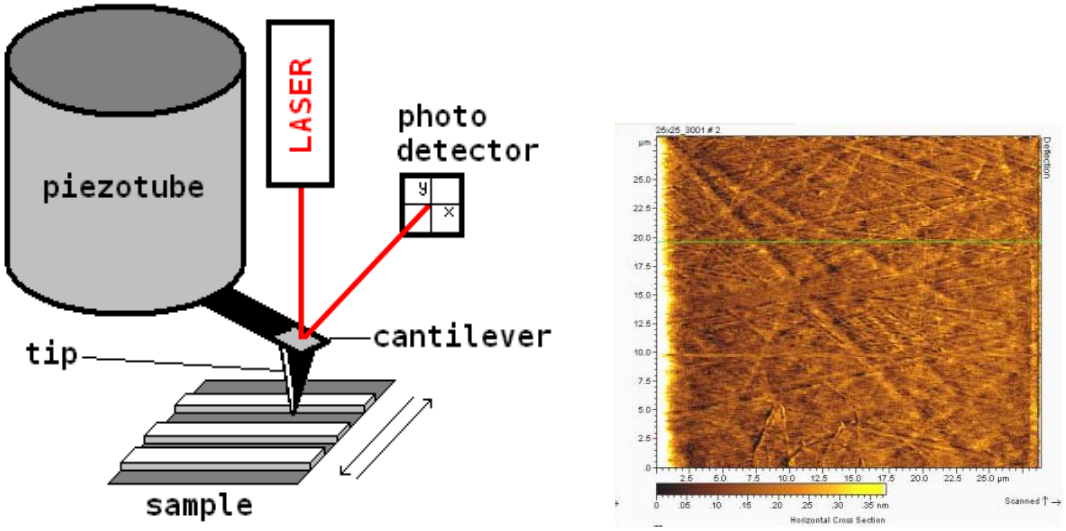

Figure 4.21 Atomic Force Microscopy. The tip scans the surface of interest and cantilever reflects back the laser beam on a photo-detector. All data are collected by computer and converted into an image.

4.10 Langmuir-Blodgett deposition method

Film transfer involves the vertical movement of a solid substrate through the monolayer/air interface with the simultaneous control of the surface pressure (Π) that is determined by measuring the surface tension with the Wilhelm plate method: $\Pi = \gamma_{water} - \gamma_{monolayer}$ where γ_{water} is the surface tension in absence of a monolayer and $\gamma_{monolayer}$ is the surface tension with the monolayer present (Figure 4.22).

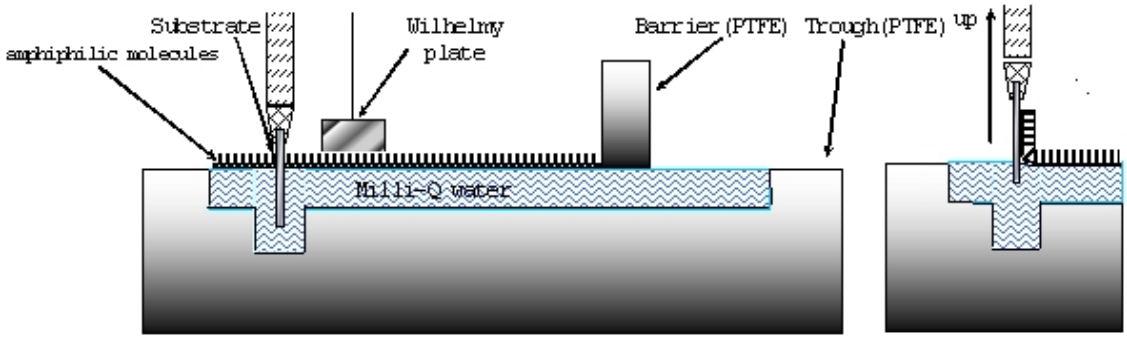

Figure 4.22. The Langmuir-Blodgett method is constituted by a trough and a barrier, made in PTFE (Teflon); in the trough the sub-phase is ultra-pure water Milli-Q. The polymer is spread on the water-air interface and its surface pressure is controlled by Wilhelm plate. In the interface between air and water the polymer molecules orient themselves following hydrophobic and hydrophilic interactions. The up or down process is selected depending on hydrophobic or hydrophilic desired modification of the substrate.

The surface pressure of the monolayer is controlled by a computer program connected to the Wilhelm plate. The instrument pushes the barrier until the desired surface pressure is obtained and keeps the surface pressure constant by moving the barrier during the deposition process [341].

For a surface hydrophobic interaction, the deposition of the polymer on the substrate is conducted by immersing the chip in the sub-phase. The monolayer attaches to the PMMA and is transferred with different surface pressure [342].

The driving force for rearrangement of molecules on the sub-phase is given by the interactions between the hydrophobic chains of Eudragit L100 and PLLA and the hydrophilic substrate of PMMA with the formation of hydrogen bonds between them. The single most important indicator of the monolayer properties of a material is given by

a plot of surface pressure as a function of the area of water surface available to each molecule. The isotherm calculated is important to determine the right surface pressure to have the layer of molecules in a condensed phase.

Furthermore with a large surface area the surfactant molecules are widely separated and are considered to lie quite flat on the surface [342].

The interactions between the molecules are small and as a result the monolayer has relatively little effect on the sub-phase surface tension. In this position the monolayer can be considered as a two dimensional “gas”.

On compression of the gas state the pressure rises until a two dimensional liquid begins to form. The liquid state is often distinguished in a liquid expanded (LE) and a liquid condensed (LC) state. In the liquid expanded state the hydrophobic portions are assumed to have a more or less random orientation (Figure 4.23).

In the LC state the monolayer molecules are more closely packed. Further compression produces a closely-packed solid (S) or condensed film which is highly incompressible. Attempts to compress the solid film further will lead to film collapse: molecules are forced out of the monolayer to form agglomerates called micelles [342].

The highest pressure to which a monolayer can be compressed is called the collapse pressure. When this is exceeded, micelles start to form.

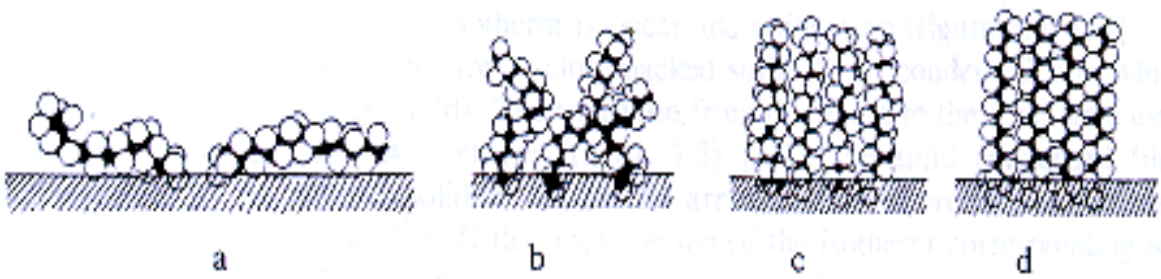

Figure 4.23 Schematic representation of the molecular arrangement in: a) gaseous; b) liquid-expanded LE; c) liquid condensed LC; d) solid condensed state. Image source is [342].

5. RESULTS AND DISCUSSION

5.1 pH fluorescence sensing on glass capillary and on PMMA

A suitable transparent substrate was required for the development of the optical sensors.
A silica glass capillary was firstly used as flow chamber to detect the fluorescence signal of dyes dissolved in buffer pH solutions.
After calibration of the system, the interrogation of fluorescent signals of biological solutions was performed using silanisation as immobilisation procedure.
A disposable chemical compound such as APTES was able to covalent bind the substrate on the glass and a pH-sensitive fluorescent molecule on the other side.
The concentration of the silane was a basilar starting point from an optical and mechanical point of view to test the resistance to the continuous flow of buffers, thus ensuring a stable and durable signal.
Different percentages of polymer/solvent content can in fact generate different thicknesses of the material deposited on the substrate affecting the intensity of the recorded optical signal.
More generally, the study of several chemical treatments of the substrate and of different types of polymer is an essential issue in biosensor chemistry.
An optimal concentration of the right polymer, a proper deposition of it on the substrate and a reproducible method were researched.
Attachment of fluorescent chemical compounds, such as fluorescein and cyanine derivative dyes onto the substrate enabled a direct control of the fluorescence optical signal providing information on the stability and reproducibility of the modified layer.
The fluidic apparatus, consisting in a peristaltic pump with tygon tubes, was interfaced with the optical system,
The optical device enabled the interrogation of a glass capillary through which the sample is flowing (Figure 5.1).

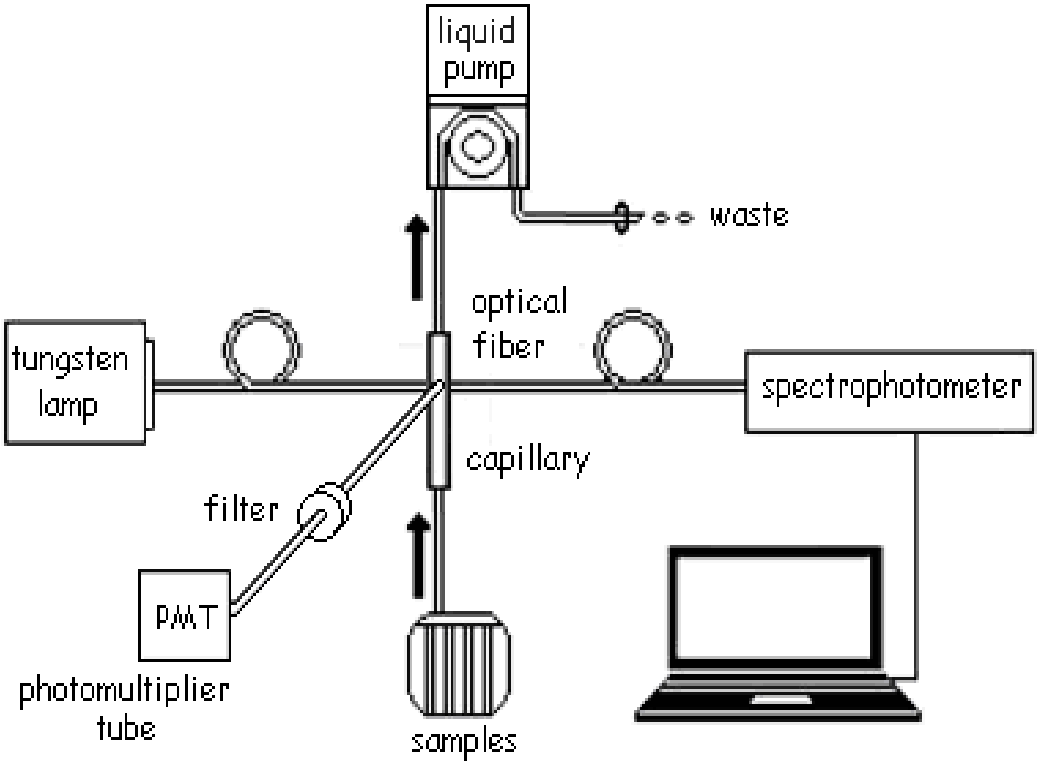

Figure 5.1 The optical system for the collection of absorbance and fluorescence spectrum. The samples flow inside the sensor capillary and are interrogated by means of optical fibres positioned perpendicularly to the capillary. Optical data are collected by a spectrophotometer and a photomultiplier tube.

The fluorescein molecule was chosen to test the optical system with a fluorescent dye that had been studied already [321-323] and the optical coupling between the capillary and the optical fibres was optimised.

The main objectives were a good separation of the optical signal between the excitation and the emission light and a high fluorescence signal. Ideally, the immobilised fluorescent layer should be resistant to water flow for several hours giving a constant fluorescence signal and avoiding a loss of dye.

Light scattering and multiple reflections of the excitation radiation, due to the geometry of the capillary, can increase significantly the background signal at the photodetector.

All these issues were considered in the optimisation of the chemical protocols of the bioassays and in the integration of the optical setup.

Another fluorescent dye, a cyanine derivative named Cy5, was used for the experiments. The usefulness of long wavelength fluorophores has been shown in numerous applications [324-326], mainly in biological analysis, because degradation is considerably reduced at higher wavelength and fluorescence of the sample matrix (i.e.

intrinsic fluorescence of PMMA) in the visible region is a source of interference. Cyanine reagents have been shown to be useful as fluorescent labels for biological compounds [326-331]. These dyes are intensively fluorescent and water soluble, providing significant advantages over other existing fluorophores. Cy5 dye produces an intense signal in the far-red region of the spectrum. Although not recommended for visual applications, this dye is ideally suited for detection using CCD cameras, PMT, or red-sensitive films [326-331].

To test the efficiency of the optical system, fluorescein or cyanine derivatives were immobilised on the internal wall of the capillary and the intensity was recorded to monitor the resistance of a sensing layer in flow conditions.

Fluorescence and absorbance spectra were recorded using a spectrophotometer when optical fibres were used or by using a photomultiplier tube. Data were recorded by Hamamatsu spectrophotometer and analysed with Excel and Origin software's.

A Gilson peristaltic pump generated a controlled and stable flow of the samples under test. The plastic tubes were made of tygon which is highly inert, extremely flexible and commonly used in industrial applications.

In summary, a double detector system was set up in order to capture both absorption and fluorescence signals at the same time. An optical interferential filter was positioned between the capillary and the PMT reducing the scattering noise due to the excitation source.

5.1.2 pH sensing of fluorescein solutions in glass capillary

The light source was a blue led at 490 nm coupled with a BP filter 488 nm.

The choice of the best arrangement was carried out by performing measurements of sodium salt fluorescein dissolved in solvent solutions.

Different concentrations of fluorescein were dissolved in McIlvaine buffer solution, pH 8.0 in a range between 10^{-4} - 10^{-9} M and measurements in fluorescence were performed by means of photomultiplier tube (PMT) connected to a frequency photon counter.

5.1.3 Input filtering

Three different calibration curves were obtained with one low-pass (LP) filter at 480 nm, and with two or three of these types of filter in a cascade configuration (Figure 5.2). The log of the concentrations of fluorescein are shown on the x axis, while on the y axis are

shown the log of counts in Hz measured by the frequency counter connected to the PMT. The use of three filters resulted in a lower detection limit as aspected; the emission tail, due to the light emitting diode source, and the scattering light were almost denied at λ > 500 nm. The enhancement is more evident in the nanomolar region.

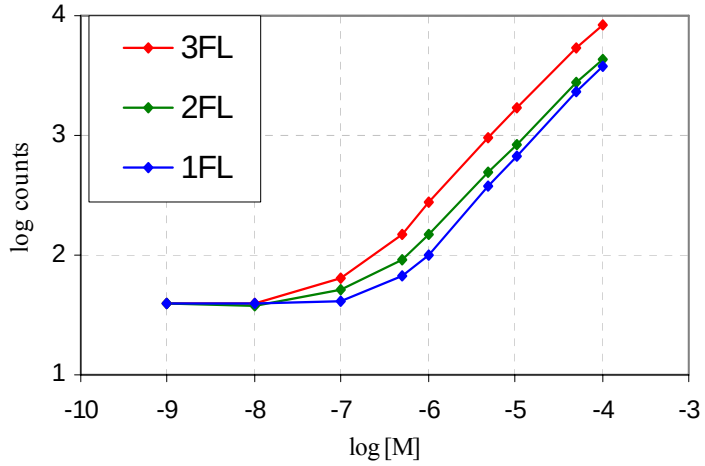

Figure 5.2 Comparison between calibration curves using input low pass filters at 480 nm in cascade at the input and no filtering in output was applied.

5.1.4 Output filtering

Two different output filters were compared, one high pass (HP) at 546 nm and one band pass (BP) at 525 nm. Calibration curves of the fluorescence signal of sodium salt fluorescein dissolved in different pH buffers were compared. The difference between the red and blue lines is not appreciable, but in order to be sure that interfering light was not captured at longer wavelengths, the BP filter 525 nm configuration was selected because a lower background noise due to the source was observed (Figure 5.3).

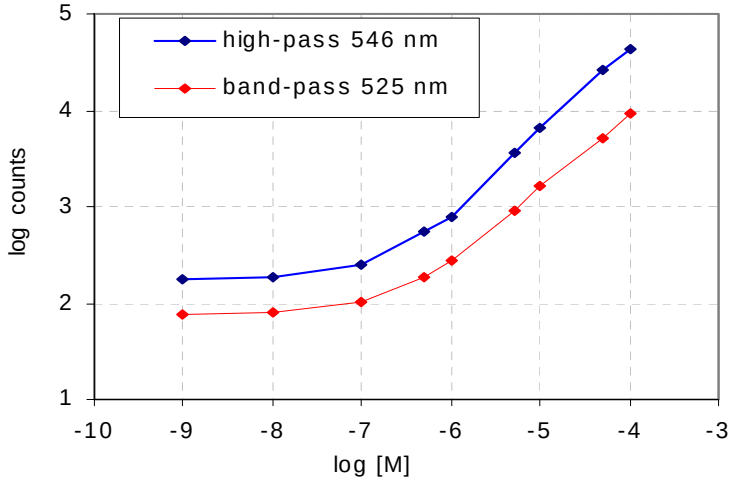

Figure 5.3 Comparison between output filters, a high-pass filter at 546 nm (blue) and a band pass filter at 525 nm (red). These calibration curves were obtained using one entrance filter LP at 480 nm.

5.1.5 Calibration curve

The calibration curve shown in figure 5.4 was obtained in accord with the instrumental setup described in Figure 5.1 and with the results in Figure 5.2 and 5.3, adding three input low pass (LP) filters in cascade at 480 nm and one output band pass (BP) filter at 525 nm. The linear range was considered satisfactory for concentrations between 10^{-4}-10^{-7} M.

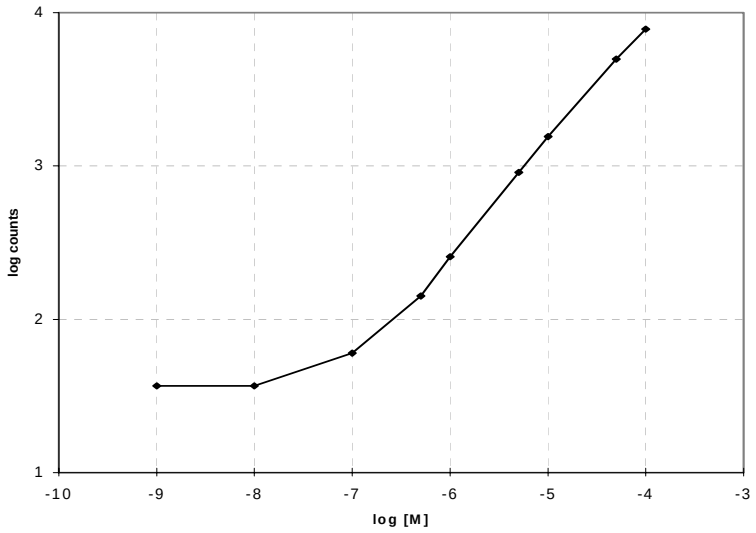

Figure 5.4 Calibration curve was obtained with solutions of fluorescein flowing inside a bare glass capillary adding three low pass filters (480 nm) at the input and one band pass filter (525 nm) at the output.

This calibration curve represented just the starting point for the sensitivity of the optical system and will be subjected to an enhanced improvement through research conducted in this thesis.

5.2 pH sensor glass capillary

5.2.1 Development of a first optical system for the glass capillary

The silanisation is a chemical procedure well known in sensor chemistry [321-323, 333-335]. A particular attention was focussed on the covalent attachment of fluorophores inside the capillary. The internal surface of the capillary was oxidised by a mixture of H_2SO_4/H_2O_2. After preliminary trials which took in consideration the type of silane (APTMS, APTES), the concentration of the silanes and the temperature of evaporation of the solvent, an appropriate silanisation protocol was selected.

A solution made of APTES at 30% in EtOH was inserted to fill the entire capillary and was dried in oven overnight at 80°C. A solution 10^{-3} M of the dye dissolved in solvent was then inserted in the silanised capillary (Figure 5.5) and was dried overnight at 80°C.

Figure 5.5 This image was captured on an optical microscope by digital camera. Left: a bare empty capillary as reference (Ø external=1 mm; Ø internal=0.5 mm. Centre: a second empty capillary after silanisation overnight in the oven at 80°C. Right: a third empty capillary after the total evaporation of EtOH in which fluorescein dye was dissolved.

The light source was a white tungsten lamp coupled with an optical fibre. As previously described, the white light was applied perpendicular to the capillary.

To obtain the absorption measurement, the signal was transported by a second optical fibre, in axis with the first one, and signal was collected by a spectrophotometer.

A third optical fibre, disposed perpendicularly to the capillary and to the other two optical fibres, collected the fluorescence signal into a photomultiplier tube.

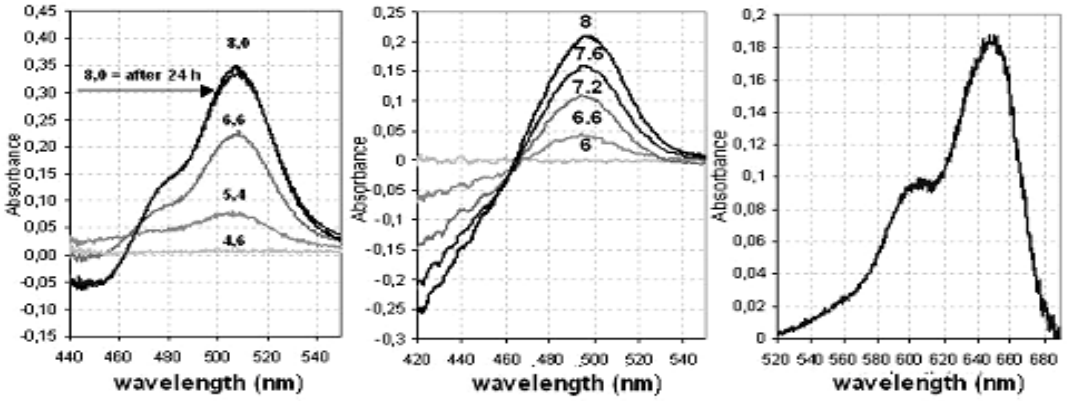

Figure 5.6 Absorbance spectra of the fluorophores FITC (left), FAM-X SE (center), and Cy5 (right) molecules immobilized on the internal wall of the capillary. In the case of FITC, the white light was turned on and the absorption spectra was collected again after 24 hours of flow, revealing that the loss of dye was almost insignificant. Numbers on the plots refers to pH values.

In figure 5.6 absorbance spectras of three different fluorophore dyes (FITC, 5-FAM-X-SE and Cy5) immobilised in the glass capillary are shown during flow of pH buffers using the capillary fibre system.

To speed up the process, APTES and FITC were then mixed together and few drops of the cocktail were deposited by a siringe in the central part of the capillary to localise the silanisation. (Figure 5.7)

Figure 5.7 Image at the microscope of a controlled silanisation of the substrate using the cocktail made with APTES 30% in EtOH and FITC 10^{-3} M.

The sensor was then inserted and interrogated with the capillary fibre system. The results shown in Figure 5.8 were recorded during flow of pH buffers at 10 µl/min demonstrating to be in good accord with theory [332].

The three LP filters at 480 nm were substituted, in this case, with one BP filter (505 nm). The signal output was not filtered to observe the separation between the led peak and the fluorescence signal.

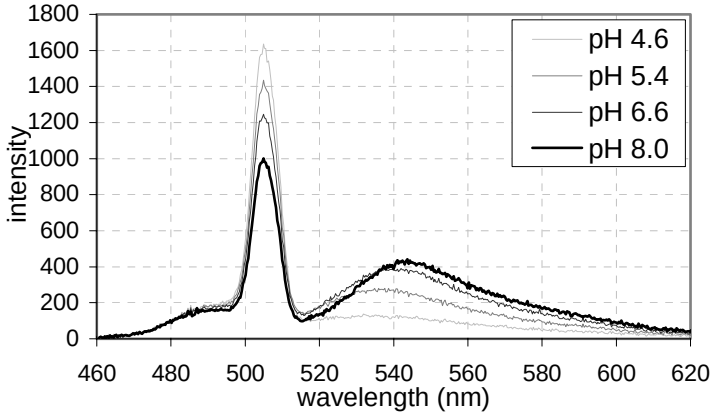

Figure 5.8 Right: Optical spectra of the sensing layer immobilised on the capillary wall during the flow of buffers at 4 different pH values .

The contribution of scattered light coming from the source and amplified by the rounded geometry of the capillary was studied registering the signal in the case of a bare capillary and in the case of a modified fluorescent capillary. (Figure 5.9)

The measurement confirmed that the loss of the dye and the photobleaching effects are really limited in a 3 hour experiment, thanks to a good silanisation procedure and to the implicit low power light typical for a led source.

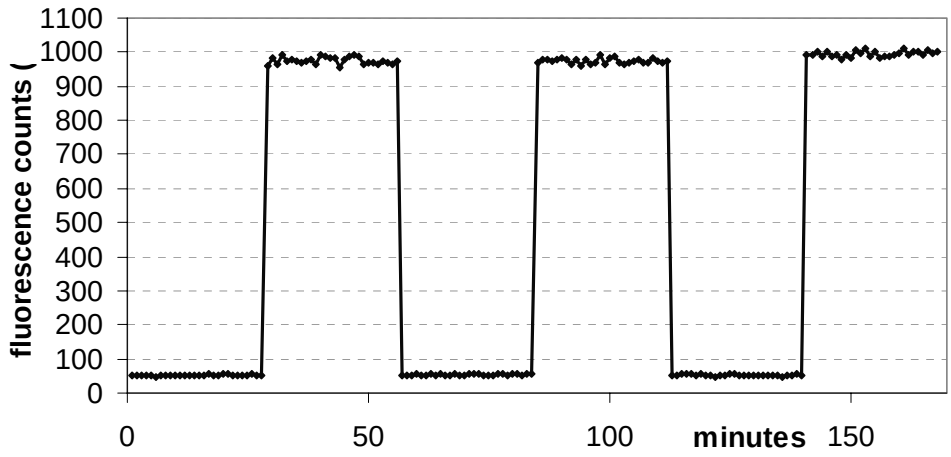

Figure 5.9 On-line measurement of the light signal of the capillary functionalised with FITC compared to a bare one during the flow of buffer pH 8.0. The fluorescence signal contribution is much higher than scattering signal deriving from the light source. Loss of dye and photobleaching effect can be considered almost irrelevant.

The result demonstrated that the contribution deriving from scattered light is about 6% of of the fluorescence one (60 Hz vs 1000 Hz) and represented a significant background which could be avoided if a better geometrical separation is engineered.

The contribution of the scattering light can represent an undesired background value, especially if low concentrations of fluorescence detection have to be reached.

So, a new optical system was ideated to enhance signal avoiding the contribution derived from scattered light.

5.2.2 Development of a second optical system for the glass capillary

A second setup for the optical recording of a fluorescence signal is shown in Figure 5.10 and was developed to improve the optical efficiency by collecting a higher proportion of the signal [343]. The idea consisted in to use a capillary as waveguide to collect the fluorescence signal separated from the source signal. The setup was studied in order to obtain a better geometrical separation between the signal of emission and excitation.

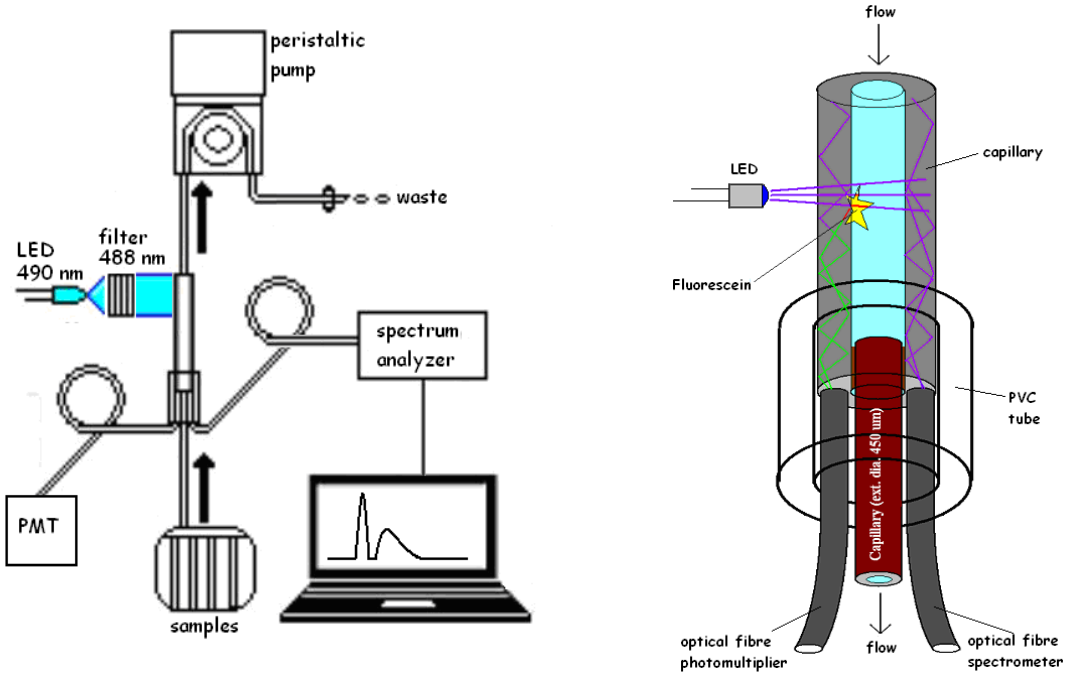

Figure 5.10 Left: a blue LED enlighten the capillary with fluorescein immobilized inside. The optical system was studied to collect the fluorescence signal geometrically separated from the LED source.
Right: source-capillary optical setup and guided fluorescence collected by two optical fibres connected to a photomultiplier tube and a spectrophotometer.

Two fibres were used for the collection of the fluorescence emitted by the immobilised layer (Fig. 5.11), using the capillary as waveguide and coupling it with a spectrophotometer and a photomultiplier tube simultaneously.

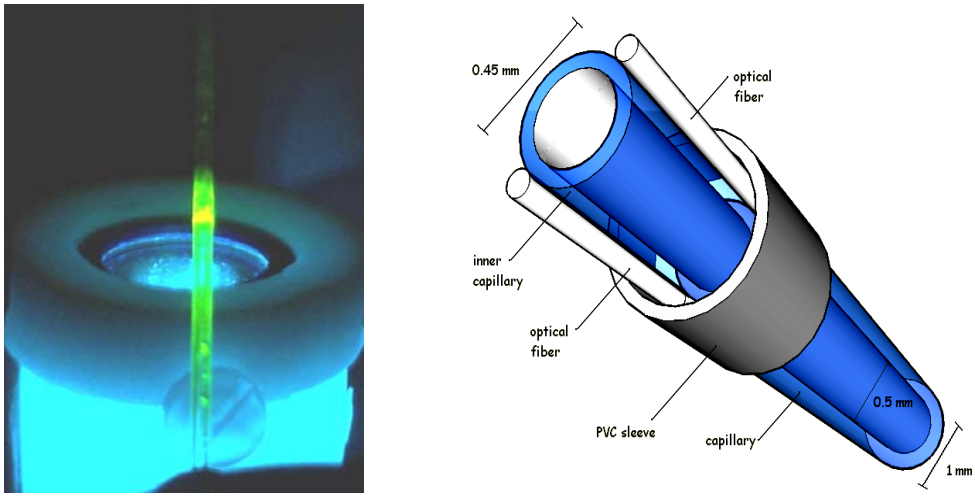

Figure 5.11 Left: a photo image in true colour of lateral section of the capillary with fluorescein silanised when a buffer pH 8 is flowing inside. Right: 3D-image of the technical particular of the coupling between capillary and optical fibres.

Tests on the efficiency of the system were carried out with fluorophores (FITC and Cy5) covalently immobilised directly on the internal wall of the glass capillary using the silanisation process.

Figure 5.12 shows the results obtained with fluorescein: high intensity fluorescence signal was collected during pH buffers flow. The result is impressive in the increase of the fluorescence signal and also in the decrease of guided light coming from the source.

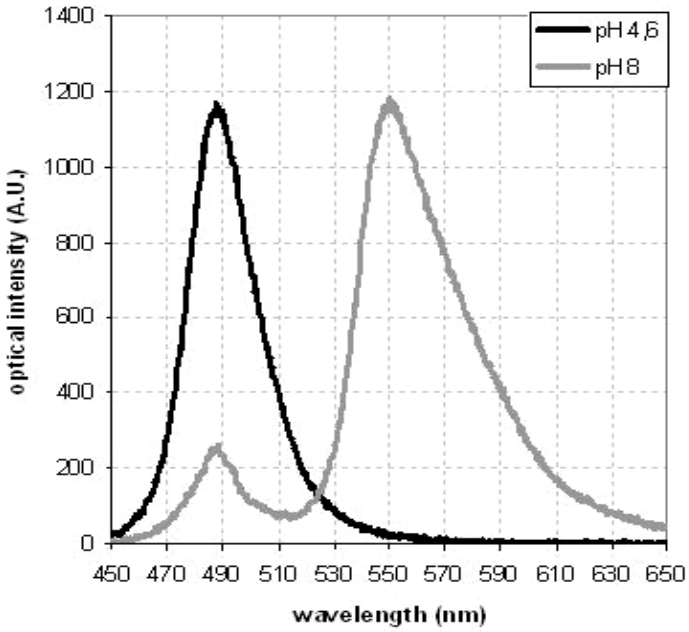

Figure 5.12 Optical spectra collected with the Ocean Optics spectrometer in the case of fluorescein (FITC) immobilised in the glass capillary. The two spectra correspond to buffer at different pH values (4.6 and 8) flowing inside the capillary.

Flow of buffer at pH 7.4 was monitored for 25 hours to gain information on the stability of the fluorescent layer at physiological pH ranges.

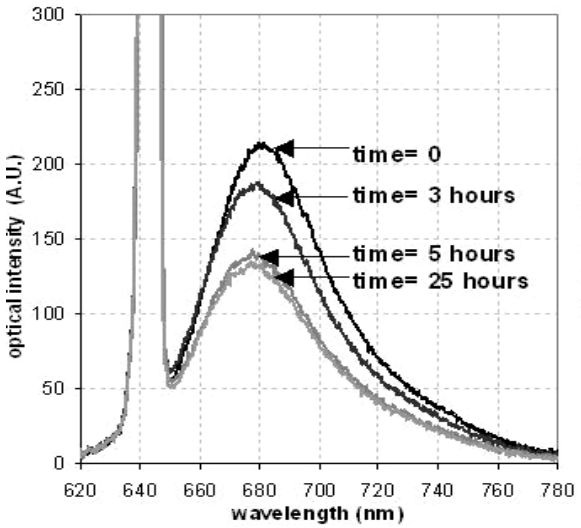

Figure 5.13 Optical spectra collected with the Ocean Optics spectrometer in the case of Cy5 immobilised in the glass capillary. After 5 hours of buffer flow in the capillary it was possible to observe a decrease of the signal of fluorescence due to the loss of not covalently bound Cy5.

After 5 hours, the signal almost stopped to decrease confirming that a deep washing procedure was necessary to delete the adsorbed dye rather than the covalently bound.

In general, the results obtained with the glass capillary were quite good, but the reproducibility of the deposited layer in the internal wall was poor.

This was mainly caused by the geometry of the capillary, in which the evaporation of the solvent is particularly difficult and maybe predictable only by complicate mathematical models.

Experiments about the changes in the temperature of silanisation determined the quality of the layer: higher is the temperature (>100°C) and lower is the time for the silane to attach the glass oxidized surface, because ethanol evaporate too fast.

On the other side, lower is the temperature (<100°C) and less strong is the covalent attachment of the silane in the internal wall of the capillary because evaporation of the water does not occur, and this fact cause not proper attachment of the silane.

A compromise temperature was found keeping the capillary at 80° C for 24 hours; so, the silane had enough time to react and water had enough time to evaporate.

Anyway, the best solution was found avoiding the central part of the capillary as deposition location of the silane trying to cause the solvent evaporation on one exit side of the capillary.

Eventually, an occluded part can form inside the capillary; this was handily broken leaving an integral side able to couple with the optical fibres for the detection of fluorescence [344].

All these troubles suggested starting thinking about a different substrate, based on transparent PMMA, which was considered as an alternative to the glass capillary.

5.3 Anisotropic emission on PMMA

Experiments were carried out in order to study the anisotropy of the fluorescence emitted by an immobilised layer of dyes on the PMMA.

The anisotropy of electric dipoles (excited fluorophores), when the distance from a dielectric interface is comparable with the emitted wavelength, is a well known phenomenon [345-347].

Therefore, an analysis of the preferential directions of the emitted fluorescence was carried out, with a mixture of FITC/Eudragit RL 100 dropped on the PMMA cover, to study anisotropic emission on a PMMA-water interface (Figure 5.14) under flow at pH 8 buffer.

Both the fluorescence emitted light at 539 nm and the scattered signal at 488 nm, coming from the source, were measured by means of a collecting fibre positioned at different angles respect to the flow direction.

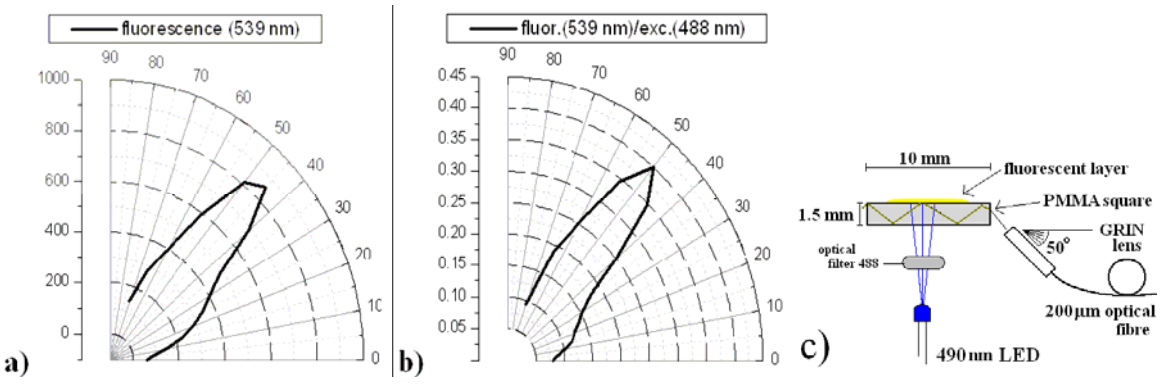

Figure 5.14 The fluorescence emission is reported in Figure a), while the efficiency, i.e. the ratio of the fluorescence and the scattered signal, is reported in Figure b). Optical optimisation of the setup for small planar squares is reported in Figure c).

Data were collected every 5 degree angle. From these results it was possible to optimize the detected signal by choosing a collection angle of 50°, as shown in Figure 5.17.
It is important to note that the collection of the fluorescence at 50° angle implies an amplification of roughly one order of magnitude in the ratio between the fluorescence signal and the scattered light.

5.4 pH sensor in PMMA chip

An initial characterisation of the optical multi-channel chip was carried out by immobilising a pH sensing layer on the PMMA cover.
Solutions of FITC/EtOH (1 mM) and Eudragit RL100/EtOH (0.1 mM) were mixed 1:1; few drops of the cocktail formed a stable fluorescent layer sensible to the change in pH of buffered solutions flowing inside (Figure 4.15).

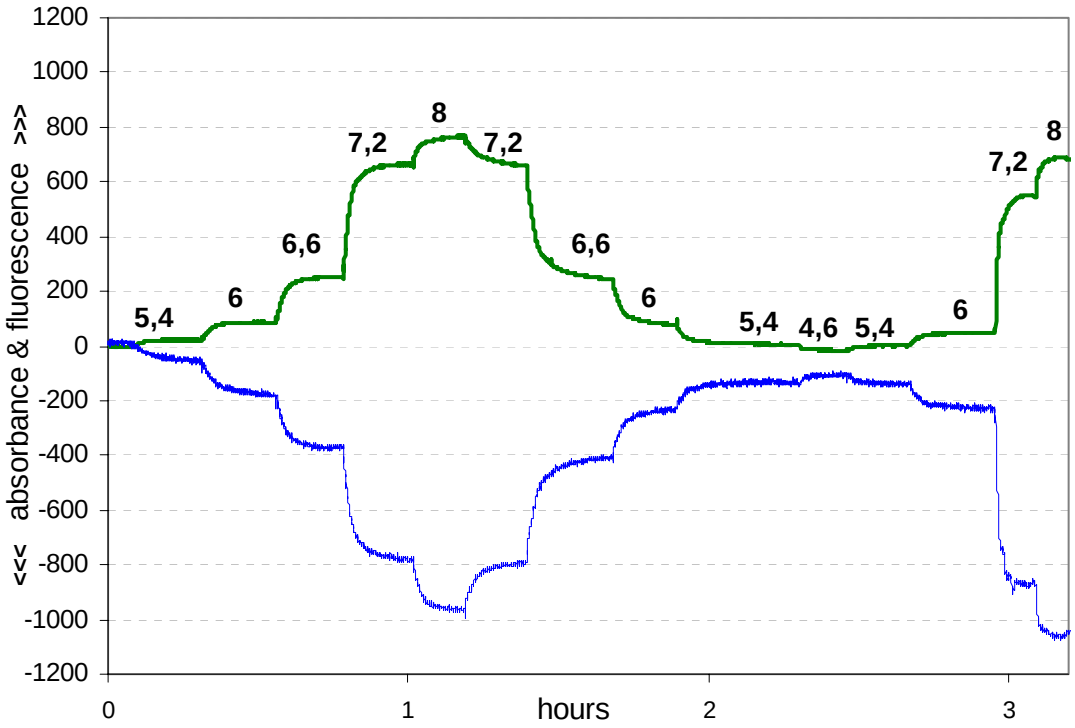

Figure 5.15 Response of absorbance and fluorescence with time for a pH sensor based on Eudragit RL100 and FITC immobilised on a microchannel of the PMMA chip under flow of buffers at different pH values. Both fluorescence signal at 525 nm (green line) and absorption signal at 488 nm (blue line) are shown.

The fluorescence signal and the source signal were monitored during a flow of pH buffer (Figure 5.15). The decrease in absorbance at 488 nm (in blue) reflects the increase of the fluorescence signal at 525 nm (in green) as expected from literature [348].

The pH change depends from the characteristics of the fluorophore dye and this result reflects exactly what is known in literature about fluorescein [349].

This result was really satisfactory because demonstrated clearly the capability of the optical chip in terms of sensitivity to the analyte in solution, good detection efficiency, fast response time, and honest reproducibility.

5.5 Development of a new optical biosensing platform for IgG/anti-IgG

The potentiality of the PMMA chip, its ease of use and its convenient geometrical configuration for a simple replacement encouraged a depth examination.

The validation of a prototype for affinity biosensors necessitated a study on how interactions between antigen and antibody are occurring on the PMMA substrate.

For this purpose, inexpensive proteins (IgG and anti-IgG) were selected and purchased for a deep investigation.

The research key step consisted in to find the best arrangement in terms of physics and chemistry, in order to obtain an immunosensor based on mouse IgG (bioreceptors) and goat antimouse IgG labelled Cy5 (analytes).

The plan strategy involved the modification of PMMA surface in order to obtain the most effective deposition of carboxylic groups. This choice was preferred in order to obtain mainly the covalent bond between amino groups of the variable region of IgG bioreceptors [131]. This treatment was carried out to achieve an entrapment of fluorescent antigens close to the surface where the outcome of the fluorescent light is guided in a more effective manner.

Small squares of PMMA were used as planar substrates in order to identify the best immobilisation procedure.

Polymer depositions of PLLA [336] or Eudragit L100 [362] were compared with surface treatments (NaOH in dmso/water or pyridine/water) to obtain exposed carboxyl groups. Immobilisation of an excess quantity of mouse-IgG (50 µl drop, 1 mg/ml) was carried out via EDC/NHS [Pierce], and its interaction with a concentrated solution of antimouse-IgG-Cy5 in PBS buffer was analysed.

An optical setup similar to the one shown in figure 5.14c was used.

The result in the anisotropic angle using Cy5 was in agreement with the one using fluorescein so the optical fibre at the output was interfaced with one lateral side of the planar square with an angle of 50° (Figure 5.16).

A diode laser at 635 nm was preferred to the led source and no filter was added between the source and the PMMA substrate.

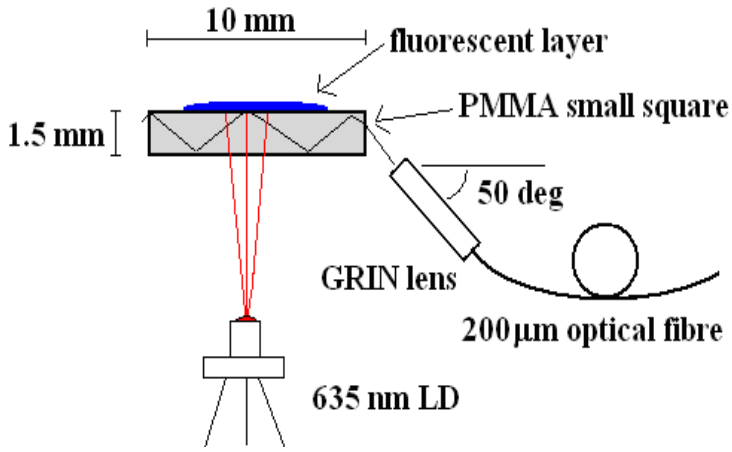

Figure 5.16 The source, a diode laser He/Ne at 635 nm, is perpendicularly directed on a PMMA square surface on which mouse IgG were immobilised. Their interactions with a solution of antiIgG-Cy5 were considered and studied. The emission signal in fluorescence is guided through the channel and collected using an optical fibre and a spectrophotometer.

The red laser diode source was driven by a current of 30 mA and the Ocean Optics spectrometer was adjusted with an integration time of 5000 msec.

The choice of the source at 635 nm, where the excitation efficiency of Cy5 is roughly 65%, follows the criterion of achieving a good separation between the excitation and emission wavelengths used.

Figure 5.17 shows a typical optical spectrum of the PMMA small squares treated with a polymer such as PLLA, with a concentration that ranged from 0.01 mM to 10 mM.

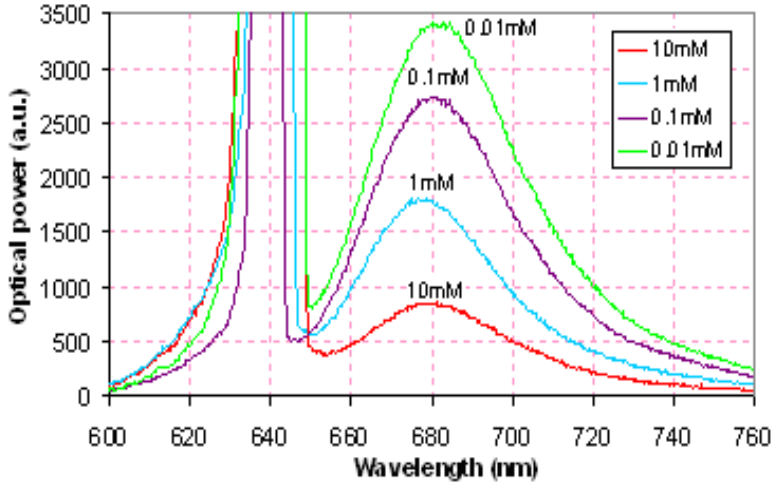

Figure 5.17 Optical spectra of the PMMA small squares treated with a PLLA concentration ranging from 0.01 mM to 10 mM; then EDC/NHS in MES 0.1 M and 50 µl of IgG (1mg/ml) to immobilise the antibodies for antiIgG-Cy5 revelation in flow. PBS buffer was used to rinse step by step. The measurement was performed with the optical setup shown in Figure 4.16. The contributions coming directly from the source (centred at 640 nm) and from the sensing layer (λ>650 nm) are shown.

The results are summarised in the histogram shown in Figure 5.18, in which the columns were obtained by evaluating the integral of the fluorescence spectra between 650-750 nm.

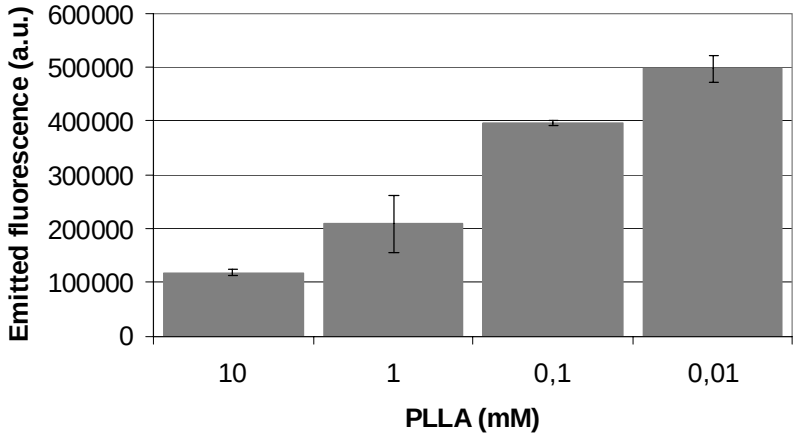

Figure 5.18 Histogram of the emitted fluorescence of the small squares treated with PLLA at different concentrations (10-0.01 mM) evaluated by considering the area of the collected spectra shown in Figure 4.17 between 650 nm and 750 nm. The error bar gives the standard deviation on three measurements performed on three different squares.

The error bar was the standard deviation of three measurements made on three different squares. As can be seen from the histogram, the concentration of carboxylic groups on the PMMA surface was a critical value: the measured fluorescence increased with a decrease in the PLLA concentration, i.e. with a decrease in the COOH concentrations on the PMMA surface. This can be easily explained by the fact that an overly large concentration of exposed functional groups led to an excessive and disordered immobilisation of IgG molecules.

The consequent steric hindrance and interaction among the IgG themselves implied a lower affinity toward the labelled anti-IgG. Moreover, a thick polymer substrate turn out to be non convenient, resulting in a wide separation between the sensing layer and the substrate resulting in a non appropriate optical coupling on a nano meter scale.

On the other hand, it was reasonable to wait for a decrease of fluorescence if the COOH concentration decreased too much.

This was observed in the case of the treatment of the PMMA surface with Eudragit L100. Figure 5.19 shows the histogram for six different concentrations of Eudragit L100. The trend was the same as the one observed for PLLA: by decreasing the concentration of Eudragit, an increase of the detected fluorescence was observed. However, a further

decrease beyond 0.01 mM implied a decrease in the detected signal, showing that the optimum concentration of Eudragit L100 on the PMMA surface was 0.01 mM.

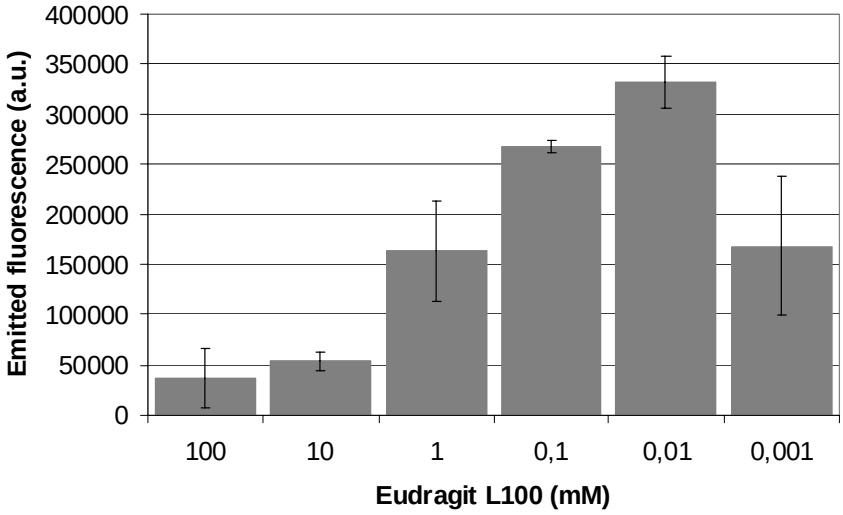

Figure 5.19 Histogram of the emitted fluorescence of the small squares treated with Eudragit L100 at different concentrations (100-0.001 mM), evaluated by considering the area of the collected spectra between 650 nm and 750 nm. The error bar gives the standard deviation of three measurements performed on three different squares.

The results obtained with NaOH are summarised in Figure 5.20. The treatment with NaOH in pure water was not very effective. Better results were obtained with NaOH dissolved in a 1:1 mixture of water and DMSO since this increased the wetting ability of the PMMA and implies a better interaction of the solution with surface.

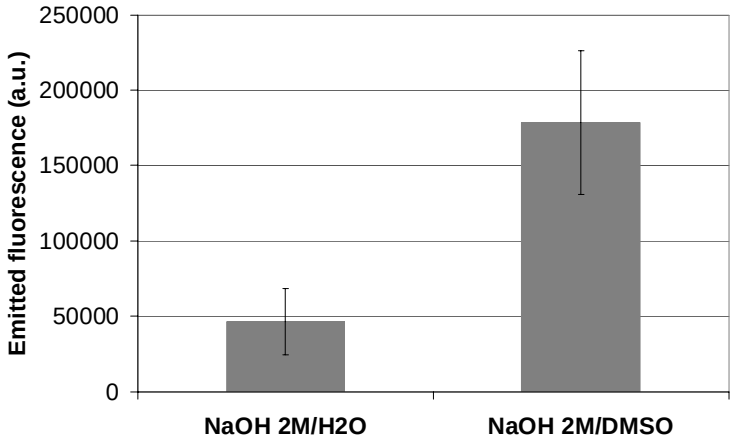

Figure 5.20 Histogram of the emitted fluorescence of the small squares treated with NaOH 2M in H_2O and with NaOH 2M in a 1:1 mixture of water and DMSO, evaluated by considering the area of the collected spectra between 650 nm and 750 nm. The error bars give the standard deviation of three measurements performed on three different squares.

The results obtained with pyridin/H_20 treatment at different ratio (1:1 and 95:5) and for different minutes (5, 20, 30 minutes) of drop deposition are summarized in Figure 5.21. The best chemical treatment in this case was found to be a mixture 1:1 for 30 minutes of deposition. However, the treated surface showed a lost in transparency and the formation of a thin white layer on the top of the surface, probably due to the aggressive action of pyridine. This was sufficient to enhance the scattering signal causing a large decrease in the signal to noise ratio. For this main reason the pyridine/water treatment was excluded from further analysis.

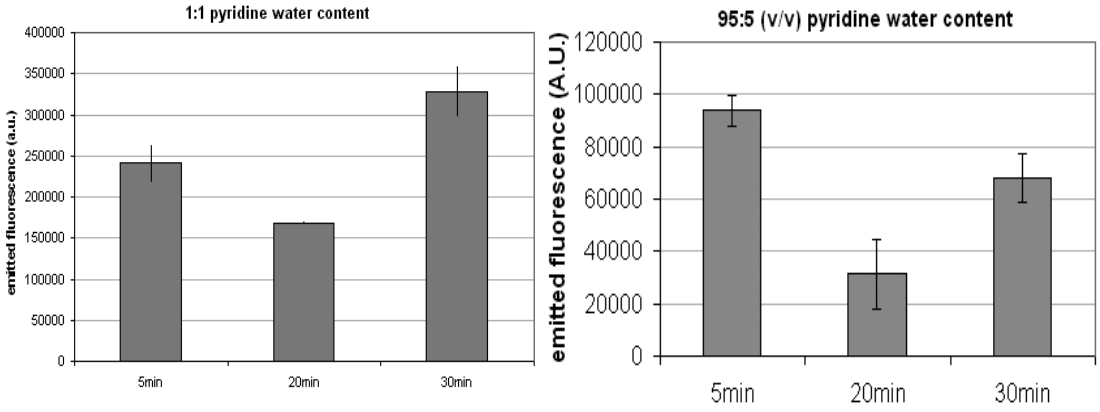

Figure 5.21 Histogram of the emitted fluorescence of the small squares treated with NaOH 2M in H_2O and with NaOH 2M in a 1:1 mixture of water and DMSO, evaluated by considering the area of the collected spectra between 650 nm and 750 nm. The error bars give the standard deviation of three measurements performed on three different squares.

The non-specific binding of labelled anti-IgG on the treated PMMA was tested by carrying out a one-hour incubation with the labelled anti-IgG on small squares with the immobilised IgG (specific binding) and on small squares with only activated carboxylic groups without immobilised IgG (non specific binding). In this second case, the unreacted carboxyl groups were treated with tris-HCl 0.2 M, pH 7.5 in order to block the activated surface for covalent immobilisation. After the incubation, the small squares were rinsed abundantly with PBS and the fluorescence spectra were collected. These tests were performed on small squares treated with Eudragit L100 (0.01 mM), PLLA (0.01 mM) and NaOH 2M (in 1:1 water/DMSO mixture) and the resulting fluorescence spectra are shown in Figure 5.22 a) b) and c), respectively. In all the cases, the non-specific binding was negligible, with the best performance exhibited by the surface treated with Eudragit L100. In these experiments, the contribution coming from the source was filtered using the HP filter (cut-on at 650 nm) with the consequent almost total removal of the source peak.

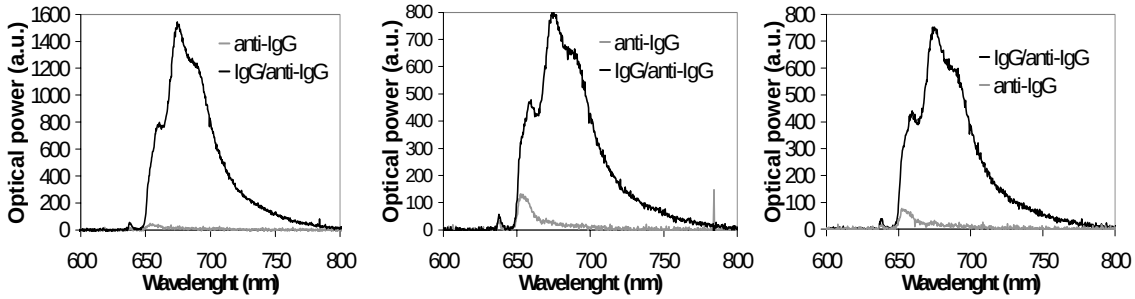

Fig. 5.22 Fluorescence spectra of the PMMA small squares treated with: a) Eudragit L100 0.01 mM, b) PLLA 0.01 mM, c) NaOH 2M (in 1:1 H_2O/DMSO mixture), and with (black spectrum) and without (grey spectrum) immobilised IgG, after 1-hour incubation with the labelled antiIgG-Cy5. Measurements were carried out with the optical set up shown in Figure 4.16 with the addiction of an HP filter cut on at 650 nm which decrease almost totally the source peak at 640 nm.

5.6 IgG/anti-IgG sensor in PMMA biochip

The sensitivity of the PMMA multiarray biochip was tested for a IgG/anti-IgG immunoassay with an optical system (Figure 5.23) built around the chip as first prototype.

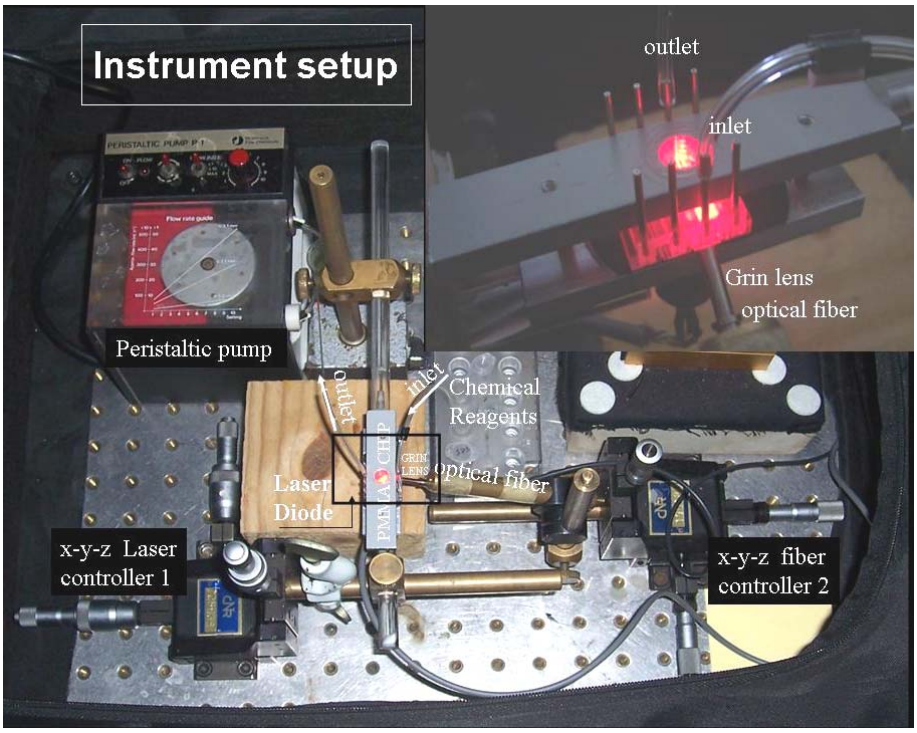

Figure 5.23 Optical setup for the PMMA multi-channel biochip. Top right is shown the detail of the coupling between the biochip, the diode laser and the optical fibre.

From the previous results, Eudragit L100 0.01 mM demonstrated to be the optimal concentration of polymer for IgG immobilisation.

In order to identify the optimal concentration of IgG for the sensing layer on the PMMA chip, three different IgG concentrations (0.005-0.05-0.5 mg/ml) were deposited on the chip. After one-hour incubation with 0.1 mg/ml of labelled anti-mouse-IgG, the chip was interrogated with the optical configuration shown in Figure 5.23, without the cylindrical lens and the input BP filter at 635 nm. The results obtained are shown in Figure 5.24. The fluorescence signal was centred at 670 nm, whereas the peak was around 655 nm due to the contribution coming directly from the source as a result of scattering.

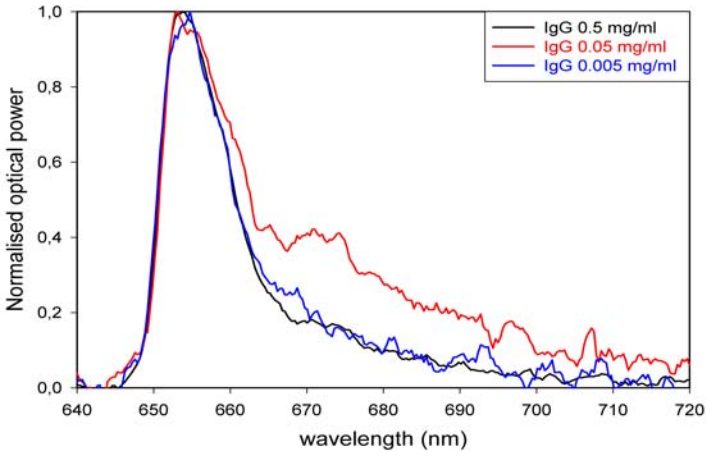

Figure 5.24. Optical intensity detected with the PMMA chip in the case of three different mouse IgG concentrations used for the formation of the sensing layer. The signal was recorded after 1-hour incubation with 0.1 mg/ml of labelled anti-IgG.

Although the signal levels and the efficiency of the fluorescence collection are low, the results shown in Figure 5.24 give a clear indication that 0.05 mg/ml was the optimal concentration of IgG to cover the PMMA surface. The reason for the low signal levels obtained with the PMMA chip compared with the small squares, is due to two main factors:

1) The different dimension of the luminous spot used to produce fluorescence; in the case of the small squares, the surface carrying the labelled anti-IgG was almost the whole surface of the square (1 cm^2) whereas in the case of the channel in the PMMA chip this surface was limited by the dimension of the flow channel. Since the lateral dimension of the flow channel was 0.5 mm, the illuminated surface usefully producing fluorescence can be estimated to be in the range of 0.05 cm^2.

2) The labelled anti-IgG concentration used in the experiments shown in Figure 5.24 was 0.1 mg/ml, ten times smaller than the concentration used in the chip experiments (Figure 5.17-5.22).

The optical efficiency of the system was improved by positioning a cylindrical lens on the top of the PMMA chip in correspondence with the sensing layer, which allowed the LD beam to be focussed on the immobilised sensing layer. Also the contribution from the scattered light coming from the source, represented by the peak at 655 nm, was noticeably reduced by placing the BP filter at 635 nm in front of the source. A further improvement in sensitivity was obtained by replacing the Ocean Optics spectrometer (based on CMOS technology) with an Hamamatsu spectrometer integrated with back-thinned type CCD image sensor.
The response of both the spectrometers to the optical signal coming from the same chip is reported in Figure 5.25, demonstrating a signal to noise ratio (SNR) improvement of about two orders of magnitude (difference in sensitivity between CMOS and CCD).

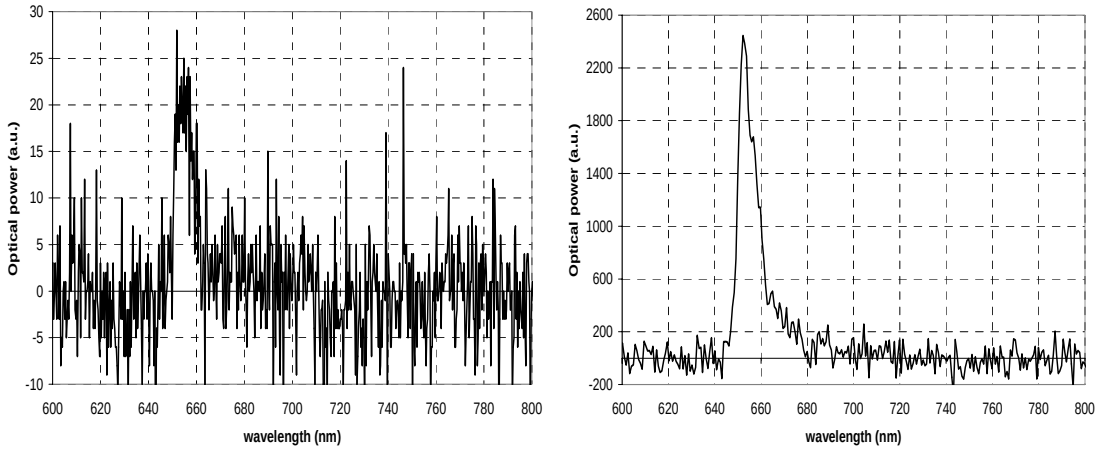

Figure 5.25 Response to the same optical signal of the Ocean Optics (left) based on CMOS technology, and the Hamamatsu (right) spectrometer based on CCD technology. The Hamamatsu SNR is about two orders of magnitude better.

On the basis of the results shown in Figure 5.24, the IgG/anti-IgG assay was then carried out by immobilising IgG 0.05 mg/ml on the PMMA chip, previously treated with either Eudragit L100 0.01 mM or PLLA 0.01 mM or NaOH 2M in DMSO/H_2O. The level of the improvement in the optical efficiency can be appreciated in Figure 5.26, which shows the fluorescence spectra in the case of treatment with Eudragit L100, for different

concentration of labelled anti-IgG (the spectra should be compared with those shown in Figure 5.24).

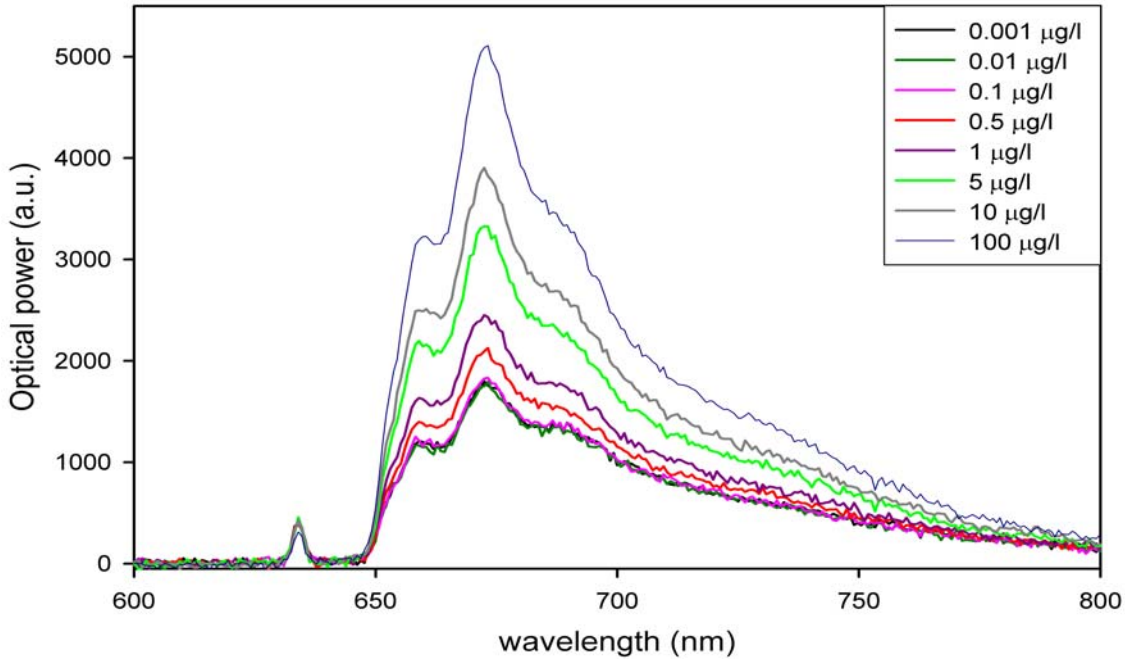

Figure 5.26 Optical spectra coming from the PMMA chip in the case of treatment with Eudragit L100, for different concentration of antiIgG-Cy5 The flow chamber is one channel of the PMMA biochip. The source is red diode laser. One filter at the input (BP-640) and a second filter at the output (HP >650) were applied to the optical system. The incubation time for each measurement was 15 minutes. The measurement was collected after 5 minutes more of buffer flow to exclude the presence of any aspecific interaction between antiIgG and the surface rich in IgG receptors. Every measurement is the average of ten spectra captured in a session of two minutes.

The measurements were carried out under flowing conditions at 10 µl/min. It is also important to stress the fact that in this case the incubation time (flow of anti-IgG) was reduced to 15 minutes. This is a very important parameter in the design and development of clinical assays, especially those for point-of-care applications, where reduction of the duration of the assay is an essential requirement. The spectra were recorded after washing for 5 minutes with PBS. Each spectrum is the average of ten spectra acquired with an integration time of 10 sec. It is important to observe the presence of a fluorescence signal also in the case of PBS buffer alone, without any labelled molecules bound to the IgG layer. The spectrum in this case overlaps with the 0.001 µg/ml spectrum, shown in Figure 5.26, and this spectrum represents the zero for this series of measurements. This effect is due to the autofluorescence of PMMA, which implies the presence of an intrinsic background in the detected signals. It is important to stress the fact that the PMMA, if

produced by injection moulding, is characterised by low autofluorescence, when excited in the red region [350]. In our case the provider of PMMA was unable to give this information. Figure 5.27 shows the calibration curves for IgG/anti-IgG assay in the three different cases: PMMA treatment with NaOH, Eudragit L100 and PLLA.

The fitting of the experimental points with a sigmoid curve is also shown. The contribution of the PMMA autofluorescence to the fluorescence signal was ignored, considering that the value obtained using pure PBS sample was equal to zero.

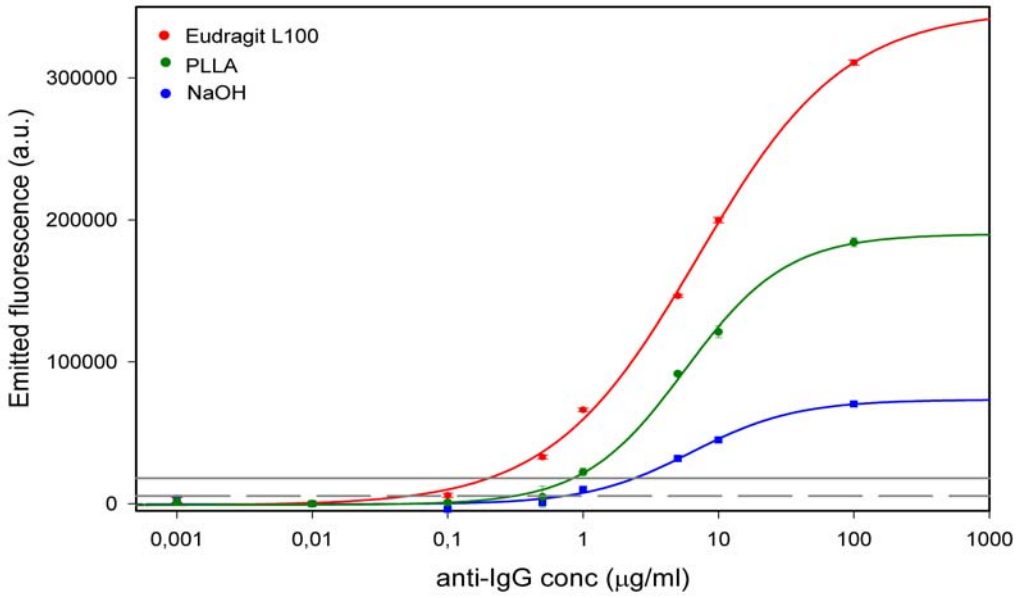

Fig. 5.27 Calibration curves of the IgG/anti-IgG assay for the three different treatments of the PMMA surface. The horizontal lines represent three times (dashed line) and ten times (solid line) the highest value of the standard deviation calculated for the different points for the curve related to Eudragit L100.

The integral between 650 and 750 nm of each spectra was evaluated and each point of the graph was obtained by calculating the average value of a total of ten recorded spectra. The standard deviation for each point is also shown and is in the range of the dimension of the points. The best performance was obtained with Eudragit L100. In this case the limit of detection and the limit of quantification were evaluated: the horizontal lines shown in Figure 5.27 represent three times (dashed line) and ten times (solid line) the highest value of the standard deviation calculated for the different points for the curve related to Eudragit L100.

The intercept of the calibration curve gives the limit of detection, 0.05 µg/ml, and the limit of quantification was 0.2 µg/ml for the IgG/anti-IgG assay.

5.6.1 Potential improvements in the optical efficiency of the PMMA biochip

Further improvements could be obtained by minimisation of the background noise of PMMA due to autofluorescence. Two different types of transparent PMMA derivatives (Topas and Zeonex) were compared to the one used above. The results shown in Figure 5.28 demonstrated that Zeonex is the minor autofluorescent material and should be used to fabricate the chip.

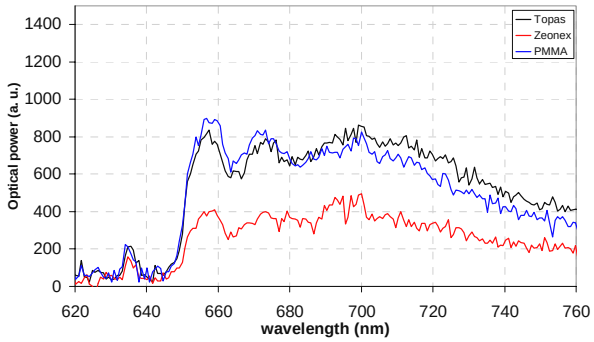

Figure 5.28 Excitation source is 635 nm. Comparison between optical spectra for three different type of transparent PMMA polymers.

Another potential improvement could be obtained by using chemical vapour deposition of aluminium and silver on one of the two angular sides of the PMMA biochip. The result for a bare mirror channel was compared to a normal chip channel (in water) is shown in Figure 5.29. The experiment demonstrated that more fluorescence signal (in this case the autofluorescence of PMMA) could be collected to improve the optical efficiency.

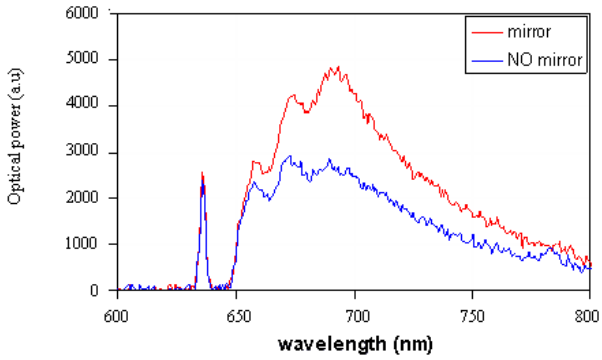

Figure 5.29 Comparison between a normal PMMA cover and a mirror PMMA cover. Excitation source was at 635 nm. The autofluorescence of PMMA (λ >650 nm) increases evidently with the addition of a micromirror on the second side of the channel. This micromirror was obtained by chemical vapour deposition of several layers made of aluminium and silver.

5.7 A biosensor for NF-kB1: A study of interactions by means of fluorescence between DNA kB site, p50 homodimer and antibody C19-Cy5 in a sandwich assay

An exhaustive introduction about the importance to detect NF-kB in nuclear cell extracts is fully explained in the Introduction of this thesis.

The optical system used for these experiments regarded the one used for PMMA multi-channel biochip shown in Figure 5.23.

The DNA sequence (kB site) specific for NF-kB detection possess amino group on its loop as shown in Figure 5.30 and it was synthesized in the laboratories of IFC-CNR in Pisa.

Fig. 5.30 NF-kB decoy, the DNA sequence able to capture the target protein. A specific ssDNA sequence was synthesised with a loop part modified with primary amino groups. In the complementary part the DNA bend on itself in a dsDNA configuration.

The DNA was dissolved in pure deionised water in a concentration of 0.1μM and then inserted into a PMMA channel previously treated with Eudragit L100/EtOH (0.01mM) and activated with EDC/NHS activation. The immobilisation of NF-kB decoy was carried out at a constant flow speed of 10 μl/min for 30 minutes. Ethanolamine was used, after DNA, to deactivate the surface and to avoid further undesirable covalent binding.

The unreacted ethanolamine was removed by washing for five minutes with the binding buffer for p50 (binding buffer: 10mM HEPES pH=7.9, 50 mM KCl, 0.1M EDTA, 2.5 mM DTT, 10% glycerol and 0.05% NP-40).

The p50 solution was dissolved in binding buffer in a concentration of 0.1 μM and was inserted for 30 minutes in the channel where interaction between DNA and p50 was expected. PBS was used to wash out in flow for 5 minutes the unreacted p50, then the signal was recorded (PMMA autofluorescence signal).

A specific antibody for p50 detection, called clone 19 (C19), was labelled with Cy5, and then was inserted in flow in the channel in a concentration of 0.1 μM for 15 minutes at 10

µl/min; then the channel was washed for 5 minutes with PBS and the signal was recorded (Figure 5.31).

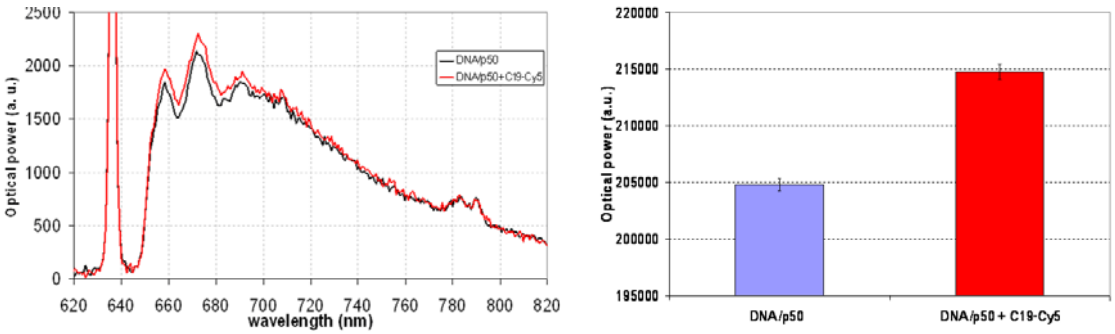

Figure 5.31 Left: optical spectra. Right: fluorescence area in the range 650-750 nm. The autofluorescence of PMMA is represented with light blue colour. The interaction between the p50 bound to DNA and the antibody specific for p50 is represented with red colour.

A control experiment was carried out to ensure the antibody C19-Cy5 is binding only at p50 sites and is not adsorbed (aspecific binding) to the surface. A channel was prepared with the same procedure but, after DNA immobilisation, the p50 protein was not added. Then the C19-Cy5 was added to determine if it binds to the surface where DNA is immobilised. The result obtained (Figure 5.32) was not satisfactory because in this case p50 is not inside the channel, so C19-Cy5 must not bind to anything.

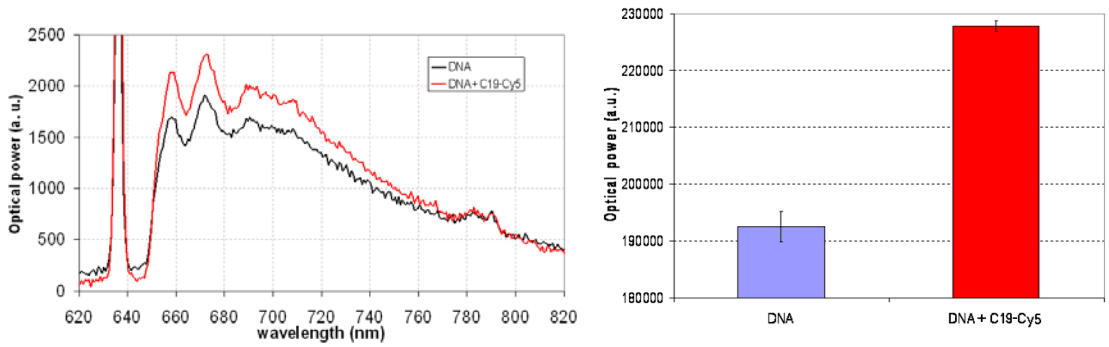

Figure 5.32 Left: Optical spectra. Right: fluorescence area is in the range 650-750 nm. The autofluorescence of PMMA is represented with light blue colour. The interaction between the surface (with DNA immobilised) and the antibody specific for p50 is represented with red colour. The difference between these two areas had to be zero to ensure that C19-Cy5 interact just with p50 and not with the surface. This is not the case. This result demonstrate that C19-Cy5 interact with the surface and means that something wrong is occurring inside the channel.

This result means that antibody C19-Cy5 binds not only to p50 but also non specifically, in part or totally, to the free sites of the PMMA.

To avoid aspecific binding of the fluorescent antibody (C19-Cy5) on the PMMA surface, the use of bovine serum albumin (BSA), reported in the literature [353], was considered.

A solution of BSA in PBS at 10% (w/v) was prepared to cover all the free sites of the channel and to avoid aspecific binding of proteins to the surface.

The same protocol described before was repeated and besides ethanolamine, BSA was used. The result obtained for BSA treatment was satisfactory (Figure 5.33).

BSA protein inactivate all the free sites present on the PMMA surface and avoid aspecific binding of C19-Cy5 antibody to the surface.

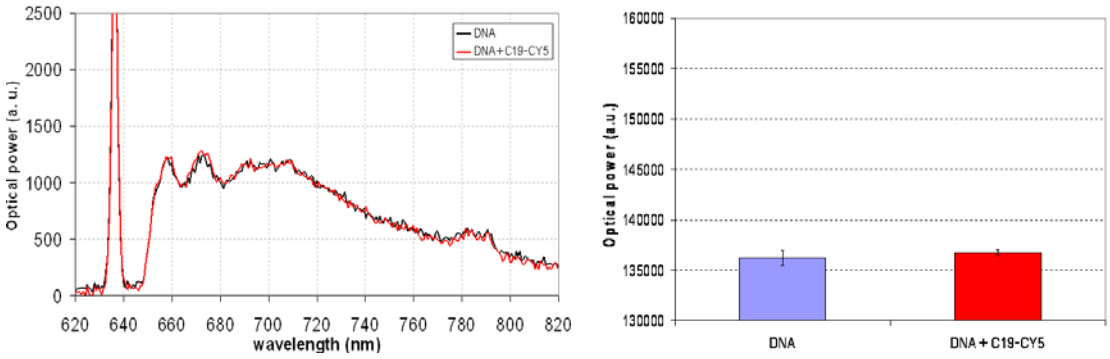

Figure 5.33 Left: Optical spectra. Right: fluorescence area in the range 650-750 nm. The autofluorescence of PMMA is represented with light blue colour. The interaction between the surface and the antibody specific for p50 is represented with red colour. The difference between these two areas had to be zero to ensure that C19-Cy5 interact just with p50. This is the right case. Aspecific binding of C19-Cy5 was avoided using BSA besides ethanolamine in the pre-treatment inactivation of the surface.

Inactivation of the surface with BSA 10% (w/v) in PBS was carried out and the first experiment using p50 was repeated. The signal of C19-Cy5 resulted now specific for p50 detection bound to the DNA decoy and the experiment result shown in Figure 5.34 was considered successful.

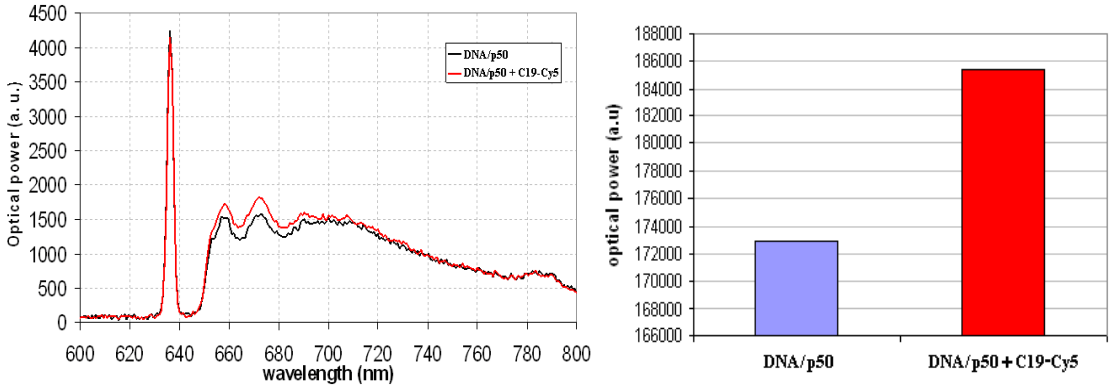

Figure 5.34. Left: Optical spectra. Right: fluorescence area in the range 650-750 nm. The autofluorescence of PMMA is represented with light blue colour. The interaction between the sensing surface and the antibody specific for p50 is represented with red colour. The difference between these two areas is proportional to the quantity of p50 present inside the channel.

5.7.1 Regeneration by SDS

Regeneration of the sensing surface is highly desirable for a biosensor system.
This was achieved by flowing SDS 10% for 20 minutes. The complex DNA/p50 + C19-Cy5 was washed with SDS and the signal decreased because all the proteins were washed out (p50 and C19-Cy5). SDS tightly binds to proteins and washes those, but not DNA which is imperturbable by SDS treatment [354]; the decoy for NF-kB was regenerated by this method and the measurement with p50 and C19-Cy5 was repeated again (Fig. 5.35).

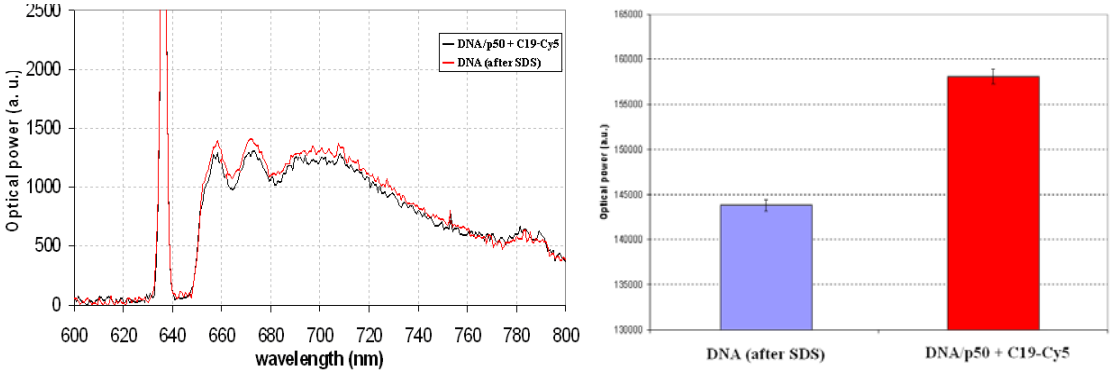

Figure 5.35 Regeneration of the biosensor with SDS (10%). Left: Optical spectra. Right: fluorescence area in the range 650-750 nm. The autofluorescence of PMMA is represented with light blue colour. The interaction between the sensing surface and the antibody specific for p50 is represented with red colour. The difference between these two areas is proportional to the quantity of p50 and C19-Cy5 washed inside the channel.

The regenerated biosensor was used a second time to reveal different quantities of p50; two treatments with different concentrations of p50 (0.01 µM and 0.1µM) were tested.
The concentration of C19-Cy5 in this case was kept constant (0.1 µM).

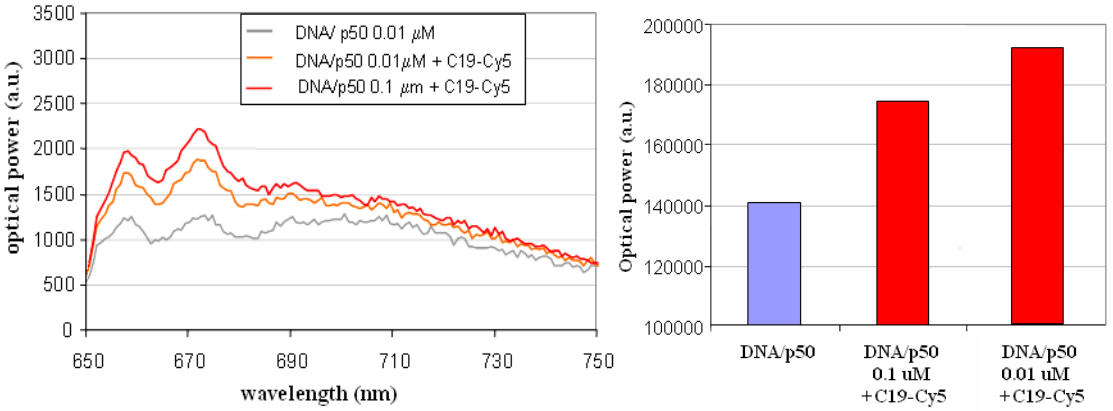

Fig. 5.36 Detection of two different concentrations of p50 (0.01 µM, 0.1 µM) using C19-Cy5 (antibody specific for p50). Left: Optical spectra. Right: fluorescence area in the range 650-750 nm. The autofluorescence of PMMA is represented with light blue colour. The interaction between the sensing

surface and the antibody specific for p50 at different concentrations is represented with red colour. The difference between these two areas is proportional to the quantity of p50 present inside the channel.

The results shown in Figure 5.36 reveal that for more concentrated solution the fluorescence increased as expected, because C19-Cy5 bind to more accessible p50 bound to the DNA decoy.

The interaction between DNA and NF-kB p50/p50 is reported in literature [175, 176] and is considered biologically as the precursor step for NF-kB p50/p65 revelation.

As it was plenty described in the introduction, although most of the NF-kB proteins are transcriptionally active, some combinations are thought to act as inactive complexes. P50/p65, p50/c-Rel, p65/p65, and p65/c-Rel are all transcriptionally active, whereas p50 homodimer (the one used in these experiments) and p52 homodimer repress transcription [174]. It is important to notice also that stimulation of cells with agents that activate NF-kB causes an increase in the p50/p65 content [181].

It is also known from theory that p50/p65 binds more tightly to DNA decoy replacing p50/p50 [173, 176].

So a future plan for the research to obtain a NF-kB biosensor is to insert in the channel with DNA decoy immobilised, the active heterodimer p50/p65, and calibrate the system with it using C19-Cy5 antibody which demonstrated to be trusty and reliable for the detection of p50.

Another future plan in the research to obtain a NF-kB biosensor is to insert p50/p65 in the channel with DNA immobilised and with p50/p50 bound to it, in order to determine the replacement of p50/p50 by p50/p65. This shift could be measured using C19-Cy5, pointing out that the fluorescence signal should decrease of half in the case of p50/p65 compared to p50/p50, just because this heterodimer contains half quantity of p50.

Unfortunately the heterodimer protein p50/p65 is not freely available in the market, so it will be necessary to synthesise or to extract it biologically in order to perform a calibration curve for this protein.

In literature is present only one work about detection by fluorescence of p50 homodimer bound to DNA [168], and in that case FRET (Forster Resonance Energy Transfer) method was employed, using a fluorescent compound for DNA labelling and a quencher (that absorbs the emission at the same wavelength) compound for p50 labelling.

Anyway, also in this case, was not possible to detect the p50/p65, but only p50/p50 for the same reason explained before (unavailability of p50/p65 on the market).

5.8 Biosensor for MGMT: A study of interactions by means of fluorescence between target RNA and synthetic 2'OMe-RNA probes covalently bound on PMMA

In order to attach thiol-modified 2'OMe-RNA probes using the SMCC cross-linker, it was necessary to obtain amino groups on the PMMA surface.

Quantification of amino groups obtained by several chemical treatments on the surface was performed using a sulfo-SDTB [351-352] which reacts with amino groups releasing, in perchloric acid, the dimethoxytrityl dye molecule (absorbance at 498 nm).

The different treatments considered are reported as follows:

b) Drop deposition of Eudragit L100 (x2);

b,c,d) acid hydrolysis of ester groups on PMMA (H_2SO_4 3M; H_2SO_4 1M; HCl 1M)

e,f) alkaline hydrolysis of ester groups (NaOH 4M; NaOH 1M) with PMMA planar square immersed in the solution for 3 h.

g) PMMA chip immersed in HMDA 1M in DMSO;

h) Drop deposition of HMDA 1M in DMSO (x2).

i) bare PMMA;

In Figure 5.37 is shown the calibration curve obtained with s-SDTB.

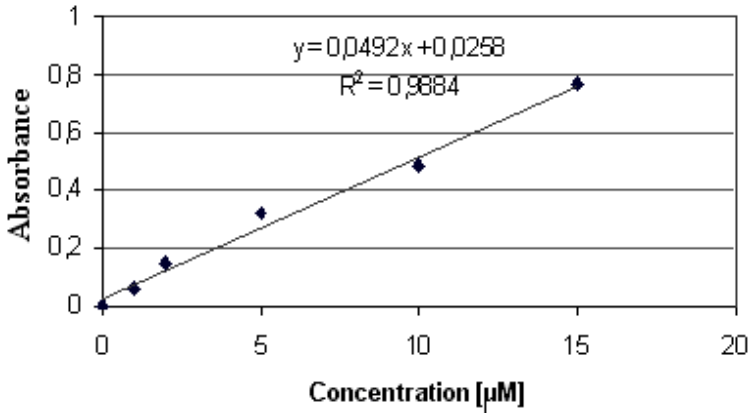

Figure 5.37 s-SDTB calibration curve was obtained measuring absorbance at 498 nm for different concentrations of the released dye after perchloric acid treatment.

In Figure 5.38 the results in the surface density of amino groups, obtained measuring the absorbance spectra at this wavelength with a spectrophotometer, was reported: a) and h) were the most efficient treatments, and the drop method was preferred to the immersion method. In particular, the treatment with Eudragit L100 was chosen for the immobilisation of the RNA oligonucleotide by means of SMCC cross-linking.

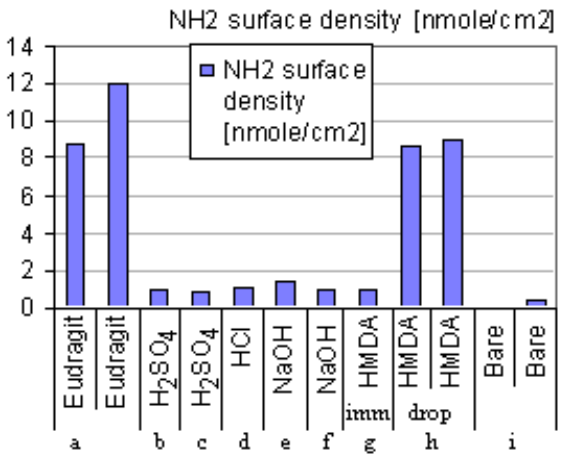

Figure 5.38 Surface density (in nmol/cm^2) of amino groups bound to the surface. The drop method offered better performance compared to the immersion method. In the case of the drop method the area considered was one face of the PMMA chip. In the case of immersed method the total surface area of the volumetric PMMA chip was considered. Buffer for SDTB was $NaHCO_3$ at pH 8.5.

A further control experiment was performed to be sure of no interaction between Cy5 and bare PMMA and to understand the entity of the fluorescence signal in the case of HMDA treatment of the surface. In this case HMDA acts as a crosslinker between bare PMMA and Cy5 dye. Two different planar squares were prepared with a solution of Eudragit L100/EtOH (0.01 mM); 50 µl of this solution was dropped on the surface and let dry at 25°C. In the first planar square a solution of HMDA 100 mM in DMSO was dropped to the surface. After 1 hour this was washed with pure water and a solution of Cy5 in DMF (0.1 mM) was dropped on the surface, reacted for 30 minutes and then washed with water. In the second planar square (control with no HMDA) a solution of Cy5 0.1 mM was dropped directly on the surface treated with Eudragit L100 and washed with pure water after 30 minutes. The results in Figure 5.39 demonstrated that if HMDA was deposited, Cy5 reacted with it; if amino groups were not present (no HMDA), Cy5 did not bind to the surface. The result was clearly evident without filtering of the source.

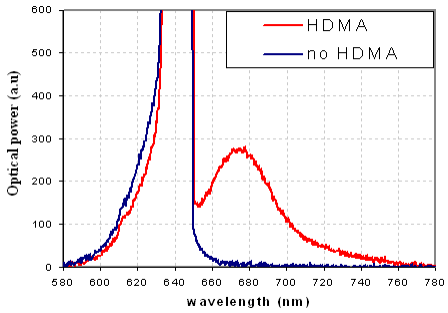

Figure 5.39 Signal of fluorescence of Cy5 covalently bound to exposed amino groups of the PMMA chip. The excitation source was a red diode laser at 635 nm.

5.8.1 MGMT: Results for Target 7/Probe 7 RNA/RNA duplex

The next step aimed to immobilise a thiol-modified RNA, by means of SMCC cross-linking action. The immobilized bioreceptor RNA probes were as follows:

Probe 7: 5'-GUGCGUUUCAUUUCACAAUCCUUGU-3'

Characteristics: 2'OMe, SH at 3', conc. 0.1mM.

*Probe 7' mismatched: 5'-GUGCGU**A**UCAUU**G**CACAA**G**CCUUGU-3'*

Characteristics: 2'OMe, SH at 3', conc. 0.1mM.

The RNA target 7 is complementary to probe 7:

Target 7 (7): 3'-CACGCAAAGUAAAGUGUUAGGAACA-5'*

Characteristics: 2'OMe, FITC-labelled, conc. 0.1mM.

2'-O-methyl-RNA probes (7 and 7') were spotted on two PMMA planar squares of 1 cm^2 pre-treated with Eudragit L100/EtOH, HDMA/DMSO, SMCC and washed step by step with PBS buffer.

The immobilised bioreceptors were the probe 7, a sequence complementary to the target 7*, and the probe 7', a mismatched sequence with three nucleotides of difference to the probe 7 (evidenced in bold). Target 7* was labelled with FITC fluorophore (Figure 5.40).

The RNA probes were dissolved in pure water, whereas the RNA targets were dissolved in an hybridisation buffer (2X) made of 5 ml of formamide (50%), 5 ml of SSC (10X), 0.2 ml of SDS (10%). SSC (20X) buffer was prepared adding NaCl 3 M, sodium citrate 0.3 M and EDTA 1 mM.

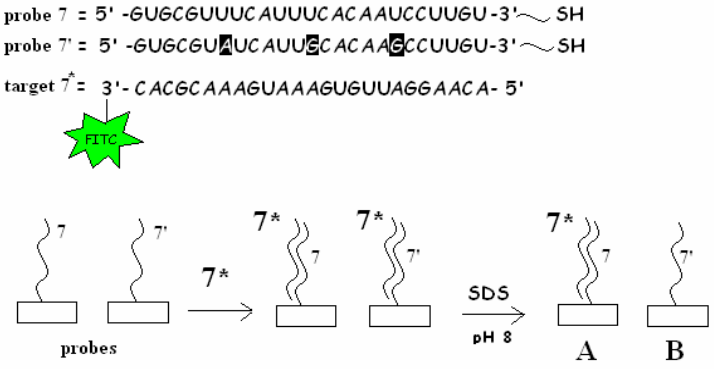

Figure 5.40 Procedure to test the detection and the specificity of target 7*. Two probes (7, 7') were immobilised on the planar surface and let react with a solution of target 7*. After hybridisation occurred, the planar square were washed accurately with an SDS solution in order to take out the not hybridised oligos. The ideal case is shown on the right, where the complementary is attached to the probe whereas the non complementary is washed out. The differences in the bases between the two probes are highlighted on the top; anyway both 2'OMe-RNA were modified with a thiol group as functional group for immobilisation on the surface.

The led source (490 nm) was not filtered at the input and output, and the signal for 2'OMe-RNA/RNA duplex (Figure 5.41) was collected.

Letter "A" represent the interaction between the complementary RNA strands probe 7 and target 7*, while letter "B" represent the interaction between a mismatched probe 7' and target 7* as it was reported previously, in Figure 5.40.

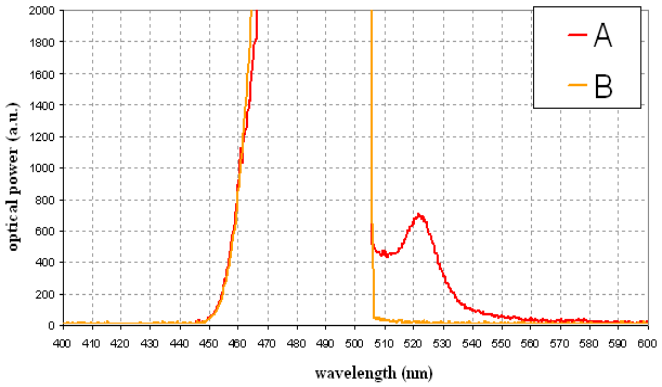

Figure 5.41 Optical spectra signal for two different planar square on which probe 7 and probe 7' were immobilised. A blue LED 488 nm is the source. Not filters were applied at the input and output. The letter A represent the hybridisation for probe 7 and target 7*, whereas the letter B represent the hybridisation (not occurring) for probe 7' and target 7*. This experiment confirm the proper specificity of probe 7 to target 7.

5.8.2 Specificity of the probe 7 to the T7* in a T7*/T46 solution

Further experiments on the specificity of probe 7 were executed by immobilising probes 7 and probe 46 and observing the interaction with a mixture 1:1 of targets (T7* and T46). This experiment was accomplished in order to obtain a sandwich system (probe 7-mRNA-probe 46) as it was described in the introduction part.

Figure 5.42 shows optical spectra obtained for this experiment which was performed to understand if the probe 7, in a T7*/T46 solution, interact only with T7* and not with the T46. The specificity of the probe 7 to the T7* in a T7*/T46 solution is an essential requirement, in order to avoid unwanted cross reactions for the obtainment of a proper sandwich construct. Probe 7 represents, in fact, in the strategy plan thought, the first site of attachment for the mRNA target, whereas probe 46 represents the second site (sandwich locking up).

Therefore, sixteen PMMA planar squares were investigated by means of fluorescence coming from hybridised target 7* using the optical setup shown in Figure 5.14c. Drops of

5 µl of three solutions were spread on the PMMA surface pre-treated with cross-linker SMCC. The three solutions were probe 7, probe 46, and a mix 1:1 of probe 7 and 46.
Two kind of carboxylic polymers were compared (PLLA and Eudragit L100) and on all the planar squares two different solutions were deposited; 50 µl of T7* in annealing buffer solution (1:1) and 50 µl of T7* and T46 (1:1) were let react for two hours.
The planar squares were then washed abundantly with buffer.
The optical system was not filtered to understand any variation of the fluorescence signal.

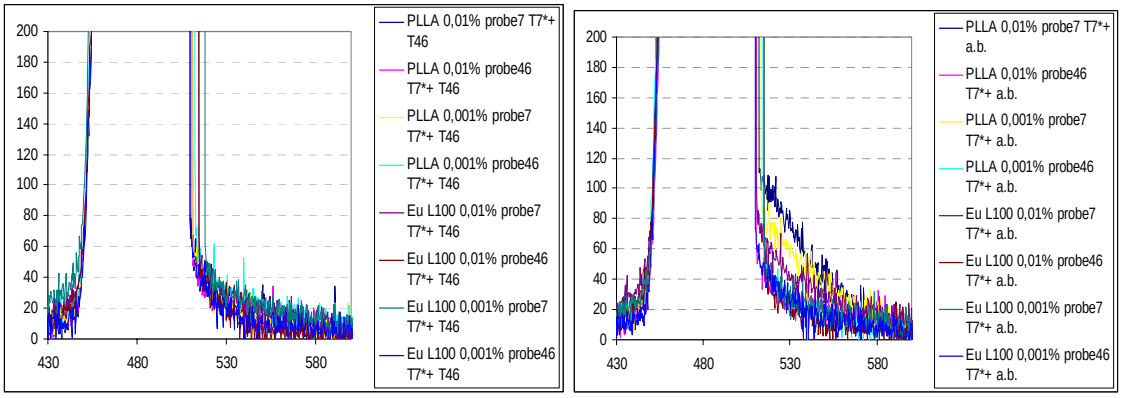

Figure 5.42 Left: Optical spectra of the interactions between probe 7 or probe 46 with a mixture 1:1 of T7*/T46; Right: Optical spectra of the interactions between probe 7 or probe 46 with a solution 1:1 of T7*/buffer.

The results, partially covered by a high signal of noise due to PMMA autofluorescence, can be simplified if considered from another perspective (Figure 5.43).

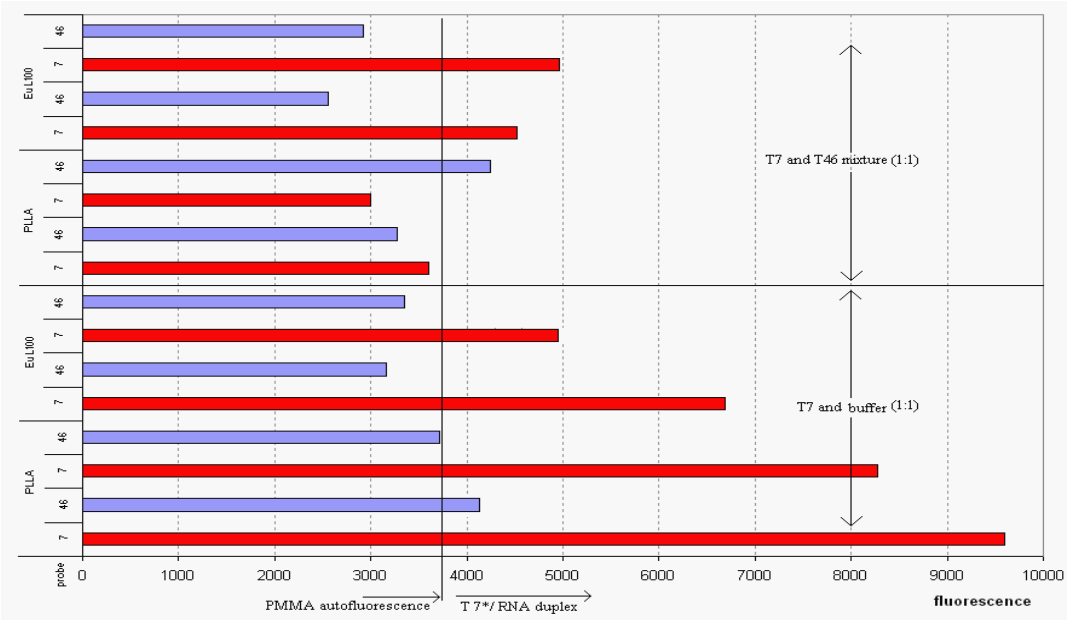

Figure 5.43 Results in fluorescence for bioreceptor probes 7 and 46 immobilised on the PMMA planar squares. On the sensing surface two solutions were dropped: as first the target 7*, and as second a mixture solution of target 7* and 46 (1:1). Fluorescence area of probe 7 immobilised are shown in light blue colour

whereas area of probe 46 immobilised are shown in red colour. On the Y axis is shown the type of polymer employed (PLLA or Eudragit L100) and the type of solution adopted (T7/buffer, 1:1 and T7/T46, 1:1). On the X axis is shown the intensity of fluorescence due to PMMA and due to the occurred hybridisation.

In particular, in red are shown the area of the fluorescence signals for the probe 7 immobilised, whereas in light blue are shown the signals for probe 46 immobilised on the surface.

It is important to stress the fact that for this experiment a concentration of T7* (and T46) ten times smaller than the previous experiment (Figure 5.41) was used and for this reason, the optical signals seems to be not "clean" as usual.

In future plans will be important to repeat the same experiment filtering the input and output signals in order to collect a better spectral resolution.

The fluorescence signal was calculated considering the area in the range between 515-585 nm.

In this area the autofluorescence of PMMA was quite high and so, to understand any variation of the fluorescence signal, a vertical line was drawn to separate at the left the PMMA autofluorescence contribution and at the right the fluorescence derived by T7* binding (Figure 5.46).

A second horizontal line divides the signals obtained using a mixture of targets (T7 and T46) or a single target (T7).

Hybridization between probe 7 and T7* was detected in the case of a solution containing only T7*. This seems to be in accord with the result obtained in Fig. 5.44.

In a mixture solution of both targets (T7* and T46) the hybridization between probe 7 and T7* seems to be partially impeded or disturbed, in particular in the case of PLLA polymer. This effect is less relevant in the case of Eudragit L100.

As described in the introduction part, the probes were chosen from a computational method described in literature [318, 320], which was exploited for selecting accessible regions of the probes in the human MGMT transcript.

The program analyses the score of pairing events among the different structures nucleotide by nucleotide (the freedom of each nucleotide), considering the probability of existence of each structure.

A set of potential probes for MGMT mRNA were considered and some of the most favourable ones were selected as probes for T7 and for T46 detection [320].

In a future plan research will be opportune to try the same experiment carried out on probe 46 using other kind of probes, such as probe 64 and probe 41.

The sequences can be found considering the article reported in literature [320].
Unfortunately, in this case, the literature is poor for this argument revealing a certain limitation in the comprehension of this argument.

5.8.3 Calibration curve probe 7-target 7* in PMMA chip:

The detection of RNA target 7* was accomplished: so, a calibration curve (Figure 5.44) was obtained for the experiments carried out in flow conditions.
The PMMA substrate of the multi-channel chip was previously modified with Eudragit L100/ EtOH (0.01 mM) and then activated with EDC/NHS treatment; 2'OMe-RNA (probe 7) was inserted in flow at 10 µl/min of speed for 30 minutes for immobilisation on the channel. In this case the immobilisation procedure was simplified using a 2'Ome-RNA modified with amino groups (probe 7), and the complementary target 7* was labelled with Cy5, in order to match the optical characteristics for a red diode laser.
The target solution was inserted in the channel at flow speed of 10 µl/min for 15 minutes, starting from the more diluted solution to the more concentrated one, with intermediate washing steps of 5 minutes with buffer. The signal was finally registered after every washing step in the spectral region between 650-750 nm.
The collected spectra signals were recorded as the medium average of ten measurements using 10 sec of integration time in a total period of 100 seconds. The area of fluorescence was plotted (Figure 5.44) and standard deviations were reported for each point measured.

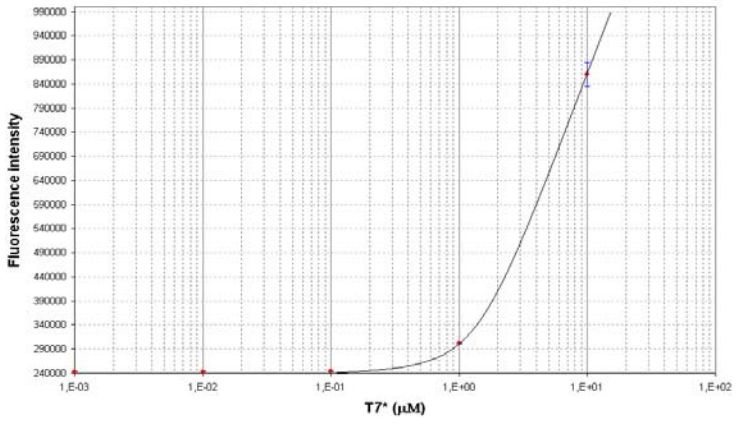

Figure 5.44. Calibration curve for the detection of RNA target 7* for MGMT using as bioreceptor the probe 7. The sensing ability of the bioreceptor used and of the optical chip adopted reaches about 0.5µM as low detection limit. The standard deviation error bar is shown for each measurement.

5.9 Characterisation of IgG/anti-IgG interactions by means of AFM and anisotropic fluorescence using LB method to enhance the sensitivity of the optical biochip

The final part of this thesis is divided in three parts and relates generally to the research for the obtainment of an optimised immobilisation of proteins on PMMA:

- The first study describes the characterization of IgG and anti-IgG covalently bound on the PMMA surface by capturing images of the biosensor surface using atomic force microscopy (AFM). An implementation of the immobilisation procedure on the PMMA chip was obtained using Langmuir-Blodgett (LB) technique on planar surface of PMMA. The result obtained on the small square chips was then transferred, using the same deposition method, on the multi-channel PMMA chip and compared with the deposition method (by micropipette) of the polymer for the IgG/anti-IgG assay.
- The second study relates to the immobilisation and characterisation of Photosystem II (PSII) proteins covalently bound on PMMA chip, using fluorescence measurements and AFM.
- The third study relates to the possibility to scratch the PMMA surface to obtain wells with controlled dimensions on a micrometer scale.

5.9.1 AFM imaging for IgG/Anti-IgG immobilised on a PMMA chip

Protein immobilisation is a common thread in the obtainment of a proper biosensing layer and requires reagents that can guarantee a covalent attachment of antibodies on the surface. This fact represents a key step to ensure enough reliability for a biosensor, ensuring enough resistance to the dynamic conditions involved in continuous flow measurements. For this reason the research pointed to capture images, as first, of antibodies immobilised to the PMMA surface and, as second, of antibodies-antigens complexes [361].

The image in Fig. 5.45 shows a first approach to the PMMA surface, cleaned with Triton X surfactant (0.1%), composed by long woven filaments of 10 to 50 nm diameters.

The surface seem to be a reticular net-like structure. This image was captured as control sample in order to recognize further biological compounds attached to the surface.

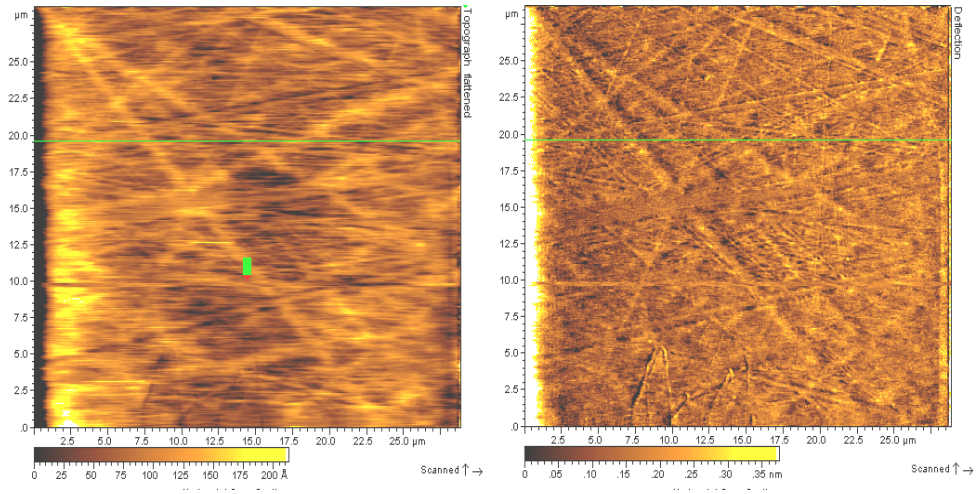

Figure 5.45 Bare PMMA. Topography and deflection images of polymethylmethacrylate surface. AFM contact mode. Image size: 28x28 µm.

Several methods for antibody immobilisation on PMMA surface are reported on literature including modifications of the substrate with carboxyl or amino groups [356], ultraviolet grafting of polymers [357], reactive ion etching by oxygen plasma treatment [358], periodate oxidation of PMMA microbeads through hydroxyl groups [359], and coatings of this material with gold nanoparticles functionalised with biocomposites [360].

Here a direct treatment of the surface was carried out using a copolymer of PMMA avoiding instrumental techniques (UV, plasma) and expensive (gold nanobeads) or dangerous chemicals (oxidizers). Hence, Eudragit L100 was dissolved in ethanol, 0.01 mM and the polymer was dropped directly onto the surface, waiting for EtOH evaporation, and rinsed after few minutes with ultra-pure H_2O.

The substrate was then treated with EDC/s-NHS in order to create stable succinimidyl ester groups on the surface.

These functional groups reacted with primary amino groups to form a covalent bond between the surface and the proteins. The protein treatments of the surfaces were executed immobilising on two different chips, by drop deposition, mouse IgG (1 mg/ml) and mouse IgG/anti-mouse IgG (1 mg/ml), using an incubation time of one hour.

These chips were washed accurately with PBS, dried with N_2 and stored in a Petri dish.

Captured images of these two chips are shown in Figure 5.46 and 5.47; the two upper images represent topography (top view) and deflection (of the cantilever axis) snapshots, whereas the lower images provide information on cut section and render a 3D picture of the surface. In both images are visible round particles of different diameter size (from 10 to 100 nm). In Figure 5.46 a particular attention was focalised on a group of four

presumptive proteins. Their medium height of 14 nm reflects in fact what is known from theory [131].

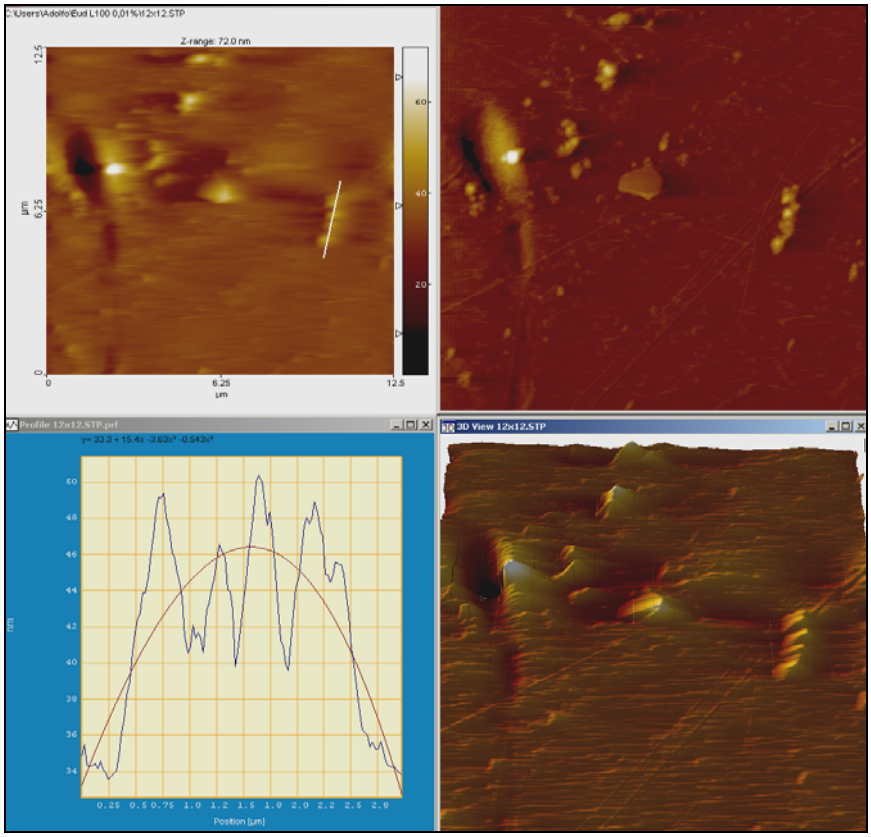

Figure 5.46 PMMA, Eudragit L100 and IgG**.** UP: topography and deflection images. BOTTOM: section analysis (12-15 nm) of upper image and 3D view. AFM contact mode. Image size: 12x12 µm.

The figure 5.47 depicts some particles similar to the ones described above. In addition to those, more large particles are visible on the surface. The cut section reveals the height of these in a range between 20 to 28 nm.

The height of these particles is quite in accord with theory [361], to the height of IgG/anti-IgG complex, in which the dimensions of a single immunoglobulin almost redouble.

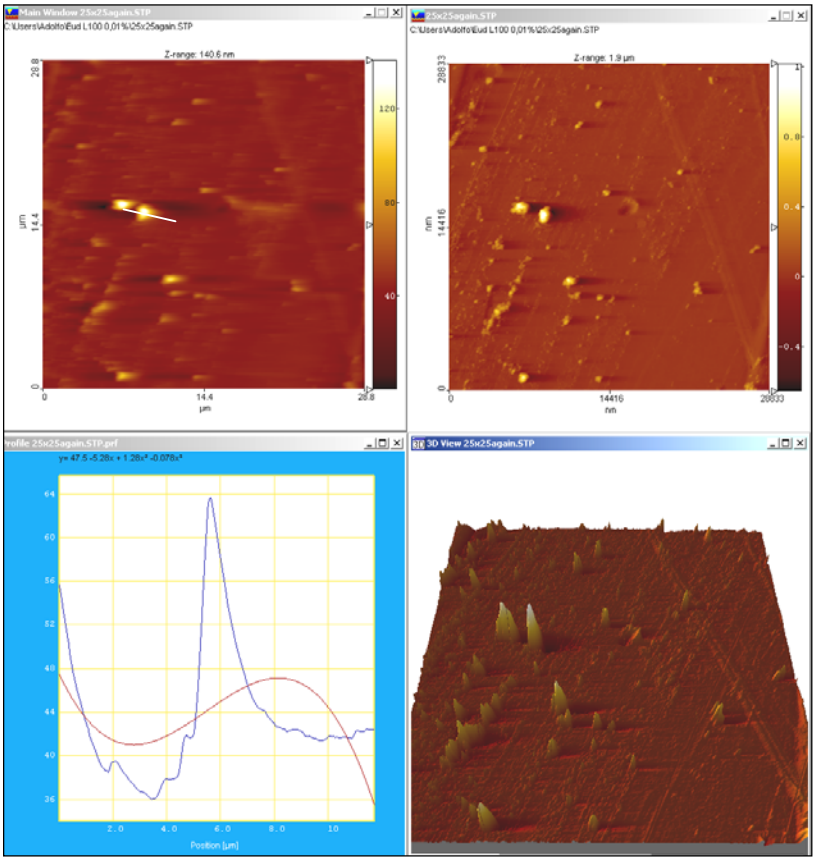

Figure 5.47 PMMA, Eudragit L100, IgG and anti-IgG. TOP: topography and deflection images. BOTTOM left: cut section of a large complex particle; right: 3D image**.** AFM contact mode. Image size: 28x28 µm.

A second polymer, polylactic-L-acid or PLLA, usually used in bioengineering tissues [336], was spread on the PMMA surface.

On a first chip a solution of PLLA was dissolved in $CHCl_3$ (0.01 mM) in order to create a polymeric structure abundant in ester groups.

The polylactic acid created a thin smooth layer made of ester groups on the PMMA surface and is able to react in a NaOH 2M to form carboxylic groups.

The surface was then treated with an EDC/s-NHS mixture (50 µl) and a drop of 5 µl of IgG (1 mg/ml) was spread on the active surface, and then washed with PBS.

Figure 5.48 evidenced two zoom images which reveal single protein detection of IgG antibodies and their respective cut section.

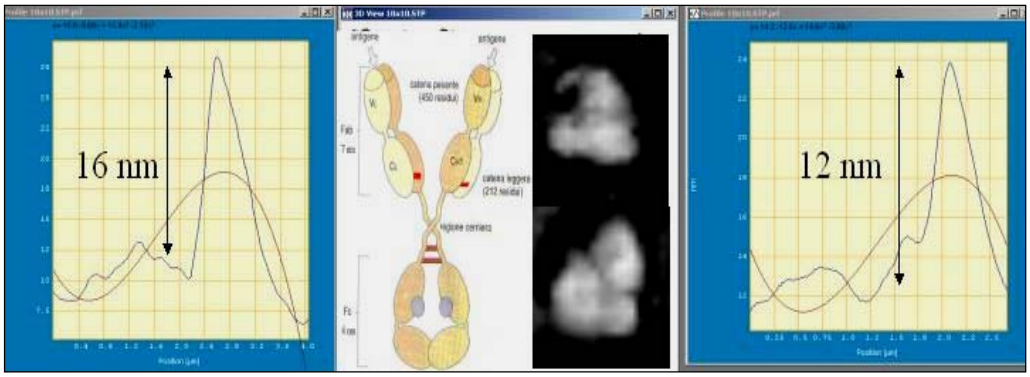

Figure 5.48 PMMA, PLLA and IgG. Middle: images at 30 x 30 nm of two immunoglobulins detected and the theoretical structure describing a shape of three balls, perfectly in accord with what is shown. Left, right: cut sections of IgG antibodies. AFM contact mode.

On a second PMMA chip treated with PLLA and IgG, a drop of 5 µl of AntiIgG-Cy5 (1 mg/ml) was allowed to interact with the surface for 1 hour incubation time.

In figure 5.49 is clear a disordered structure of the polymer in the background (PLLA matrix), in which some immunoglobulins are put in evidence inside white circles.

A particular attention was devoted to the circle line where a more large structure was evident.

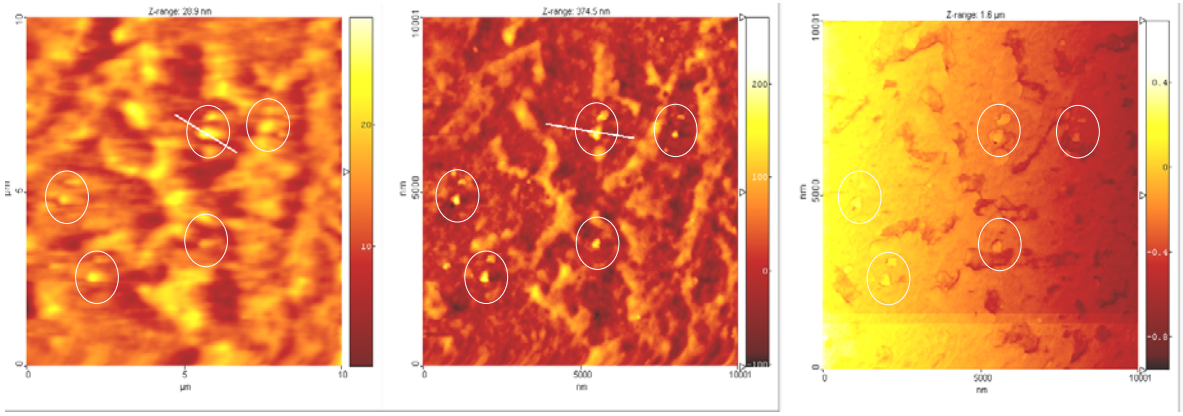

Figure 5.49 PMMA, PLLA, IgG/anti-IgG. Topography, deflection and friction images. The IgG are white circled. The PLLA polymer is evident in the background. AFM contact mode. Image size: 10x10 µm.

The presence of an interaction IgG /anti-IgG in a larger structure is quite clear because the complex is bigger.

These clusters are mostly evident in the images reported in Figure 5.50 ere cut section analysis was carried out to understand the height of them (almost 30 nm).

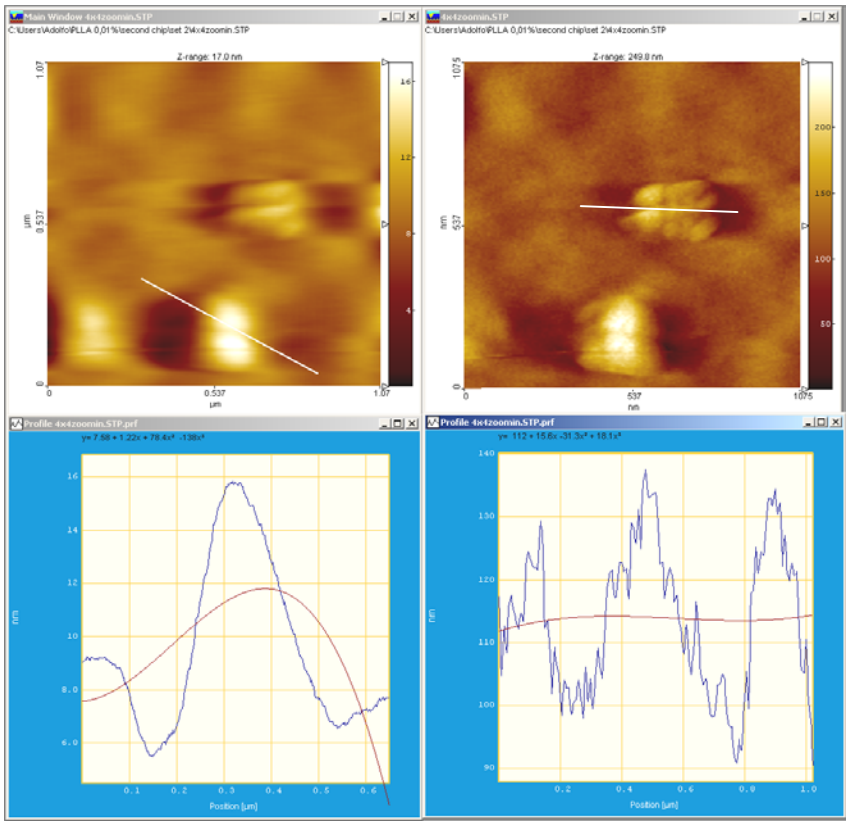

Figure 5.50 PMMA, PLLA, IgG/anti-IgG. Top: topographic and deflection images. Down: cut sections of revealed clusters of IgG/AntiIgG of 30 nm size. AFM contact mode. Image size: 1x1 μm.

5.10 Langmuir Blodgett evaluation of the polymer thickness

In order to develop a sensing layer more effective for the immobilisation of IgG antibodies, a further experiment was carried out depositing a film of Eudragit L100 on the chip surface.

The sensitivity of the fluorescent layer is extremely dependent on the thickness of the polymer, considering that the collected signal, in the case of the PMMA chip, is carried out by the guided light coming from the chip itself. On the other side, a deposition of PLLA by this method was not suggested because its closed ring structure does not permit a controlled deposition method.

If a previous activation of this polymer with NaOH could partially solve the problem, the opened ring structure presents hydrophilic groups on both sides causing a not reproducible liquid condensed state, necessary condition for a reproducible film formation by LB method. For this reason PLLA deposition was not considered for the obtainment of a reproducible layer by LB method.

The main aim of this experiment pointed out to study the difference in terms of deposition between the drop method and the Langmuir-Blodgett (LB) method; hence, three chips were modified using Eudragit L100 polymer.

Three different surface pressure values (Π = 20, 30, 35 mN/m) were examined to obtain a reproducible layer enriched in carboxylic groups.

The chips were then analysed by means of AFM in order to understand the proper thickness of deposition.

The first deposition (Π = 20 mN/m) produced a polymer thickness of 5 nm.

The polymer appears to be homogeneous over the PMMA surface (Figure 5.51). On the upper image on the right, is visible also the friction image (also called lateral force, or lateral deflection image) which provide informations about the strength in tip-sample interactions.

On the bottom images is presented in addition the Abbott curve, which shows the height distribution of the surface. Several roughness parameters are deduced from the Abbott curve.

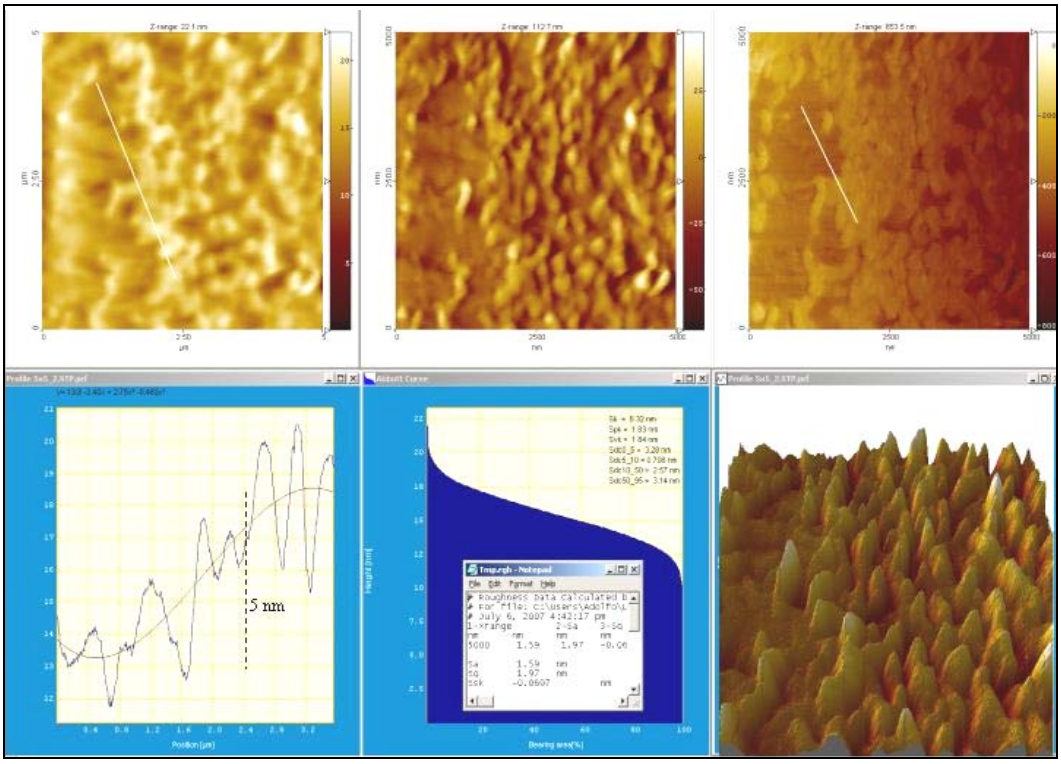

Figure 5.51 PMMA, Eudragit L100 at 20 mN/m. Top: topography, deflection and friction images. Bottom: thickness of the polymer (5 nm); Abbott curve; 3D image. AFM contact mode. Image size: 5 x 5 μm.

A second picture of the deposited coating is displayed in Figure 5.52. Further two cut sections of the film layer confirmed the homogeneity in the thickness of about 5 nm.

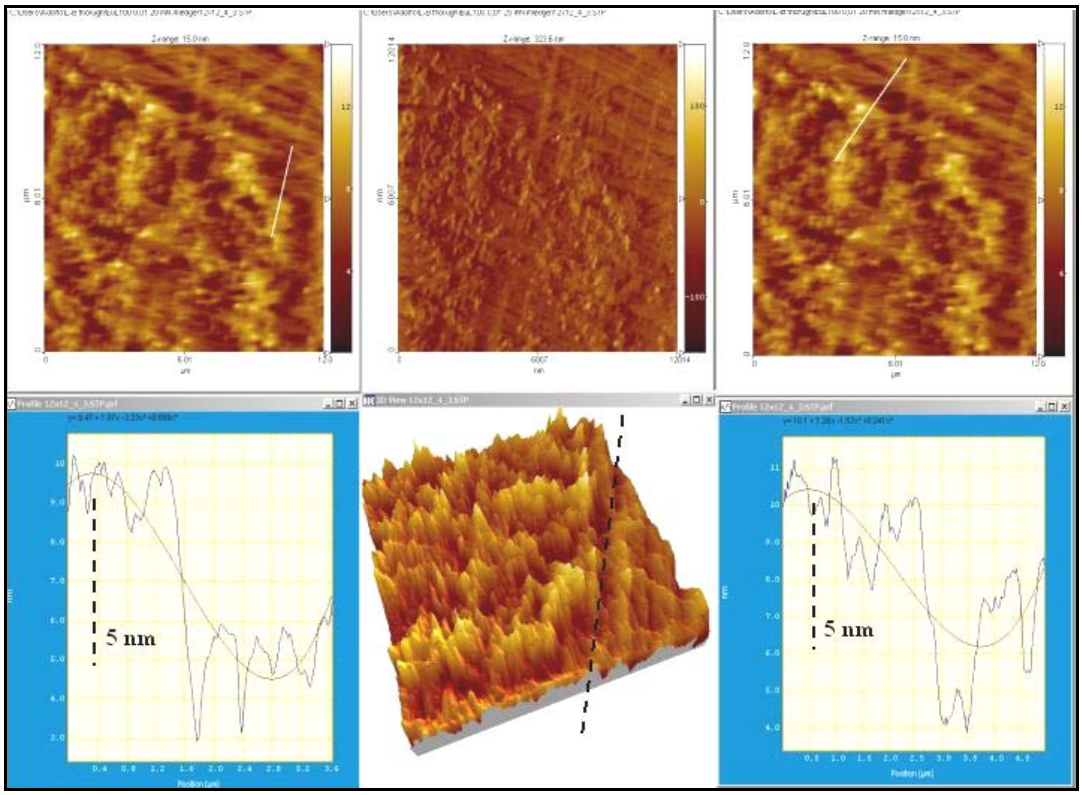

Figure 5.52 PMMA, Eudragit L100 at 20 mN/m. Top: topography deflection and topography again. Bottom: left and right cut section views of the thickness; middle: 3D image. AFM contact mode. Image size: 12 x 12 μm.

Higher is the surface pressure on a water-layer interface, more compressed is the film of polymer, and higher it is the thickness deposited on the surface.

The second deposition ($\Pi = 30$ mN/m) produced a polymer thickness in the range between 7-14 nm.

The polymer appears to be less homogeneous than in the deposition at 20 mN/m.

In fact in Figure 5.53 and 5.54 is shown an increase (in blue) in the slope of the bearing area (roughness of the surface).

This is demonstrated then by the presence on the surface of several thicknesses, caused by a partial overlapping of the condensed films for the enhancement of the surface pressure value from 20 to 30 mN/m.

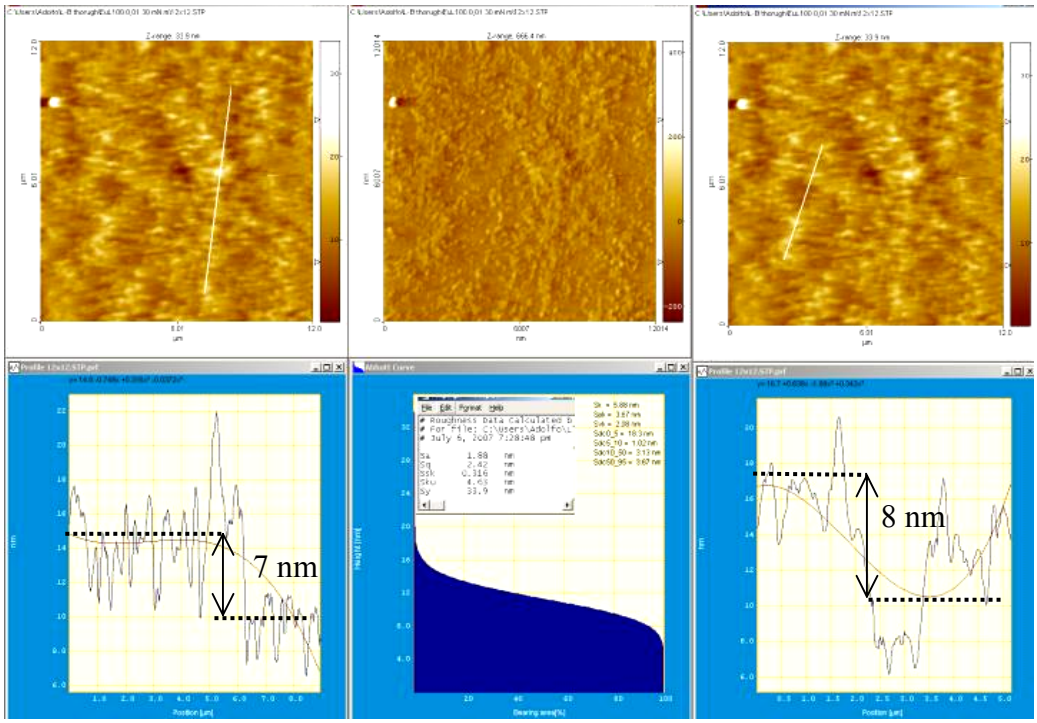

Figure 5.53 PMMA, Eudragit L100 at 30 mN/m. Top: topography deflection and topography images. Bottom: left and right, section views reveal 7-8 nm of thickness; Abbott curve. AFM contact mode. Image size: 12 x 12 µm.

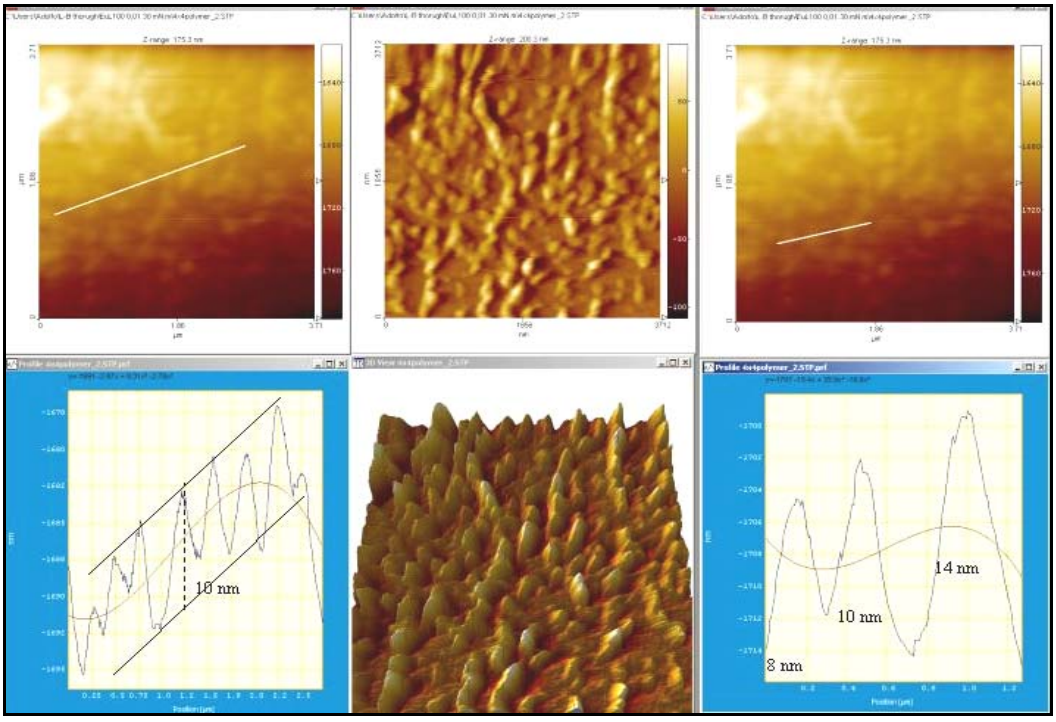

Figure 5.54 PMMA, Eudragit L100 at 30 mN/m. Top: topography deflection and topography images. Bottom: section views that show 10 nm of thickness. 3D image. Other particles of different size (8, 10, 14 nm) are shown on the right. AFM contact mode. Image size: 4 x 4 µm.

In the third deposition, at higher surface pressure (Π = 35mN/m), the polymer layer was lost and a lot of clusters made of overlapped molecules are seen on the surface (Figure 5.55).

Too much surface pressure, as expected, caused the collapse of the polymer into bigger nanoparticles (20-50 nm) which were neither useful nor reproducible.

The result shows clearly that the deposition of a monolayer of Eudragit L100 on PMMA at this surface pressure is not convenient.

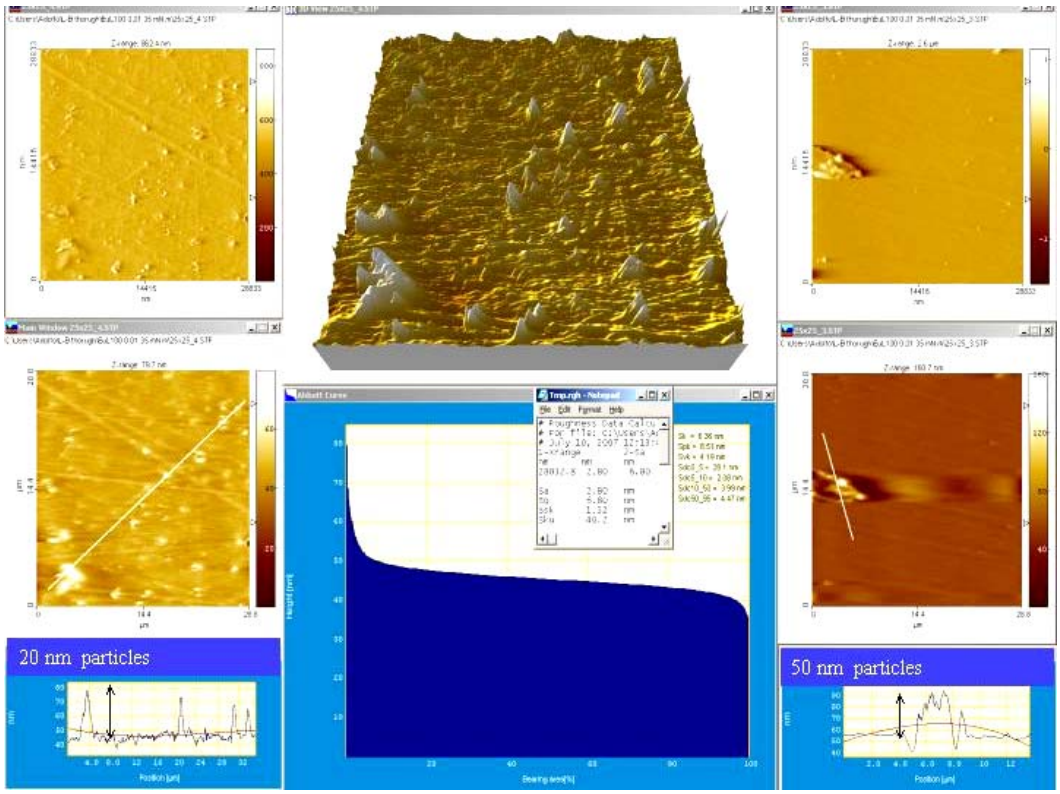

Figure 5.55 PMMA, Eudragit L100 at 35 mN/m. Left: topography, deflection and section images of the polymer surface deposited on PMMA.Middle: 3D image and Abbott curve. Right: topography, deflection and section images of the polymer. AFM contact mode. Image size: 28 x 28 μm.

The results obtained show that the most effective treatments of the surface were at 20mN/m and 30mN/m.

Treatment at 20mN/m had the advantage of keeping the sensing layer close to the PMMA surface with potentially better coupling of the emitted fluorescence.

This type of deposition was chosen and transferred on channel of the PMMA cover plate of the multi-channel biochip.

Therefore the deposition by LB method at 20mN/m was tested with an IgG/Anti-IgG assay in order to compare it to the previous results obtained by micropipette deposition represented previously at fig. 5.27.

In Figure 5.56 is shown a comparison of the calibration curve with an LB film with the calibration curve obtained with Eudragit L100 dropped on the PMMA surface.

The improvement in the performance of the assay was immediately apparent and impressive.

Every measured point is an average of ten measurements of the fluorescence signal collected in a ten seconds integration time period.

The standard deviation for these points was calculated to be in the range of the dimension of the point and for this reason is not displayed on the graph.

The standard error bar, displayed on the graph, was calculated as the ratio between:

1) standard deviation relative to two different measurements executed on two different PMMA channels.

2) the square root of the number of measurements (in this case two).

Anyway, the standard error bar gives an idea about the reproducibility of the method.

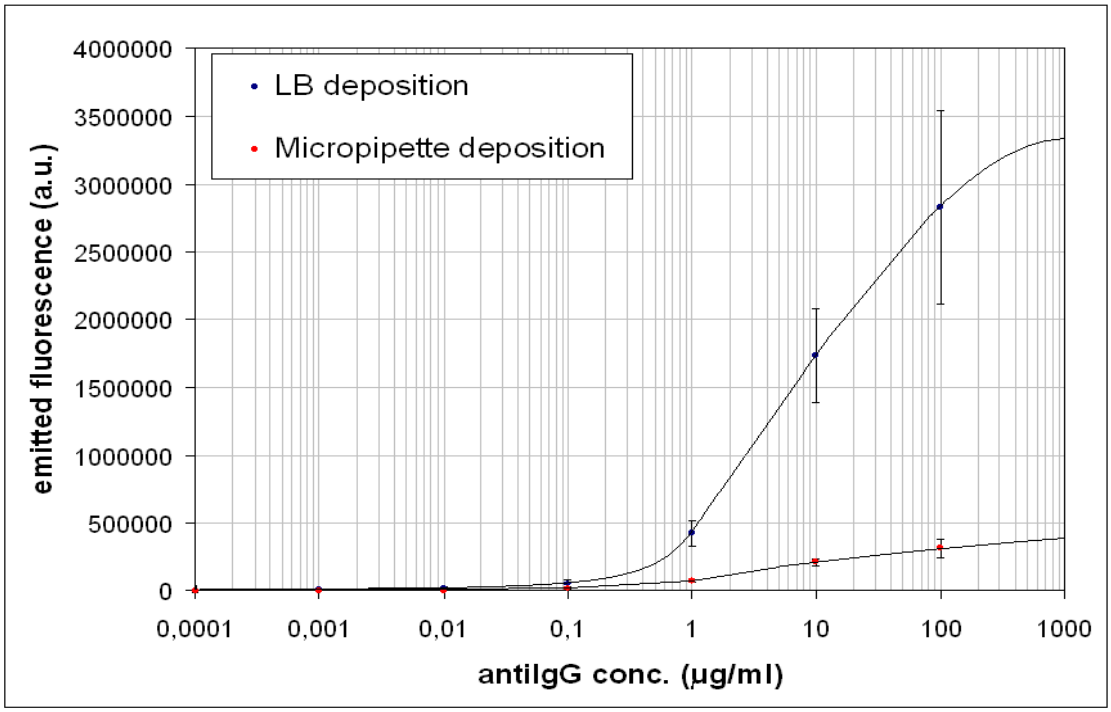

Figure 5.56 Eudragit L100 deposition method. Comparison between micropipette deposition at 0.01 mM and LB deposition at 20 mN/m.

Finally, a characterization by AFM imaging of IgG and anti-IgG covalently bound on a PMMA surface was carried out.

The immobilisation was carried out on Eudragit L100 copolymer and on poli-L-lactic acid (PLLA). Eudragit L100 revealed a better and homogeneous polymer layer.

The antibodies were photographed and their cut sections confirmed the theoretical size known from literature.

An implementation of the immobilisation procedure on the PMMA chip was obtained by using Eudragit L100 and depositing a monolayer of 5 nm of thickness by Langmuir-Blodgett (LB) method using a surface pressure of 20 mN/m.

This deposition method, previously carried out on small planar square and then on a channel of the biochip, was compared, for an IgG/antiIgG assay, to the previous depositions of the polymer applied by micropipette.

The deposition by LB method enhanced the performance of the chip of at least on order of magnitude in sensitivity.

Future plans can be pointed out on the obtainment, by using Langmuir-Blodgett methodology, of smooth transparent surfaces with an ordered structure of monomers able to enhance sensitivity towards concentrations lower than 1 ng/ml.

Deposition of LB layers involve a big variety in the research plans to obtain in the future more sensitive coatings. Surface pressure variation can determine a high reproducibility of the system and a further optimisation of the system thanks to enhanced sensitivity obtained by LB method and to research on low kind of autofluorescent PMMA, thus increasing SNR.

A1. Characterisation of immobilised PSII proteins on a PMMA substrate by means of anisotropic fluorescence, AFM and L-B methodology

In this addendum chapter is presented a work carried out on protein extracts from spinach membrane fragments enriched in Photosystem II (PSII) covalently immobilised on to a PMMA surface at various concentrations and analyzed by means of AFM and anisotropic fluorescence activity. An improved sensitivity was resulted using Langmuir-Blodgett methodology for the deposition of the polymer which binds to PMMA and to the proteins.

A1.1 Chlorophyll fluorescence

Chlorophyll fluorescence analysys has become one of the most powerful and widely used techniques available to plant physiologists and ecophysiologists [363].

Chlorophyll fluorescence can be used to study components of the photosynthetic apparatus and their reactions to changes in the environment as well as photosynthesis. This is interesting in the fact that photosynthesis is a good indicator of the adaptation of a plant to its surrounding environment.

Since the measurements are non-intrusive, fast and reliable, this makes chlorophyll fluorescence an attractive tool for environmental research and for breeding purposes.

In particular, the oxygen evolution of a plant is directly correlated into the estimation of the photoactivity of PSII. For the same reason, the fluorescence correlated to the concentration of these proteins can suggest several informations on the oxygen activity of a plant [364]. Furthermore, a close correlation has been found between change in the dark level of fluorescence F_0 and necrosis test after heat stress in a large number of plant species [365]. Upon exposure to increasing temperature, the dark level of fluorescence F_0 increases. From its theoretical expression, an increase of fluorescence can be interpreted as a reduction of the rate constant of energy trapping by PSII centers [366].

This is the result of a physical dissociation of light harvesting complex from PSII core as it has been observed in several plant species as a result of heat damage [367].

A1.2 PSII proteins

PSII is a trans-membrane chlorophyll-protein complex which consists of a large number of subunits, which catalyse the photo-oxidation of water. Light is harvested by means of the LHCII complex and the chlorophyll-binding subunits [368].

PSII is embedded in the lipid matrix of the thylakoid membranes of chloroplasts coming from higher plants. It is also present in other microorganisms such as algae and cyanobacteria [369].

PSII is one of the multisubunit protein membrane complexes which are involved in the "light reactions" of the photosynthesis: it strictly cooperates with Photo System I (PSI) and the Cytochrome b_6f complex [370] (Figure A1.1).

PSII can be extracted from chloroplast cells of spinach leaves and then stabilised as a suspension using a suitable buffer, according to the following steps of a standardised procedure [371].

PSI and PSII contain chlorophylls and other pigments that harvest light and funnel its energy to a reaction centre. Energy that has been captured by the reaction centre induces the excitation of specialised reaction-centre chlorophylls (primary electron donors; a special chlorophyll pair in PSI), which initiates the translocation of an electron across the membrane through a chain of cofactors.

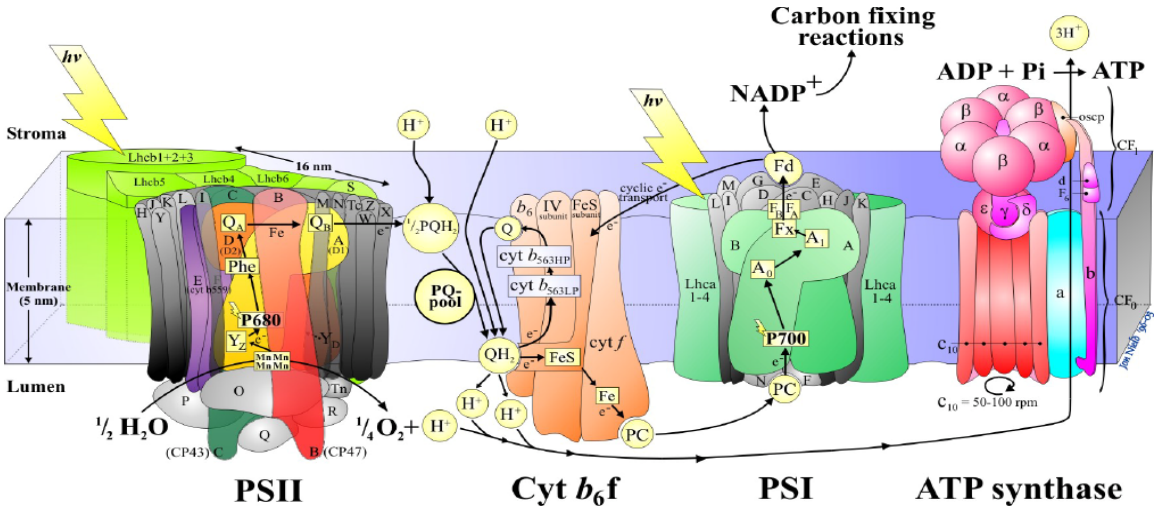

Figure A1.1. Light reactions are represented by this diagram also known as "Z-scheme". The image source is at http://www.bio.ic.ac.uk/research/barber/psIIimages/PSII.html

PSII catalyses a unique process of water oxidation and provides almost all of the earth's oxygen. The evolution of PSII was therefore crucial for the emergence and endurance of aerobic organisms. The mechanism of oxygen production involves the oxidation of two

water molecules to make molecular oxygen (O_2) in a combined mechanism that requires the absorption of four light quanta. Two weakly coupled chlorophylls known as P_{680} function as the primary electron donor (680 nm is the peak of the lowest-energy absorption band of P_{680}). After absorption of the first of the light quanta, an electron is translocated from P_{680} through accessory chlorophyll and pheophytin molecule to the tightly bound quinone Q_A, and this is followed by the reduction of a mobile quinone Q_B [372]. The oxidized P_{680}^+ has the highest redox potential observed in a biological system (> 1 V), and is able to oxidize a nearby tyrosine (Y_Z). Y_Z then extracts an electron (and perhaps a proton) from a cluster of four manganese ions, which binds two substrate water molecules and has a calcium ion, a chloride ion and a bicarbonate ion as necessary cofactors. After another photochemical cycle, the doubly reduced Q_B (Q_B^{2-}) takes up two protons from the stroma to form Q_BH_2 and is released into the lipid bi-layer to be replaced by an oxidized quinone from the membrane quinone pool. This pool consists of oxidized (PQ) and reduced (PQH_2) plastoquinones (plastoquinone, rather than quinone, is specified when it is the predominant quinone) [373]. After two more photochemical cycles, the manganese cluster is provided with four oxidizing equivalents, which are used to oxidize two water molecules to produce O_2 (photo-oxidation of water) by following the reaction: $2H_2O + PQ + h\nu \rightarrow O_2 + 2H^+ + PQH_2$

PSII can have biotechnological applications in the environmental field, because it is very sensitive to some herbicides (derivatives of phenylurea, triazine, diazine and phenolic types). The triazine herbicides bind to the PSII complex, displacing the plastoquinone (PQ), and inhibit the light-driven electron transfer system in photosynthesis. Many detection methods using photosynthetic proteins, such as D1 protein [374], PSII particles [375], and thylakoid membranes [376], have been reported.

Many of these assessed inhibition of the light-driven electron transport by herbicides [377]. The signals of herbicide binding to the photosynthetic reaction centres of the protein can be detected directly by measuring the reduction in photocurrent due to the decrease of oxygen generation.

Thylakoid membranes are plenty enriched in photosystem II (PSII) complexes: thylakoid proteins, commonly present inside these membranes, are rich in chlorophyll (α, β) molecules with Mg^{2+} porphyrin fluorescent molecules that reveal an absorption signal in the region nearby 635 nm and an emission at 680 nm. In this work, thylakoid proteins extracted from spinach membranes [378] and dissolved in MNBC buffer solution (3.0 mg/ml) were purified for the attachment on a PMMA substrate.

A1.3 Experimental part

The substrates used were planar square surfaces made of PMMA of 1 cm^2 and thick 0.15 cm. Drops of two different polymers (Eudragit L100 and PLLA followed by activation with NaOH) were deposited in order to obtain a surface enriched in carboxylic groups.

In particular the effectiveness of the deposition method (by drop or by Langmuir-Blodgett) of Eudragit L100 was investigated by means of fluorescence. Three different protocols were carried out as follow: 1) Eudragit L 100 (0.01mM in EtOH) solution was dropped onto the PMMA surface. 2) PLLA (0.01mM in $CHCl_3$) was dropped onto the PMMA surface followed by activation with NaOH 2M. 3) Eudragit L 100 film was obtained by LB method with a controlled deposition at surface pressure Π= 20 mN/m.

The activation of the surface was achieved using the EDC/s-NHS method in MES buffer 0.1 M, pH 6.2 in order to obtain a surface enriched in carboxylic groups activated for protein binding.

Protein solutions at five different concentrations (3.0, 0.3, 0.03, 0.003, 0.0003 mg/ml) were spread on fifteen chips (five for each polymer treatment) on the active surface using MNBC, which is a derivative, more rich in salt ions, of MES buffer.

The optical system used for the characterization of the chips is shown in Figure A1.2. The source consisted in a He/Ne laser at 632 nm. There was no need to apply filters to the optical system. The detected signal was collected at fluorescence anisotropic angle [379], using a multimode optical fibre connected to an USB2000 Ocean Optics spectrophotometer and analysed using SpectraSuite software.

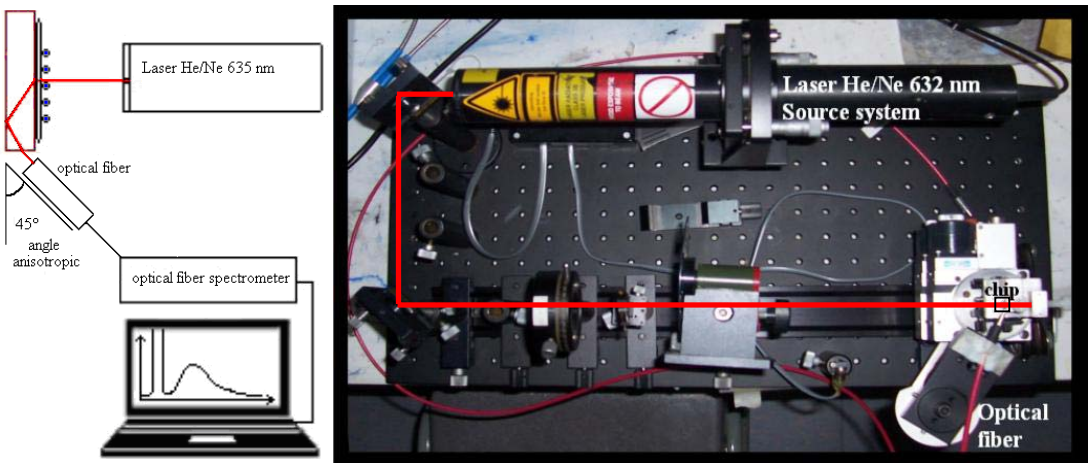

Figure A1.2. Instrumental setup for fluorescence measurements. The excitation source hit the surface in the upper part of the chip. The fluorescence from the PMMA surface dictated the best signal collection angle of 45° due to the effect of anisotropic emission.

A1.4 Results and discussion

Fluorescence measurements:

The results of the fluorescence studies are shown in Figures A1.3-A1.5.

On the left side the optical spectra collected are shown whereas a calibration curve (concentration vs fluorescence) is shown on the right.

In the region nearby 630 nm is visible the excitation signal of the He/Ne laser whereas the peak at higher wavelength (650-800 nm) is the fluorescence signal.

On the right side is plotted the area of the fluorescence (in the spectral region between 680±25 nm) versus the concentration of the protein.

Comparing the depositions by drop method, the fluorescence signal in the case of Eudragit L100 (figure A1.3) was found to be three times higher than in the case of PLLA (figure A1.4). In particular the gap (17000 vs 47000 arbitrary units) is quite evident at higher concentration (3 mg/ml).

Considering the depositions by LB method, the fluorescence signal for treatment with Eudragit L100 polymer (Figure A1.5), demonstrated to be really good in sensitivity and linearity at lower concentrations (0.3 to 0.0003 mg/ml).

This measurement confirmed that an enhanced sensitivity of the system could be obtained using a LB controlled deposition method. In this case, a calibration curve was captured with a limit of detection of approximately 1 μg/ml.

The optical spectra captured are the average of ten measurements collected at 10 seconds of integration time using spectrophotometer USB2000 from Ocean Optics Inc.

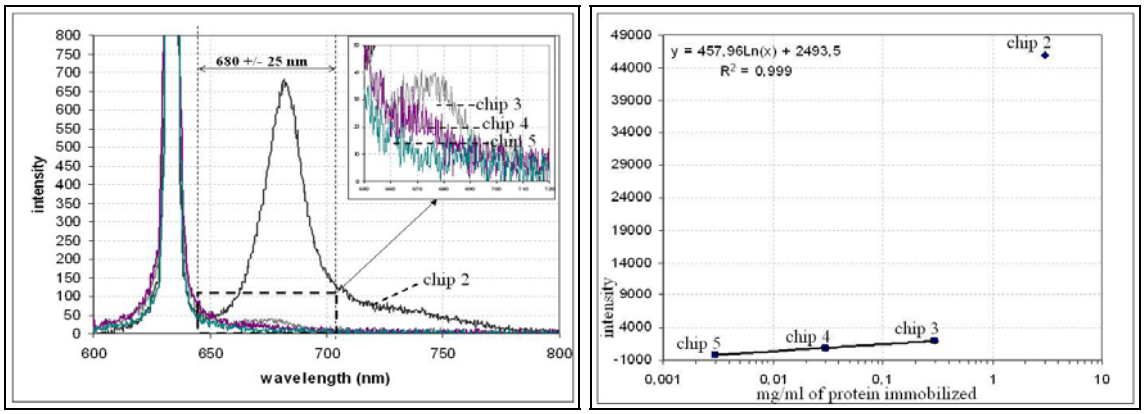

Figure A1.3. Eudragit 0.01 mM dropped on PMMA chip. Left: Optical spectra were collected with the instrumental setup in Fig.13. Four different chips with different concentrations of proteins were deposited. Right: calibration curve obtained with the four concentration chips; in the y axis the fluorescence area between 655 and 705 nm was considered.

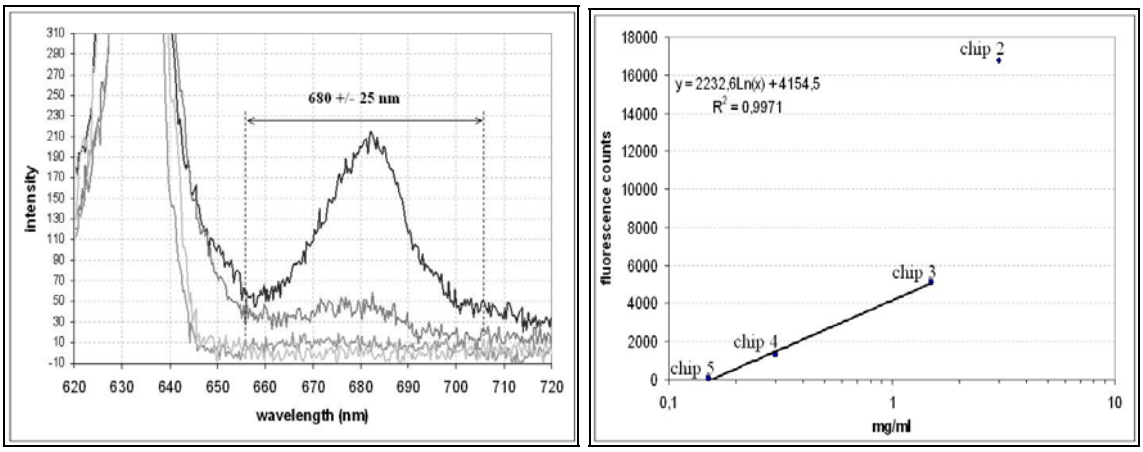

Figure A1.4. PLLA 0.01mM dropped on PMMA chip Left: Optical spectra were collected with the instrumental setup in Fig.13. Four different chips with different concentrations of proteins were deposited. Right: calibration curve obtained with the four concentration chips; in the y axis the fluorescence area between 655 and 705 nm was considered.

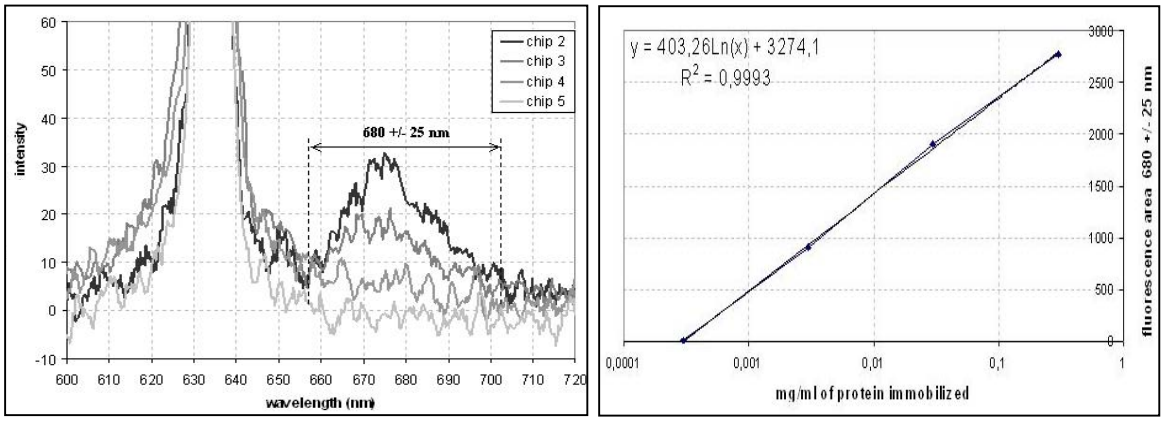

Figure A1.5. Eudragit in EtOH deposition by LB method at 20 mN/m**.** Left: Optical spectra were collected with the instrumental setup in Fig.13. Four different chips with different concentrations of proteins were deposited. Right: calibration curve obtained with the four concentration chips; in the y axis the fluorescence area between 655 and 705 nm was considered.

AFM measurements:

Three different PMMA chips with the highest concentration in protein content (3mg/ml) were analysed by means of AFM. The first image captured is shown in Figure A1.6. On the upper images topography, deflection and friction pictures are displayed. On the PMMA matrix treated by Eudragit, some little particles are visible. Two of those, covalently bound on a PMMA thread, were considered for cut section analysis, in order to understand their effective size avoiding any dimension contribution coming from the net structured background. The particles measured were 4-5 nm high and 50-100 nm wide. Their dimensions in width reflects the dimensions of PSII proteins known from theory [380] but their height (in theory are reported height between 30 to 50 nm) suggested that these proteins were partially included inside the Eudragit matrix. When

Eudragit was deposited on the surface, time was waited for the evaporation of EtOH solvent and then after 1 hour deposition of the protein was carried out. Anyway the deposition of the polymer was carried out at room temperature (total evaporation of EtOH occurs at 79°C). So, could be possible that not all the solvent was evaporated leaving sacks of the solvent and the proteins inserted parts of their structure inside it.

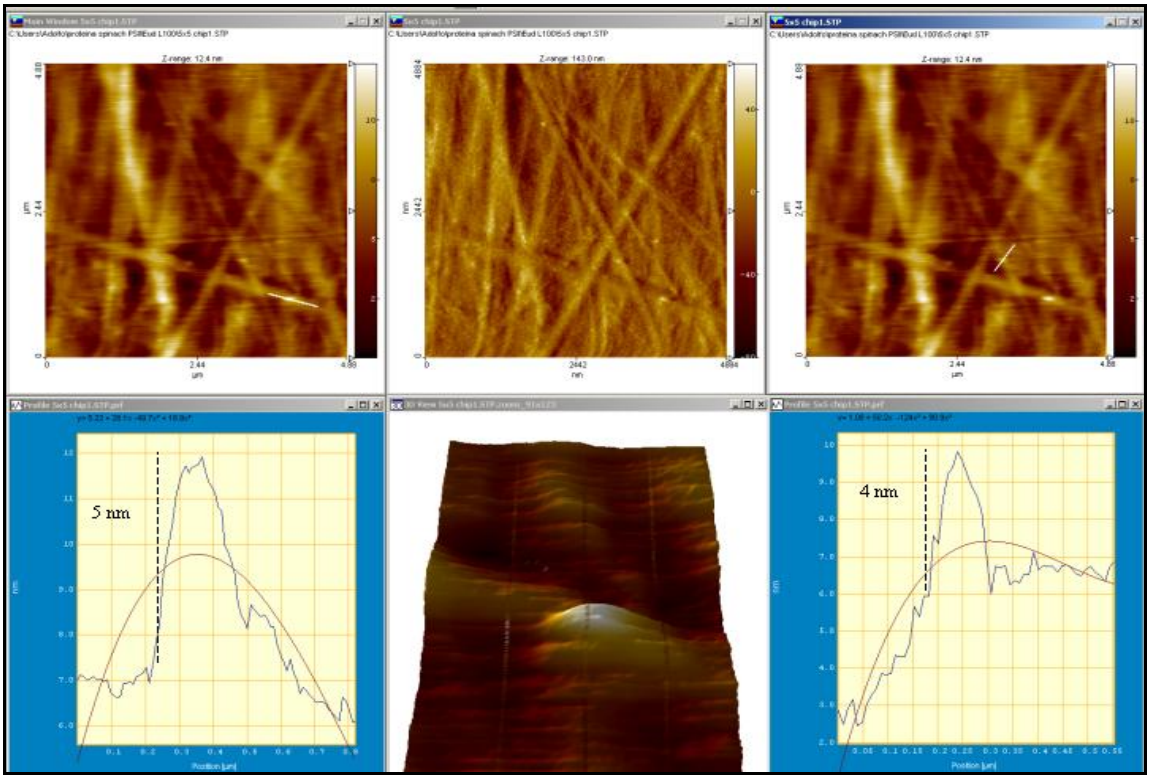

Figure A1.6. PMMA + Eudragit 0.01 mM by drop method. PSII proteins: Top: from left to right Topography, deflection and 3D images. Bottom: Relative cut section of the protein immobilized on the surface. AFM contact mode. Image size: 5 x 5 μm image.

Figure A1.7 show the immobilization of PSII proteins on a monolayer of Eudragit obtained by LB deposition. The deposition of these proteins occurred several days after the polymer deposition so the effect previously described should be minimal. Despite that, the same effect of before is visible. The sacks of EtOH not evaporated do not explain the little dimension in height revealed by these proteins. A second explanation more exhaustive can be described this effect for a better understanding. These proteins are delicate macromolecular structures that probably suffer the immobilisation procedure or the tip scanning and for this reason they tend to spread their shape on the surface. This explanation was mainly suggested by their wide extension (400 nm), really unusual for their size. Anyway, it is almost clear that in these conditions the proteins possessed a

fluorescence activity but degraded from a three dimensional structure into a two dimensional flatten shape.

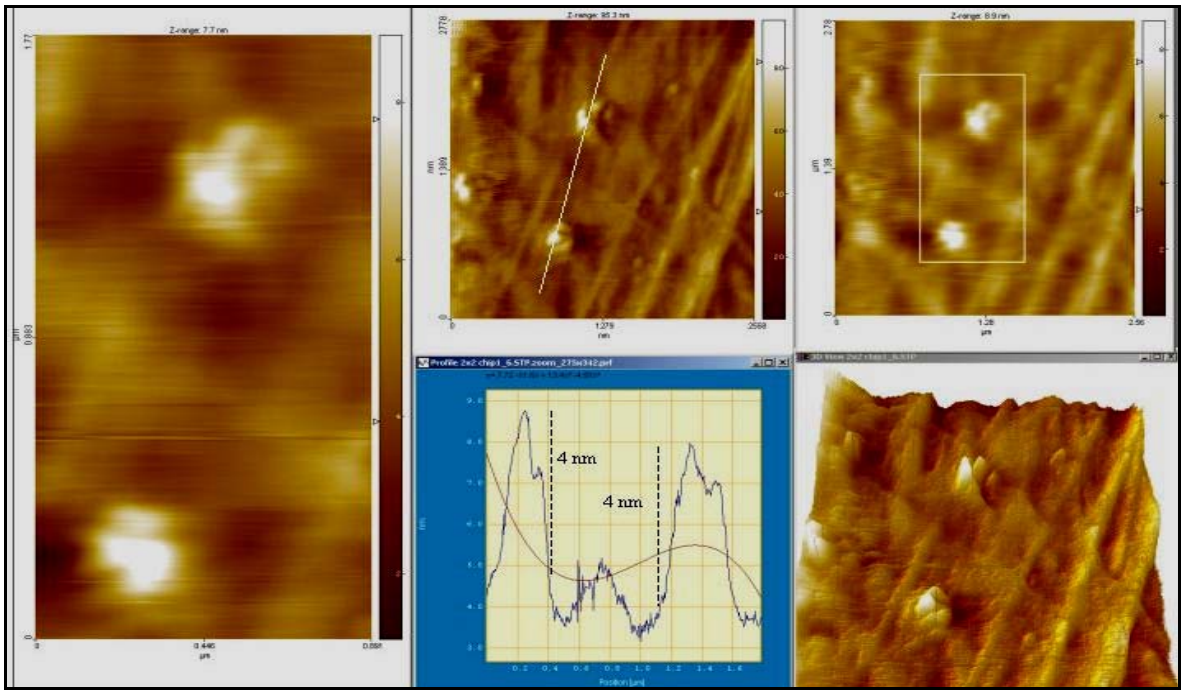

Figure A1.7. PMMA + Eudragit L100 by LB method at 20mN/m. PSII proteins: topography, deflection, 3D and zoom images. Relative cut section of proteins immobilised on the surface. AFM contact mode. Image size: 2.5 x 2.5 μm.

Figure A1.8 show the proteins immobilised on to a PLLA matrix, revealing an height of 1-2 nanometer and a width section of 50-200 nm.

To regulate the force of tip is enough to adjust the force of set point values.

A curious experiment was conducted by manipulating the proteins using the AFM tip as a nanoscale arm that can move proteins from point to an external side of the image.

This experiment is shown in figure A1.9, where two proteins were detected on the surface and one of these was moved on one side (out of image) leaving an empty hole on the PLLA polymer.

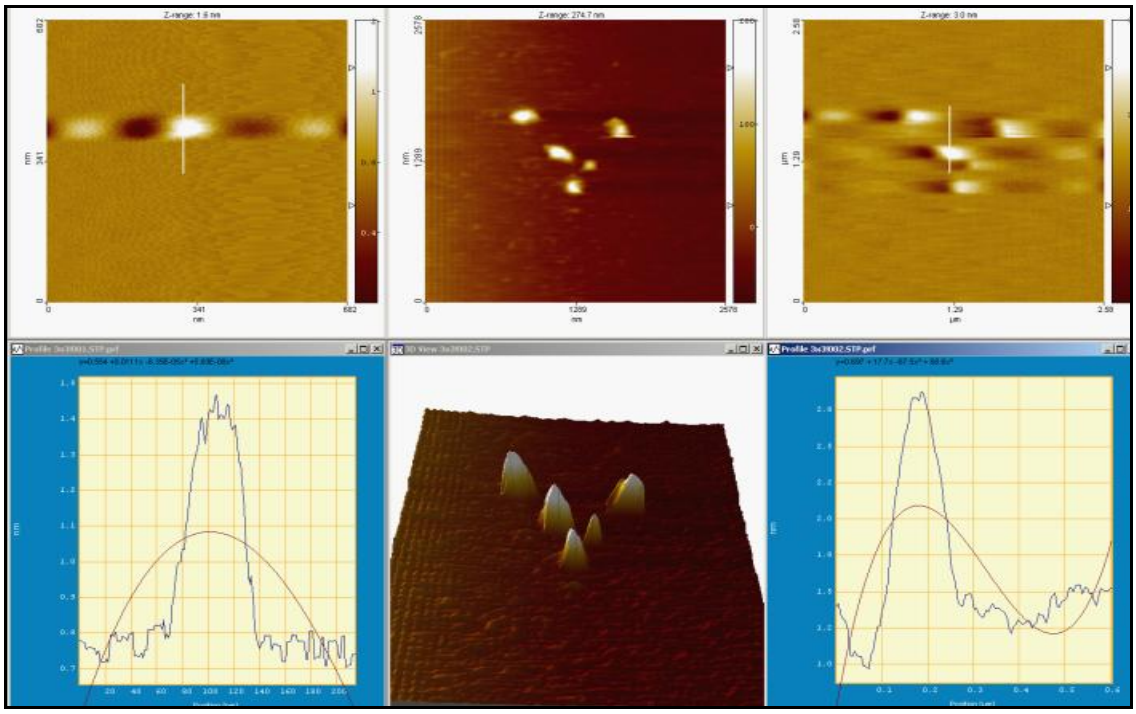

Figure A1.8..PMMA + PLLA 0.01mM by drop method. Topograpy, 3D and deflection images. Relative cut sections of the proteins detected on the surface. AFM contact mode. Image size: 2.5 x 2.5 µm.

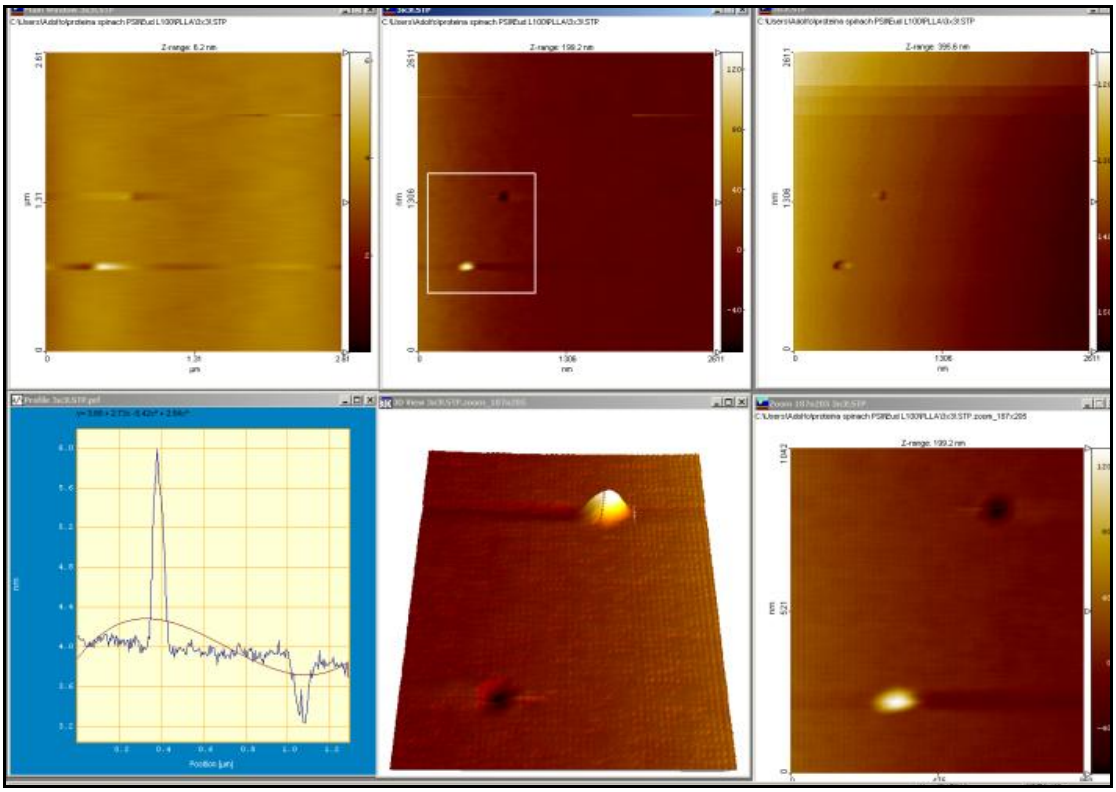

Figure A1.9. PMMA + PLLA 0.01mM dropped and activated by NaOH (2M) on PMMA chip. Top:: topography, deflection and 3-D images. Bottom: Relative cut section and zoom in of one protein and of one hole leaved by one protein removed by AFM tip. AFM contact mode. Image size: 2.5 x 2.5 µm.

A1.5 Well experiment

Dip-Pen Nanolithography (DPN) is a scanning probe nanopatterning technique in which an AFM tip is used to deliver molecules to a surface via a solvent meniscus, which naturally forms in the ambient atmosphere. This direct-write technique offers high-resolution patterning capabilities for a number of molecular and biomolecular 'inks' on a variety of substrates, such as metals, semiconductors, and monolayer functionalized surfaces. It's becoming a work-horse tool for the scientist interested in fabricating and studying soft- and hard-matter on the sub-100nm length scale [381].

DPN allows one to precisely pattern multiple patterns with near-perfect registration. It's both a fabrication and imaging tool, as the patterned areas can be imaged with clean or ink-coated tips. The ability to achieve precise alignment of multiple patterns is an additional advantage earned by using an AFM tip to write, as well as read nanoscopic features on a surface. These attributes make DPN a valuable tool for studying fundamental issues in colloid chemistry, surface science, and nanotechnology [382].

The possibility to build, by scratching with an AFM tip, controlled wells on a nanometer scale for multi-analyte detection can offer several interesting solutions, especially in a "lab on a chip" technology.

Biomedical science needs to obtain biosensors for virus diseases (AIDS-HIV, HPV ecc.) which involves multi-genotypes detection, where more than one hundred of different genes are involved in biorecognition of sample analytes.

So, previously acquired capabilities in the manipulation of proteins (Figure A1.9), suggested a research work which was orientated into the realisation of a substrate characterised by wells in a specific region, in order to understand the control possibilities of etching by AFM tip in terms of resolution and depth.

The image in Figure A1.10 shows the results of experiments conducted on the PMMA surface and demonstrated that it can easily be scratched by an AFM tip and modelled for specific purposes. The procedure consists into take a picture of a 1 micron length in an unexplored zone. By adjusting the force of the set point value was possible to take another image with a lower force on the tip across a 5 micron length.

Finally, an image was taken across a 10 micron length, revealing everything that was scratched before using a lighter atomic force. The cut section revealed a depth in the central square hole of 25 nm and 15 nm in the external square one.

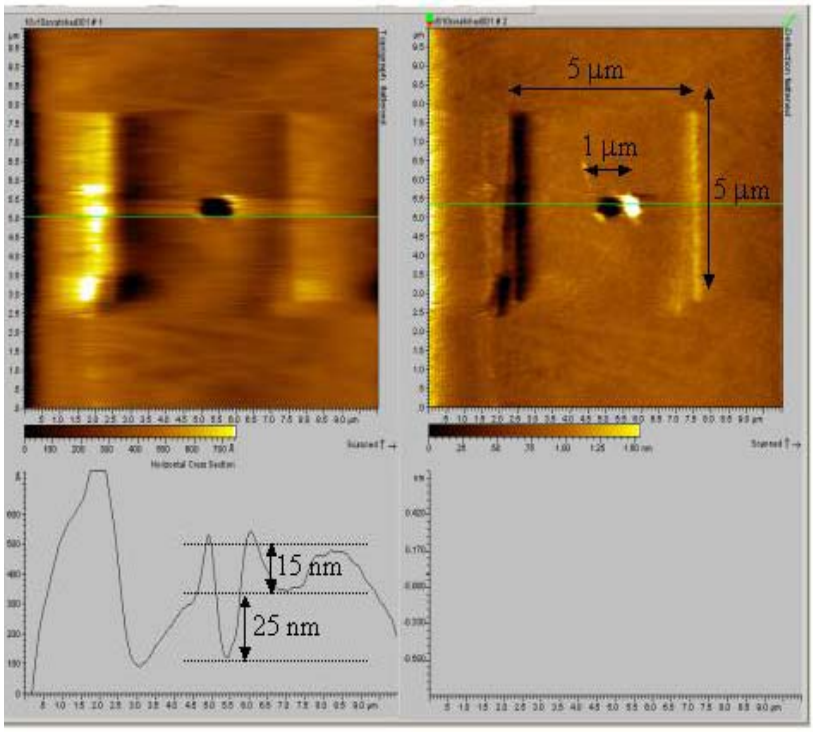

Figura A1.10. Bare PMMA. Building a well of 1µm^2 inside a 5 micron side square pool using atomic force set point is possible to scratch PMMA with the tip of AFM. The pool where the well was built is 15 nm deep and the well is 25 nm deep. AFM contact mode, Cranfield University. Image size: 10 x 10 µm.

A second experiment similar was carried out with the AFM tip to understand the level of control of the instrumentation on an x-y region for a controlled scratching of the surface to obtain multi-wells (Figure A1.11).

Starting from a central well of 1 µm^2, the tip was moved 2 µm in x direction to the right and 2 µm in y direction to the top to build a second well.

This type of movement did not excelled in perfection (see figure A1.11). The force on the tip was kept constant and moving just only the x direction of 4 µm on the left a third well was built. The cut section revealed that keeping the same force on the tip (keeping the same set point value), a reproducible well in terms of depth is obtainable.

This fact had a confirmation in the building of a fourth micro-well (just moving to down in y direction for 4 µm) when the same tip force was maintained. In the fifth and last micro-well, moving again on x direction for 4 µm to the right, the force tip was diminished, determining a change in depth from 150 nm to 100 nm.

This result suggested that further studies will be required to discover the dependence for PMMA between the force set point values and the depth of the holes in order to arrange a

perfect combination between the geometry of the substrates and its possibility in multi-genotypes detection.

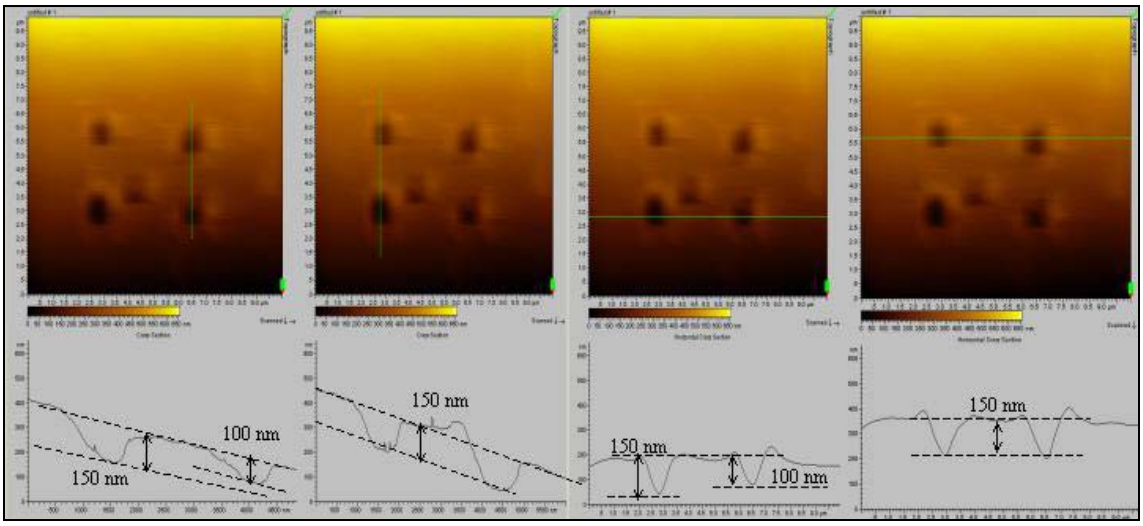

Figure A1.11. Bare PMMA. Topography images of 5 wells of 1μm^2 scratched on a bare PMMA surface. Relative cut section analysis are captured. AFM contact mode. Image size: 10 x 10 μm.

In the figure A1.12 is shown a PMMA scratched surface with holes of 100 x 100 nm, 100 x 200nm, 300 x 300 nm and 500 x 500 nm dipped using different set point values and creating different holes with a controlled depth.

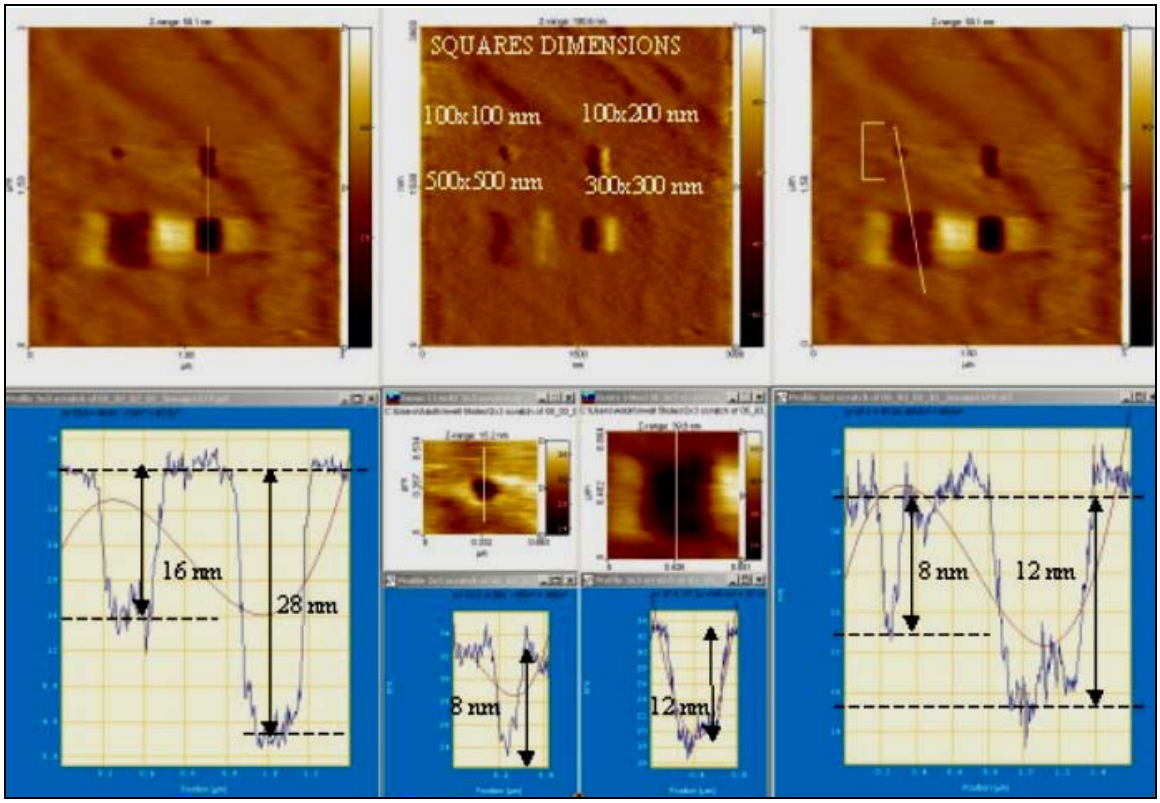

Figure A1.12. Bare PMMA. Topograhy, deflection and topography images. The depth of the wells was controlled by adjusting the set point value of the tip force tip.

A1. Conclusions

In this final chapter of the thesis a work carried out on protein extracts from spinach membrane fragments enriched in Photosystem II (PSII) covalently bound on to a PMMA surface and analyzed by means of AFM and fluorescence activity at various concentration was presented.

Two different polymers were evaluated, Eudragit L100 and PLLA; the first one demonstrates, by fluorescence evidence, a protein binding capacity three times superior than the second. A comparison between a drop deposition and a Langmuir-Blodgett deposition was carried out by means of fluorescence and the second method was considered the most effective, especially for lower concentration of the proteins. Detection by AFM imaging was also carried out and revealed the presence of these proteins attached on the surface on a flatten position and confirmed the effectiveness of the immobilisation method on this substrate.

Moreover, the last images revealed that manipulation of these proteins on a nanometer scale on a surface was also possible by the control in position and strength of the tip.

By adjusting the force of the tip is conceivable to build micro and nano-wells on the PMMA surface to develop ordered substrates for biosensors multi-purposes.

CONCLUSIONS

Object of this Ph.D. thesis was the development of a novel optical chip for affinity biosensors. The research carried out was highly interdisciplinary since not only were chemical and biochemical aspects faced during the course of the three years, but the activity also dealt with optical aspects. The main results achieved are summarized below:

1) A novel fluorescence-based optical platform for multiple bioassay was designed and developed in order to optimise the collection of the fluorescence emitted by the sensing layer. The fluorescence anisotropy, which is exhibited whenever a discontinuity of refractive index is present, was used to develop a novel optical configuration characterized by high collection efficiency and a very good separation between excitation and emission. In principle, the optical efficiency of the system could be improved further improved if the spectrum analyser were replaced by a photomultiplier or a powerful detector, without discriminating the detected wavelength. On the other hand the described system, equipped with the spectrum analyser, was essential in the identification of the better working wavelengths and in the discrimination of the optical signal coming from the chip (fluorescence and scattered light). It is also important to stress the particular configuration of the chip with multiple channels which was potentially useful for multi-analyte assay, with each single channel designed for the detection of different analytes.

2) A careful study on the optimisation of the substrate for the immobilisation of the bioreceptor was carried out in order to identify the best chemical treatment of the surface: the best polymer was found to be 0.01mM Eudragit L100 for drop deposition; PLLA was another affordable solution. Eudragit L100 was also shown to be an appropriate solution for a reaction with an amino-linker. Further studies, verified by chip measurements, demonstrated that the optimal concentration by drop deposition was 0.01 mM. The best method for deposition of Eudragit L100 was by using the Langmuir Blodgett method with 20mN/m surface pressure in order to obtain a thin monolayer of 5 nm. This increased by at least one order of magnitude the sensitivity of the entire optical system.

3) The system was fully characterised with the IgG/anti-IgG direct assay with the definition of a protocol for the implementation of the assay. IgG and Anti-IgG interactions were plenty characterized also by atomic force microscopy imaging. The

increased efficiency of the optical system by Langmuir-Blodgett deposition was obtained for this type of assay.

4) The potential of the optical platform was tested with a sandwich assay for NF-kB1, using a double stranded DNA (dsDNA) sequence as the specific capture bioreceptor immobilised on the PMMA surface and a Cy5-labelled antibody (clone C-19) as detection bioreceptor.

5) The hybridization of the RNA/RNA duplex for the MGMT detection was verified on the optical platform detecting target 7 in flow, after the immobilization of the suitable probe (probe 7) on the PMMA surface.

6) The optimised immobilization procedure of proteins on PMMA was also used for the detection of PSII proteins extracted from thylakoid membranes of spinach leaves. A characterization of these surfaces was carried out by measurements of anisotropic fluorescence and by means of atomic force microscopy.

The significance of this work can be summarised as the title of this thesis declares. A novel optical biochip for multi-analyte detection is born.

This biochip represent the core part of the integrated project called CARE-MAN (HealthCARE by Biosensor Measurements And Networking) of the 6th EU RTD Framework Programme.

Integration of potentials in nanotechnology and information technology is an urgent objective in the economy of Europe, aiming at the transition towards a knowledge-based society and sustainable development.

Accordingly, support of e-health by development of new diagnosis equipment for healthcare based on biosensing with integrated data pre-treatment and networking capabilities is intended by the joint call IST-NMP-2 in the Sixth Framework Programme and considered within eEurope2002 Action Plan Health.
The achievement of the objectives of the Integrated project CARE-MAN will provide significant benefits to the effectiveness of the European healthcare in general as well as to large segments of the European population profiting from the knowledge generated within this project because of its focus on major diseases prevailing in European societies. As these diseases are closely linked to the issue of the ageing European population, CARE-MAN will contribute to meet this major societal challenge.
At present, diagnostics at hospitals is based either on large-scale automated equipment or ELISA techniques based on bioassays which are not suitable for bedside and emergency medicine. To overcome these restrictions, the Integrated Project CARE-

MAN has first a long-term objective as the development of a new medical instrument being an intelligent diagnosis equipment for healthcare, representing a development for the future and the potential of down-scaling for the use in general practices, and second the vision to provide a new automated, self-controlled equipment for patient homecare, either in case of post-operative checks or for permanent surveillance in case of chronic diseases. CARE-MAN will provide a validated, intelligent, fully automated diagnostic device with a modular technological system based on biosensor technology, combining successful transduction principles, biochemical recognition methods and communication capabilities to allow a multi parameter measurement characterising diseases defined by doctors and needs in hospitals, like cardiovascular disease, coagulation disorders, chronic/acute inflammation, cancer, thyroid disorders.

The CARE-MAN 5-year project has a total budget of nearly € 18 million of which about € 11.55 million is funded by the European Commission.

CARE-MAN integrates partners from academia, industry and medical science into a coordinated interdisciplinary research between nanotechnology, nanoscience and information technology.

BIBLIOGRAPHY

1. Turner A.P.F., BIOCHEMISTRY: Biosensors--Sense and Sensitivity, *Science*, 2000, Vol. **290**, no. 5495, pp. 1315-1317.
2. Homola J., Lu H.B., Nenninger G.G., Dostàlek J., Yee S.S., A novel multichannel surface plasmon resonance biosensor, 2001, Sensors and Actuators B, **76**: 403-410.
3. Gauglitz G., Brecht A., Kraus G., Mahm W., Chemical and biochemical sensors based on interferometry at thin (multi-) layers, Sensors and Actuators B, 1993, **11**: 21-27.
4. Dieterle F., Belge G., Betsch C., Gauglitz G., Quantification of the refrigerants R22 and R134a in mixtures by means of different polymers and reflectometric interference. Analytical and Bioanalytical Chemistry, 2002, **374**: 858-867.
5. Ligler F.S., Rowe Taitt C., Shriver-Lake L.C., Sapsford K.E., Shubin Y., Golden J.P., Array biosensor for detection of toxins, Analytical and Bioanalytical Chemistry, 2003, **377**: 469-477.
6. Barzen C., Brecht A., Gauglitz G., Optical multiple-analyte immunosensor for water pollution control, Biosensors and Bioelectronics, 2002 **17**: 289-295.
7. Epstein J.R., Biran I., Walt D.R., Fluorescence-based nucleic acid detection and microarrays, Analytica Chimica Acta, 2002 **469**: 3-36.
8. Proll G., Tschmelak J., Gauglitz G., Fully automated biosensors for water analysis, Analytical and Bioanalytical Chemistry, 2005, **381**: 61-63.
9. Proll G, Steinle L, Proll F, Kumpf M, Moehrle B, Mehlmann M, Gauglitz G., Potential of label-free detection in high-content-screening applications, Journal of Chromatography A, 2007, **1161**: 2-8.
10. Moreno-Bondi M.C., Rowe Taitt C., Shriver-Lake L.C., Ligler F.S., Multiplexed measurement of serum antibodies using an array biosensor, Biosensors and Bioelectronics, 2006, **21**: 1880-1886.
11. IUPAC Compendium of Chemical Terminology, Blackwell Scientific Publications, 2nd edition, 1997, edited by A D McNaught and A Wilkinson.
12. Turner A.P.F., Biosensors '90: an introduction, Biosensors and Bioelectronics, 1991, Vol. **6**, 177-178.
13. Van der Pol J.J., De Gooijer D.C., Biselli M., Wandrey C., Tramper J., automation of selective assays for on-line bioprocess monitoring by flow-injection analysis, Trends in Biotechnology, 1996, Vol. **14**, 471-477.

14. Brooks S.L., Higgins I.J., Newman J.D. and Turner A.P.F., Biosensors for process control, Enzyme Microbial Technology, 1991, Vol. **13**, 946-955, 1991
15. White S.F., and Turner A.P.F, Encyclopedia of Bioprocess Technology: Fermentation, Biocatalysis and Bioseparation. M.C. Flickinger and S.W. Drew, eds. 1997, Wiley, New York.
16. Maccà C., Response time of ion-selective electrodes. Current usage versus IUPAC recommendations", Analytica Chimica Acta, 2004, **512**, 183-190.
17. Sutherland RM, Dähne C, Place JF, Ringrose AS., (Optical detection of antibody-antigen reactions at a glass-liquid interface. Clin Chem. 1984, 30 (9): 1533-1538
18. Place JF, Sutherland RM, Dähne C., Opto-electronic immunosensors: a review of optical immunoassay at continuous surfaces. Biosensors 1985, 1 (4): 321-353.)
19. Flanagan M.T., Java Scientific Library
20. D.L. Lee, Electromagnetic Principles of Optics, John Wiley and Sons, New York, (1986) pp 86-89.
21. Sloper A.N. and Flanagan M.T., Metal phosphate planar waveguides for biosensors, Applied Optics, 33, (1994) 4230-4240.
22. Sloper A.N., Deacon J.K. and Flanagan M.T., A planar indium phosphate monomode waveguide evanescent field immunosensor, Actuators and Sensors, B1,(1989) 589-591.
23. Sloper A.N. and Flanagan M.T., Novel iron phosphate optical waveguides fabricated by a low temperature process, Electronic Letters, 24, (1988) 353-355.
24. Flanagan M.T. and Sloper A.N., Waveguide sensor with input and reflecting gratings and its use in immunoassay, U.S. Patent 5,081,012, 1992. [http://www.freepatentsonline.com/5081012.pdf]
25. Carniglia C.K., Mandel L. Absorption and emission of evanescent photons. J. Opt. Soc. Am. 63, 479-480 (1972).
26. Lee E.H., Bremmer R.E., Fenn J.B., Chang E.K. Angular distribution of fluorescence from liquids and monodispersed spheres by evanescent wave excitation. Appl. Opt. 18, 862-868 (1979).
27. Sutherland RM, Dähne C, Place JF, Ringrose AS., (Optical detection of antibody-antigen reactions at a glass-liquid interface. Clin.Chem. 1984, 30 (9): 1533-1538)
28. Yalow E.S., Berson S.A. Immunoasaay of endogenous plasma insulin in man. Journal of Clinical Investigation,1960, 39: 1157-1170.
29. Kirkhasn KE, Hunter WM, Eds. Radioimmunoassay Methods, Churchill-Livingstone Press, Edinburgh, 1971.

30. Hunter WM, Come JT, Eds. Immunoassays for Clinical Chemistry,.Churchill-Livingston Press, Edinburgh, 1983.
31. Harrick NJ. Internal Reflection Spectroscopy, Wiley Interscience, New York, NY, 1967.
32. Yang RT, Low MJD. Quantitative analysis of aqueous nitrite/nitrate solutions by infrared internal reflection spectrometry. Anal Chem 45, 2014-2018 (1973).
33. Mattson JS, Smith CA, Paulsen KE. Infrared internal reflection spectrometry of aqueous protein films at the germanium-water interface. Anal Chem 47, 736-738 (1975).
34. Gendreau EM, Leininger RI, Winters S, Jacobsen RJ. Fourier transform infrared spectroscopy for protein-surface studies. In InterfacialPhenomena and Applications, SL Cooper, NA Peppas, Eds., (Adu Chem Ser 199), Interscience, John Wiley & Sons, New York, NY, 1982, pp 351-370.
35. Van Wagenen R.A., Rockhold S., Andrade J.D. Probing protein adsorption: Total internal reflection intrinsic fluorescence. Ibid. pp 370-389.
36. Kromck MN, Little WA. A new immunoassay based on fluorescence excitation by internal reflection spectroscopy. J Immunol Methods 8, 235-240 (1975).
37. Thompson N.L., Axelrod D., Immunoglobulin surface-binding kinetics studied by total internal reflection with fluorescence correlation spectroscopy. Biophys. J. **43,** 103-114 (1983).
38. Sutherland EM, Dahne C, Place JF. Preliminary results obtained with a no-label, homogeneous, optical immunoassay for human immunoglobulin G. *AnolLett* 17(B1), 43-55 (1984).
39. Sutherland R.M., Dähne C., Place J.F. and Ringrose A.R., Immunoassays at a quartz-liquid interface: theory, instrumentation and preliminary application to the fluorescent immunoassay of human immunoglobulin G, Journal of Immunological Methods, 1984, Vol. 74, (2): 253-265.
40. Shanks et al., 1987, U.S. Patent No. 4,810,658.
41. Badley, R. A.; Drake, R. A. L.; Shanks, I. A.; Smith, A. M.; Stephenson, P. R., Optical Biosensors for Immunoassays: The Fluorescence Capillary-Fill Device, Philosophical Transactions of the Royal Society of London. Series B, Biological Sciences, 1987, Vol. 316, (1176): 143-160).
42. Flanagan M.T., Surface optics for biodetection. Biosensors: A Viable Monitoring Technology?, IEE Colloquium on 1991: pp. 6/1-6/3).

43. Badley R.A., Drake L., Shanks I.A., Smith A.M. and Stephenson P.R., 1987, Phil. Trans Royal Society of London, B316, 143-160.

44. Parry R. P., Love C.A. and Robinson G. A., Detection of rubella antibody using an optical immunosensor**,** Journal of Virological Methods**,** , 1990, Vol. 27, (1): 39-48.

45. Deacon J. K., Thomson A. M., Page A. L., Stops J. E., Roberts P. R., Whiteley S.C., Attridge J.W., Love C.A., Robinson and G. P. Davidson G.A.**,** An assay for human chorionic gonadotrophin using the capillary fill immunosensor, Biosens Bioelectron. 1991;6(3):193-199.

46. Daniels P.B, Fletcher J.E., O'Neill P.M., Stafford C.G., Bacarese-Hamilton T., Robinson G.A., A comparison of three fluorophores for use in an optical biosensor for the measurement of prostate-specific antigen in whole blood, Sensors and Actuators B, 26-27, (1995): 447-451.

47. Catalona W.J., Smith D.S., Ratcliff T.L., Dodds K.M., Coplen D.E., Yaun J.J., Petros J.A. and Andriole G.L., Measurement of prostate-specific antigen in serum as a screening test for prostate cancer, *N. Engl. J. Med., 324* (1991) 1156-1161.

48. Flanagan M.T., Surface optics for biodetection. Biosensors: A Viable Monitoring Technology?, IEE Colloquium on 1991: pp. 6/1-6/3).

49. Attridge J W, Daniels I.B, Deacon J K, Robinson G A and Davidson G P, 1991 Biosensors and Bioelectronics 6, 201-214.

50. J. W. Attridge, P. B. Daniels, J. K. Deacon**,** G. A. Robinson and G. P. Davidson, Sensitivity enhancement of optical immunosensors by the use of a surface plasmon resonance fluoroimmunoassay Biosensors and Bioelectronics, Vol. 6, 3, 1991: 201-214.

51. William H. Scouten, John H. T. Luong and R. Stephen Brown, Enzyme or protein immobilization techniques for applications in biosensor design, Review, Trends in Biotech. 1995, Vol. 13, Elsevier Science ed.

52. Blodgett, K.B. and Langmuir I. (1937) Phys. Rev. 51, 964-982

53. Sugawara M., Kojima K., Sazawa H. and Umezawa Y. Anal. Chem. 59, 2842-2846.

54. Wolfbeis O.S. and Schaffar B.P.H. (1987) Anal. Chim. Acta 198, 1-12.

55. Scouten W.H., Luong J.H.T. and Brown R.S., Enzyme or protein immobilization techniques for applications in biosensor design, Review, Trends in Biotech. 1995, Vol. 13, Elsevier Science ed.

56. MacCraith B.D., McDonagh C., Enhanced Fluorescence Sensing Using Sol-Gel Materials, Journal of Fluorescence, Vol. 12, No. 3/4, 2002

57. MacCraith B.D., Optical chemical sensors based on sol-gel-derived films, in sol-gel and polymer photonic devices, Andrews M.P. Najafi S.I. (eds.), SPIE, 1997, Bellingham, Washington.
58. Watts H.J., Lowe C.R., Pollard-Knight D.V., Optical biosensor for monitoring microbial cells, Anal. Chem. 1994, 66, 2465-2470.
59. Slop, A. N.; Deacon, J. K.; Flanagan, M. T. Sens. Actuators 1990, B1, 589-591.
60. J.-F. Gouin, A. Doyle and B.D. MacCraith, Fluorescence capture by planar waveguide as platform for optical sensors, Electronics letter, 1998, Vol. 34, No. 17: 1685-1687.
61. Brinker C.J., Scherer G.W., Sol-gel Science (Academic Press, New York, 1990)
62. McDonagh C., MacCraith B.D. and McEvoy A.K.: Tailoring of sol-gel films for optical sensing of oxygen in gas and aqueous phase, Anal. Chem., 1991, Vol. 1-2.
63. Lippitsch M.E., Draxler S., and Kieslinger D., Luminescence lifetime-based sensing: new materials, new devices, Sens. actuators B Chem. 1997, 38-39: 96-102).
64. Ekins, R.; Chu, R., Clin. Chem.. 1993, 39, 369-370.
65. Ekins, R., Chu, F., Biggart, E., Clin. Chim. Acta 1990, 194, 91-114.
66. Herron, J. N., Christensen, D. A., Wang, H.-K., Caldwell, K. D., Janatova, V., Huang, S.C., U.S. Patent 5677196, 1997.
67. Abel, A. P.; Weller, M. G.; Duveneck, G. L.; Ehrat, M.; Widmer, H. M. Anal.Chem., 1996, 68: 2905-12.
68. Blawas, A. S.; Oliver, T. F.; Pirrung, M. C.; Reichert, W. M. *Langmuir* 1998, *14*, 4243-50.
69. Brecht, A., Klotz, A., Barzen, C., Gauglitz, G., Harris, R. D., Quigley, G. R., Wilkinson, J. S., Sztajnbok, P., Abuknesha, R., Gasco´n J., Oubin˜a, A.; Barcelo D., Anal. Chim. Acta 1998, 362, 69-79.
70. Bakaltcheva, I. B.; Shriver-Lake, L. C.; Ligler, F. S. *Sens. Actuators*, *B* 1998, 51, 46-51.
71. Narang, U., Gauger P. R., Kusterbeck A. W., Ligler F. S., *Anal. Biochem.*1998, 255, 13-19.
72. Kakabakos, S. E.; Christopoulos, T. K.; Diamandis, E. P. Clin. Chem. 1992, 38, 338-342.
73. Parsons, R. G.; Kowal, R.; LeBlond, D.; Yue, V. T.; Neagarder, L.; Bond, L.; Garcia, D.; Slater, D.; Rogers, P. Clin. Chem. 1993, 39, 1899-1903.
74. Frebel, H.; Chemnitius, G.-C.; Cammann, K.; Kakerow, R.; Rospert, M.; Mokwa, W. Sens. Actuators, B 1997, 43, 87-93.

75. Berger, C. E. H.; Beumer, T. A. M.; Kooyman, R. P. H.; Greve, J. Anal.Chem. 1998, 70, 703-706.

76. Wadkins, R.M., Golden, J.P., Pritsiolas, L.M., Ligler, F.S. Biosens. Bioelectron. 1998, 13: 407-15.

77. Wadkins, R. M.; Golden, J. P.; Ligler, F. S. J. Biomed. Opt. 1997, 2: 74-79.

78. Rowe C.A., Tender L.M., Feldstein M.J., Golden J.P., Scruggs S.B., MacCraith B.D., Cras J.J., Ligler F. S., Array biosensor for simultaneous identification of Bacterial, Viral, Protein anlytes, Anal. Chem. 1999, 71, 3846-3852.

79. Rowe, C. A.; Scruggs, S. B.; Feldstein, M. J.; Golden, J. P.; Ligler, F. S. Anal. Chem. 1999, 71, 433-439.

80. Marose S., Lindemann C., Ulber R. and Scheper T., Optical sensor systems for bioprocess monitoring, Trends in Biotech., Vol. 17, 1999, Elsevier Science.

81. Junker, B. H., Reddy, J., Gbewonyo, K. and Greasham, R. (1994) *Bioprocess Eng.* 10, 195–207

82. Wu, P., Ozturk, S. S., Blackie, J. D., Thrift, J. C., Figueroa, C. and Naveh, D. (1995) Biotechnol. Bioeng. 45, 495–502.

83. Konstantinov, K., Chuppa, S., Sajan, E., Tsai, Y., Yoon, S. and Golini, F., 1994, Trends Biotechnol. 12, 324–333.

84. Olsson, L. and Nielsen, J., 1997, Trends Biotechnol. 15, 517–522.

85. Hatch, R. T. and Veilleux, B. G., 1995, Biotechnol. Bioeng. 46, 371–374

86. Naimimohasses, R., Barnett, D. M., Green, D. A. and Smith, P. R., 1995, Sci. Technol. 6: 1291–1300.

87. Montague, G. and Morris, J., 1994, Trends Biotechnol. 12, 312–324

88. Suhr, H. et al. Biotechnol. Bioeng., 1995, 47, 106–116.

89. Watts, H. J., Yeung, D. and Parkes, H. (1995) Anal. Chem. 67, 4283–4289.

90. Chung H., Arnold M.A., Rhiel, M. and Murhammer D.W., 1995, Appl. Biochem. Biotechnol. 50:109–125.

91. Riley, M. R., Rhiel, M., Zhou, X., Arnold, M. A. and Murhammer, D. W. (1997) Biotechnol. Bioeng. 55, 11–15.

92. Macalony, G., Draper, I., Preston, J., Anderson, K. B. and Rollins, M. J. (1996) Food Bioprod. Process. 74, 212–220.

93. Vaccari G., Dosi E., Campi A.L., Gonzalez R.A. Matteuzzi D. and Mantovani G., 1994, Biotechnol. Bioeng. 43, 913-917.

94. Eberl R., and Wilke J., 1996, Sens. Actuators B. 32, 203-208.

95. Schügerl, K., Bioprocess Monitoring (1st ed.), J. Wiley & Sons, 1997: 372–375.

96. Marose S., Lindemann C. and Scheper T., 1998, Biotechnol. Prog. 14, 63–74.

97. Bambot S.B., Lakowicz J.R. and Rao G., 1995, Trends Biotechnol. 13, 106–115.

98. Sipior, J., Randers-Eichhorn L., Lakowicz J. R., Carter G.M. and Rao G., 1996, Biotechnol. Prog. 12, 266–271.

99. Inman, S. M., Thibado, P., Theriault, G. A. and Liebermann, S. H. (1990) Anal. Chim. Acta 239, 45–51.

100. Szmacinski, H. and Lakowicz, J. R. (1996) Sens. Actuat. B 30, 207–215.

101. Malins C., Niggemann M. and MacCraith B. D., Multi-analyte optical chemical sensor employing a plastic substrate, Meas. Sci. Technol. 11 (2000) 1105–1110.

102. L'ubosˇ Polerecky´ , Jaroslav Hamrle, and B.D. MacCraith, Theory of the radiation of dipoles placed within a multilayer system, Applied Optics, , 2000, Vol. 39, No. 22: 3968-3977.

103. Rabbany S., Donner B., and Ligler F., "Optical immunosensors" Crit. Rev. Biomed. Eng. **22,** 307–346 (1994).

104. Stuart H. and Hall D., Enhanced dipole–dipole interaction between elementary radiators near a surface, Phys. Rev. Lett. 80**,** 5663–5666, 1998.

105. Enderlein J., Ruckstuhl T., and Seeger S., Highly efficient optical detection of surface-generated fluorescence, Appl. Opt. **38,** 724–732 (1999).

106. McDonagh C., Kolle C., McEvoy A.K., Dowling D.L., Cafolla A.A., Cullen S.J., MacCraith B.D., Phase fluorometric dissolved oxygen sensor, Sensors and Actuators B, 2001, 74,: 124-130.

107. Wong, R.L. *et al.* (1997) Validation parameters for a novel biosensor assay which simultaneously measures serum concentrations of a humanized monoclonal antibody and detects induced antibodies. J. Immunol. Methods 209, 1–15.

108. Tsoka, S. *et al.* (1998) Rapid monitoring of virus-like particles using an optical biosensor: a feasibility study. J. Biotechnol. 63, 147–153.

109. Baker, K. et al., Real-time monitoring of recombinant protein concentration in animal cell cultures using an optical biosensor, Genet. Eng. Biotechnol., 1997, 17, 69–74.

110. Gill, A. et al., Bioprocess monitoring: an optical biosensor for rapid bioproduct analysis. J. Biotechnol., 1998, 65, 69–80.

111. Jonsson, U. and Malmqvist, M. (1992) Real-time biospecific interaction analysis. The integration of surface plasmon resonance, detection, general biospecific interface chemistry and microfluidics into one analytical system. *Adv. Biosensors* 2, 291–336.

112. Baker K.N., Rendall M.H., Patel A., Boyd P., Hoare M., Robert B. Freedman and David C. James, Rapid monitoring of recombinant protein products: a comparison of current technologies, Trends in Biotechnology Vol.20, No.4, 2002.

113. Qian S. and Bau H.H., A mathematical model of lateral flow bioreactions applied to sandwich assays, Analytical Biochemistry 2003, 322: 89–98.

114. Qian S. and Bau H.H., Analysis of lateral flow biodetectors: competitive format, Analytical Biochemistry (2004) **326**: 211–224

115. Abrams WR, Barber CA, McCann K, Tong G, Chen Z, Mauk MG, Wang J, Volkov A, Bourdelle P, Corstjens PL, Zuiderwijk M, Kardos K, Li S, Tanke HJ, Sam Niedbala R, Malamud D, Bau H., Development of a microfluidic device for detection of pathogens in oral samples using upconverting phosphor technology (UPT). Ann N Y Acad Sci. 2007 Mar; 1098: 375-88.

116. Corstjens PL, Chen Z, Zuiderwijk M, Bau HH, Abrams WR, Malamud D, Sam Niedbala R, Tanke H.J., Rapid assay format for multiplex detection of humoral immune responses to infectious disease pathogens (HIV, HCV, and TB). Ann. N.Y.Acad.Sci. 2007 Mar; 1098:437-45.

117. Chen Z., Mauk M.G., Wang J., Abrams W.R., Corstjens P.L., Niedbala R.S., Malamud D., Bau H.H., A microfluidic system for saliva-based detection of infectious diseases. Ann. N. Y. Acad. Sci. 2007, 1098: 429-36.

118. Stranik O., McEvoy H.M., McDonagh C., MacCraith B.D., Plasmonic enhancement of fluorescence for sensor applications, Sensors and Actuators B 107 (2005) 148–153

119. Rechberger W., Hohenau A., Leitner A., Optical properties of two gold nanoparticles, Opt. Commun., 2003, 220, 137–141.

120. Oberthaler M.K., One-, two- and three-dimensional nanostructures with atom lithography, J. Phys.: Condens. Matter , 2003, 15 (6): R233–R255.

121. Link S., Wang Z.L., Alloy formation of gold-silver nanoparticles and the dependence of the plasmon absorption on their composition, J. Phys. Chem. B 103 (1999) 3529–3533.

122. Everett D.H., Basic Principles of Colloid Science, Royal Society of Chemistry, 1988.

123. Zach M.P., Penner R.M., Size-monodisperse and nanocrystalline nickel nanoparticles, Adv. Mater., 2000, 12, 878.

124. Al-Rawashdeh N.A., Sandrock M.L., Seugling C.J., Visible region polarization spectroscopic studies of template-synthesized gold nanoparticles oriented in polyethylene, J. Phys. Chem. B 1998, 102: 361–371.

125. Rowe C.A., et al., Array biosensor for simultaneous identification of bacterial, viral and protein analytes, Anal. Chem., 1999, 71: 3846-3852.

126. Blue R., Kent N., Polerecky L., McEvoy H., Gray D. and MacCraith B.D., Platform for enhanced detection efficiency in luminescence-based sensors, Electronics letters 2005 Vol. 41 No. 12.

127. Ruckstuhl T., Verdes, D., Supercritical angle fluorescence (SAF) microscopy, Opt. Express, 2004, 12, pp. 4246–4254.

128. Ligler F.S., Sapsford K.E., Golden J.P., Shriver-Lake L.C., Taitt C.R., Dyer M.A., Barone S., and Myatt C.J. The Array Biosensor: Portable, Automated Systems Analytical Science, 2007, Vol. 23

129. Golden J.P., Taitt C.R., Shriver-Lake L.C., Shubin Y.S. and Ligler F.S. A portable automated multianalyte biosensor, 2005, Talanta, 65, ed. Elsevier.

130. Mauk M.G., Ziober B.L., Chen Z., Thompson J.A., Bau H.H. Lab-on-a-chip technologies for oral-based cancer screening and diagnostics: capabilities, issues, and prospects. Ann. N. Y. Acad. Sci. 2007, 1098: 467-75.

131. Ajello L. et al., La Placa - Principi di microbiologia medica, , 10th ed., 2005, edited by Esculapio.

132. Kasper D.L., Braunwald E., Fauci A.S., Hauser S.L., Longo D.L., Jameson J.L., Harrison - Principi di medicina interna, 16th ed., 2007, edited by McGraw Hill.

133. Roitt I., Brostoff J., Male D., Immunology, 3rd ed., 1996, edited by Zanichelli.

134. Latchman D.S., Transcription factors: An overview, International Journal of Biochemistry and Cell Biology, 1997, **29** (12): 1305-1312.

135. Karin M., Too many transcription factors: positive and negative interactions, New Biol. 1990, **2** (2): 126-131.

136. Roeder R.G., The role of general initial factors in transcription by RNA polymerase II, Trends in Biochemical Science, 1996, **21** (9): 327-335.

137. Nikolov D.B., Burley S.K., RNA polymerase II transcription initiation: a structural view, Proceedings of National Academy of Sciences USA, 1997, 94 (1): 15-22.

138. DiDonato J., Mercurio F., Rosette C., Wu-Li J., Suyang H., Ghosh S., Karin M., Mapping of the inducile IkappaB phosphorylation sites that signal its ubiquination and degradation, Molecular Cell Biology 1996, **16** (4): 1295-1304.

139. Schmitz M.L., Bacher S., Kracht M., IκB-independent control of NF-κB activity by modulatory phosphorylations, Trends in Biochemical Science 2001, **26** (3): 186-190.

140. McClean P., http://www.cc.ndsu.nodak.edu/instruct/mcclean/plsc731/transcript/transcript1.htm
141. Sen R., Baltimore D., Multiple nuclear factors interact with the immunoglobulin enhancer sequences, Cell 1986, **46**: 705-716.
142. Baeuerle P.A., Baltimore D., Activation of DNA-binding activity in an apparently cytoplasmic precursor of the NF-κB transcription factor, Cell 1988, **53**: 211-217.
143. Grilli M., Chiu J.J.S., Lenardo M.J., NF-kappa-B and rel – Participants in a multiform transcriptional regulatory system, International Review of Citology – A survey of Cell Biology, 1993, 143: 1-62.
144. Kopp E.B., Ghosh S., NF-kappa-B and rel proteins in innate immunity, Advances in Immunology, 1995, **58**: 1-27.
145. Gonzalez-Crespo S., Levine M., Related target enhancers for dorsal and NF-kappa B signaling pathways, Science, 1994, Vol. **264** (5156): 255-258.
146. Steward R., Dorsal an embryonic polarity gene in Drosophila, is homologous to the vertebrate proto-oncogene c-rel, Science, 1987, **238** (4827): 692-694.
147. Ip Y.T., Reach M., Engstrom Y., Kadalayil L., Cai H., Gonzalez-Crespo s., Tatei K., Levine M., Dif, a dorsal-related gene that mediates an immune response in Drosophila, Cell 1993, Vol. **75**: 753-763.
148. Dushay M.S., Asling B., Hultmark D., Origins of Immunity: Relish, a compound rel-like gene in the anti-bacterial defense of Drosophila, Proceedings of National Academy of Sciences USA, 1996, **93** (19): 10343-10347.
149. Govind, S., Steward, R., Dorsoventral pattern formation in *Drosophila*: signal transduction and nuclear targeting, Trends in Genetics 1991, **7** (4): 119-125.
150. Hashimoto C., Hudson K.L., Anderson K.V., The Toll gene of Drosophila, required for dorsal-ventral embryonic polarity, appears to encode a transmembrane protein, , Cell 1988, **52** (2): 269-279.
151. Shelton C.A., Wasserman S.A., pelle encodes a protein kinase required to establish dorsoventral polarity in the Drosophila embryo, Cell. 1993, **72** (4): 515-25.
152. Cao Z., Xiong J., Takeuchi M., Kurama T., Goeddel D.V., TRAF6 is a signal transducer for interleukin-1, Nature 1996, **383** (6599): 443-446.
153. R. Geisler, A. Bergmann, and Y. Hiromi, *et al.,* Cactus, a gene involved in dorsoventral pattern formation of Drosophila, is related to the IkB gene family of vertebrates, Cell 1992, **71**: 613-621.

154. Kidd. S., Characterization of the Drosophila cactus locus and analysis of interactions between cactus and dorsal proteins, Cell 1992, **71**: 623-635.

155. Belvin M. P., Jin Y., Anderson K.V., Cactus protein degradation mediates Drosophila dorsal-ventral signalling 1995, Genes & development **9**: 783-793.

156. Whalen A.M. and Steward R., Dissociation of the dorsal-cactus complex and phosphorylation of the dorsal protein correlate with the nuclear localization of dorsal, the Journal of Cell Biology 1993, **123**: 523-534.

157. Gillespie S.K., Wasserman S.A., Dorsal, a Drosophila Rel-like protein, is phosphorylated upon activation of the transmembrane protein Toll, Molecular and Cellular Biology 1994, **14** (6): 3559-3568.

158. Hultmark D., Immune reactions in Drosophila and other insects: a model for innate immunity, Trends in Genetics 1993, **9** (5): 178-183.

159. Baumann H., Gauldie J., the acute phase response, Immunology Today 1994, **15** (2): 74-80.

160. Lemaitre B., Nicolas E., Michault L., Reichhart J.M., Hoffmann J.A., The dorsoventral regulatory gene cassette spatzle/Toll/cactus controls the potent antifungal response in Drosophila adults, Cell 1996, **86** (6): 973-983.

161. Nicolas E., Nappi A.J., Lemaitre B., Expression of antimicrobial peptide genes after infection by parasitoid wasps in Drosophila, Developmental and Comparative Immunology 1996, **20** (3): 175-181.

162. Whitham S., Dinesh-Kumar S.P., Choi D., Hehl R., Corr C., Baker B., The product of the tobacco mosaic virus resistance gene N: Similarity to toll and the interleukin-1 receptor,
Cell 1994, **78**: 1101-1115.

163. Ryals J., Weymann K., Lawton K., Friedrich L., Ellis D., Steiner H.Y., Johnson J., Delaney T.P., Jesse T., Vos P., Uknes S., The Arabidopsis NIM1 protein shows homology to the mammalian transcription factor inhibitor I kappa B, Plant Cell. 1997, **9** (3): 425–439.

164. Medzhitov R., Preston-Hurlburt P., Janeway Jr C.A., A human homologue of the Drosophila Toll protein signals activation of adaptive immunity, letters to Nature 1997.

165. Yamamoto Y., Gaynor R. B., Therapeutic potential of inhibition of the NF-κB pathway in the treatment of inflammation and cancer, Journal of Clinical Investigation 2001, **107**: 135-142.

166. Sampath D., Castro M., Look D. C., Holtzman M. J., Constitutive activation of an epithelial signal transducer and activator of transcription (STAT) pathway in asthma, Journal of Clinical Investigation 1999,**103**: 1353-1361.

167. T.D. Gilmore, The Rel/NF-kappaB signal transduction pathway: introduction. Oncogene **18** (49): 6842-6844.

168. Giannetti A., Citti L., Domenici C., Tedeschi L., Baldini F., Wabuyele B.M., Vo-Dinh T., FRET-based protein DNA binding assay for detection of active NF-kB, Sensors and Actuators B Chemical., 2006, **119** (2): 649-654.

169. Baldwin A.S**.**, The NF-kB and IkB proteins: new discoveries and insights, Annual Review of Immunology 1996, 14: 649–681.

170. Verma, I. M., Stevenson, J. K., Schwarz, E. M., Van Antwerp, D. and Miyamoto, S. Rel/NF-kB/IkB family: intimate tales of association and dissociation, Genes & Development 1995, **9**: 2723-2735.

171. Huxford T., Huang D.B., Malek S., Ghosh G., The crystal structure of the IkB/NF-kB complex reveals mechanisms of NF-kB Inactivation, , Cell 1998, **95**: 759-770.

172. Kunsch C., Ruben S.M., Rosen C.A., Selection of optimal kappa B/Rel DNA-binding motifs: interaction of both subunits of NF-kappa B with DNA is required for transcriptional activation, Molecular and Cellular Biology 1992, **12** (10): 4412-21.

173. Chen, F.E., Huang, D.B., Chen, Y.Q., Ghosh, G., Crystal structure of p50/p65 heterodimer of transcription factor NF-kappaB bound to DNA, 1998, Nature **391:** 410-413.

174. Plaksin D., Baeuerle P.A., Eisenbach L., KBF1 (p50 NF-kappa B homodimer) acts as a repressor of H-2Kb gene expression in metastatic tumor cells, Journal of experimental Medicine 1993, Vol. **177**: 1651-1662.

175. C.W. Muller, Fèlix A.Rey, Mikiko Sodeoka, Gregory L.Verdine, S.C.Harrison, Structure of the NF-κB p50 homodimer bound to DNA, Nature, 1995, **373**: 311- 317.

176. Ghosh G., Van Duyne G., Ghosh S., Sigler P.B., Structure of NF-κB p50 homodimer bound to a κB site, Nature, 1995, **373**: 303- 310.

177. Cramer P., Larson C.J., Verdine G.L., Muller C.W., Structure of the human NF-kappaB p52 homodimer-DNA complex at 2.1 A resolution, European Molecular Biology Organization (EMBO) Journal, 1997, **16** (23): 7078-7090.

178. Chen F. E., Huang D.B., Chen Y.Q., Ghosh G., Crystal structure of p50/p65 heterodimer of transcription factor NF-kappa B bound to DNA, Nature, 1998, **391** (6665): 410-413.

179. Fan C.M., Maniatis T., Generation of p50 subunit of NF-*k*B by processing of p105 through an ATP-dependent pathway, Nature, 1991 **354**: 395 – 398.

180. Karin M., Lin A., NF-κB at the crossroads of life and death, Nature Immunology, 2002**,** **3**: 221 – 227.

181. Lin L., Ghosh S., A glycine-rich region in NF-kappaB p105 functions as a processing signal for the generation of the p50 subunit. Molecular Cell Biology, 1996, **16** (5): 2248-54.

182. Heusch M., Lin L., Geleziunas R., Greene W.C., The generation of NFkB2 p52: mechanism and efficiency, Oncogene, 1999, **18** (46): 6201-8.

183. Jacobs M. D. and Harrison S. C., Structure of an IκBα / NF-κB Complex, Cell 1998, Vol. **95:** 749-758.

184. Chiao P. J., Miyamoto S., Verma I.M., Autoregulation of I\kappaB\alpha Activity, Proceedings of the National Academy of Sciences of the United States of America, 1994, Vol. **91**, No.1: 28-32.

185. Thompson J.E., Phillips R.J., Erdjument-Bromage H., Tempst P. and Ghosh S., IkB-β regulates the persistent response in a biphasic activation of NF-kB, Cell 1995, **80**: 573-582.

186. Franzoso G., Bours V., Azarenko V., Park S., Tomita-Yamaguchi M., Kanno T., Brown K., Siebenlist U, The oncoprotein Bcl-3 can facilitate NF-kB-mediated transactivation by removing inhibiting p50 homodimers from select kB sites, EMBO Journal 1993, **12**: 3893-3901.

187. Nolan G.P., Fujita T., Bhatia K., Huppi C., Liou H-C., Scott M. and Baltimore D. The bcl-3 proto-oncogene encodes a nuclear IkB-like molecule that preferentially interacts with NF-kB p50 and p52 in a phosphorylation-dependent manner. Molecular and Cellular Biology, 1993, **13**: 3557-3566.

188. Bours V., Franzoso G., Azarenko V., Park S., Kanno T., Brown K., Siebenlist U., The oncoprotein Bcl-3 directly transactivates through kB motifs via association with DNA-binding p50B homodimers. Cell 1993, **72**: 729-739.

189. Liou H-C, Nolan G.P., Ghosh S., Fujita T.,Baltimore D., The NF-kB p50 precursor, p105, contains an internal IkB-like inhibitor that preferentially inhibits p50. EMBO Journal 1992, **11**: 3003-3009.

190. Lin L., DeMartino G.N., Greene W.C., Cotranslational biogenesis of NF-kB p50 by the 26S proteasome. Cell 1998, **92**: 819-828.

191. Israël A., The IKK complex: an integrator of all signals that activate NF-kB? Trends in Cell Biology 2000, **10**: 129-133.

192. Li Y., Kang J., Friedman J., Tarassishin L., Ye J., Kovalenko A., Wallach D. and Horwitz M.S., Identification of a cell protein (FIP-3) as a modulator of NF-kB activity and as a target of an adenovirus inhibitor of tumor necrosis factor alpha-induced apoptosis. Proceedings of the National Academy of Sciences USA, 1999, **96**: 1042-1047.

193. Garg A. and Aggarwal B.B., Nuclear transcription factor-kB as a target for cancer drug development, Leukemia 2002, **16**: 1053-1068.

194. Yamaoka S., Courtois G., Bessia C., Whiteside S.T., Weil R., Agou F., Kirk H.E., Kay R.J. and Israël A. Complementation cloning of NEMO, a component of the IkB kinase complex essential for NF-kB activation. Cell 1998, **93**: 1231-1240.

195. Rothwarf D.M., Zandi E., Natoli G. and Karin M. IKK-γ is an essential regulatory subunit of the IkB kinase complex. Nature 1998, **395**: 297-300.

196. Delhase M., Hayakawa M., Chen Y. and Karin M., Positive and negative regulation of the IkB kinase activity through IKKβ subunit phosphorylation. Science, 1999, **284**: 309-313.

197. Karin M., The beginning of the end: IkB kinase (IKK) and NF-kB activation. Journal of Biological Chemistry, 1999, **274**: 27339-27342.

198. Christman J.W., Blackwell T.S. and Juurlink B.H., Redox regulation of nuclear factor kB: therapeutic potential for attenuating inflammatory responses. Brain Pathology, 2000, **10**: 153-162.

199. Hanson J. L., Anest V., Reuther-Madrid J., Baldwin A. S., Oncoprotein suppression of TNF-induced NF-kB activation is independent of Raf-controlled pathways, J.ournal of Biological Chemistry, 2003, Vol. **278** (37): 34910-34917,

200. Schreck R., Albermann K. and Baeuerle P.A. Nuclear factor kB: an oxidative stress-responsive transcription factor of eukaryotic cells. Free Radical Research Communications 1992, **17**: 221-237.

201. Iuvone T, D'Acquisto F, Van Osselaer N, Di Rosa M, Carnuccio R and Herman AG (1998) Evidence that inducible nitric oxide synthase is involved in LPS-induced plasma leakage in rat skin through the activation of nuclear factor-kB. British Journal of Pharmacology **123** 1325-1330.

202. Deng J., Xia W., Miller, S.A., Wen Y., Wang H. Y., Hung M.c., Crossregulation of NF-kB by the APC/GSK-3β/β-catenin pathway, Molecular Carcinogenesis, 2004, Vol. **39** (3): 139-146.

203. Gius D., Botero A., Shah S. and Curry H.A., Intracellular oxidation/reduction status in the regulation of transcription factors NF-kB and AP-1. Toxicology Letters, 1999, **106**: 93-106.

204. Mohan S., Koyoma K., Thangasamy A., Nakano H., Glickman R.D., Mohan **N.,** Low shear stress preferentially enhances IKK activity through selective sources of ROS for persistent activation of NF-κB in endothelial cells, Am. J. Physiology and Cell Physiology, 2007, **292**: C362-C371.

205. Yang J, Merin JP, Nakano T, Kato T, Kitade Y and Okamoto T Inhibition of the DNA-binding activity of NF-kB by gold compounds in vitro. Federation of European Biochemical Society (FEBS) Letters, 1995, **361**: 89-96.

206. MacMicking J. D., Nathan C., Hom G., Chartrain N., Fletcher D. S., Trumbauer M., Stevens K., Xie Q.W., Sokol K., Hutchinson N., Chen H., Mudget J.S., Altered responses to bacterial infection and endotoxic shock in mice lacking inducible nitric oxide synthase Cell, 1995, Vol. **81**: 641-650.

207. Pfeffer, K., Matsuyama, T., Kuendig, T.M., Wakeham, A., Kishihara, K., Shahinian, A., Wiegmann K., Ohashi, P.S., Kroenke, M., Mak, Tak W., Mice deficient for the 55 kd tumor necrosis factor receptor are resistant to endotoxic shock, yet succumb to L. monocytogenes infection. Cell. 1993, Vol. 73 (3): 457-467.

208. Behl C., Davis J.B., Lesley R. and Schubert D., Hydrogen peroxide mediates amyloid b protein toxicity. Cell 1994, **77**: 817-827.

209. Pahl H.L. and Baeuerle P.A., Expression of influenza virus hemagglutinin activates transcription factor NF-kB. Journal of Virology, 1995, **69** 1480-1484.

210. Barnes P.J. and Karin M., Nuclear factor-kB: a pivotal transcription factor in chronic inflammatory diseases. New England Journal of Medicine, 1997, **336**: 1066-1071.

211. Valen G., Paulsson G., Vaage J., Induction of inflammatory mediators during reperfusion of the human heart. Annals of Thoracic Surgery, 2001, **71**: 226-232.

212. Valen G., Yan Z.Q., Hansson G.K., Nuclear factor kB and the heart, Journal of the American College of Cardiology 2001 **38**: 307-314.

213. Barkett M., Gilmore T.D., Control of apoptosis by Rel/NF-kB transcription factors. Oncogene, 1999, **18**: 6910-6924.

214. Ashkenazi A., Pai R.C., Fong S., Leung S., Lawrence D.A., Marsters S.A., Blackie C., Chang L., McMurtrey A.E., Hebert A., DeForge L., Koumenis I.L., Lewis D., Harris L., Bussiere J., Koeppen H., Shahrokh Z. and Schwall R.H., Safety and antitumor activity of recombinant soluble Apo2 ligand. Journal of Clinical Investigation 1999, **104**: 155-162.

215. Van Antwerp D.J., Martin S.J., Verma I.M. and Green D.R. Inhibition of TNF-induced apoptosis by NF-kB. Trends in Cell Biology, 1998, **8**: 107-111.

216. Hsu H., Shu H-B, Pan M-G and Goeddel D.V., TRADD-TRAF2 and TRADD-FADD interactions define two distinct TNF receptor 1 signal transduction pathways. Cell 1996, **84**: 299-308.

217. Ozes O.N., Mayo L.D., Gustin J.A., Pfeffer S.R., Pfeffer L.M. and Donner D.B., Reply to: Kinase regulation in inflammatory response., Nature, 2000, **406**: 368.

218. Grilli M., Pizzi M., Memo M. and Spano P.F., Neuroprotection by aspirin and sodium salicylate through blockade of NF-kB activation. Science. 1996, **274**: 1383-1385.

219. Bales K.R., Du Y., Dodel R.C., Yan G-M, Hamilton-Byrd E. and Paul S.M. The NF-kB/Rel family of proteins mediates Ab-induced neurotoxicity and glial activation. Molecular Brain Research, 1998, **57**: 63-72.

220. Gahring L.C., Meyer E.L. and Rogers S.W., Nicotine-induced neuroprotection against N-methyl-d-aspartic acid or beta-amyloid peptide occur through independent mechanisms distinguished by pro-inflammatory cytokines. Journal of Neurochemistry, 2003, **87**: 1125-1136.

221. DeLuca C., Kwon H., Pelletier N., Wainberg M.A. and Hiscott J., NF-kB protects HIV-1-infected myeloid cells from apoptosis. Virology 1998 **244**: 27-38.

222. Westendorp M.O., Shatrov V.A., Schulze-Osthoff, Frank R., Kraft M., Lose M., Krammer P.H., Droge W. and Lehmann V. HIV-1 Tat potentiates TNF-induced NF-kB activation and cytotoxicity by altering the redox state. EMBO Journal 1995, **14**: 546-554.

223. Van Antwerp D.J. and Verma I.M., Signal-induced degradation of IkBa: association with NF-kB and the PEST sequence in IkBa are not required. Molecular and Cellular Biology, 1996, **16**: 6037-6045.

224. Giri D.K., Mehta R.T., Kansal R.G. and Aggarwal B.B. Mycobacterium avium-intracellular complex activates nuclear transcription factor kB in different cell types through reactive oxygen intermediates. Journal of Immunologa, 1998, **161**: 4834-4841.

225. Nakshatri H., Bhat-Nakshatri P., Martin D.A., Goulet Jr R.J. and Sledge Jr G.W. Constitutive activation of NF-kB during progression of breast cancer to hormone-independent growth. Molecular and Cellular Biology, 1997, **17**: 3629-3639.

226. Waddick K.G. and Uckun F.M., Innovative treatment programs against cancer: II. NF-kB as a molecular target. Biochemical Pharmacology, 1999, **57**: 9-17.

227. Kalgutkar A. S., Zhao Z. Discovery and design of selective cyclooxygenase-2 inhibitors as non-ulcerogenic, anti-inflammatory drugs with potential utility as anti-cancer agents. Curr. Drug Targets. 2001, **2** (1): 79-106.

228. Loukinova E., Chen Z., Van Waes C. and Dong G. Expression of proangiogenic chemokine Gro 1 in low and high metastatic variants of Pam murine squamous cell carcinoma is differentially regulated by IL-1alpha, EGF and TGF-beta1 through NF-kB dependent and independent mechanisms. International Journal of Cancer 2001, **94**: 637-644.

229. Luo D., Luo Y., He Y., Zhang H., Zhang R., Li X., Dobrucki W.L., Sinusas A.J., Sessa W.C. and Min W. Differential functions of tumor necrosis factor receptor 1 and 2 signaling in ischemia-mediated arteriogenesis and angiogenesis. American Journal of Pathology 2006, **169**: 1886-1898.

230. Collart MA, Baeuerle PA and Vassalli P (1990) Regulation of tumor necrosis factor alpha transcription in macrophages: involvement of four kB-like motifs and of constitutive and inducible forms of NF-kB. Molecular and Cellular Biology 10 1498-1506

231. Whelan J., Ghersa P., Hooft van Huijsduijnen R., Gray J., Chandra G., Talabot F. and DeLamarter J.F. An NFkB-like factor is essential but not sufficient for cytokine induction of endothelial leukocyte adhesion molecule 1 (ELAM-1) gene transcription. Nucleic Acids Research, 1991 **19**: 2645-2653.

232. Iademarco M.F., McQuillan J.J., Rosen G.D. and Dean D.C. Characterization of the promoter for vascular cell adhesion molecule-1 (VCAM-1). The Journal of Biological Chemistry, 1992, **267**: 16323-16329.

233. Dong G., Chen Z., Kato T. and Van Waes C. The host environment promotes the constitutive activation of nuclear factor-kB and proinflammatory cytokine expression during metastatic tumor progression of murine squamous cell carcinoma. Cancer Research, 1999, **59**: 3495-3504

234. Koong A., Chen E., Mivechi N., Denko N., Stambrook P. and Giaccia A. Hypoxic activation of NF-kB is mediated by a Ras and Ras signaling pathway and does not involve MAP kinase (ERK1 or ERK2). Cancer Research 1994, **54**: 5273-5279.

235. Koong A.C., Chen E.Y. and Giacca A.J. Hypoxia causes the activation of nuclear factor kB through the phosphorylation of IkBa on tyrosine residues. Cancer Research 1994, **54**: 1425-1430.

236. Miyamoto S., Chiao P.J. and Verma I.M. Enhanced IkBa degradation is responsible for constitutive NF-kB activity in mature murine B-cell lines. Molecular and Cellular Biology, 1994, **14**: 3276-3282.

237. Bargou R.C., Emmerich F., Krappmann D., Bommert K., Mapara M.Y., Arnold W., Royer H.D., Grinstein E., Greiner A., Scheidereit C. and Dörkin B. Constitutive NF-kB-RelA activation is required for proliferation and survival of Hodgkin's disease tumor cells. Journal of Clinical Investigation, 1997, **100**: 2961-2969.

238. O'Connell M.A., Bennett B.L., Mercurio F., Mannin A.M. and Machman N. Role of IKK1 and IKK2 in lipopolysaccharide signaling in human monocytic cells. Journal of Biological Chemistry, 1998 **273**: 30410-30414.

239. Kordes U., Krappmann D., Heissmeyer V., Ludwig W.D. and Scheidereit C. Transcription factor NF-kB is constitutively activated in acute lymphoblastic leukemia cells. Leukemia 2000, **14**: 399-402.

240. Visconti R., Cerutti J., Battista S., Fedele M., Trapasso F., Zeki K., Miano M.P., de Nigris F., Casalino L., Curcio F., Santoro M. and Fusco A. Expression of the neoplastic phenotype by human thyroid carcinoma cell lines requires NFkB p65 protein expression. Oncogene, 1997, **15**: 1987-1994.

241. Palayoor S.T., Youmell M.Y., Calderwood S.K., Coleman C.N. and Price B.D. Constitutive activation of IkB kinase a and NFkB in prostate cancer cells is inhibited by ibuprofen. Oncogene, 1999, **18**: 7389-7394.

242. Wang C.Y., Cusack J.C. Jr, Lin R., Baldwin A.S. Jr. Control of inducible chemoresistance: enhanced anti-tumor therapy through increased apoptosis by inhibition of NF-kB. Nature Medicine, 1999, **5**: 412-417.

243. Wang C.Y., Guttridge D.C., Mayo M.W. and Baldwin Jr A.S. NF-kB induces expression of the Bcl-2 homologue A1/Bfl-1 to preferentially suppress chemotherapy-induced apoptosis. Molecular and Cellular Biology, 1999, **19**: 5923-5929.

244. Zhang Z.W., He Z.M., Zhou M., Zhang Q., Yu Y.H. and Chen Z.C. Effects of Epstein-Barr Virus Latent Membrane Protein 1 mediated by nuclear factor-kB on transformation and tumorigenesis of rat-1 cells. Ai Zheng, 2007, **26**: 118-122.

245. Rayet B., Fan Y. and Gelinas C. Mutations in the v-Rel transactivation domain indicate altered phosphorylation and identify a subset of NF-kB-regulated cell death inhibitors important for v-Rel transforming activity. Molecular and Cellular Biology 2003, **23**: 1520-1533

246. Rayet B. and Gelinas C. Aberrant rel/nfkb genes and activity in human cancer. Oncogene, 1999, **18**: 6938-6947.

247. Karin M. and Hunter T. Transcriptional control by protein phosphorylation: signal transmission from the cell surface. Current Biology, 1995, **5**: 747-757.

248. Siebenlist U., Franzoso G. and Brown K. Structure, regulation and function of NF-kB. Annual Review of Cell Biology, 1994, **10**: 405-455.

249. Baeuerle P.A., IkB-NF-kB structures: at the interface of inflammation control. Cell 1998, **95**: 729-731.

250. Stark G.R., Kerr I.M. Interferon-dependent signaling pathways: DNA elements, transcription factors, mutations, and effects of viral proteins. Journal of Interferon Research 1992 Jun;12(3):147–151.

251. Bonaiuto C., McDonald P.P., Rossi F. and Cassatella M.A. Activation of Nuclear Factor-kB by beta-amyloid peptides and interferon-gamma in murine microglia. Journal of Neuroimmunology 1997, **77**: 51-56.

252. Roulston A., Beauparlant P., Rice N. and Hiscott J. Chronic human immunodeficiency virus type I infection stimulates distinct NF-kB/rel DNA binding activities in myelomonoblastic cells. Journal of Virology, 1993, **67**: 5235-5246.

253. Bex F. and Gaynor R.B. Regulation of gene expression by HTLV-I Tax protein. Methods, 1998, **16**: 83-94.

254. Baichwal V.R. and Baeuerle P.A., Apoptosis: activate NF-kB or die? Current Biology 1997, **7**: R94-R96.

255. Sonenshein G.E. Rel/NF-kB transcription factors and the control of apoptosis. Seminars in Cancer Biology, (T.D. Gilmore, ed.), 1997, **8**: 113-119.

256. Gilmore T.D. Regulation of Rel transcription complexes. In, Frontiers in Molecular Biology: Eukaryotic Gene Transcription (ed. S. Goodbourn), Oxford University Press, Oxford, England, 1995, pp. 102-131.

257. Grilli M. and Memo M. Nuclear Factor-kB/Rel proteins: a point of convergence of signalling pathways relevant in neuronal function and dysfunction. Biochemical Pharmacology, 1999, **57**: 1-7.

258. Foxwell B., Browne K., Bondeson J., Clarke C., de Martin R., Brennan F. and Feldmann M. Efficient adenoviral infection with IkBa reveals that macrophage tumor necrosis factor alpha production in rheumatoid arthritis is NF-kB dependent, 1998, Proceedings of the National Academy of Sciences of USA, **95**: 8211-8215.

259. Barnes P.J., Anti-inflammatory actions of glucocorticoids: molecular mechanisms. Clincial Science, 1998, **94**: 557-562.

260. Neurath M.F., Fuss I., Schurmann G., Pettersson S., Arnold K., Muller-Lobeck H., Strober W., Herfarth C. and Buschenfelde K.H. Cytokine gene transcription by NF-kB family members in patients with inflammatory bowel disease. Annals of the New York Academy of Sciences, 1998, **859**: 149-159.

261. Palombella V.J., Rando O.J., Goldberg A.L. and Maniatis T. The ubiquitin-proteasome pathway is required for processing the NF-kB1 precursor protein and the activation of NF-kB. Cell 1994, **78**: 773-785.

262. Epinat J.C. and Gilmore T.D. Diverse agents act at multiple levels to inhibit the Rel/NF-kB signal transduction pathway. Oncogene, 1999, **18**: 6896-6909.

263. Rothe M., Xiong J., Shu H-B, Williamson K., Goddard A. and Goeddel D.V. I-TRAF is a novel TRAF-interacting protein that regulates TRAF-mediated signal transduction. Proceedings of the National Academy of Sciences USA, 1996, **93**: 8241-8246.

264. Malinin N.L., Boldin M.P., Kovalenko A.V. and Wallach D. MAP3K-related kinase involved in NF-kB induction by TNF, CD95 and IL-1. Nature, 1997, **385**: 540-544.

265. Song H.Y., Régnier C.H., Kirschning C.J., Goeddel D.V. and Rothe M. Tumor necrosis factor (TNF)-mediated kinase cascades: bifurcation of nuclear factor-kB and c-jun N-terminal kinase (JNK/SAPK) pathways at TNF receptor-associated factor 2. Proceedings of the National Academy of Sciences USA, 1997, **94**: 9792-9796.

266. Jang I.K., Lee Z.H., Kim Y.J., Kim S.H., Kwon B.S., Human 4-1BB (CD137) signals are mediated by TRAF2 and activate nuclear factor-kappa B. Biochem. Biophys. Res. Commun. 1998, **242** (3): 613-20.

267. DiDonato J.A., Hayakawa M., Rothwarf D.M., Zandi E. and Karin M. A cytokine-responsive IkB kinase that activates the transcription factor NF-kB. Nature, 1997, **388**: 548-554.

268. Mercurio F., Zhu H., Murray B.W., Shevchenko A., Bennett B., Li J.W., Young D., Barbosa M., Mann M., Manning A. and Rao A. IKK-1 and IKK-2: cytokine-activated IkB kinases essential for NF-kB activation. Science. 1997, **278**: 860-866.

269. Zandi E., Rothwarf D.M., Delhase M., Hayakawa M. and Karin M. The IkB kinase complex (IKK) contains two kinase subunits, IKKa and IKKb, necessary for IkB phosphorylation and NF-kB activation. Cell 1997, **91**: 243-252.

270. Ling L., Cao Z. and Goeddel D.V. NF-kB-inducing kinase activates IKK-a by phosphorylation of Ser-176. Proceedings of the National Academy of Sciences USA, 1998, **95**: 3792-3797.

271. Régnier C.H., Song H.Y., Gao X., Goeddel D.V., Cao Z., Rothe M., Identification and characterization of an IkappaB kinase. Cell. 1997, **90** (2): 373-83.

272. Woronicz J.D., Gao X., Cao Z., Rothe M. and Goeddel D.V. IkB kinase-b: NF-kB activation and complex formation with IkB kinase-a and NIK. Science. 1997, **281**: 866-870.

273. Bowen B., Steinberg J., Laemmli U.K., Weintraub H. The detection of DNA-binding proteins by protein blotting. Nucleic Acids Res. 1980 **8** (1): 1-20.

274. Miskimins W.K., Roberts M.P., McClelland A., Ruddle F.H. Use of a protein-blotting procedure and a specific DNA probe to identify nuclear proteins that recognize the promoter region of the transferrin receptor gene. Proc. Natl. Acad. Sci. USA. 1985 **82** (20): 6741-4.

275. Engvall E., Perlman P.. Enzyme-linked immunosorbent assay (ELISA). Quantitative assay of immunoglobulin G. Immunochemistry,1971, **8** (9): 871-4.

276. Ruscher K, Reuter M, Kupper D, Trendelenburg G, Dirnagl U and Meisel A (2000) A fluorescence based non-radioactive electrophoretic mobility shift assay. J. of Biotech. **78**: 163-170.

277. II Hamdan, Skellern G.G. and Waigh R.D., Use of capillary electrophoresis in the study of ligand-DNA interactions. Nucelic acid research, Oxford University Press, 1998, **26** (12), 3053-3058.

278. Carlsen H., Alexander G., Austenaa L.M., Ebihara K. and Blomhoff R. Molecular imaging of the transcription factor NF-kB, a primary regulator of stress response. Mutation Research, 2004, **551**: 199-211.

279. Yang M., Baranov E., Moossa A.R., Penman S., Hoffman R.M. Visualizing gene expression by whole-body fluorescence imaging. Proc. Natl. Acad. Sci. USA. 2000, **97** (22): 12278-12282.

280. Weissleder R., Tung C.H., Mahmood U., Bogdanov A. Jr., In vivo imaging of tumors with protease-activated near-infrared fluorescent probes. Nat. Biotechnol. **17** (4): 375-8.

281. Tjuvajev J.G., Stockhammer G., Desai R., Uehara H., Watanabe K., Gansbacher B., Blasberg R.G. Imaging the expression of transfected genes in vivo. Cancer Res., 1995 **55** (24): 6126-32.

282. Gambhir S.S., Barrio J.R., Phelps M.E., Iyer M., Namavari M., Satyamurthy N., Wu L., Green L.A., Bauer E., MacLaren D.C., Nguyen K., Berk A.J., Cherry S.R., Herschman H.R., Imaging adenoviral-directed reporter gene expression in living animals with positron emission tomography. Proc. Natl. Acad. Sci. U S A, 1999, **96** (5): 2333-2338.

283. Tjuvajev J.G., Finn R., Watanabe K., Joshi R., Oku T., Kennedy J., Beattie B., Koutcher J., Larson S., Blasberg R.G. Noninvasive imaging of herpes virus thymidine kinase gene transfer and expression: a potential method for monitoring clinical gene therapy. Cancer Res. 1996, **56** (18): 4087-95.

284. Hofmann B., Bogdanov A. Jr, Marecos E., Ebert W., Semmler W., Weissleder R., Mechanism of gadophrin-2 accumulation in tumor necrosis. J Magn Reson Imaging. 1999; **9** (2): 336-341.

285. Contag P.R., Olomu I.N., Stevenson D.K., Contag C.H. Bioluminescent indicators in living mammals. Nat Med. 1998, **4**(2): 245-7.

286. Wang J.K., Li T.X., Bai Y.F., Lu Z.H. Evaluating the binding affinities of NF-kappaB p50 homodimer to the wild-type and single-nucleotide mutant Ig-kappaB sites by the unimolecular dsDNA microarray. Analytical Biochemistry 2003, **316** (2):192-201.

287. Gerson S.L., Clinical relevance of MGMT in the treatment of cancer. Journal of Clinical Oncology, 2002, **20** (9): 2388-2399.

288. Ryan J. Hansen, Ramamoorthy Nagasubramanian, Shannon M. Delaney, Leona D. Samson, and M. Eileen Dolan, Role of O6-methylguanine-DNA methyltransferase in protecting from alkylating agent-induced toxicity and mutations in mice. Carcinogenesis 2007, **28** (5): 1111-1116.

289. Rye P.T., Delaney J.C., Netirojjanakul C., Sun D.X., Liu J.Z., Essigmann J.M. Mismatch repair proteins collaborate with methyltransferases in the repair of O(6)-methylguanine. DNA Repair (Amst). 2008, **7** (2):170-176.

290. Gonzaga P.E., Potter P.M., Niu T.Q., Yu D., Ludlum D.B., Rafferty J.A., Margison G.P., Brent T.P., Identification of the cross-link between human O6-methylguanine-DNA methyltransferase and chloroethylnitrosourea-treated DNA. Cancer Res. 1992, **52** (21):6052-8.

291. Komine C., Watanabe T., Katayama Y., Yoshino A., Yokoyama T., Fukushima T., Promoter hypermethylation of the DNA repair gene O6-methylguanine-DNA methyltransferase is an independent predictor of shortened progression free survival in patients with low-grade diffuse astrocytomas. Brain Pathology 2003, **13** (2): 176-184.

292. Esteller M., Garcia-Foncillas J., Andion E., Goodman S.N., Hidalgo O.F., Vanaclocha V., Baylin S.B., Herman J.G. Inactivation of the DNA-repair gene MGMT and the clinical response of gliomas to alkylating agents. New England Journal of Medicine, 2000; **343** (19):1350-4.

293. Stern M.C., Conti D.V., Siegmund K.D., Corral R., Yuan J.M., Koh W.P., Yu M.C. DNA repair single-nucleotide polymorphisms in colorectal cancer and their role as modifiers of the effect of cigarette smoking and alcohol in the Singapore Chinese Health Study. Cancer Epidemiol. Biomarkers Prev. 2007, **16** (11): 2363-72.

294. Parkinson J.F., Wheeler H.R., Clarkson A., McKenzie C.A., Biggs M.T., Little N.S., Cook R.J., Messina M., Robinson B.G., McDonald K.L. Variation of O(6)-methylguanine-DNA methyltransferase (MGMT) promoter methylation in serial samples in glioblastoma. J Neurooncol. 2008, **87** (1): 71-78.

295. Wiewrodt D., Nagel G., Dreimüller N., Hundsberger T., Perneczky A., Kaina B., MGMT in primary and recurrent human glioblastomas after radiation and chemotherapy and comparison with p53 status and clinical outcome. Int J. Cancer. 2008 **122** (6): 1391-1399.

296. Kovacs K., Scheithauer B.W., Lombardero M., McLendon R.E., Syro L.V., Uribe H., Ortiz L.D., Penagos L.C. MGMT immunoexpression predicts responsiveness of pituitary tumors to temozolomide therapy. Acta Neuropathol. 2008 **115** (2): 261-262.

297. Felini M.J., Olshan A.F., Schroeder J.C., North K.E., Carozza S.E., Kelsey K.T., Liu M., Rice T., Wiencke J.K., Wrensch M.R. DNA repair polymorphisms XRCC1 and MGMT and risk of adult gliomas. Neuroepidemiology 2007, **29** (1-2): 55-58.

298. Marchesi F., Turriziani M., Tortorelli G., Avvisati G., Torino F., De Vecchis L. Triazene compounds: mechanism of action and related DNA repair systems. Pharmacol. Res. 2007, **56** (4): 275-287.

299. Wagner LM, McLendon RE, Yoon KJ, Weiss BD, Billups CA, Danks MK. Targeting methylguanine-DNA methyltransferase in the treatment of neuroblastoma. Clin Cancer Res. 2007, **13** (18 Pt 1): 5418-5425.

300. Hegi M.E., Diserens A.C., Gorlia T., Hamou M.F., de Tribolet N., Weller M., Kros J.M., Hainfellner J.A., Mason W., Mariani L., Bromberg J.E., Hau P., Mirimanoff R.O., Cairncross J.G., Janzer R.C., Stupp R. MGMT gene silencing and benefit from temozolomide in glioblastoma. New England Journal of Medicine 2005, **352** (10): 997-1003.

301. Paus C., Murat A., Stupp R., Regli L., Hegi M., Role of MGMT and clinical applications in brain tumours [Article in French] Bull. Cancer. 2007, **94** (9): 769-773.

302. Crosbie P.A., McGown G., Thorncroft M.R., O'Donnell P.N., Barber P.V., Lewis S.J., Harrison K.L., Agius R.M., Santibáñez-Koref M.F., Margison G.P., Povey A.C., Association between lung cancer risk and single nucleotide polymorphisms in the first intron and codon 178 of the DNA repair gene, O6-alkylguanine-DNA alkyltransferase. Int. J. Cancer. 2008 **122** (4): 791-795.

303. Henken F.E., Wilting S.M., Overmeer R.M., van Rietschoten J.G., Nygren A.O., Errami A., Schouten J.P., Meijer C.J., Snijders P.J., Steenbergen R.D. Sequential gene promoter methylation during HPV-induced cervical carcinogenesis. British Journal of Cancer. 2007, **97** (10): 1457-1464.

304. Srivenugopal K.S., Ali-Osman F., The DNA repair protein, O(6)-methylguanine-DNA methyltransferase is a proteolytic target for the E6 human papillomavirus oncoprotein. Oncogene. 2002, **21** (38): 5940-5945.

305. Guo W., Liu X., Lee S., Park N.H., High O6-methylguanine methyl transferase activity is frequently found in human oral cancer cells with p53 inactivation. Int. J. Oncology **15** (4): 817-821.

306. Kuo C.C., Liu J.F., Chang J.Y., DNA repair enzyme, O6-methylguanine DNA methyltransferase, modulates cytotoxicity of camptothecin-derived topoisomerase I inhibitors. J. Pharmacol. Exp. Therapy 2006, **316** (2): 946-954.

307. Tsourkas A., Behlke M.A., Bao G., Hybridization of 2'-O-methyl and 2'-deoxy molecular beacons to RNA and DNA targets. Nucleic Acids Res. 2003, **31** (6): 5168-5174.

308. Schmitz J.C., Yu D., Agrawal S., Chu E. Effect of 2'-O-methyl antisense ORNs on expression of thymidylate synthase in human colon cancer RKO cells. Nucleic Acids Res. 2001, **29** (2): 415-422.

309. Citti L., Eckstein F., Capecchi B., Mariani L., Nevischi S., Poggi A., Rainaldi G. Transient transfection of a synthetic hammerhead ribozyme targeted against human MGMT gene to cells in culture potentiates the genotoxicity of the alkylation damage induced by mitozolomide. Antisense Nucleic Acid Drug Dev. 1999, **9** (2): 125-133.

310. Esteller M., Hamilton S.R., Burger P.C., Baylin S.B., Herman J.G. Inactivation of the DNA repair gene O6-methylguanine-DNA methyltransferase by promoter hypermethylation is a common event in primary human neoplasia. Cancer Res. 1999, **59** (4): 793-797.

311. Egyházi S., Ma S., Smoczynski K., Hansson J., Platz A., Ringborg U., Novel O6-methylguanine-DNA methyltransferase SNPs: a frequency comparison of patients with familial melanoma and healthy individuals in Sweden. Human Mutation 2002, **20** (5): 408-9.

312. Daniels DS, Mol CD, Arvai AS, Kanugula S, Pegg AE, Tainer JA. Active and alkylated human AGT structures: a novel zinc site, inhibitor and extrahelical base binding. EMBO J. 2000, **19** (7): 1719-30.

313. Daniels D.S., Woo T.T., Luu K.X., Noll D.M., Clarke N.D., Pegg A.E., Tainer J.A., DNA binding and nucleotide flipping by the human DNA repair protein AGT. Nat. Struct. Molecular Biology, 2004, **11:** 714-720.

314. Hyperthermostable protein structure maintained by intra and inter-helix ion-pairs in archaeal O6-methylguanine-DNA methyltransferase. Journal of Molecular Biology, 1999, **292** pp. 707-716.

315. Banerjee A.R., Jaeger J.A., Turner D.H. Thermal unfolding of a group I ribozyme: the low-temperature transition is primarily disruption of tertiary structure.Biochemistry. 1993, **32** (1):153-163.

316. Jaeger J.A., SantaLucia J. Jr, Tinoco I. Jr. Determination of RNA structure and thermodynamics. Annu. Rev. Biochem. 1993; **62**: 255-87.

317. Zuker M., Computer prediction of RNA structure. Methods in Enzymology 1989, **180**: 262-288.

318. Mercatanti A, Rainaldi G, Mariani L, Marangoni R, Citti L. A method for prediction of accessible sites on an mRNA sequence for target selection of hammerhead ribozymes. Journal of Computational Biology, 2002 **9** (4): 641-53.

319. Zhang O., Ohannesian D.W., and Erickson L.C., hammerhead ribozyme-mediated sensitization of human tumour cells after treatment with 1,3-Bis(2-chloroethyl)-1-nitrosourea, Journal of Pharmacology and Experimental Therapeutics **309**: 506-514, 2004.

320. Tedeschi L., Citti L., Domenici C., An integrated approach for the design and synthesis of oligonucleotide probes and their interfacing to a QCM-based RNA biosensor, Biosensors and Bioelectronics (2005) **20**: 2376–2385, 2381.

321. Ming-Ren S.Fuh, Burgess L.W., Hirschfeld T., Christian G.D., Wang F., Single Fibre optic Fluorescence pH Probe, Analyst, 1987, **112**: 1159-1163.

322. Kawabata Y., Tsuchida K., Imasaka T., Ishibashi N., Fiber-optic pH sensor with monolayer indicator, Analytical Sciences, 1987, Vol. **3**, No. 1: 7-9.

323. Saari L., pH sensor based on Immobilized Fluoresceinamine, Anal. Chem. 1982, **54**: 821-823.

324. Daehne S., Resch Genger U., Wolfbeis O.S., Near infrared dyes for high technology applications, Proceedings of the NATO Advanced Research Workshop on Syntheses, Optical Properties and Applications of Near-Infrared (NIR) Dyes in High Technology Fields, Trest, Czech Republic, September 24-27, 1997 Series: NATO Science Partnership Sub-Series: 3: Vol. 52.

325. Mank A.J.G., Lingeman H., Gooijer C., Diode laser-based detection in liquid chromatography and capillary electrophoresis Trends Anal.Chem., 1996, **15**, 1: 1-11.

326. Rahavendran S.V., Karnes H.T., Solid-state diode laser-induced fluorescence detection in high-performance liquid chromatography. Pharm. Res. 1993, **10** (3), 328-334.

327. Mujumdar R.B., Ernst L.A., Mujumdar S.R., Lewis C.J., Waggoner A.S. Cyanine dye labeling reagents: sulfoindocyanine succinimidyl esters. Bioconjugate Chemistry, 1993, **4** (2): 105-111.

328. Southwick, P.L., Ernst L.A., Tauriello E.W., Parker S.R., Mujumdar R.B., Mujumdar S.R., Clever H.A., Waggoner A.S., Cyanine dye labeling reagents--carboxymethylindocyanine succinimidyl esters. Cytometry, 1990, **11** (3): 418-430.

329. Smith L.M., Fung S.,,Hunkapiller M.W., Hunkapiller T.J., Hood L.E., The synthesis of oligonucleotides containing an aliphatic amino group at the 5' terminus: synthesis of fluorescent DNA primers for use in DNA sequence analysis. Nucleic Acids Research, 1985, **13** (7): 2399-2412.

330. Wessendorf, M.W. and Brelje, T.C., Which fluorophore is brightest? A comparison of the staining obtained using fluorescein, tetramethylrhodamine, lissamine rhodamine, Texas red, and cyanine 3.18. Histochemistry. 1992, **98** (2): 81-85.

331. Yu H., Chao J., Patek D., Mujumdar R., Mujumdar S., Waggoner A.S., Cyanine dye dUTP analogs for enzymatic labeling of DNA probes. Nucleic Acids Research, 1994, **22** (15): 3226-3232.

332. www.probes.com/Handbook.

333. Offenbacher H., Wolfbeis O.S., Furlinger E., Fluorescence optical sensors for continous determination of near-neutral pH values, Sens. and Act., 1986, **9** : 73-84.

334. Yguerabide J., Talavera E.M., Alvarez J.M.and Quintero B. Steady-state fluorescence method for evaluating excited estate proton reactions: application to fluorescein, Photochem. Photobiol., 1994, **60**: 435- 441.

335. H.Stuart, D.Hall, Enhanced dipole-dipole interaction between elementary radiators near a surface, Phys. Rev. Lett. 1998, **80**: 5663–5666.

336. Po-Chun Chang, Bu-Yuan Liu, Cheng-Meei Liu, Hsin-Hua Chou, Ming-Hua Ho, Hwa-Chang Liu, Da-Ming Wang, Lein-Tuan Hou, Bone tissue engineering with novel rhBMP2-PLLA composite scaffolds. J. Biomed. Mater. Res. A. 2007.

337. Bieniarz, C., Husain M., Barnes G., King C.A., Welch C.J. Extended Length Heterobifunctional Coupling Agents for Protein Conjugations, 1996, Bioconjug. Chem. **7**: 88-95.

338. Chrisey, L.A., Lee U.G.,O'Ferrall C.E., Covalent attachement of synthetic DNA to self-assembled monolayers, Nucleic Acids Research, 1996, **24** (15): 3031-3039.

339. Brinkley M.A., A survey of methods for preparing protein conjugates with dyes, haptens and crosslinking reagents. Bioconjugate Chem., 1992, 3: 2-13.

340. Mattson G., Conklin E., Desai S., Nielander G. , Savage M. D. and Morgensen S., A practical approach to crosslinking, Molecular Biology Reports, 1993, 17: 167-183.

341. Gaines Jr. G.L., Insoluble monolayers at Liquid-Gas Interfaces, Interscience publishers, New York, 1966.

342. Ulman A., An introduction to Ultrathin Organic Films from LB to self assembly, Academic Press, San Diego, 1991.

343. Dhawal H.S., Kemp P., Aller J., Dantzler M.M., Capillary waveguide nucleic acid based biosensor, Analytica Chimica Acta, 2004, 501: 205-217.

344. Baldini F., Giannetti A., Mencaglia A.A.Optical sensor for interstitial pH measurements. Journal of Biomedical Optics, 2007, **12** (2): 024024.

345. J.R.Lakowicz, Topics in Fluorescence Spectroscopy,Vol.4, Plenum Press, New York, USA,1994.

346. Polerecky, L., Hamrle, J., and MacCraith, B.D.: Theory of the radiation of dipoles within a multilayer system', Appled Optics, 2000, **39** (22), 3968–3977.

347. Lee K-B, Park S-J, Mirkin A.C., Smith J.C., Mrksich M., Protein Nanoarrays Generated By Dip-Pen Nanolithography.

348. P.A. Wallace, M.Campbell, Y. Yang, Holmes-Smith A.S., M.Uttamlal, A distributed optical fibre fluorosensor for pH measurement, Journal of Luminescence, 1997, 72-74, 1017-1019.

349. Moorthy J.N., Shevchenko T., Magon A., Biohne C., Paper acidity estimation: Application of pH-dependent fluorescence probes, Journal of Photochemistry and Photobiology A: Chemistry, 1998, 113: 189-195.

350. Piruska A., Nikcevic I., Lee S.H., Ahn C.,. Heineman W.R., Limbacha P.A., Seliskar C.J., The autofluorescence of plastic materials and chips measured under laser irradiation, 2005, Lab Chip 5: 1348–1354.

351. Donald J. Dempsey, Phaneuf M.D., LoGerfo F.W., Quist W.C., Donald 2002: Development of a Bioactive Surface for Titanium Implant Devices; ©2002 SOCIETY FOR BIOMATERIALS 28th Annual Meeting Transactions.

352. Gaur R.K, and Gupta K.C. A spectrophotometric method for the estimation of amino groups on polymer supports. Analytical Biochemistry, 1989, 180: 253-258.

353. Putnam W.F., The Plasma Proteins: Structure, Function and Genetic Control, Academic Press, New York, 1975, 2nd ed., Vol. 1: 141, 147.

354. Zhitkovich A., Costa M.A. Simple, sensitive assay to detect DNA-protein crosslinks in intact cells and in vivo. Carcinogenesis, 1992, **13** (8): 1485-1489.

355. Kim S.J., Gobi K.V., Iwasaka H., Tanaka H., Miura N. Novel miniature SPR immunosensor equipped with all-in-one multi-microchannel sensor chip for detecting low-molecular-weight analytes. Biosensor and Bioelectronics 2007, **23** (5):701-7

356. Wang B., Oleschuk R.D., Petkovich P.M., Horton J.H. Chemical force titrations of antigen- and antibody-modified poly(methylmethacrylate).Colloids Surf B Biointerfaces. 2007, **55** (1): 107-114.

357. Jones B.J., Hayes M.A. Surface modification methods for enhanced device efficacy and function. Methods Mol. Biol. 2006, **339**: 49-56.

358. Rucker V.C., Havenstrite K.L., Simmons B.A., Sickafoose S.M., Herr A.E., Shediac R. Functional antibody immobilization on 3-dimensional polymeric surfaces generated by reactive ion etching. Langmuir. 2005, **21** (17): 7621-7625.

359. Pişkin E., Ayhan H., Bulmuş E.V., Rad A.Y., Falkenhagen D., Weber C. Protein A carrying monosize PMMA microbeads for the removal of HIgG from human plasma. Int. J. Artif. Organs. 1996, **19** (5): 311-317.

360. Luo L., Zhang Z., Hou L., Development of a gold nanoparticles based chemiluminescence imaging assay and its application. Anal. Chim. Acta. 2007, **584** (1): 106-111.

361. Zhang P.C., Bai C., Ho P.K., Dai Y., Wu Y.S. Observing interactions between the IgG antigen and anti-IgG antibody with AFM. IEEE Eng. Med. Biol. 1997, **16** (2): 42-46.

362. Baldini F, Carloni A, Giannetti A, Porro G, Trono C. A new optical platform for biosensing based on fluorescence anisotropy. Anal. Bioanal Chem. 2008 Jul; 391(5): 1837-44. Epub 2008 Feb 15.

363. Maxwell K. and Johnson G.N., Chlorophyll fluorescence—A practical guide, Journal of Experimental Botany, Vol. **51**, No.345, pp. 659-668, April 2000. Review.

364. Ventrella A., Catucci L., Villari V., Scolaro L.M., Agostiano A. Focus on the aggregation processes of Photosystem II complexes. Bioelectrochemistry, 2007, **70** (1): 33-8.

365. Bilger H.W., Schreiber U. and Lange O.L. Determination of Leaf Heat-Resistance - Comparative Investigation of Chlorophyll Fluorescence Changes and Tissue Necrosis Methods. Oecologia, 1984, **63**: 256-262.

366. Havaux M. 1993. Characterisation of Thermal damage to the photosynthetic electron transport system in potato leaves. Plant Science 94: 19-33.

367. Armond P.A., Bjorkman O. and Staehelin L.A. Dissociation of Supramolecular Complexes in Chloroplast Membranes - a Manifestation of Heat Damage to the Photosynthetic Apparatus. Biochim Biophys Acta, 1980, 601: 433-442.

368. Vink M., Zer H., Alumot N., Gaathon A., Niyogi K., Herrmann R.G., Andersson B., Ohad I. Light-modulated exposure of the light-harvesting complex II (LHCII) to protein kinase(s) and state transition in Chlamydomonas reinhardtii xanthophyll mutants. Biochemistry. 2004, **43** (24): 7824-7833.

369. Ferreira K. N., Iverson T.M, Maghlaoui K., Barber J., Iwata S. Architecture of the photosynthetic oxygen-evolving center. Science. 2004, **303** (5665):1831-1838.

370. Barber J. Photosystem II: a multisubunit membrane protein that oxidises water. Curr.Opin.Struct.Biol.2002,12(4):523-30.

371. Lu Y.K. and Stemler A.J., Extrinsic Photosystem II Carbonic Anhydrase in Maize Mesophyll Chloroplasts Plant Physiol. 2002 February; 128(2): 643–649.

372. Paddock M. L., Chang C., Xu Q., Abresch E. C., Axelrod H. L., Feher G., and Okamura M. Y., Quinone (Q_B) Reduction by B-Branch Electron Transfer in Mutant Bacterial Reaction Centers from Rhodobacter sphaeroides: Quantum Efficiency and X-ray Structure, Biochemistry 2005., **44** (18): 6920 -6928.

373. Hundal T., Forsmark-Andrée P., Ernster L., and Andersson B. Antioxidant Activity of Reduced Plastoquinone in Chloroplast Thylakoid Membranes, Archives of Biochemistry and Biophysics 1995, Vol. **324** (1): 117-122.

374. Piletskaya E.V., Piletsky S.A., El'skaya A.V., Sozinov A.A., Marty J.-L. and Rouillon R., D1 protein – an effective substitute for immunoglobulins in ELISA for the detection of photosynthesis inhibiting herbicides, Analytica Chimica Acta 1999, Vol. **398**, (1), 49-56.

375. Koblizek M, Masojidek J, Komenda J, Kucera T, Pilloton R, Mattoo AK, Giardi MT. A sensitive photosystem II-based biosensor for detection of a class of herbicides. Biotechnol. Bioeng. 1998, **60** (6): 664-9.

376. Laberge D, Rouillon R, Carpentier R. Comparative study of thylakoid membranes sensitivity for herbicide detection after physical or chemical immobilization. Enzyme Microb. Technol. 2000, **26** (5-6): 332-336.

377. Tamura N, Kuwahara M, Sasaki Y, Wakamatsu K, Oku T. Redox dependence for photoligation of manganese to the apo-water-oxidizing complex in chloroplasts and photosystem II membranes. Biochemistry. 1997, **36** (20): 6171-6177.

378. Ventrella A, Catucci L, Mascolo G, Corcelli A, Agostiano A. Isolation and characterization of lipids strictly associated to PSII complexes: focus on cardiolipin structural and functional role. Biochim Biophys Acta. 2007, **1768** (6): 1620-1627.

379. Optical PMMA chip for multianalyte detection Baldini F., Carloni A., Falciai R., Giannetti A., Mencaglia A., Porro G., Trono C., Proceedings of SPIE -- Volume 6619, Third European Workshop on Optical Fibre Sensors, Cutolo A., Culshaw B., López-Higuera J. M., Editors, 661923 (Jul. 2, 2007).

380. Trudel E., Gallant J., Mons S., Mioskowski C., Lebeau L., Jeuris K., Foubert P., De Schryver F., and Salesse C., Design of Functionalized Lipids and Evidence for Their Binding to Photosystem II Core Complex by Oxygen Evolution Measurements, Atomic Force Microscopy, and Scanning Near-Field Optical Microscopy. Biophysical Journal, 2001, Vol. **81**, No. 1, p. 563-571.

381. Zhang, H., Lee, K.-B., Li, Z., Mirkin C. A., Biofunctionalized Nanoarrays of Inorganic Structures Prepared by Dip-Pen Nanolithography, Nanotechnology 2003, 14, 1113-1117.

382. Liu, X.; Guo, S.; Mirkin, C.A. "Surface and Site-Specific Ring-Opening Metathesis Polymerization Initiated by Dip-Pen Nanolithography" Angew. Chem. Int. Ed. 2003, 115, 4933-4937.

PUBLICATIONS

1) Baldini F.; Carloni A.; Falciai R.; Giannetti A.; Mencaglia A.; Porro G.; Trono C., *Optical PMMA chip for multianalyte detection,* (Proceedings Paper) Proceedings Vol. 6619. Third European Workshop on Optical Fibre Sensors, Antonello Cutolo; Brian Culshaw; José Miguel López-Higuera, Editors, 661923, 2 July 2007

2) Baldini F., Carloni A., Giannetti A., Porro G., Trono C., *A new optical platform for biosensing based on fluorescence anisotropy*. Anal. Bioanal. Chem. 2008 Feb 15.

3) "Bioprocess Technology", Chapter book A. Carloni, A.P.F.Turner, M. Flickinger, Encyclopedia of Bioprocess Technology, Wiley & Sons ed., Feb 2008.

POSTERS

- New Frontiers in Micro and Nano Photonics, 23 - 26 April 2008, Firenze, Italy. Poster: "CRP assay with a novel optical chip".
- Elettrottica Congress 2008, 10-12 June 2008, Milano, "Un nuovo chip ottico per la rivelazione di bioanaliti di interesse clinico".
- European Workshop on Optical Fibre Sensors, July 2007, Napoli, Italy,. Poster: "Optical PMMA chip for biosensing applications".
- Associazione Italiana Sensori e Microsistemi Congress, February 2007, Napoli, Italy. Poster: "Optical PMMA chip for multianalyte detection".

- Advanced School on chemical and optical sensors, September 2006, Tihanj, Hungary. (7 days courses).
- EUROPTRODE 2006, Tuebingen, Germany, April 2006. (3 days courses).
- CARE-MAN 2005 (6° Framework European project), November 2005.
- AISEM 2005 (Italian Association of Sensors and Microsystems), Firenze, Italy, February 2005.

Personal Reference:

Adolfo Carloni - Dr. in Industrial Chemistry
Birth: 9th December 1978 in Pavullo nel Frignano, Modena, Italy
Position: from January 2008 at European Laboratory of Non linear Spectroscopy (LENS)
Office: +39 055 457 2476
Lab: +39 055 457 2018
Mobile: +39 320 246 3550
E-mail: adolfo.carloni@gmail.com
